

**Massachusetts Institute of Technology
Woods Hole Oceanographic Institution**



**Joint Program
in Oceanography/
Applied Ocean Science
and Engineering**



DOCTORAL DISSERTATION

The Temporal Dynamics of Terrestrial
Organic Matter Transfer to the Oceans:
Initial Assessment and Application

by

Nicholas J. Drenzek

June 2007

20070927454

MIT/WHOI

2007-14

**The Temporal Dynamics of Terrestrial Organic Matter Transfer to the Oceans:
Initial Assessment and Application**

by

Nicholas J. Drenzek

Massachusetts Institute of Technology
Cambridge, Massachusetts 02139

and

Woods Hole Oceanographic Institution
Woods Hole, Massachusetts 02543

June 2007

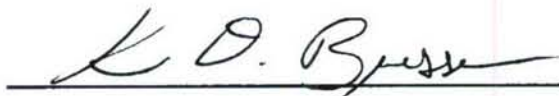
DOCTORAL DISSERTATION

Funding was provided by the National Science Foundation through grants OCE-9907129, OCE-052626800, OCE-0137005, DEB-0447281, and the Stanley Watson Chair for Excellence in Oceanography. There was additional support by the Schlanger Ocean Drilling Program, the Environmental Protection Agency's Science to Achieve Results (STAR) Program, as well as by the WHOI Academic Programs Office.

Reproduction in whole or in part is permitted for any purpose of the United States Government. This thesis should be cited as: Nicholas J. Drenzek, 2007. The Temporal Dynamics of Terrestrial Organic Matter Transfer to the Oceans: Initial Assessment and Application. Ph.D. Thesis. MIT/WHOI. 2007-14.

Approved for publication; distribution unlimited.

Approved for Distribution:

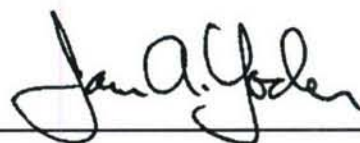


Ken O. Buesseler, Chair

Department of Marine Chemistry and Geochemistry



Paola Malanotte-Rizzoli
MIT Director of Joint Program



James A. Yoder
WHOI Dean of Graduate Studies

**THE TEMPORAL DYNAMICS OF TERRESTRIAL ORGANIC MATTER TRANSFER TO THE
OCEANS: INITIAL ASSESSMENT AND APPLICATION**

By

Nicholas J. Drenzek

B.S., Rensselaer Polytechnic Institute, 2000

Submitted in partial fulfillment of the requirements for the degree of

Doctor of Philosophy

at the

MASSACHUSETTS INSTITUTE OF TECHNOLOGY

and the

WOODS HOLE OCEANOGRAPHIC INSTITUTION

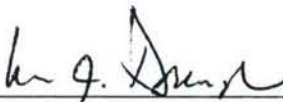
June 2007

© 2007 *Nicholas J. Drenzek*

All rights reserved.

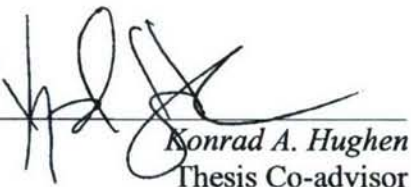
The author hereby grants to MIT and WHOI permission to reproduce paper and electronic copies of this thesis in whole or in part and to distribute them publicly.

Signature of Author

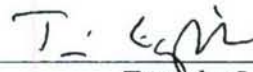


Joint Program in Oceanography / Applied Ocean Science and Engineering
Massachusetts Institute of Technology
and Woods Hole Oceanographic Institution
May 11, 2007

Certified by

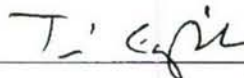


Konrad A. Huguen
Thesis Co-advisor



Timothy I. Eglinton
Thesis Co-advisor

Accepted by



Timothy I. Eglinton
Chair, Joint Committee in Chemical Oceanography
Woods Hole Oceanographic Institution

THE TEMPORAL DYNAMICS OF TERRESTRIAL ORGANIC MATTER TRANSFER TO THE OCEANS: INITIAL ASSESSMENT AND APPLICATION

By

Nicholas J. Drenzek

Submitted to the MIT/WHOI Joint Program in Oceanography on May 11, 2007, in partial fulfillment of the requirements for the degree of Doctor of Philosophy in the field of Marine Chemistry

THESIS ABSTRACT

This thesis employs compound-specific stable carbon and radiocarbon isotopic analysis of organic biomarkers to (a) resolve petrogenic from pre-aged vascular plant organic carbon (OC) in continental margin sediments, (b) investigate the underlying mechanisms controlling the anomalously old ages that are often observed for the terrestrial component of sedimentary OC, and (c) address the associated consequences for biomarker-based climate reconstructions. In Chapters 2 and 3, coupled molecular isotope mass balances demonstrate that the amount of petrogenic OC residing on the Beaufort Shelf (Arctic Ocean) and the Eel River Margin (coastal California) has been previously overestimated due to the presence of significantly 'pre-aged' terrestrial OC. However, even though the contribution of organic matter emanating from sedimentary rocks may be smaller, these results reinforce the emerging notion that it is not completely oxidized during weathering and subsequent seaward transport. In Chapter 4, comparison of the down-core radiocarbon profiles for certain vascular plant biomarkers extracted from Cariaco Basin (Caribbean Sea) and Saanich Inlet (coastal British Columbia) sediments with the radiocarbon evolution of atmospheric carbon dioxide reveals that the vast majority of the terrestrial OC experiences multi-millennial residence times on land prior to entering the sea. Most of the remaining inventory is deposited in sediments within one or two decades, providing direct evidence that very little terrestrial organic matter is rapidly transferred to the marine environment. With this in mind, the striking modulation in the signal amplitude of a biomarker-based tropical paleoaridity record presented in Chapter 5 was instead used to evaluate the role of low versus high latitude forcing in abrupt paleoclimate oscillations during the last full glacial cycle. Seasonal variations in the position of the Intertropical Convergence Zone were interpreted to be a response to both high latitude adjustments in meridional overturning circulation and precessionally-driven modifications in local insolation. Finally, Chapter 6 addresses the broader implications of multi-millennial terrestrial residence times for paleoclimate records based on vascular plant biomarkers.

ACKNOWLEDGEMENTS

How does one condense six years of grad school (and, somewhat synonymously, life) into a few paragraphs? For starters, I've been profoundly lucky to have two amazing advisors guide me through the experience. Konrad Huguen was a veritable fountain of energy and scientific curiosity; Tim Eglinton supplied interminable patience, much-appreciated humor, and (along with his wife Lorraine) the best Indian fare in town. Both allowed me to pursue my rather diverse interests, and somehow managed to provide an endless stream of money to fund the (seemingly) equally endless succession of analyses/conferences/cruises that went along with it. Many thanks also go to Ed Boyle, the oracle of all things Earth science. His contributions to this thesis as a member of my committee were invaluable. And then there's Daniel Montluçon, effectively my third advisor, dear friend, and most would say my natural foil. I learned practically everything I know about how things work both in the laboratory and at sea from him. As one of my esteemed predecessors once observed, Daniel, Matt Makou, Gesine Mollenhauer, Enno Schefuß, Ana Lima, Jeomshik Hwang, Jens Holtvoeth, Angie Dickens, James Saenz, Nao Ohkouchi, Ann Pearson, Alison Olcott, and honorary Eglinton Empire members Li Xu and Pascale Poussart made Fye 111 much more like home than a mere place of work.

I've also been blessed to make some of the best friends on the planet during my time here. Matt Makou and I laughed, cried, and griped together as housemates and lab mates. I'll always admire his ability to find humor in everything and offense in nothing. Paul Craddock is a small Brit with a bit heart, not to mention a mean pool game. Together we went through some of the best (and occasionally worst) bottles of wine out there, all while simultaneously going through our pay checks. Rachel Wisniewski (aka Sushi) and I commiserated about life and love over many a trailer tirade, walk, coffee run, and cocktail. Rachel Stanley is one of the sweetest, most sincere people I've ever met. Rachel, you're truly lit from within. Linda Kalnejais was my swimming buddy and (thus not surprisingly) one of my closest confidants through thick and thin. To Eoghan 'the torch is passed' Reeves and Laura Hmelo – long live Fye After Dark! Desiree Plata and I think so much alike (well, except for politics) that it's scary, but that's nurtured a dearly treasured friendship. Rose Came, Kristy Dahl, Dreux Chappell, Jeff Standish, Cara Santelli, Margaret Boettcher, Nathalie Goodkin, Mea Cook, Emily Peacock (and Rose), Sharon Hoffman, Mary Lardie, Casey Saenger, and Louisa Morrison also made my time in Woods Hole so very memorable. More thanks are owed to Linda, Margaret, Cara, Paul, Eric, Sheean, Andy, Sarah, Heather, Dreux, Enno, Jens, Greg, and past and present members of School St. (my alma mater) and Millfield for all those swingin' parties over the years. What a blast we had!

I'm indebted to Chanda Bertrand, Marley Bice, Alex Sessions, Ellen Druffel, John Southon, Guaciara dos Santos, Ellen Roosen, Margaret Sulanowska, Li Xu, and the staff at NOSAMS and KCCAMS for all the help at various points; this thesis benefited greatly from their involvement. Marsha Gomes, Julia Westwater, Judy McDowell, and Christine Charette made the Academic Programs Office a wonderful place to visit and

provided much of the heart and soul of the Joint Program. Sheila Clifford, Donna Mortimer, Lauren Ledwell, Mary Zawoysky, and Alla Skorokhod are all also thanked for the many ways in which they made life easier for me (and everyone else) every single day.

To my close family – Mom, Dad, Tony, Bachie Lizak and Bachie Drenzek: Without your support, none of this would have been possible. This thesis is dedicated to my late grandfather, James Lizak, “Dziadzi”. We lost him suddenly a few months after I started grad school, but not before he imprinted the qualities that made him so beloved into our minds and hearts.

The scientific analyses described herein were funded by the National Science Foundation through grants OCE-9907129 (T.I.E.), OCE-052626800 (T.I.E.), OCE-0137005 (T.I.E. and K.A.H.), DEB-0447281 (K.A.H.), and the Stanley Watson Chair for Excellence in Oceanography (T.I.E.). N.J.D.’s tuition and stipend were supported by the graduate fellowships from the Stanley Watson Foundation, Schlanger Ocean Drilling Program, and Environmental Protection Agency’s Science to Achieve Results (STAR) Program, as well as by the WHOI Academic Programs Office.

TABLE OF CONTENTS

ABSTRACT	3
ACKNOWLEDGEMENTS	5
TABLE OF CONTENTS	7
TABLE OF FIGURES	9
TABLE OF TABLES	11
 CHAPTER 1 – GENERAL INTRODUCTION	 13
 CHAPTER 2 – CONSTRAINTS ON THE ORIGIN OF SEDIMENTARY ORGANIC CARBON IN THE BEAUFORT SEA FROM COUPLED MOLECULAR ^{13}C AND ^{14}C MEASUREMENTS	 19
ABSTRACT	19
2.0 INTRODUCTION	21
2.1 METHODS	27
2.1.1 LIPID EXTRACTION & ISOLATION	27
2.1.2 DEMINERALIZATION AND OFFLINE PYROLYSIS	30
2.1.3 PYROLYSIS – GAS CHROMATOGRAPHY	32
2.1.4 COMPOUND-SPECIFIC $\delta^{13}\text{C}$ AND $\Delta^{14}\text{C}$ MEASUREMENTS	32
2.2 RESULTS & DISCUSSION	34
2.2.1 BULK CHARACTERISTICS	34
2.2.2 MOLECULAR DISTRIBUTIONS	35
2.2.3 MOLECULAR ISOTOPIC COMPOSITIONS	38
2.2.4 A QUALITATIVE VIEW OF OC CYCLING	44
2.2.5 COUPLED ISOTOPE MASS BALANCE CALCULATIONS	47
2.3 CONCLUSIONS	56
ACKNOWLEDGEMENTS	57
REFERENCES	58
 CHAPTER 3 – APPLICATION OF THE COUPLED MOLECULAR ISOTOPE APPROACH TO A NON-STEADY STATE SYSTEM: THE EEL RIVER MARGIN	 65
ABSTRACT	65
3.0 INTRODUCTION	67
3.1 METHODS	71
3.2 RESULTS & DISCUSSION	73
3.2.1 CHRONOLOGY DEVELOPMENT	73
3.2.2 ELEMENTAL AND ISOTOPIC PROFILES	77
3.2.3 MASS BALANCE CALCULATIONS	80
3.3 CONCLUSIONS	83
ACKNOWLEDGEMENTS	84
REFERENCES	85

CHAPTER 4 – TEMPORAL CONSTRAINTS ON THE DELIVERY OF TERRESTRIAL BIOMARKERS TO MARINE SEDIMENTS	89
ABSTRACT	89
4.0 INTRODUCTION	91
4.1 METHODS	99
4.1.1 SAMPLE RECOVERY	99
4.1.2 CHRONOLOGY DEVELOPMENT	101
4.1.3 BULK ELEMENTAL AND ISOTOPIC ANALYSIS	102
4.1.4 FATTY ACID ISOLATION	102
4.1.5 COMPOUND-SPECIFIC $\delta^{13}\text{C}$ ANALYSIS	106
4.1.6 COMPOUND-SPECIFIC $\Delta^{14}\text{C}$ ANALYSIS	106
4.2 RESULTS & DISCUSSION	109
4.2.1 BULK ELEMENTAL AND ISOTOPIC DISTRIBUTIONS	109
4.2.2 MOLECULAR DISTRIBUTIONS AND ISOTOPIC SIGNATURES	112
4.2.3 QUANTITATIVE MODEL DEVELOPMENT AND APPLICATION	123
4.3 CONCLUSIONS	133
ACKNOWLEDGEMENTS	135
REFERENCES	136
CHAPTER 5 – ATLANTIC INTERTROPICAL CONVERGENCE ZONE VARIABILITY OVER THE LAST FULL GLACIAL CYCLE	147
ABSTRACT	147
5.0 INTRODUCTION	148
5.1 METHODS	160
5.1.1 FATTY ACID EXTRACTION AND ISOLATION	160
5.1.2 COMPOUND-SPECIFIC ISOTOPE ANALYSIS	161
5.1.3 CHRONOLOGY DEVELOPMENT	162
5.2 RESULTS & DISCUSSION	165
5.2.1 STABLE CARBON ISOTOPE RECORD	165
5.2.2 DEUTERIUM ISOTOPE RECORD	171
5.2.3 CLIMATE IMPLICATIONS	173
5.3 CONCLUSIONS	182
ACKNOWLEDGEMENTS	184
REFERENCES	185
CHAPTER 6 – CONCLUSIONS AND THOUGHTS ON FUTURE RESEARCH DIRECTIONS	195
APPENDICES	201

TABLE OF FIGURES

CHAPTER 2

FIGURE 2.1 – MAP OF THE BEAUFORT SHELF

FIGURE 2.2 – BULK ELEMENTAL MEASUREMENTS OF BEAUFORT SHELF SEDIMENTS

FIGURE 2.3 – PYROLYSIS GC CHROMATOGRAM FOR BEAUFORT STATION 5

FIGURE 2.4 – FATTY ACID & ALKANE ABUNDANCES FOR ALL BEAUFORT SHELF STATIONS

FIGURE 2.5 – COMPOUND-SPECIFIC $\delta^{13}\text{C}$ COMPOSITIONS AND ^{14}C AGES OF BEAUFORT SHELF FATTY ACIDS

FIGURE 2.6 – COMPOUND-SPECIFIC $\delta^{13}\text{C}$ COMPOSITIONS AND ^{14}C AGES OF BEAUFORT SHELF EXTRACTABLE ALKANES

FIGURE 2.7 – COMPOUND-SPECIFIC $\delta^{13}\text{C}$ COMPOSITIONS AND ^{14}C AGES OF BEAUFORT SHELF PYROLYSATE ALKANES

FIGURE 2.8 – COUPLED MOLECULAR ISOTOPE MASS BALANCE RESULTS FOR BEAUFORT SEDIMENTS

CHAPTER 3

FIGURE 3.1 – MAP OF THE EEL RIVER MARGIN

FIGURE 3.2 – PHOTOGRAPH OF GGC 5

FIGURE 3.3 – CHRONOLOGY DEVELOPMENT FOR GGC 5 AND MC 36

FIGURE 3.4 – DOWN-CORE PROFILES OF VARIOUS BULK AND MOLECULAR PARAMETERS IN GGC 5

FIGURE 3.5 – FATTY ACID ABUNDANCES FOR GGC 5

FIGURE 3.6 – COMPOUND-SPECIFIC $\delta^{13}\text{C}$ COMPOSITIONS OF GGC 5 FATTY ACIDS

FIGURE 3.7 – COUPLED MOLECULAR ISOTOPE MASS BALANCE RESULTS FOR EEL RIVER MARGIN SEDIMENTS

CHAPTER 4

FIGURE 4.1 – SCHEMATIC DIAGRAM OF THE GLOBAL CARBON CYCLE

FIGURE 4.2 – MAP OF THE CARIACO BASIN AND SAANICH INLET

FIGURE 4.3 – CHRONOLOGY DEVELOPMENT FOR CARIACO SEDIMENTS

FIGURE 4.4 – CHRONOLOGY DEVELOPMENT FOR SAANICH SEDIMENTS

FIGURE 4.5 – DOWN-CORE PROFILES OF VARIOUS BULK AND MOLECULAR PARAMETERS IN CARIACO SEDIMENTS

FIGURE 4.6 – DOWN-CORE PROFILES OF VARIOUS BULK AND MOLECULAR PARAMETERS IN CARIACO SEDIMENTS

FIGURE 4.7 – CROSS PLOT OF CARIACO AND SAANICH BULK $\delta^{13}\text{C}$ VERSUS TOC/TN

FIGURE 4.8 – FATTY ACID ABUNDANCES FOR CARIACO SEDIMENTS

FIGURE 4.9 – FATTY ACID ABUNDANCES FOR SAANICH SEDIMENTS

- FIGURE 4.10 – COMPOUND-SPECIFIC $\delta^{13}\text{C}$ COMPOSITIONS OF CARIACO AND SAANICH FATTY ACIDS
- FIGURE 4.11 – $\delta^{13}\text{C}$ AND $\Delta^{14}\text{C}$ PROFILES OF CARIACO AND SAANICH DIC
- FIGURE 4.12 – COMPOUND-SPECIFIC $\Delta^{14}\text{C}$ PROFILES OF CARIACO AND SAANICH FATTY ACIDS AND TOC ALONG WITH THE $\Delta^{14}\text{C}$ HISTORY OF ATMOSPHERIC CO_2
- FIGURE 4.13 – BEST-FIT MODEL CURVES TO COMPOUND-SPECIFIC $\Delta^{14}\text{C}$ PROFILES OF CARIACO AND SAANICH FATTY ACIDS

CHAPTER 5

- FIGURE 5.1 – AVERAGE WINTER AND SUMMER PRECIPITATION ESTIMATES FOR SOUTH AMERICA
- FIGURE 5.2 – C_3 VS C_4 VEGETATION MAP FOR NORTHERN SOUTH AMERICA
- FIGURE 5.3 – CHRONOLOGY DEVELOPMENT FOR ODP CORE 1002D
- FIGURE 5.4 – AGE VS DEPTH RELATIONSHIP FOR ODP CORE 1002D
- FIGURE 5.5 – CROSS PLOT OF THE COMPOUND-SPECIFIC $\delta^{13}\text{C}$ AND δD COMPOSITIONS OF LONG CHAIN FATTY ACIDS FROM ODP CORE 1002D
- FIGURE 5.6 – COMPOUND-SPECIFIC $\delta^{13}\text{C}$ AND δD RECORDS FROM THE CARIACO BASIN PLOTTED ALONGSIDE GISP2 $\delta^{18}\text{O}$ AND 10°N NOVEMBER INSOLATION FOR THE PAST 180 KYR
- FIGURE 5.7 – COMPOUND-SPECIFIC $\delta^{13}\text{C}$ AND SEDIMENT REFLECTANCE RECORDS FROM THE CARIACO BASIN PLOTTED ALONGSIDE GISP2 $\delta^{18}\text{O}$ FOR 10 – 75 KYR
- FIGURE 5.8 – SPECTRAL ANALYSIS OF THE COMPOUND-SPECIFIC $\delta^{13}\text{C}$ RECORD FROM THE CARIACO BASIN

CHAPTER 6

- FIGURE 6.1 – CARIACO 1002D $\delta^{13}\text{C}$ RECORD PASSED THROUGH RESIDENCE TIME BOX MODEL

TABLE OF TABLES

CHAPTER 2

TABLE 2.1 – BULK GEOCHEMICAL PARAMETERS FOR BEAUFORT SHELF SEDIMENTS

CHAPTER 4

TABLE 4.1 – BEST-FIT SOLUTIONS TO BIOMARKER TERRESTRIAL RESIDENCE TIME MODEL
VARIABLES

CHAPTER 1

GENERAL INTRODUCTION

Ten years ago, Hedges et al. (1997) posed the question, “What happens to terrestrial organic matter in the ocean?” in a seminal review of the subject. These authors highlighted the ‘geochemical conundrum’ that although rivers supply enough dissolved and particulate organic carbon (DOC and POC, respectively) to the ocean on an annual basis to account for the turnover of all of the DOC in its waters and the POC accumulating in underlying sediments, little (< 10 %) of this terrigenous material is actually found there (e.g. Schlunz and Schneider, 2000). Although Burdige (2005) recently re-examined this problem and concluded that the discrepancy might not be so severe, it is still clear that the large majority of terrigenous OC does not escape remineralization upon entry into the marine environment. The mechanism(s) allowing some component to persist while the majority succumb to diagenetic attack, and the associated consequences for the global cycles of carbon and oxygen (Berner, 1989; Crowley, 1995; Petsch, 2003), remain relatively ill-understood. An array of explanatory hypotheses have nonetheless been advanced including structure and composition (Hedges, 1992), oxygen exposure time (Hedges and Keil, 1995), photochemistry (Miller and Zepp, 1995), and mineral protection (Hedges and Keil, 1995; Keil et al., 1997). The inherent age of terrigenous OC has the potential to influence all of these parameters. For example, the old radiocarbon (^{14}C) ages of certain fluvial DOC and POC fractions

(Raymond and Bauer, 2001) may reflect pre-aging of vascular plant detritus in various continental reservoirs such as soils, wetlands, and freshwater sediments, where both biological and abiotic processes can alter the chemical composition of that detritus and potentially increase its association with inorganic mineral grains. Such old ages might also (at least partially) reflect the presence of petrogenic (or ‘fossil’) material weathered from ancient OC-rich sedimentary rocks (shales) that has resisted complete destruction by diagenetic and catagenetic forces for millions of years (Di-Giovanni et al., 2002). In this context, the age of terrigenous (vascular plant + petrogenic) OC can be considered something of a master variable controlling its fate upon introduction to the marine environment.

Bulk level isotopic investigations, however, afford little resolution of these parameters. Fortuitously though, Hedges et al.’s review coincided with the initial $\Delta^{14}\text{C}$ measurements of individual lipid biomarkers isolated from marine sediments by preparative capillary gas chromatography (PCGC) (Eglinton et al., 1997). A suite of additional analyses in the ensuing decade targeting compounds thought to derive from vascular plants (Pearson, 1999; Uchida et al., 2000, 2001, 2005; Pearson et al., 2001; Ohkouchi et al., 2003) have reinforced the notion that this material is significantly pre-aged on land, probably in an array of multi-annual to multi-millennial pools, before delivery to the ocean. These observations not only suggest that such ‘terrestrial residence times’ may influence the preservation of vascular plant OC in marine sediments, but also imply that biomarker-based investigations of both the contemporary and paleo carbon cycle (Meyers, 1997; Pancost and Boot, 2004) encumber temporal offsets. Both of these

effects are likely sensitive to the proportion of terrestrial material sequestered in relatively short (annual to centennial) versus relatively long (multi-millennial) reservoirs, but until now there were few quantitative constraints on the importance of these reservoirs in relation to one other or to a petrogenic endmember.

The overall goals of this thesis are therefore to (a) develop an initial framework in which the ^{14}C age of terrigenous OC can be more quantitatively expressed in terms of several pre-aged terrestrial constituents and a truly fossil component [Chapters 2 – 4], and (b) address the consequences of these findings for terrestrial biomarker-based climate reconstructions [Chapters 5 – 6]. Unbound fatty acids and alkanes are almost exclusively employed as biomarkers of choice in these studies because they are (a) often highly abundant in marine sediments, thus affording sufficient mass for compound-specific radiocarbon analysis (CSRA) at fairly fine down-core resolution, (b) relatively easily extracted and isolated for isotope analysis, and (c) contain information about different sources within the same homologues series. With this in mind, Chapter 2 introduces the concept of a coupled molecular isotope ($\delta^{13}\text{C}$, $\Delta^{14}\text{C}$) approach to sedimentary OC source apportionment and demonstrates its utility in the climatically-sensitive Beaufort Sea (Arctic Ocean). Chapter 3 then applies this approach to develop a more robust budget of pre-aged terrestrial vs. petrogenic OC buried on the Eel River Margin (California), a site thought to be representative of many small mountainous river/shelf systems world-wide. Chapter 4 relates down-core $\Delta^{14}\text{C}$ profiles developed for several long chain fatty acid homologues from the Cariaco Basin (Caribbean) and Saanich Inlet (British Columbia) to that of atmospheric CO_2 in an effort to further resolve the terrestrial component into those

delivered on annual, decadal, and millennial timescales. Chapter 5 presents a high resolution, biomarker-based record of aridity in northern South America over the last ~ 180,000 years, and in light of the results from Chapter 4, introduces a new approach to evaluate the role of the tropics in abrupt climate change. Finally, Chapter 6 summarizes the main conclusions of the thesis and offers some perspectives on future research avenues.

REFERENCES

- Berner, R.A., 1989. Biogeochemical cycles of carbon and sulfur and their effect on atmospheric oxygen over Phanerozoic time. *Palaeogeography Palaeoclimatology Palaeoecology*, 73: 97-122.
- Burdige, D.J., 2005. Burial of terrestrial organic matter in marine sediments: A reassessment. *Global Biogeochemical Cycles*, 19: doi: 10.1029/2004GB002368.
- Crowley, T.J., 1995. Ice age terrestrial carbon changes revisited. *Global Biogeochemical Cycles*, 9: 377-389.
- Di-Giovanni, C., Disnar, J.R., Macaire, J.J., 2002. Estimation of the annual yield of organic carbon released from carbonates and shales by chemical weathering. *Global and Planetary Change*, 32: 195-210.
- Eglinton, T.I., Benitez-Nelson, B.C., Pearson, A., McNichol, A.P., Bauer, J.E., Druffel, E.R.M., 1997. Variability in radiocarbon ages of individual organic compounds from marine sediments. *Science*, 277: 796-799.
- Hedges, J.I., 1992. Global biogeochemical cycles: progress and problems. *Marine Chemistry*, 39: 67-93.
- Hedges, J.I., Keil, R.G., 1995. Sedimentary organic matter preservation: An assessment and speculative synthesis. *Marine Chemistry*, 49: 81-115.
- Hedges, J.I., Keil, R.G., Benner, R., 1997. What happens to terrestrial organic matter in the ocean? *Organic Geochemistry*, 27: 195-212.
- Keil, R.G., Mayer, L.M., Quay, P.D., Richey, J.E., Hedges, J.I., 1997. Loss of organic matter from riverine particles in deltas. *Geochimica et Cosmochimica Acta*, 61: 1507-1511.
- Meyers, P.A., 1997. Organic geochemical proxies of paleoceanographic, paleolimnologic, and paleoclimatic processes. *Organic Geochemistry*, 27: 213-250.
- Miller, W.J., Zepp, R.G., 1995. Photochemical production of dissolved inorganic carbon from terrestrial organic matter: Significance to the oceanic coastal organic carbon cycle. *Geophysical Research Letters*, 22: 417-420.
- Ohkouchi, N., Eglinton, T.I., Hayes, J.M., 2003. Radiocarbon dating of individual fatty acids as a tool for refining Antarctic margin sediment chronologies. *Radiocarbon*, 45: 17-24.
- Pancost, R.D., Boot, C.S., 2004. The paleoclimate utility of terrestrial biomarkers in marine sediments. *Marine Chemistry*, 92: 239-261.
- Pearson, A., 1999. Biogeochemical applications of compound-specific radiocarbon analysis. Ph.D. Thesis, MIT/WHOI Joint Program, Woods Hole, MA.
- Pearson, A., McNichol, A.P., Benitez-Nelson, B.C., Hayes, J.M., Eglinton, T.I., 2001. Origins of lipid biomarkers in Santa Monica Basin surface sediments: A case study using compound-specific $\Delta^{14}\text{C}$ analysis. *Geochimica et Cosmochimica Acta*, 65: 3123-3137.
- Petsch, S.T., 2003. The global oxygen cycle. In: *Treatise on Geochemistry, Vol 8*, H.D. Holland and K.K. Turekian (eds): 515-555.

Raymond, P.A., Bauer, J.E., 2001. Use of ^{14}C and ^{13}C natural abundances for evaluating riverine, estuarine, and coastal DOC and POC sources and cycling: A review and synthesis. *Organic geochemistry*, 32: 469-485.

Schlünz, B., Schneider, R.R., 2000. Transport of terrestrial organic carbon to the oceans by rivers: Re-estimating flux and burial rates. *International Journal of Earth Sciences*, 88: 599-606.

Uchida, M., Shibata, Y., Kawamura, K., Kumamoto, Y., Yoneda, M., Ohkushi, K., Harada, N., Hirota, M., Mukai, H., Tanaka, A., Kusakabe, M., Morita, M., 2001. Compound-specific radiocarbon ages of fatty acids in marine sediments from the western North Pacific. *Radiocarbon*, 43: 949-956.

Uchida, M., Shibata, Y., Kawamura, K., Yoneda, M., Mukai, H., Tanaka, A., Uehiro, T., Morita, M., 2000. Isolation of individual fatty acids in sediments using preparative capillary gas chromatography (PCGC) for radiocarbon analysis at NIES-TERRA. *Nuclear Instruments and Methods in Physics Research B*, 172: 583-588.

Uchida, M., Shibata, Y., Ohkushi, K., Yoneda, M., Kawamura, K., Morita, M., 2005. Age discrepancy between molecular biomarkers and calcareous foraminifera isolated from the same sediment horizons of Northwest Pacific sediments. *Chemical Geology*, 218: 73-89.

CHAPTER 2

This manuscript was previously published in:
Marine Chemistry (2007), vol. 103, pp 146-162
It is reprinted here with permission of the publisher.

CONSTRAINTS ON THE ORIGIN OF SEDIMENTARY ORGANIC CARBON IN THE BEAUFORT SEA FROM COUPLED MOLECULAR ^{13}C AND ^{14}C MEASUREMENTS

Nicholas J. Drenzek^{a*}, Daniel B. Montluçon^a, Mark B. Yunker^b, Robie W. Macdonald^c,
and Timothy I. Eglinton^a

^aDepartment of Marine Chemistry and Geochemistry, Woods Hole Oceanographic Institution, Woods Hole,
MA, USA

^b7137 Wallace Dr., Brentwood Bay, BC, Canada

^cDepartment of Fisheries and Oceans, Institute of Ocean Sciences, Sidney, BC, Canada

ABSTRACT

The type and flux of organic carbon (OC) delivered from the continents to the sea can both influence, and be influenced by, climate change on regional and global scales. In order to develop a more complete view of OC delivery in the climatically sensitive Arctic region, we measured the stable carbon and radiocarbon isotopic signatures of individual lipid biomarkers and products of kerogen pyrolysis from the surficial sediments of several sites on the Mackenzie Shelf and adjacent slope of the Beaufort Sea. Even carbon number fatty acids exhibit a trend of increasing ^{14}C age with increasing chain length, from 'modern' values for the $n\text{C}_{14}$ – $n\text{C}_{18}$ homologues to several thousand

years old for those $\geq nC_{24}$. Such depleted ^{14}C values for longer-chain fatty acids likely reflect supply of vascular plant OC that has been ‘pre-aged’ on the continents for several millennia prior to delivery to the Beaufort Sea. Their corresponding $\delta^{13}C$ values support a C_3 land plant source. The molecular distributions and ^{14}C and ^{13}C signatures of solvent-extractable alkanes point to at least two sources: higher plant leaf waxes and a ^{14}C -‘dead’ component likely derived from erosion of organic-rich sedimentary rocks exposed within the Mackenzie River drainage basin. The $\delta^{13}C$ and $\Delta^{14}C$ values of straight chain n -hydrocarbon pyrolysis products from the corresponding demineralized sediments also suggest a mixed supply of ancient kerogen and pre-aged vascular plant-derived precursors to the Beaufort Sea. On a bulk level, the trend in sedimentary OC contents, C/N ratios, and $\delta^{13}C$ values point to an overall decrease in the terrigenous input (mainly from the Mackenzie river) with increasing distance offshore, whereas bulk $\Delta^{14}C$ measurements exhibit no trend suggesting a somewhat constant pre-aged component.

A dual molecular isotopic mass balance approach based on the lipid $\delta^{13}C$ and $\Delta^{14}C$ signatures is used to construct a budget of terrestrial, marine, and petrogenic OC burial on the shelf. Results indicate that roughly 40-50% of the carbon currently being buried in the Beaufort Sea is derived from the weathering of ancient sedimentary rock. The balance is composed of marine and terrestrial input, supporting the qualitative description of OC sources given by the bulk and molecular patterns above. This suggests that mass balances utilizing the $\delta^{13}C$ and $\Delta^{14}C$ signatures of biomarkers as endmembers can be used to semi-quantitatively deconvolve multiple sources of organic carbon in marine sediments.

2.0 INTRODUCTION

The flux of organic carbon (OC) to marine sediments includes autochthonous contributions from primary production in overlying waters as well as allochthonous inputs from terrigenous sources such as vascular plants, soils, ancient sedimentary rocks (shales), and anthropogenic contaminants (Hedges et al., 1997). The relative proportion of these carbon pools dictates the composition and burial efficiency of OC in sediments and influences the atmospheric oxidation state on geologic timescales (Bernier, 1989; Petsch, 2003). Many studies, therefore, have aimed to quantify these components in rivers and on continental shelves using bulk characteristics such as %OC, C/N ratios, $\delta^{13}\text{C}$, and $\Delta^{14}\text{C}$ (e.g. Megens et al., 2001; Raymond and Bauer, 2001, and references therein) as well as the distributions and stable carbon isotopic compositions of source-specific biomarkers (e.g. Prahl et al., 1994; Yunker et al., 1995; Goñi et al., 1998, 2000; Belika et al., 2002; Yunker et al., 2005). Within this framework, isotopic mass balance calculations used to assess the fractional abundance of modern and ancient OC (Blair et al., 2003, 2004; Goñi et al., 2005) indicate that fully 50% or more of the total carbon preserved in some recent river-dominated shelf sediments is not of recent origin, but instead originates from ‘pre-aged’ continental reservoirs such as soils (Masiello and Druffel, 2001; Rethemeyer et al., 2004a,b) and wetlands (Trumbore et al., 1999), or ‘petrogenic’ fossil sources liberated upon sedimentary rock weathering (Di-Giovanni et al., 2002). These pools of reduced carbon are presumably highly refractory and therefore, once mobilized from continental reservoirs, have been hypothesized to escape extensive remineralization in the marine water column and underlying sediments.

However, isotopic mass balances utilizing bulk $\Delta^{14}\text{C}$ and $\delta^{13}\text{C}$ measurements in sediments cannot alone independently discriminate between pre-aged terrestrial, petrogenic, and marine OC since the stable and radiocarbon signatures of terrestrial OC often lie in between the latter two ($\Delta^{14}\text{C} \sim -1000$ ‰, $\delta^{13}\text{C} = -24$ to -30 ‰ and $\Delta^{14}\text{C} \sim 0$ ‰, $\delta^{13}\text{C} = -14$ to -20 ‰ respectively). In particular, distinguishing and quantifying pre-aged terrestrial OC of vascular plant origin and ancient OC from rock erosion can be particularly difficult because each may be depleted in both ^{14}C and ^{13}C . Nevertheless, distinguishing between vascular plant and shale OC is extremely important since the very different rates at which OC cycles through these reservoirs impacts global biogeochemical cycles (Hedges and Oades, 1997). The isotopic compositions of all three endmembers are thus either assumed (Goñi et al., 2005), inferred from their spatial trends (Blair et al., 2003), or measured on samples taken from the source rock itself (Komada et al., 2004).

This problem may be more directly addressed by measuring both the ^{14}C and ^{13}C content of individual biomarkers specific to each of these endmembers. The source specificity of these compounds avoids the need for assumptions or ancillary sample collections outside of the sediment in which they are contained, and allows for direct determination of signatures which have the potential to vary during delivery to, and subsequent deposition (and re-deposition) over, the seafloor. Such coupled molecular $\delta^{13}\text{C}$ and $\Delta^{14}\text{C}$ measurements have been previously used to establish the provenance of natural and anthropogenic compounds in sediments (Eglinton et al., 1997; Pearson and Eglinton, 2000; Pearson et al., 2001), freshwaters, groundwaters, and soils on the

continents (Schiff et al., 1997; Agnelli et al., 2002), aerosols (Matsumoto et al., 2001; Eglinton et al., 2002), and the marine water column (Guo et al., 1996). These signatures can also be used to solve a set of simultaneous isotopic mass balance expressions to yield the fractional abundances of the OC sources they represent. Since the provenance of organic matter contained within continental shelf sediments has been traditionally cited as one of the features controlling its ability to survive early diagenesis (Hedges et al., 1997), this approach provides a useful window into the factors controlling the composition and sequestration of organic matter in marine sediments.

The Arctic Ocean contains 20% of the world's continental shelf area (Macdonald et al., 1998) and receives input from many major and minor rivers whose collective drainage area contains half of the global soil carbon inventory (Dixon et al., 1994). The Mackenzie River is the largest fluvial source of both sediment and particulate organic carbon (POC) to the Arctic Ocean at about $125 \times 10^9 \text{ kg yr}^{-1}$ and $2.1 \times 10^9 \text{ kg yr}^{-1}$ respectively, with approximately 60% of this POC subsequently buried in the sediments of its delta and the adjacent Mackenzie Shelf (Macdonald et al., 1998, 2004; Rachold et al., 2004). Most of this flux (~90%) is associated with the spring/summer freshet, a period from May through September when ~70% of the annual freshwater discharge ($3.3 \times 10^{11} \text{ m}^3$) occurs (Macdonald et al., 1998). The Mackenzie River drainage basin spans the western alpine region of the Cordillera Mountains to the Canadian Shield and includes forests, swamps, grasslands, and permafrost soils interspaced with numerous lakes, smaller streams, and wetlands. The Mackenzie River thus effectively integrates an array of OC sources including those eroding from sedimentary rock, fixed by land plants,

sequestered in soils, produced by algae, and recycled through bacteria. Immature bitumens, shales, or coals from the Devonian Canol formation that outcrop into the lower Mackenzie River valley have been established as the most likely source of petrogenic OC to the Beaufort Sea (Yunker et al., 2002). In addition to similarities in petroleum biomarker composition between the Canol and the Mackenzie River, this formation is near-surface and outcrops in high relief areas in the western side of the basin. Some

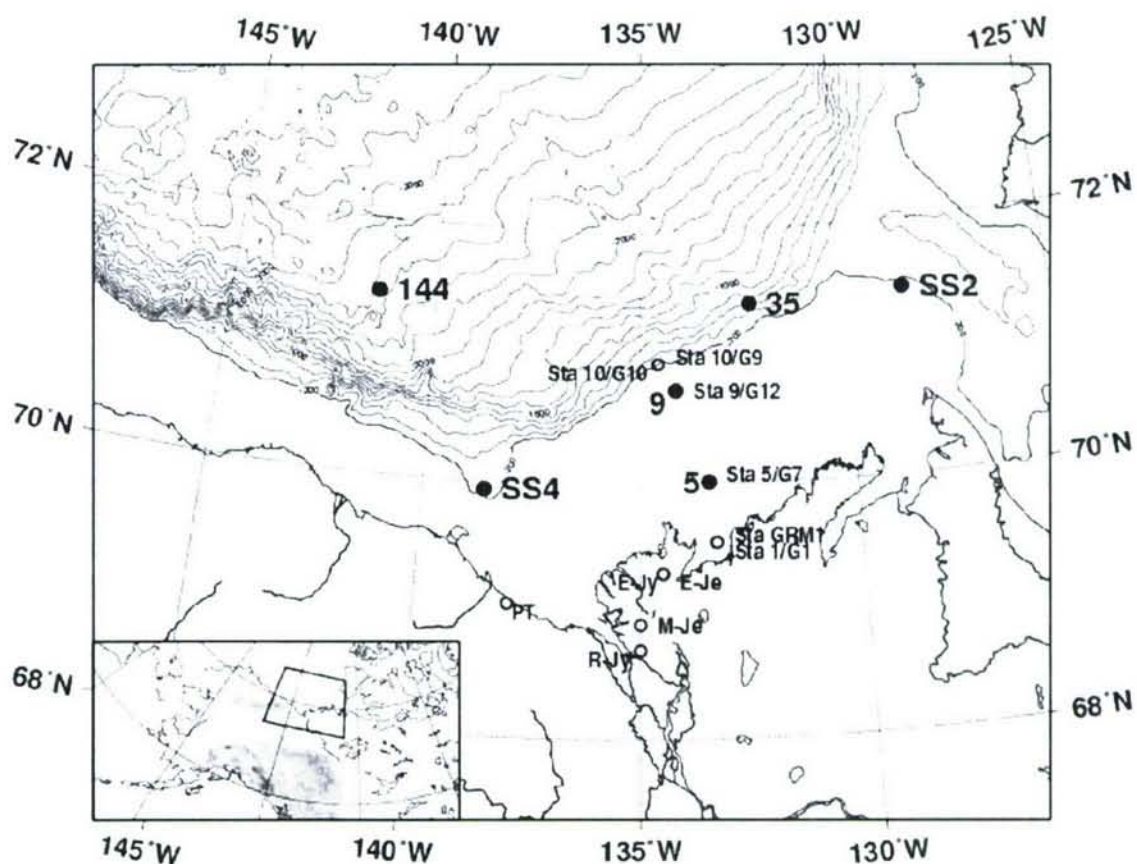


FIGURE 2.1 – Map of the Beaufort Shelf / Slope study area with sample collection sites shown (large black circles). Sediment and Mackenzie River suspended matter collection sites from Goñi et al. (2000) are plotted as small open circles. Isobaths are contoured every 200m.

petrogenic material could also originate from the shales underlying the Canadian Shield to the east (Milot et al., 2003), although small tributary sizes and large headwater lakes (that efficiently trap particles) on the east flank of the river lead Carson et al. (1998) to estimate that these sources supply less than 5% of the sediment delivered to the Mackenzie Delta annually. Nonetheless, significantly old ^{14}C ages of both fluvial POC and sedimentary OC on the shelf suggest that petrogenic OC is actively cycling through this system (Goñi et al., 2005; Table 2.1) likely in the form of refractory hydrocarbons (Yunker et al., 1993, 2002) and kerogen.

Widespread permafrost soils in the Arctic rim have the ability to retain this material, as well as that from terrestrial vegetation, for many millennia. However, recent warming trends in the Arctic (Hassol, 2004) could potentially lead to the retreat of permafrost conditions (Stendel and Christensen, 2002), promoting rapid weathering of the vast reduced carbon archive these soils contain (Goulden et al., 1998; Guo et al., 2004). An increased flux and compositional change of terrigenous OC entering the Beaufort Sea, together with altered aquatic primary production due to change in shelf upwelling and/or nutrient supply by rivers, promises to alter the amount and composition of carbon buried in shelf sediments. Therefore, establishing the current type and rate of OC delivery to Beaufort Sea sediments would provide a benchmark against which climate change in the Arctic may be assessed. The origin of OC and, just as importantly, its rate of transport must therefore be determined in order to fully assess the impact of climate change in the Arctic Ocean. Here we apply a coupled isotopic mass balance to quantify the amount of petrogenic, terrestrial, and marine detrital carbon being delivered

	Station 5/G7*	Station 9/G12*	Station 35	Station SS2	Station SS4	Station 144
Depth (m)	25	61	460	167	255	2650
Latitude	70.017°N	70.737°N	71.408°N	71.462°N	69.935°N	71.433°N
Longitude	133.433°W	134.165°W	132.333°W	128.563°W	138.573°W	141.400°W
<i>Bulk Sediment</i>						
% C	2.16	1.86	1.77	1.63	1.85	1.34
C:N	12.3	9.9	9.6	12.4	10.6	8.1
<i>Carbonate-free</i>						
$\delta^{13}\text{C}$ (‰)	-26.0	-24.9	-24.9	-24.8	-25.4	-23.8
$\Delta^{14}\text{C}$ (‰)	-737.8	-618.6	-726.8	-681.6	-722.1	-725.4
^{14}C Age (yr BP)	10700	7690	10350	9140	10250	10350
% C	1.56	1.44	1.39	1.32	1.43	1.11
C:N	4.7	5.7	4.3	4.8	4.9	4.8
<i>Demineralized</i>						
% C	15.26	17.63				14.74
C:N	15.2	17.0				16.0

*Station designations after Goñi et al., 2000

TABLE 2.1 – Water depths, positions, and isotopic and elemental values for sediment from each site, as well as elemental values for carbonate-free and HF digested sediments.

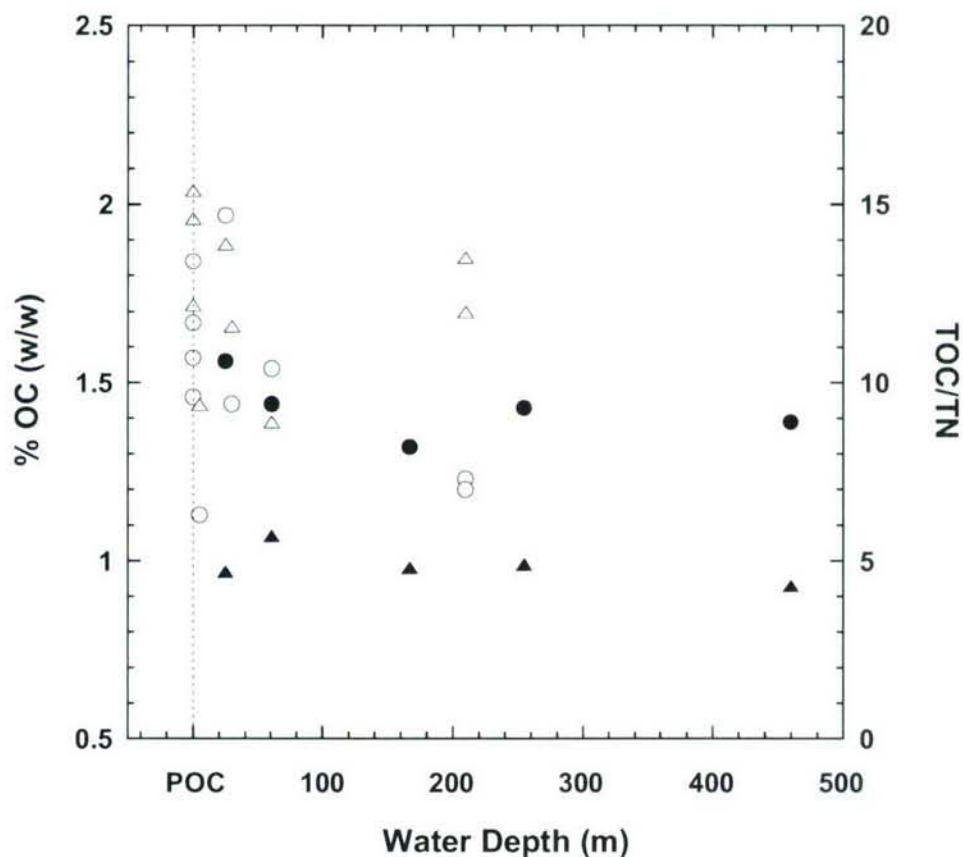
to Beaufort Sea sediments using molecular $\delta^{13}\text{C}$ and $\Delta^{14}\text{C}$ measurements on a subset of their respective lipid components.

2.1 METHODS

2.1.1 Lipid extraction & isolation

Sediments from five sites on the Mackenzie shelf and shelf edge (stations 5, 9, 35, SS2, and SS4; Figure 2.1) were collected in July and August 1987 by a Smith-McIntyre (0.12 m²) grab sampler (Macdonald et al., 1988; Yunker et al., 1993). Sediments from a sixth site near the base of the Beaufort Slope (station 144; Figure 2.1) were collected in September 1991 using a box corer (0.06 m², 50-55 cm length) with a stainless steel liner (Macdonald et al., 1992). Surface sediment (0-2cm) samples were taken from the undisturbed grab samples, while the 4-5 cm interval was used for the core from station 144. Sedimentation rates on the shelf, derived from isopach thickness since glacial retreat, generally range from 10 to 300 cm kyr⁻¹ (Harper and Penland, 1982; Macdonald et al., 1998) but rapidly decrease farther offshore to values of 1 cm kyr⁻¹, and to perhaps as little as 0.1 cm kyr⁻¹ in slope and central basin sediments (Cranston, 1997; Darby et al., 1997; Backman et al., 2004). Although ice scour in shallow regions (< ~30m), bioturbation, and for the Beaufort Slope site, turbidites (Phillips et al., 1991; Grantz et al., 1996) have the potential to expose older sediments or recycle them back up to the surface, radiocarbon analysis of marine biomarkers from the shelf stations (discussed below) imply very recent deposition. Aliquots of each sediment sample were measured for total carbon (TC) and total nitrogen (TN) by high temperature combustion on a Carlo Erba 1108 Elemental Analyzer. Total organic carbon (TOC) was measured by the same

method after carbonate removal by exposure to HCl vapor for 8-10 hours followed by addition of a drop of 2N HCl_(aq) directly onto the sample. If any effervescence was noticed, an additional drop was added after drying overnight. TN cannot be assumed to be equivalent to total organic nitrogen (TON) as a regression of TN vs. TOC exhibits a weak relationship ($r^2 = 0.23$) and has an intercept on the N axis that is equal to approximately 50% of the highest TN value (Appendix 2.1). Therefore, unlike



Ruttenberg and Goñi (1997) and Goñi et al. (2000, 2005) who used a phosphoric acid treatment, the absolute values of the C/N ratios of the carbonate-free sediments at these particular sites cannot be taken as representative of the organic matter they contain. These data and those from Goñi et al. (2005) are compared in Figure 2.2. Bulk OC $\delta^{13}\text{C}$ and $\Delta^{14}\text{C}$ data were acquired at the National Ocean Science Accelerator Mass Spectrometry (NOSAMS) facility at Woods Hole Oceanographic Institution (WHOI).

Remaining sediments (~100 – 400 gdw) were dried and soxhlet extracted for 2 days in 2:1 dichloromethane:methanol to yield their respective total lipid extracts (TLEs). Each TLE was then hydrolyzed by refluxing in 100mL of 0.5M KOH in methanol plus 20mL MilliQ water for three hours. Saponified extracts were transferred to separatory funnels and back extracted with three 25mL aliquots of a 9:1 hexane:dichloromethane solution to yield a neutral fraction (pH ~ 13 to 14). The residual saponified extracts were then reduced to a pH of ~1 by the addition of hydrochloric acid and 125mL of MilliQ water and back extracted with three 25mL aliquots of dichloromethane to yield an acid fraction. Both neutral and acid fractions were subsequently dried over sodium sulfate. The acid fractions were reduced in volume and transesterified overnight at 70°C under N_2 using 20mL of a 5:95 hydrochloric acid:methanol solution of known carbon isotopic composition ($\delta^{13}\text{C} = -47.25 \text{ ‰}$; $\Delta^{14}\text{C} = -997.7 \text{ ‰}$). The resulting fatty acid methyl esters were further purified by elution through silica gel columns (20cm long x 0.5cm in diameter, 1% de-activated) with a 2:1 dichloromethane:hexane eluent, then urea adducted to remove branched components, and finally eluted through silver nitrate (~10% w/w)

impregnated silica gel columns (20 x 0.5cm, fully activated) to provide only the saturated homologues in 1:1 dichloromethane:hexane.

The neutral lipids were separated by silica gel column chromatography (7 x 5cm, fully activated) to yield the non-polar fraction containing the hydrocarbons in hexane. This fraction was then reduced in volume, urea adducted to yield the straight-chain homologues, and analyzed by gas chromatography with flame ionization detection (Hewlett Packard 5890 Series II GC/FID, 60m x 0.32mm i.d. x 0.25 μ m film DB-5 column, H₂ carrier gas) along with the isolated fatty acid methyl esters.

2.1.2 Demineralization and offline pyrolysis

Approximately 100g of the solvent-extracted sediment residues from stations 5, 9, and 144 were loaded into 60mL acid-cleaned Teflon test tubes (~12-15g per tube). Carbonate minerals were removed using three 5mL treatments of 12M HCl, with the tubes being capped, agitated for 1 hour, centrifuged, and decanted of the supernatant after the addition of each aliquot. Silicate minerals were then removed by treating the samples with 10mL of concentrated hydrofluoric acid (50%) and 4mL hydrochloric acid (12M) for 12 hours followed by centrifugation and removal of the supernatant. This process was repeated twice more, after which any remaining hydrofluoric acid was salted out with boric acid and rinsed copiously with water. The remaining (highly OC enriched) matrix was dried and subsampled for elemental measurement, with overall mass losses from mineral removal of 94.7, 95.4, and 96.0% for stations 5, 9, and 144 respectively.

The demineralized material was then ultrasonically re-extracted with dichloromethane, with the insoluble residue then subjected to off-line pyrolysis. Briefly,

approximately 100mg aliquots were loaded into a metal boat and inserted into a quartz tube encased in a programmable ceramic oven. Prior to insertion into the oven, air was purged from the system with helium. During pyrolysis, helium was passed over the sample at a constant rate (20 ml min^{-1}) and exited the oven through a U-tube immersed in liquid nitrogen and terminating in a solvent (dichloromethane) trap. In this way, the pyrolysate effluent was either deposited inside the quartz tube, in the U-trap, or (for the most volatile compounds) in the solvent trap. The oven was heated from ambient temperature to 105°C and held for 5 minutes to remove any residual water, and then ramped rapidly at 20°C/min thereafter, holding at a final temperature of 605°C for 2 minutes before cooling. A batch of approximately 50 aliquots was pyrolyzed per sample. After each reactor cycle, the quartz and U-tubes were rinsed with dichloromethane, hexane, and methanol into separate reservoirs and concentrated once all runs of a given station were complete. Sediment mass loss for a complete experiment averaged 30.7, 28.1, and 27.4% for stations 5, 9, and 144 respectively, indicating that the majority of the organic matter was either thermally refractory or prone to charring. Aliquots of the concentrated pyrolysates were silylated (BSTFA, 70°C for 20 min) and analyzed by GC/FID and GC/MS (Thermo Finnigan Trace GC interfaced to a Tempus time-of-flight mass spectrometer) in order to ascertain their composition. Dichloromethane rinses from both the U-trap and quartz tube contained abundant homologous series of saturated and unsaturated straight chain hydrocarbons superimposed on an array of various other products. Taken together, these fractions resembled online pyrolysis GC traces acquired for the same samples (Figure 2.3, see methodology below). Thus, they were combined

with the solvent trap and eluted through silica gel columns, after which the non-polar fraction was stripped of residual branched components by urea adduction and then eluted through silver nitrate-doped silica gel columns to yield isolated series of both *n*-alkanes (in pentane) and *n*-alkenes (in dichloromethane).

2.1.3 Pyrolysis – gas chromatography

Although such ‘offline’ pyrolytic techniques allow products to be pooled for isotopic analyses, loss of some amounts of these products (especially the more volatile components) is inevitable because of the open nature of the system. It thus becomes advantageous to examine a sample by ‘online’ techniques such as pyrolysis GC as a complementary analytical step. Therefore, demineralized sediment aliquots from stations 5, 9, and 144 were pressed into a 770°C Curie-point wire and inserted into a pyrolysis head attached to a HP 5890 Series II GC equipped with an FID detector and flash pyrolyzed (~0.3 second), with the effluent transferred directly onto an initially cryo-cooled GC column and subsequently separated under a ramping oven program (Figure 2.3).

2.1.4 Compound-specific $\delta^{13}C$ and $\Delta^{14}C$ measurements

The stable carbon isotopic compositions of the solvent-extractable fatty acids and alkanes and the isolated hydrocarbon pyrolysis products were measured on a Hewlett Packard 6890 gas chromatograph coupled to a Finnigan Delta^{plus} isotope ratio mass spectrometer via a modified Finnigan GC Combustion III interface (*irmGC/MS*). Carbon isotopic compositions are reported in the delta (δ) notation referenced to the Vienna Pee-Dee Belemnite (VPDB) standard by introducing several pulses of CO₂ with a

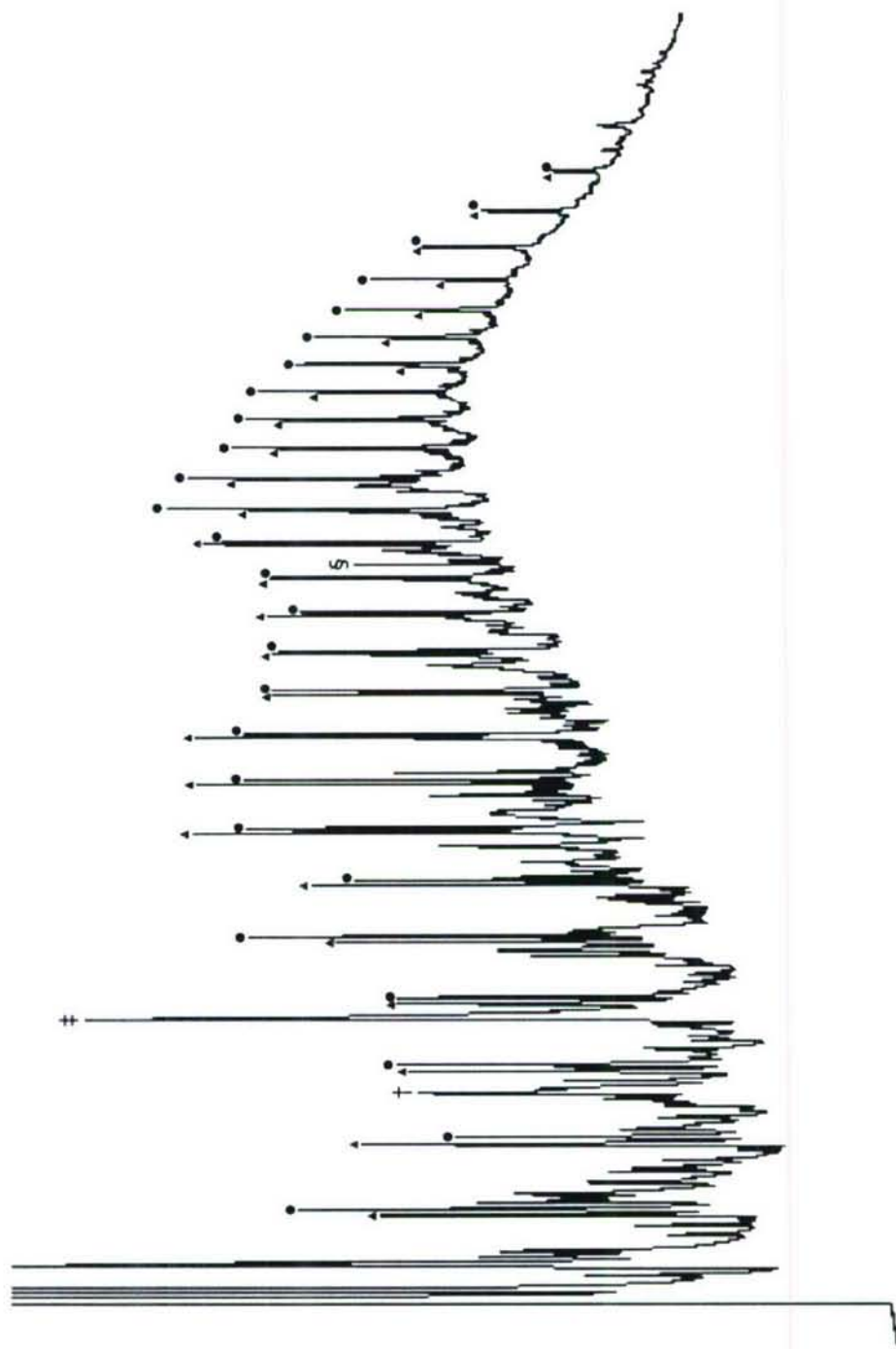


FIGURE 2.3 – Pyrolysis GC chromatogram for station 5 (those for stations 9 and 144 are analogous to station 5 and are therefore not shown). Individual major peaks are identified as follows: homologues series, annotated from C_5 to C_{30} , of n -alkanes (circles) and n -alkenes (triangles), a methylcyclopentene/benzene co-elution (\times), toluene ($+$), and prist-1-ene ($\$$).

known $^{13}\text{C}/^{12}\text{C}$ ratio relative to VPDB into the system during each run. Selected compounds were isolated from these fractions for radiocarbon analysis by preparative capillary gas chromatography (PCGC; an HP 5890 Series II GC system coupled to a Gerstel preparative fraction collector; see Eglinton et al., 1996 for a detailed description.) In order to provide sufficient mass ($>20\mu\text{g}$ carbon) for AMS ^{14}C analysis at station 144, the C_{14} , C_{16} , and C_{18} homologues, and the C_{24} , C_{26} , and C_{28} homologues were recombined after PCGC isolation to yield ‘short-chain’ and ‘long-chain’ fatty acid fractions, respectively. PCGC traps were eluted with hexane into pre-combusted quartz tubes, the hexane evaporated, and pre-combusted copper oxide added. These tubes were then attached to a vacuum line, evacuated, flame sealed, and combusted at 850°C for 5 hours. The resultant CO_2 was introduced and purified on a vacuum line, isolated in a gas sample tube dipped in liquid nitrogen, reduced to graphite, and measured for radiocarbon content at the NOSAMS facility. The $\delta^{13}\text{C}$ ratios measured on aliquots of each sample as CO_2 before graphitization are generally within 1σ analytical precision of their values as measured by *irmGC/MS*, indicating only minor influence from process blank carbon. All of the $\delta^{13}\text{C}$ and $\Delta^{14}\text{C}$ compositions of fatty acids reported below were corrected for the addition of the derivative carbon using an isotopic mass balance.

2.2 RESULTS & DISCUSSION

2.2.1 Bulk characteristics

Elemental and isotopic data for bulk sedimentary OC for all sites are shown in Table 2.1. Radiocarbon ages for these core top sediments cluster around 9000 to 10,000 yr BP, with the exception of station 9 (7690 yr BP). Total carbon contents and C/N ratios

for whole sediments generally decrease with increasing water depth (Figure 2.2). Bulk OC $\delta^{13}\text{C}$ trends to slightly more enriched values with distance offshore, consistent with an increasing contribution from marine production (Ruttenberg and Goñi, 1997; Macdonald et al., 2004). On a carbonate-free basis, although sedimentary OC contents also decrease with distance offshore, TOC/TN ratios do not vary systematically and are quite low, nominally implying a dominant marine source over the entire shelf. However, as mentioned above, the TOC/TN quotient is likely depressed by nitrogen associated with mineral phases as seen in other Arctic sediments (Schubert and Calvert, 2001) and therefore over-represents the marine contribution. Demineralized sediments from stations 5, 9, and 144 display markedly increased C/N stoichiometry, likely reflecting removal of inorganically-bound nitrogen.

2.2.2 Molecular distributions

Major lipid abundances display significant and systematic variability over the shelf and slope. The total abundances of *n*-fatty acids and *n*-alkanes (Figure 2.4) generally decrease as a function of distance offshore (with the exception of station 144) and are similar to those previously reported for the Beaufort Shelf (Yunker et al., 1995, 2002; Belicka et al., 2004) as well as those from a transect from the Lena River Delta to the Laptev Sea (Zegouagh et al., 1998; Stein and Fahl, 2004). These concentrations are anywhere from 2 to 20 times greater than those from sediments underlying the open western Arctic Ocean (Belicka et al., 2002). Embedded within this cumulative trend are molecular level patterns. For example, shorter chain homologues (C_{14} – C_{18}) are generally as abundant, or more abundant, than their longer chain counterparts (C_{22} – C_{28}),

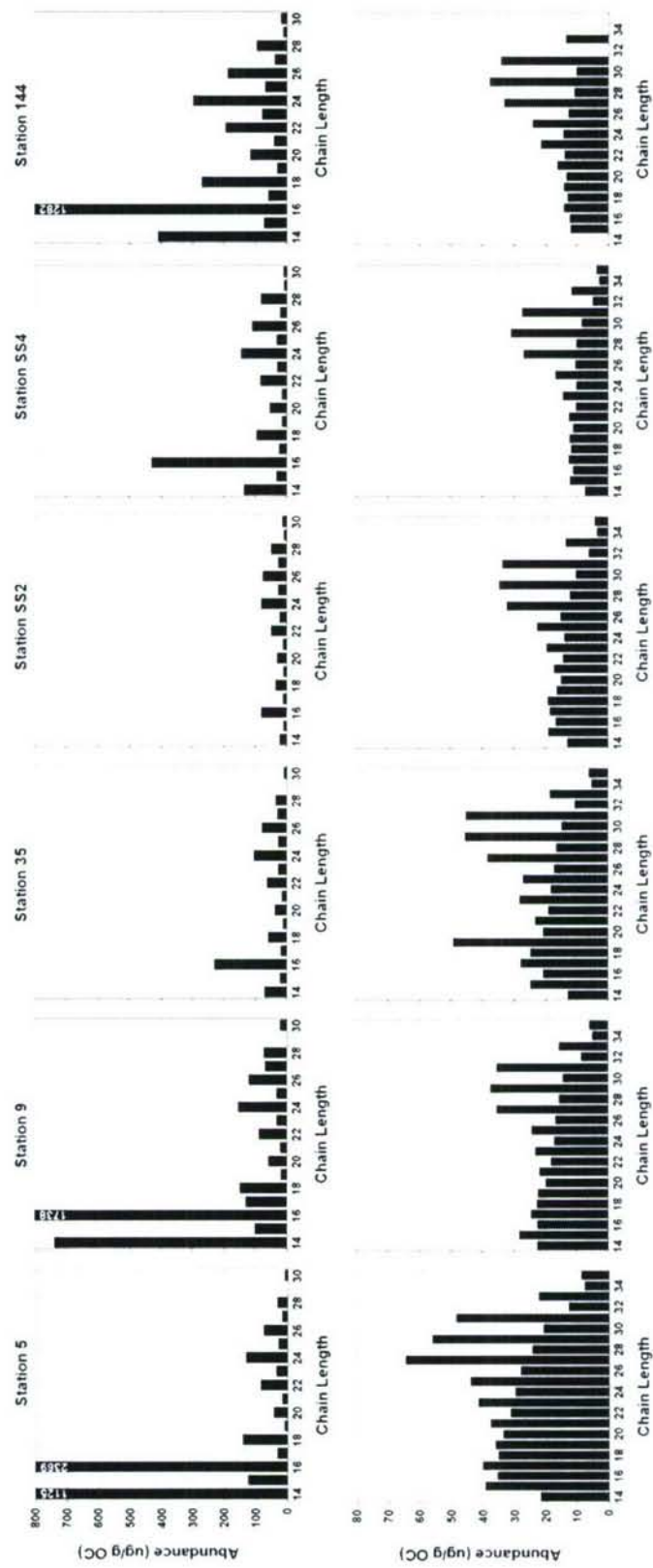


FIGURE 2.4 – Abundance of individual *n*-fatty acids (top) and *n*-alkanes (bottom) in the total lipid extract from each station. White values superimposed on histogram bars indicate the abundances for those homologues that are off-scale.

suggesting significant marine (algal or bacterial) contribution to the OC of Beaufort Sea sediments. Station 144 is unique in that there are noticeably greater concentrations of the higher chain length compounds (C_{22} – C_{28}) relative to those further inshore. This may be a consequence of differing susceptibilities of long versus short chain homologues to degradation (Camacho-Ibar et al., 2003), or could reflect hydrodynamic processes that result in preferential export of terrigenous organic matter associated with fine-grained clays and silts emanating from the Mackenzie plume to the Beaufort Slope. Elevated organic carbon contents are indeed associated with fine grain sediments in this region (Macdonald et al., 2004). The slope may also be subject to turbidite deposits (Philips et al., 1991; Grantz et al., 1996) that are sourced from sediments further inshore containing a greater amount of terrestrial OC.

Extractable *n*-alkanes are two orders of magnitude less abundant than fatty acids (Figure 2.4) but their summed concentrations exhibit similar behavior, i.e., a decrease with distance offshore. There is a distinct odd-over-even carbon number predominance at higher chain length ($>nC_{23}$) in all sites consistent with Yunker et al. (1993, 1995, 2002). Notably, carbon preference index (CPI, = $\Sigma[\text{odd numbered alkane abundances from } nC_{23}\text{--}nC_{35}]/\Sigma[\text{even numbered alkane abundances from } nC_{22}\text{--}nC_{34}]$) values systematically increase as a function of distance offshore from 1.8, to 2.7 for stations 5 and 144, respectively. The overall molecular pattern of abundant odd-carbon numbered, long chain homologues superimposed on a unimodal series ($nC_{15}\text{--}nC_{35}$) of otherwise low CPI homologues suggests contributions from both vascular plant waxes and petrogenic hydrocarbons (from bitumens, shales, or coals), respectively (Yunker et al., 1993, 2002).

The distribution of products from offline pyrolysis are dominated by sequential pairs of alkane/alkene doublets that are very similar to online Curie Point Pyrolysis-Gas Chromatographic (Py-GC) analysis of the same demineralized samples (see Figure 2.3 for a chromatogram from station 5). However, the offline pyrolysates were noticeably depleted of very short chain (C_{12}) homologues compared to their corresponding Py-GC chromatograms, pointing to either inefficient trapping or evaporative loss of volatile hydrocarbons during subsequent sample work-up. The abundance of *n*-alkyl over isoprenoidal products suggests an aliphatic biopolymeric precursor (Höld et al., 1998).

2.2.3 Molecular isotopic compositions

The stable carbon and radiocarbon isotopic signatures of individual fatty acids are shown in Figure 2.5. Short-chain acids are enriched in ^{13}C (–25 to –29 ‰) relative to their longer chain length counterparts (–29 to –33 ‰) with a defined transition occurring at the C_{19} and C_{20} homologues. Some internal structure is also apparent within the longer chain acids as even carbon-numbered compounds are consistently enriched (some by up to 2 ‰) over the neighboring odd-carbon homologues. Taken together, these data imply a predominantly marine algal and/or bacterial source for the short chain acids (C_{14} – C_{20}) and a C_3 vascular plant wax source for the even numbered, long chain acids (C_{22} – C_{30}). Their corresponding radiocarbon isotopic values support this interpretation. For stations 5 and 9, conventional radiocarbon ages for the nC_{14} – nC_{18} acids are either post modern ($\Delta^{14}C = >0$ ‰) or are within or near the estimate of the surface water dissolved inorganic carbon (DIC) reservoir age in other river influenced Arctic margins (~200 to 800 years; Forman and Polyak, 1997). In contrast, at Station 144 the average ^{14}C age is ~3800 yr

BP. Down core profiles of ^{210}Pb , ^{137}Cs , (Appendix 2.2) and the radiocarbon age of TOC (Appendix 2.3) subsequently measured for this core yields an average sedimentation rate of 1.2 cm kyr^{-1} ($r^2 = 0.99$), indicating that the ^{14}C content of the short chain fatty acids extracted from the 4-5 cm horizon is consistent with aging in sediment since deposition.

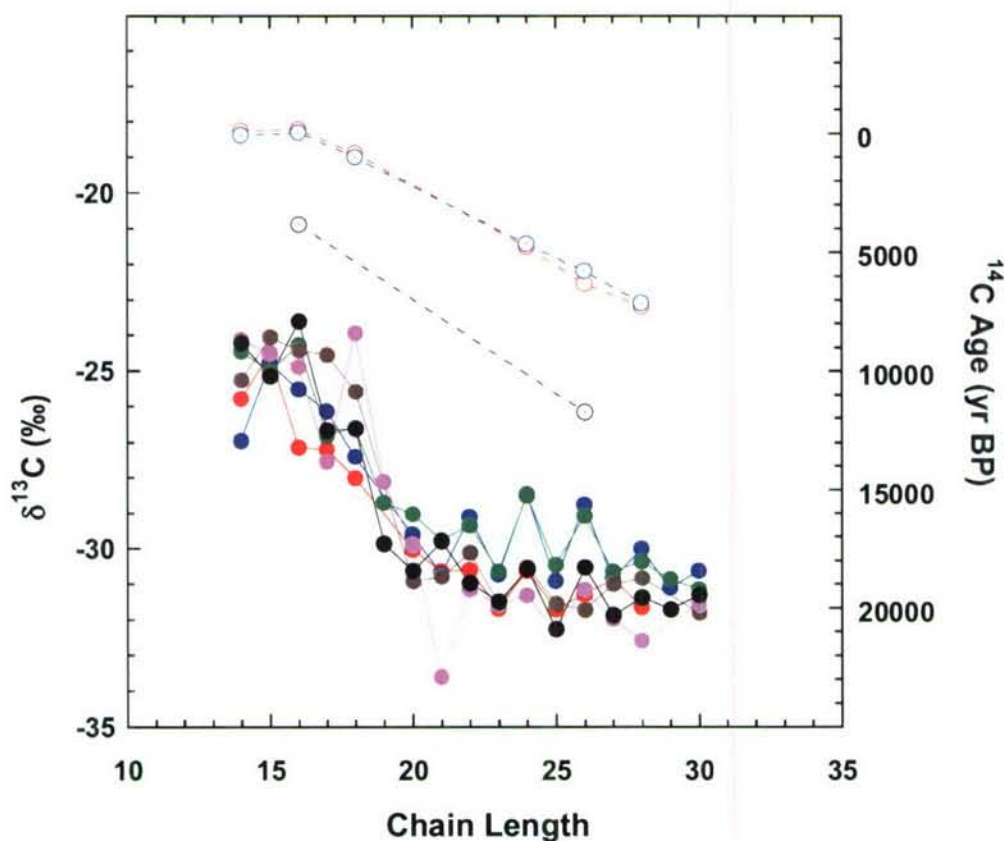


FIGURE 2.5 – Compound-specific $\delta^{13}\text{C}$ (all stations) and $\Delta^{14}\text{C}$ (stations 5, 9, and 144) compositions for fatty acids. Positive ages indicate years before present. For both isotopes, colors are as follows: stations 5 (red), 9 (blue), 35 (green), SS2 (brown), SS4 (purple), and 144 (black); $\delta^{13}\text{C}$ data points are filled, whereas $\Delta^{14}\text{C}$ data points are hollow. The data points at chain lengths 16 and 26 for Station 144 represent the combinations of the $n\text{C}_{14+16+18}$ and $n\text{C}_{24+26+28}$ homologues, respectively (the 16 and 26 homologues being the most abundant of each group.)

At all sites, the long chain acids are several thousand years older than the short chain homologues, suggesting a long residence time on land before delivery to Beaufort Shelf sediments. Old ^{14}C ages for long chain fatty acids have been previously observed for sediments in the northwestern Pacific slope (Uchida et al., 2001), Bermuda Rise (Ohkouchi et al., unpublished results), Tokyo Bay (Uchida et al., 2000), and the Ross Sea (Ohkouchi et al., 2003), as well as a continental aerosol sample (Matsumoto et al., 2001).

The stable and radiocarbon isotopic compositions of the solvent extractable *n*-alkanes are shown in Figure 2.6. The $\delta^{13}\text{C}$ signatures of short chain ($\leq n\text{C}_{26}$) homologues are relatively invariant, and centered around -30‰ . In contrast, longer odd carbon numbered homologues from all stations are between 0.5 to 2 ‰ depleted relative to both the short-chain homologues and their even carbon numbered counterparts. The latter are similar in isotopic composition to the long chain, even numbered fatty acids from these same sediments that are believed to derive from the epicuticular coatings of C_3 plant leaves (Wiesenberg et al., 2004). For the *n*-alkanes, the magnitude of this depletion increases with increasing chain length, reflecting the greatest contribution from terrestrial plants over that from petrogenic sources for the highest homologues. The higher ^{14}C content of long chain, odd numbered alkanes (C_{27} , C_{29} , & C_{31}) also points to a greater contribution of alkanes from a non-petrogenic source while the even homologues, which are not abundantly produced by extant terrestrial or marine biomass, retain a depleted ^{14}C signature. Thus, the molecular ^{13}C and ^{14}C distributions reveal that a mixture of at least two sources (terrestrial plants and petrogenic material) is responsible for the mass

abundance profiles, similar to that reported by Pearson and Eglinton (2000) in the Santa Monica Basin.

The influence of petrogenic ‘contamination’ on the $\delta^{13}\text{C}$ and $\Delta^{14}\text{C}$ values of homologues that are primarily derived from higher plants can be quantitatively assessed using mass balances for each isotope. For example, the $\delta^{13}\text{C}$ or $\Delta^{14}\text{C}$ signature of the

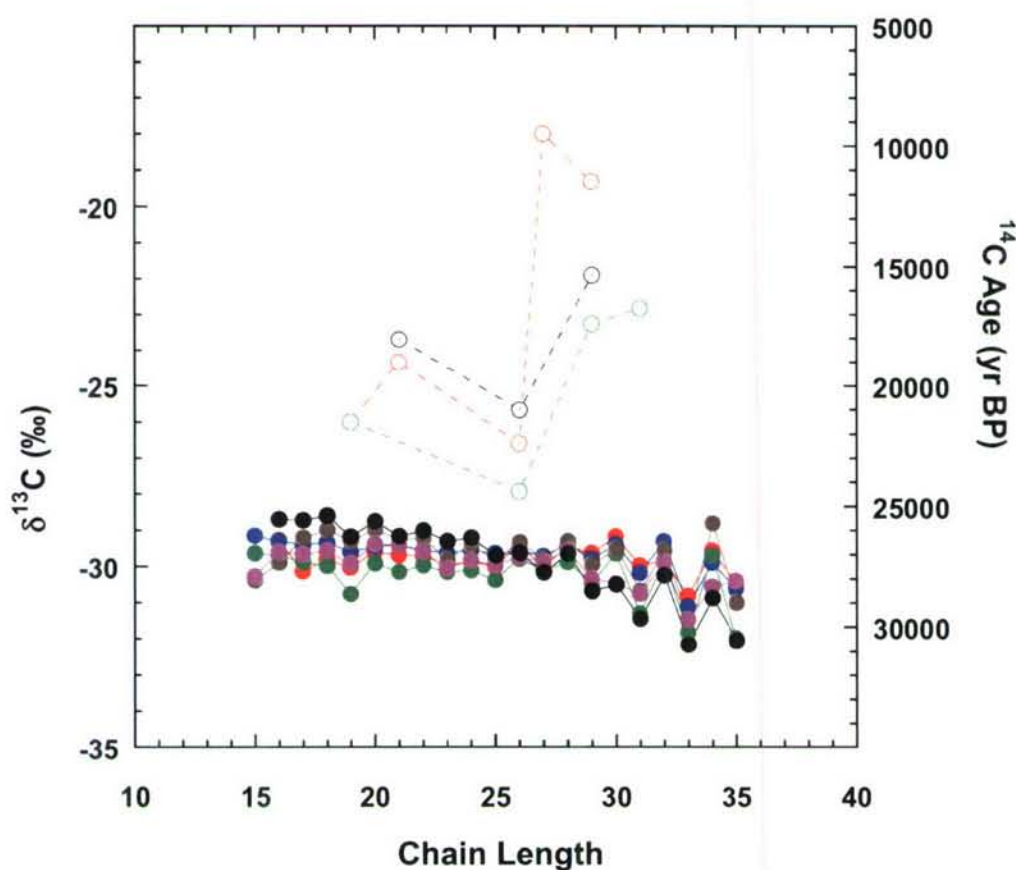


FIGURE 2.6— $\delta^{13}\text{C}$ and $\Delta^{14}\text{C}$ compositions of individual extractable alkanes. Symbols are as in Figure 2.5. The following data points are combinations of the homologues in parentheses, with the point plotted at the most abundant homologue’s chain length: Station 5 $n\text{C}_{26}$ ($n\text{C}_{26+28+30}$); Station 35 $n\text{C}_{26}$ ($n\text{C}_{26+28+30}$); Station 144 $n\text{C}_{26}$ ($n\text{C}_{26+28+30}$); Station 144 $n\text{C}_{21}$ ($n\text{C}_{19+21}$); Station 144 $n\text{C}_{29}$ ($n\text{C}_{27+29}$).

fraction of the nC_{29} homologue's total mass that is sourced from vascular plant waxes can be calculated by assuming that the even numbered homologues (in this case nC_{26} , nC_{28} , and nC_{30}) are completely petrogenic, and thus their average abundance and isotopic composition are equivalent to the abundance and isotopic composition of the petrogenic fraction of nC_{29} . This approach is modified after Huang et al. (2000), but in the absence of ancillary information on the exact distribution of higher plant n -alkanes in this region, we assume here that the even numbered homologues are overwhelmingly petrogenic. For homologue i , therefore, the measured stable carbon isotopic composition ($\delta^{13}C_{i,\Sigma}$) can be expressed as the sum of the isotopic compositions of its petrogenic ($\delta^{13}C_{i,P}$) and terrestrial ($\delta^{13}C_{i,T}$) components, each multiplied by their fractional contribution ($f_{i,P}$ and $f_{i,T}$, respectively) to the total homologue abundance ($A_{i,\Sigma}$),

$$\delta^{13}C_{i,\Sigma} = f_{i,P} \delta^{13}C_{i,P} + f_{i,T} \delta^{13}C_{i,T} \quad (1)$$

$$f_{i,P} = \bar{A}_{i\pm n} / A_{i,\Sigma} \quad (2)$$

$$f_{i,P} + f_{i,T} = 1 \quad (3)$$

where, in this case, $\bar{A}_{i\pm n}$ is the average abundance of the nC_{26} , nC_{28} , and nC_{30} homologues. Equation 1 can also be re-written for $\Delta^{14}C_{i,\Sigma}$. Performing these calculations for nC_{29} at stations 5, 35, and 144 yields $\delta^{13}C_{29,T}$ compositions that are at most 0.35 ‰ depleted relative to $\delta^{13}C_{29,\Sigma}$. The corresponding $\Delta^{14}C_{29,T}$ values, however, are enriched by approximately 210 ‰ (3300 ^{14}C years), 35 ‰ (2150 ^{14}C years), and 30 ‰ (1400 ^{14}C years) relative to $\Delta^{14}C_{29,\Sigma}$ at stations 5, 35, and 144, respectively. Thus, the ^{14}C ages for the leaf wax fraction of the nC_{29} alkane are in closer agreement with the ages of the nC_{28} fatty acid, whose source is normally attributed to higher plants alone.

The $\Delta^{14}\text{C}$ and $\delta^{13}\text{C}$ values for alkanes and the $\delta^{13}\text{C}$ values for alkenes isolated from the offline pyrolysates are shown in Figure 2.7. Similar to observations of some kerogens by Eglinton (1994) and Höld et al. (1998), the $\delta^{13}\text{C}$ signatures of both saturated and mono-unsaturated homologues are relatively invariant suggesting they may be derived from a biopolymeric source, and not a product of random condensation of

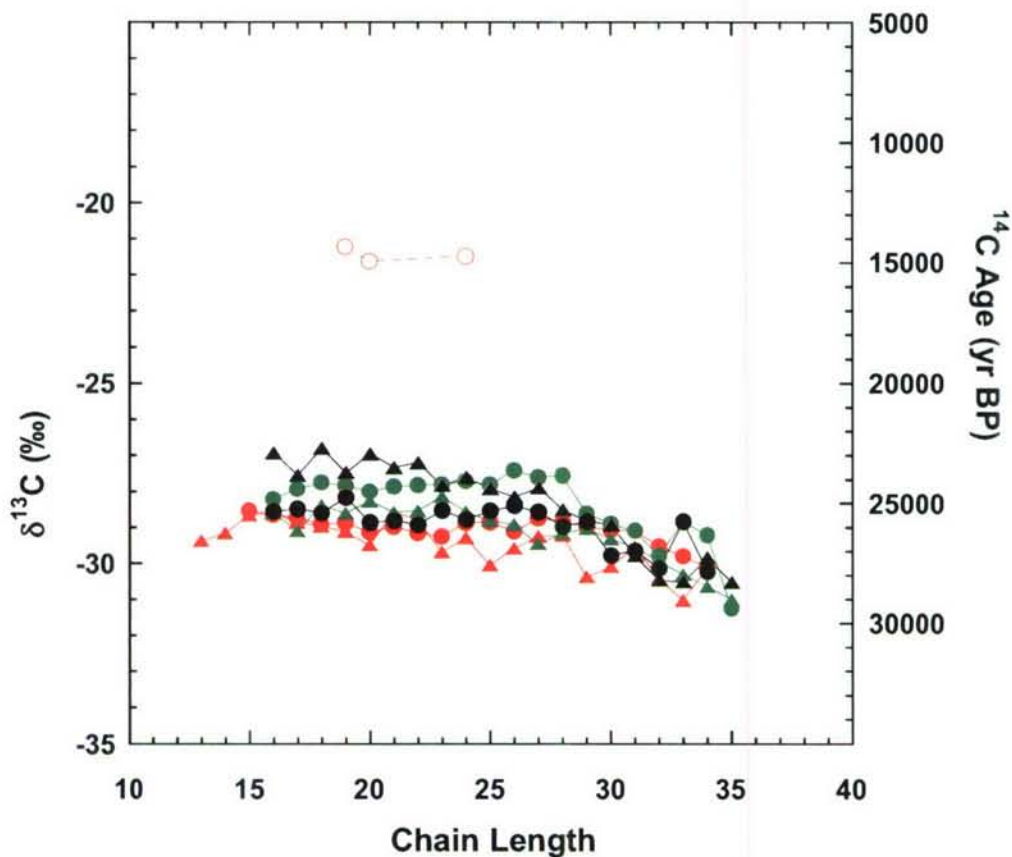


FIGURE 2.7 – $\delta^{13}\text{C}$ and $\Delta^{14}\text{C}$ compositions of pyrolysate alkanes (circles) and alkenes (triangles). Symbol colors and fill are as in Figure 5. The data point at chain length 19 represents a combination of $n\text{C}_{17}$ & $n\text{C}_{19}$ homologues, with the latter being more abundant.

structurally and isotopically distinct diagenesis products within sediments. Their corresponding old radiocarbon ages, in addition to the distributional data discussed above, imply that a significant portion this material may be derived from vascular plant cutan that spends an equivalent or somewhat longer amount of time sequestered on land before delivery to the Beaufort Sea, instead of originating exclusively from kerogen released during sedimentary rock erosion.

2.2.4 A qualitative view of OC cycling

The bulk and molecular abundance and isotopic data described above yield a dynamic picture of OC delivery to the Mackenzie shelf. The Mackenzie River supplies the vast majority of sedimentary organic matter to the region, a fact that is demonstrated by the decrease in %OC and total lipid abundances in surficial sediments with increasing offshore distance. This finding is consistent with other studies of alkane, alcohol, sterol, fatty acid, hopane, and polycyclic aromatic hydrocarbon (PAH) distributions in this region (Yunker et al., 1995, 1996, 2002; Belicka et al., 2004). The river's influence is further highlighted by the depleted $\delta^{13}\text{C}$ values as well as the higher C/N ratios for bulk sediment proximal to the shore (Table 2.1), suggesting a large depositional flux of OC ultimately derived from C_3 land plants (Ruttenberg and Goñi, 1997; Goñi et al., 2000). The overall depletion in individual long-chain fatty acids (-25 to -33 ‰) and alkanes (-28 to -32 ‰) over the whole shelf strongly supports this interpretation as well (Figures 2.5 & 2.6) (e.g. Collister et al., 1994). The bulk radiocarbon contents (Table 2.1) of these same sediments, moreover, point to a significant terrigenous contribution from either petrogenic or pre-aged terrestrial debris, or both, consistent with the characteristics of the

Mackenzie River drainage basin described above. High sedimentation rates on the shelf proper (10 to 300 cm kyr⁻¹) preclude the possibility that such ages are merely an artifact of bioturbation.

The abundance and isotopic distributions of the extracted lipids provide insights into the sedimentological processes in operation once the organic matter exits the river delta. In contrast to the bulk data, the abundance of long chain fatty acids increases at stations SS2 and 144 (Figure 2.4), consistent with an increasing vascular plant signature at the sites most distal from the Mackenzie Delta. The alkane profiles exhibit similar behavior, with escalating CPI indices with offshore distance. Vascular plant lipids have also been observed in sediments from the central Arctic Ocean indicating that some terrestrial material is exported all the way to the deep basins (Schubert and Stein, 1997; Belicka et al., 2002, 2004; Yunker et al., 2005). The stable and radiocarbon compositions of these same long chain compounds (Figures 2.5 & 2.6) confirm a source other than autochthonous production in the water column, which would be expected to yield lipids more enriched in ¹³C and with a radiocarbon age near the reservoir age of the mixed layer DIC pool (as is observed for the short chain fatty acids from stations 5 & 9; see Figure 2.5; Pearson et al., 2001; Ohkouchi et al., 2003). Rather, both isotopes point to a vascular plant origin of these long chain lipids that has subsequently resided on the continents for several millennia prior to transport to the Beaufort Sea. Lignin phenol data indicating highly degraded vascular plant debris in Mackenzie River POC and Beaufort Shelf sediments (Goñi et al., 2000, 2005) is also consistent with long terrestrial residence times.

Taken together, these observations suggest that the majority of river-derived material is deposited in the inner shelf and delta (Macdonald et al., 1998) where rapid flocculation, settling, and sedimentation likely aid the preservation of terrigenous OC. These processes, coupled with a summer flux that is particularly intense during freshet, may hinder the replacement of this material by marine OC on mineral grains as observed for other estuarine systems (Keil et al., 1997), further protecting it from remineralization (Mayer, 1994). To a first order approximation, the ‘terrestrial residence time’ of this OC is given by the ages of the long chain fatty acids to be 5,000 to 10,000 years, in good agreement with the age of suspended POC from the Mackenzie River (Goñi et al., 2005). It is likely, however, that such dates represent a weighted average of inputs spanning a continuum of ages from many different temporal reservoirs on land. A significant portion of this old material is probably physically protected via close association with larger macromolecules (e.g. biopolymers, kerogen) or detrital mineral grains, as the more labile components would likely have been degraded over the course of many millennia. The ubiquity of pyrolysis (this study) and CuO (Goñi et al., 2000, 2005) products across the shelf, and the old ages and $\delta^{13}\text{C}$ signatures of the former compounds (Figure 2.7), support this hypothesis.

Some allochthonous organic matter associated with finer grain minerals or detrital aggregates does not immediately settle out of the water column, however, and either remains in suspension or is perhaps re-suspended from deltaic and inner shelf sediments for later deposition in outer shelf, slope, and basin sediments (Macdonald et al., 1998). Even though the overall flux of terrigenous (terrestrial land plant + petrogenic) OC

relative to marine OC to surficial sediments is less on the lower slope than on the shelf proper, low sedimentation rates increase the oxygen exposure time in the sediment column, allowing a smaller amount of (presumably more labile) marine detritus to be ultimately preserved. Consequently, the 4-5cm depth interval at Station 144 appears to contain a similar, or greater, relative proportion of terrigenous OC as the surficial sediments further inshore. The depth of the mixed layer relative to the sedimentation rate is almost certainly higher in slope and basin sediments as well, allowing for a larger upward advection of older material (Yunker et al., unpublished results). Together, these observations may explain the uniformity of the bulk radiocarbon ages across the Beaufort Shelf/Slope transect.

2.2.5 Coupled isotopic mass balance calculations

A quantitative assessment of various inputs to marine sediments can be achieved by the use of elemental or isotopic mass balance calculations. Traditionally, a two endmember mixing model based on the C/N stoichiometry or $\delta^{13}\text{C}$ of bulk OC has been employed to resolve vascular plant versus marine sources, although low C/N ratios for some terrigenous OC exiting the Mackenzie River complicate such calculations in the Beaufort Sea (Macdonald et al., 2004). This approach can be refined to include the petrogenic contribution by the addition of a second isotope, ^{14}C , but relies on the extrapolation of endmember isotopic compositions and the assumption that these compositions do not change from source to sink. Molecular level $\delta^{13}\text{C}$ and $\Delta^{14}\text{C}$ measurements on compounds representing known endmembers relieves this constraint, allowing direct assessment of the fractional contribution of terrestrial, marine, and

petrogenic material to sedimentary OC at any one location to be deconvoluted independent of ancillary data. Nonetheless this approach carries two important limitations. First, source specific biomarkers such as lipids are typically only trace constituents in sediments and therefore may not always be representative of the total organic matter. In this case however, the depleted isotopic compositions of the pyrolysis products (Figure 2.7) suggest that long chain fatty acids and alkanes are likely representative of terrestrial OC on the whole. Second, differences in $\delta^{13}\text{C}$ between biomarkers and bulk biomass resulting from isotopic fractionation during biosynthesis ($\delta^{13}\text{C}_{\text{biomass}} - \delta^{13}\text{C}_{\text{lipid}}$) need to be taken in account. This is especially the case for lipids, which tend to be significantly depleted in ^{13}C . This constraint is addressed below.

Three simultaneous equations can be written describing these contributions to total organic matter,

$$f_T(\Delta^{14}\text{C}_T) + f_M(\Delta^{14}\text{C}_M) + f_P(\Delta^{14}\text{C}_P) = \Delta^{14}\text{C}_S \quad (4)$$

$$f_T(\delta^{13}\text{C}_T) + f_M(\delta^{13}\text{C}_M) + f_P(\delta^{13}\text{C}_P) = \delta^{13}\text{C}_S \quad (5)$$

$$f_T + f_M + f_P = 1 \quad (6)$$

where f is the fractional abundance and the subscripts T, M, P, and S are terrestrial, marine, and petrogenic carbon, and bulk sediment sample respectively. Based on the source assignments discussed above, these equations can be solved using the abundance-weighted mean isotopic compositions of the short chain fatty acids ($n\text{C}_{14}$, $n\text{C}_{16}$, & $n\text{C}_{18}$) for $\delta^{13}\text{C}_M$ and $\Delta^{14}\text{C}_M$, the $n\text{C}_{28}$ acid for $\delta^{13}\text{C}_T$ and $\Delta^{14}\text{C}_T$ (except for Station 144 where the combination of $n\text{C}_{24}$, $n\text{C}_{26}$, & $n\text{C}_{28}$ is used), and the mean of the even carbon numbered, unbound alkanes ($n\text{C}_{26}$, $n\text{C}_{28}$, & $n\text{C}_{30}$) for $\delta^{13}\text{C}_P$ and $\Delta^{14}\text{C}_P$. The values for $\delta^{13}\text{C}_P$ and

$\Delta^{14}\text{C}_\text{P}$ at Station 35 were substituted for those of Station 9 because the latter sample was lost during preparation for ^{14}C analysis. However the mean $\delta^{13}\text{C}$ values at all stations for these chain lengths were very similar (-29.3 , -29.4 , -29.8 , and -29.9 ‰ for stations 5, 9, 35, and 144 respectively) as were the corresponding $\Delta^{14}\text{C}$ values for stations 5, 35, and 144 (-939 , -952 , and -927 ‰, respectively) suggesting isotopic homogeneity for the petrogenic endmember. In theory, these compounds do not contain a measurable amount of radiocarbon since they are likely sourced from ancient sedimentary rocks whose age is $\gg 50,000$ years old. In practice, the $\sim 30\mu\text{g}$ carbon samples used for $\Delta^{14}\text{C}$ analysis by AMS are generally considered to be ‘radiocarbon dead’ at values below approximately -920 ‰ due to blank and precision limits (A. McNichol, pers. comm.). It might therefore be reasonable to re-assign the $\Delta^{14}\text{C}_\text{P}$ at each station a value of -1000 ‰. Over the range of lipid-to-biomass isotopic ^{13}C offsets ($\delta^{13}\text{C}_\text{biomass} - \delta^{13}\text{C}_\text{lipid}$) considered here (see below), this modification increases both f_P and f_M by ~ 0.15 units at the expense of f_T , indicating that such calculations are indeed sensitive to the current limits of AMS technology. Nonetheless, we adopt the measured $\Delta^{14}\text{C}$ values of the petrogenic alkanes here in order to demonstrate the present utility of molecular-based isotopic mass balances without the need for assumptions.

It is also important to note that the calculated values for f_T , f_M , and f_P are sensitive to the prescribed $\delta^{13}\text{C}_\text{biomass} - \delta^{13}\text{C}_\text{lipid}$ offset. The exact relationship and its potential variability have not been fully constrained, but some studies (Collister et al., 1994; Wiesenberg et al., 2004) suggests a value of 7 to 10 ‰ for vascular plants and anywhere from 5 to 10 ‰ for algae (Schouten et al., 1998; van Dongen et al., 2002). However, the

$\delta^{13}\text{C}$ signatures of lipid biomarkers can be affected by inputs from different species (Collister et al., 1994), local growth conditions and kinetics (Bidigare et al., 1997; Lockheart et al., 1997), external and *in vivo* carbon pools (Hollander and McKenzie, 1991; Hayes, 1993; Arens et al., 2000), climatic shifts (Pancost and Boot, 2004), and diagenesis (Nguyen Tu et al., 2004; Sun et al., 2004). Practically speaking, the offset is directly added to the $\delta^{13}\text{C}$ values of the short and long chain fatty acids to arrive at the isotopic composition of bulk marine ($\delta^{13}\text{C}_\text{M}$) and terrestrial ($\delta^{13}\text{C}_\text{T}$) biomass, respectively, which are then used in the isotopic mass balance calculations below. No correction is applied *a priori* to $\delta^{13}\text{C}_\text{P}$ because the short chain *n*-alkanes are assumed to be isotopically similar to that of the sedimentary rock from which they derive (Eglinton, 1994). However, Goñi et al. (2005) use the trends in $\delta^{13}\text{C}$ and $\Delta^{14}\text{C}$ of Mackenzie River POC and Beaufort Shelf sedimentary OC to imply a $\delta^{13}\text{C}_\text{P}$ value of -25 to -27 ‰, or 3 to 5 ‰ heavier than the average $\delta^{13}\text{C}$ composition of the short chain alkanes measured in this study. This discrepancy might be an artifact in Goñi et al.'s interpretation of the bulk isotopic trends, or might otherwise indicate isotopic heterogeneity in the petrogenic endmember. In any case, varying the $\delta^{13}\text{C}_\text{biomass} - \delta^{13}\text{C}_\text{lipid}$ difference for $\delta^{13}\text{C}_\text{M}$ or $\delta^{13}\text{C}_\text{T}$ by a couple of per mille in either direction influences our calculations by as much as a factor of two. For this or other molecular isotope work to be widely applied, therefore, this range will clearly need to be narrowed further.

The calculated values for f_T , f_M , and f_P at Stations 5, 9, and 144 for a $\delta^{13}\text{C}_\text{biomass} - \delta^{13}\text{C}_\text{lipid}$ variation between 7 and 9 ‰ are shown in Figure 2.8. These results indicate

that, for median values of $\delta^{13}\text{C}_{\text{biomass}} - \delta^{13}\text{C}_{\text{lipid}}$, roughly 40-50% of the OC being delivered to Beaufort Sea sediments is derived from the weathering of ancient sedimentary rocks. Both the general magnitude and ubiquity of this ancient component across the Beaufort Shelf and slope are similar to, but generally lower than, estimates made by Goñi et al. (2005) using the $\Delta^{14}\text{C}$ signatures of bulk sediment and assumed endmember compositions. Importantly, however, that study may have overestimated f_p because contributions from significantly pre-aged vascular plant matter sources could not be accounted for. The fate of this petrogenic OC in the marine environment remains unclear, but some fraction may be re-incorporated into the biological food web (Petsch et al., 2001). In any event, combining the values of f_p integrated across $\delta^{13}\text{C}_{\text{biomass}} - \delta^{13}\text{C}_{\text{lipid}}$ offsets between 7 and 9 ‰ for the shelf stations (5 and 9) ($f_{p,\text{avg}} = 0.44$) as well as for station 144 on the outer slope ($f_{p,\text{avg}} = 0.37$) with estimates of total OC burial rates in these sediments ($0.71 \times 10^9 \text{ kg yr}^{-1}$ and $0.17 \times 10^9 \text{ kg yr}^{-1}$, respectively) (Macdonald et al., 1998) yields a total petrogenic carbon burial rate of roughly $0.4 \times 10^9 \text{ kg yr}^{-1}$, or ~20% of the estimated annual OC yield from bedrock weathering in the Mackenzie basin (Di-Giovanni et al., 2002).

The fractions of marine and pre-aged terrestrial OC wax and wane with offshore distance, respectively, in line with the elemental and isotopic observations on the bulk sediments (Table 2.1). Similar to calculations made by Belicka et al. (2004) using C_{25} – C_{31} odd *n*-alkane biomarker abundance patterns, we find that shelf sediments are overwhelmed by terrigenous (terrestrial + petrogenic) carbon ($f_{\text{terrigenous}} = f_{\text{T,avg}} + f_{p,\text{avg}} = 0.43 + 0.44 = 0.87$, $f_{\text{M,avg}} = 0.13$), which gives way to a larger marine component at

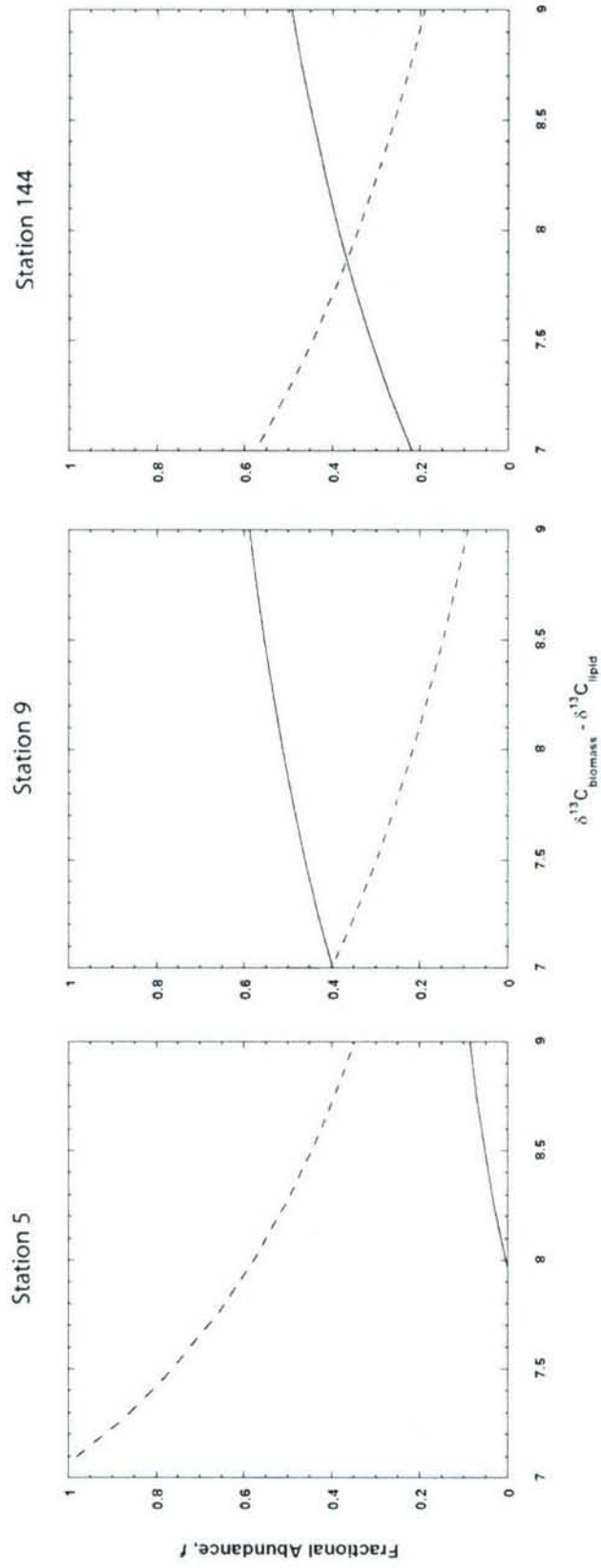


FIGURE 2.8 – Coupled isotopic mass balance results for the fractional contributions of marine (f_M , solid black), terrestrial (f_T , dashed black), and petrogenic (f_P , solid grey) OC in sediments from stations 5, 9, and 144 over a range of prescribed $\delta^{13}\text{C}_{\text{biomass}} - \delta^{13}\text{C}_{\text{lipid}}$ offsets.

station 144 ($f_{\text{terrigenous}} = f_{\text{T,avg}} + f_{\text{P,avg}} = 0.36 + 0.37 = 0.73$, $f_{\text{M,avg}} = 0.27$). The large f_{P} values are consistent with the presence of a well-defined signature of petroleum alkanes and PAHs in Mackenzie River and Beaufort Sea sediments (Yunker et al., 1993, 2002). Nevertheless, the Mackenzie River is the only large Arctic River that exhibits such a petrogenic signature, and petrogenic carbon may be less important for other Arctic rivers and shelves. For example, old radiocarbon ages of surficial sediments from the Siberian coastline have been primarily attributed to the release of pre-aged terrestrial OC from soils upon permafrost thawing (Guo et al., 2004). The calculated increase in f_{M} offshore is also based on a fairly stable component of the marine carbon, and does not include labile marine constituents that are rapidly degraded in the marine water column and surface sediments (Wakeham et al., 1997; Yunker et al., 2005). Based on the multivariate analysis of 107 biomarkers, the fraction of the labile/marine biomarkers (most notably the unsaturated fatty acids) to the stable/terrigenous biomarkers (sterols, alkanes and alcohols) in surface sediments does indeed decrease from 0.77 to 0.61 between stations 5 and 144 (Yunker et al., 2005).

Recent studies on small mountainous rivers draining active margins, where the uplift and erosion of sedimentary rock is expected to be greatest, suggest that roughly 0.5 wt.% of the POC (Komada et al., 2004) and half of the OC buried in sediments of the adjacent shelves (Blair et al., 2003, 2004) is of fossil (petrogenic) origin. Our data suggests that shelves influenced by large rivers whose extensive basins include sedimentary rock formations may bury an equivalent amount of ancient carbon. In other words, rapid physical wasting of shale and delivery to the ocean may not be a prerequisite

for high incorporation rates of petrogenic OC into marine sediments as suggested by these previous investigations. It is also equally likely that the freshet in the Mackenzie, when the vast majority of POC is transported to the Beaufort Sea, mimics the intense seasonal flow of many small mountainous rivers that has been cited as one of the main features controlling old OC erosion and reburial (Masiello and Druffel, 2001; Komada et al., 2004). Such intense discharge episodes may serve to increase the overall preservation of terrigenous POC by evading the efficient recycling machinery normally observed in estuarine environments. In this regard, ancient carbon input from large rivers may only be significant at high latitudes. Nonetheless, it is possible that the ^{14}C depleted POC in rivers draining passive margins (Raymond and Bauer, 2001) might therefore be at least partially attributed to shale weathering over and above debris leached from old soil reservoirs. The compositional nature and variability of this material is not well understood, but likely takes the form of a complex mixture of diagenetically and catagenetically altered hydrocarbons (e.g. a broad distribution of low CPI alkanes is attributed to OC weathered from shale as highlighted here, and as per Pearson and Eglinton, 2000 and Yunker et al., 2002), kerogen including ancient biopolymers (Hedges et al., 2000; Petsch et al., 2000), and graphitic black carbon (Dickens et al., 2004) depending on the source and thermal history of the sedimentary rock. Loss of OC from sedimentary rock itself can likely be represented as a kinetic competition between physical erosion and chemical oxidation (Petsch et al., 2000). Future research into the composition and reactivity of shale derived OC will likely augment our understanding of how much of it is preserved in marine sediments and, by extension, how the oxidation

state of the atmosphere is balanced, as well as whether export of some of this carbon from the shelves to the abyssal ocean in resuspension events (i.e. scour by bottom currents, turbidites, and in the polar regions, ice rafting) influences the apparently old age of DOC there (Bauer and Druffel, 1998).

The findings reported here also have implications for biomarker applications. Specifically, it is clear that the temporal fidelity of organic biomarker records in marine sediments must be carefully assessed in order to undertake accurate paleoclimatic reconstructions. Mollenhauer et al. (2003) have shown that the fine fraction of slope sediments may be influenced by allochthonous (terrigenous and marine) OC advecting in from the shelves during repeated resuspension/deposition cycles. We now show that vascular plant OC in shelf sediments themselves, from which high resolution records of continental climate are often constructed, may suffer from similar age offsets due to its terrestrial residence time. The ages of the vascular plant biomarkers reported here likely represent the weighted average of a continuum of ages, from recently synthesized leaf waxes that are rapidly delivered to the Beaufort Shelf, to those residing in soils and wetlands for many tens of thousands of years before being incorporated into the fluvial flux of material. It is similarly likely that the temporal offset varies as a function of proximity to a major river outlet. The addition of a third molecular isotope system, δD , may help to resolve these questions in future studies.

2.3 CONCLUSIONS

Coupled $\delta^{13}\text{C}$ and $\Delta^{14}\text{C}$ analyses on individual biomarkers provide a valuable new tool in apportioning the sources of OC accumulating in aquatic sediments. Application of this technique to lipids extracted from Mackenzie Shelf and Beaufort Sea sediments indicates that, on average, approximately 40-50% of the organic carbon currently being buried in this climatically sensitive region is petrogenic in origin, likely derived from the weathering of ancient sedimentary rock. The remaining OC flux is comprised of different amounts of marine detritus and pre-aged terrestrial material. A significant portion of the latter must have resided for several millennia in soils and wetlands on the continent before delivery to the sea. These results are in good agreement with a qualitative interpretation of carbon cycling in this area given by the elemental and isotopic distribution on both the bulk and molecular level. Radiocarbon analysis of the pyrolysis products of insoluble organic matter yield ages that are somewhat older than those for the coeval free lipids, suggesting either that monomeric and polymeric forms of OC are both derived from higher plants and exhibit significant terrestrial residence times or that this material is a mixture of fossil and non-fossil endmembers. Together these results indicate that far more petrogenic carbon may be being buried in continental shelf sediments globally than has been previously estimated, and that long terrestrial residence times of higher plant biomarkers may complicate paleoclimate reconstructions.

ACKNOWLEDGEMENTS

Carl Johnson and Leah Houghton are thanked for providing their analytical expertise for the $\delta^{13}\text{C}$ measurements. Suggestions from two anonymous reviewers are greatly appreciated. N.J.D. was supported by funds from the Stanley W. Watson Foundation, and Schlanger Ocean Drilling Program & EPA STAR Fellowships. This work was also supported by NSF OCE-9907129 and OCE-0137005 (T.I.E.), and the Strategic Science Fund of the Department of Fisheries and Oceans, Canada.

REFERENCES

- Agnelli, A., Trumbore, S.E., Corti, G., Ugolini, F.C., 2002. The dynamics of organic matter in rock fragments in soil investigated by ^{14}C dating and measurements of ^{13}C . *European Journal of Soil Science*, 53: 147-159.
- Arens, N.C., Jahren, A.H., Amundson, R., 2000. Can C3 plants faithfully record the carbon isotopic composition of atmospheric carbon dioxide? *Paleobiology*, 26: 137-164.
- Bauer, J.E., Druffel, E.R.M., 1998. Ocean margins as a significant source of organic matter to the deep open ocean. *Nature*, 392: 482-485.
- Backman J., Jakobsson M., Løvlie R., Polyak L., Febo LA., 2004. Is the central Arctic Ocean a sediment starved basin? *Quaternary Science Reviews*, 23: 1435-1454.
- Belika, L.L., Macdonald, R.W., Harvey, H.R., 2002. Sources and transport of organic carbon to shelf, slope, and basin sediments of the Arctic Ocean. *Deep-Sea Research I*, 49: 1463-1483.
- Belika, L.L., Macdonald, R.W., Yunker, M.B., Harvey, H.R., 2004. The role of depositional regime on carbon transport and preservation in Arctic Ocean sediments. *Marine Chemistry*, 86: 65-88.
- Berner, R.A., 1989. Biogeochemical cycles of carbon and sulfur and their effect on atmospheric oxygen over Phanerozoic time. *Paleogeography Paleoclimatology Paleoecology*, 73: 97-122.
- Bidigare, R.R., Fluegge, A., Freeman, K.H., Hanson, K.L., Hayes, J.M., Hollander, D., Jasper, J.P., King, L.L., Laws, E.A., Milder, J., Millero, F.J., Pancost, R., Popp, B.N., Steinberg, P.A., Wakeham, S.G., 1997. Consistent fractionation of ^{13}C in nature and in the laboratory: Growth rate effects in some haptophyte algae. *Global Biogeochemical Cycles*, 11: 279-292.
- Blair, N.E., Leithold, E.L., Aller, R.C., 2004. From bedrock to burial: the evolution of particulate organic carbon across coupled watershed-continental margin systems. *Marine Chemistry*, 92: 141-156.
- Blair, N.E., Leithold, E.L., Ford, S.T., Peeler, K.A., Holmes, J.C., Perkey, D.W., 2003. The persistence of memory: The fate of ancient sedimentary organic carbon in a modern sedimentary system. *Geochimica et Cosmochimica Acta*, 67: 63-73.
- Camacho-Ibar, V.F., Aveytua-Alcázar, L., Carriquiry, J.D., 2003. Fatty acid reactivities in sediment cores from the northern Gulf of California. *Organic Geochemistry*, 34: 425-439.
- Carson, M.A., Jasper, J.N., Conly, F.M., 1998. Magnitude and sources of sediment input to the Mackenzie Delta, Northwest Territories, 1974-94. *Arctic*, 51: 116-124.
- Collister, J.W., Rieley, G., Stern, B., Eglinton, G., Fry, B., 1994. Compound-specific $\delta^{13}\text{C}$ analyses of leaf lipids from plants with differing carbon dioxide metabolisms. *Organic Geochemistry*, 21: 619-627.
- Cranston, R.E., 1997. Organic carbon burial rates across the Arctic Ocean from the 1994 Arctic Ocean Section expedition. *Deep-Sea Research II*, 44: 1705-1723.

- Darby, D.A., Bischof, J.F., Jones, G.A., 1997. Radiocarbon chronology of depositional regimes in the western Arctic Ocean. *Deep-Sea Research II*, 44: 1745-1757.
- Dickens, A.F., Gélina, Y., Masiello, C.A., Wakeham, S., Hedges, J.I., 2004. Reburial of fossil organic carbon in marine sediments. *Nature*, 427: 336-339.
- Di-Giovanni, C., Disnar, J.R., Macaire, J.J., 2002. Estimation of the annual yield of organic carbon released from carbonates and shales by chemical weathering. *Global and Planetary Change*, 32: 195-210.
- Dixon, R.K., Brown, S., Houghten, R.A., Solomon, A.M., Trexler, C., Wisniewski, J., 1994. Carbon pools and flux of global forest ecosystems. *Science*, 263: 185-190.
- Eglinton, T.I., 1994. Carbon isotopic evidence for the origin of macromolecular aliphatic structures in kerogen. *Organic Geochemistry*, 21: 721-735.
- Eglinton, T.I., Aluwihare, L.I., Bauer, J.E., Druffel, E.R.M., McNichol, A.P., 1996. Gas chromatographic isolation of individual compounds from complex matrices for radiocarbon dating. *Analytical Chemistry*, 68: 904-912.
- Eglinton, T.I., Benitez-Nelson, B.C., Pearson, A., McNichol, A.P., Bauer, J.E., Druffel, E.R.M., 1997. Variability in radiocarbon ages of individual organic compounds from marine sediments. *Science*, 277: 796-799.
- Eglinton, T.I., Eglinton, G., Dupont, L., Sholkovitz, E.R., Montluçon, D., Reddy, C.M., 2002. Composition, age, and provenance of organic matter in NW African dust over the Atlantic Ocean. *Geochemistry, Geophysics, Geosystems*, 3.
- Forman, S.L., Polyak, L., 1997. Radiocarbon content of pre-bomb marine mollusks and variations in the ^{14}C reservoir age for coastal areas of the Barents and Kara seas, Russia. *Geophysical Research Letters*, 24: 885-888.
- Goñi, M.A., Ruttenberg, K.C., Eglinton, T.I., 1998. A reassessment of the sources and importance of land-derived organic matter in surface sediments from the Gulf of Mexico. *Geochimica et Cosmochimica Acta*, 62: 3055-3075.
- Goñi, M.A., Yunker, M.B., Macdonald, R.W., Eglinton, T.I., 2000. Distribution and sources of organic biomarkers in arctic from the Mackenzie River and Beaufort Shelf. *Marine Chemistry*, 71: 23-51.
- Goñi, M.A., Yunker, M.B., Macdonald, R.W., Eglinton, T.I., 2005. The supply and preservation of ancient and modern components of organic carbon in the Canadian Beaufort Shelf of the Arctic Ocean. *Marine Chemistry*, 93: 53-73.
- Goulden, M.L., Wofsy, S.C., Harden, J.W., Trumbore, S.E., Crill, P.M., Gower, S.T., Fries, T., Daube, B.C., Fran, S.-M., Sutton, D.J., Bazzaz, A., Munger, J.W., 1998. Sensitivity of boreal forest carbon balance to soil thaw. *Science*, 279: 214-217.
- Grantz, A., Phillips, R.L., Mullen, M.W., Starratt, S.W., Jones, G.A., Naidu, A.S., Finney, B.P., 1996. Character, paleoenvironment, rate of accumulation, and evidence for seismic triggering of Holocene turbidites, Canada Abyssal Plain, Arctic Ocean. *Marine Geology*, 133: 51-73.
- Guo, L., Santschi, P.H., Cifuentes, L.A., Trumbore, S.E., Southon, J., 1996. Cycling of high-molecular-weight dissolved organic matter in the Middle Atlantic Bight as revealed by carbon isotopic (^{13}C and ^{14}C) signatures. *Limnology and Oceanography*, 41: 1242-1252.

Guo, L., Semiletov, I., Gustafsson, Ö., Ingri, J., Andersson, P., Dudarev, O., White, D., 2004. Characterization of Siberian Arctic coastal sediments: Implications for terrestrial organic carbon export. *Global Biogeochemical Cycles*, 18: GB1036, doi: 10.1029/2003GB002087.

Harper, J.R., Penland, P.S., 1982. Beaufort Sea sediment dynamics. Contract report to Atlantic Geosciences Centre, Geological Survey of Canada.

Hassol, S.J., 2004. Impacts of a Warming Arctic: Arctic Climate Impact Assessment. Cambridge University Press, Cambridge.

Hayes, J.M., 1993. Factors controlling ^{13}C contents of sedimentary organic compounds: Principles and evidence. *Marine Geology*, 113: 111-125.

Hedges, J.I., Eglinton, G., Hatcher, P.G., Kirchman, D.L., Arnosti, C., Derenne, S., Evershed, R.P., Kögel-Knabner, I., de Leeuw, J.W., Littke, R., Michaelis, W., Rullkötter, J., 2000. The molecularly-uncharacterized component of nonliving organic matter in natural environments. *Organic Geochemistry*, 31: 945-958.

Hedges, J.I., Keil, R.G., Benner, R., 1997. What happens to terrestrial organic matter in the ocean? *Organic Geochemistry*, 27: 195-212.

Hedges, J.I., Oades, J.M., 1997. Comparative organic geochemistries of soils and marine sediments. *Organic Geochemistry*, 27: 319-361.

Höld, I.M., Schouten, S., Van Kaam-Peters, H.M.E., Sinninghe Damsté, J.S., 1998. Recognition of *n*-alkyl and isoprenoidal algaenans in marine sediments by stable carbon isotopic analysis of pyrolysis products of kerogens. *Organic Geochemistry*, 28: 179-194.

Hollander, D.J., McKenzie, J.A., 1991. CO_2 control on carbon-isotope fractionation during aqueous photosynthesis: A paleo- CO_2 barometer. *Geology*, 19: 929-932.

Huang, Y., Dupont, L., Sarnthein, M., Hayes, J.M., Eglinton, G., 2000. Mapping of C_4 plant input from North West Africa into North East Atlantic sediments. *Geochimica et Cosmochimica Acta*, 64: 3505-3513.

Keil, R.G., Mayer, L.M., Quay, P.D., Richey, J.E., Hedges, J.I., 1997. Loss of organic matter from riverine particles in deltas. *Geochimica et Cosmochimica Acta*, 61: 1507-1511.

Komada, K., Druffel, E.R.M., Trumbore, S.E., 2004. Oceanic export of relict carbon by small mountainous rivers. *Geophysical Research Letters*, 31: doi:10.1029/2004GL019512.

Lockheart, M.J., van Bergen, P.F., Evershed, R.P., 1997. Variations in the stable carbon isotope compositions of individual lipids from the leaves of modern angiosperms: Implications for the study of higher plant-derived sedimentary organic matter. *Organic Geochemistry*, 26: 137-153.

Macdonald, R.W., Iseki, K., O'Brien, M.C., McLaughlin, F.A., McCullough, D., Macdonald, D.M., Carmack, E.C., Adams, H., Yunker, M.B., Miskulin, G., Buckingham, S., 1988. NOGAP B.6; Volume 4: Chemical data collected in the Beaufort Sea, Summer, 1987. Canadian Data Report of Hydrography and Ocean Sciences, 60: 1-103.

Macdonald, R.W., Naidu, A.S., Yunker, M.B., Gobeil, C., 2004. The Beaufort Sea: Distribution, sources, fluxes, and burial of organic carbon. In Stein and Macdonald

(Eds.), *The Organic Carbon Cycle in the Arctic Ocean*. Springer, Berlin, Germany, pp. 177-193.

Macdonald, R.W., Sieberg, D., Pearson, R., Paton, D., O'Brien, M.C., McLaughlin, F.A., Carmack, E.C., 1992. Oceanographic data collected from the *Henry Larsen* in the Beaufort Sea, September 1991. Canadian Data Report of Hydrography and Ocean Sciences, 112: 1-108.

Macdonald, R.W., Solomon, S.M., Cranston, R.E., Welch, H.E., Yunker, M.B., Gobeil, C., 1998. A sediment and organic carbon budget for the Canadian Beaufort Shelf. *Marine Geology*, 144: 255-273.

Masiello, C.A., Druffel, E.R.M., 2001. Carbon isotope geochemistry of the Santa Clara River. *Global Biogeochemical Cycles*, 15: 407-416.

Matsumoto, K., Kawamura, K., Uchida, M., Shibata, Y., Minoru, Y., 2001. Compound-specific radiocarbon and $\delta^{13}\text{C}$ measurements of fatty acids in a continental aerosol sample. *Geophysical Research Letters*, 28: 4587-4590.

Mayer, L.M., 1994. Surface area control of organic carbon accumulation in continental shelf sediments. *Geochimica et Cosmochimica Acta*, 58: 1271-1284.

Megens, L., van der Plicht, J., de Leeuw, J.W., 2001. Temporal variations in ^{13}C and ^{14}C concentrations in particulate organic matter from the southern North Sea. *Geochimica et Cosmochimica Acta*, 65: 2899-2911.

Millot, R., Gaillardet, J., Dupré, B., Allège, C.J., 2003. Northern latitude chemical weathering rates: Clues from the Mackenzie River Basin, Canada. *Geochimica et Cosmochimica Acta*, 67: 1305-1329.

Mollenhauer, G., Eglinton, T.I., Ohkouchi, N., Schneider, R.R., Müller, P.J., Grootes, P.M., Rullkötter, J., 2003. Asynchronous alkenone and foraminifera records from the Benguela upwelling system. *Geochimica et Cosmochimica Acta*, 67: 2157-2171.

Nguyen Tu, T.T., Derenne, S., Largeau, C., Bardoux, G., Mariotti, A., 2004. Diagenesis effects on specific carbon isotope composition of plant n-alkanes. *Organic Geochemistry*, 35: 317-329.

Ohkouchi, N., Eglinton, T.I., Hayes, J.M., 2003. Radiocarbon dating of individual fatty acids as a tool for refining Antarctic margin sediment chronologies. *Radiocarbon*, 45: 17-24.

Pancost, R.D., Boot, C.S., 2004. The palaeoclimatic utility of terrestrial biomarkers in marine sediments. *Marine Chemistry*, 92: 239-261.

Pearson, A., Eglinton, T.I., 2000. The origin of n-alkanes in Santa Monica Basin surface sediment: a model based on compound-specific $\Delta^{14}\text{C}$ and $\delta^{13}\text{C}$ data. *Organic Geochemistry*, 31: 1103-1116.

Pearson, A., McNichol, A.P., Benitez-Nelson, B.C., Hayes, J.M., Eglinton, T.I., 2001. Origins of lipid biomarkers in Santa Monica Basin surface sediment: A case study using compound-specific $\Delta^{14}\text{C}$ analysis. *Geochimica et Cosmochimica Acta*, 65: 3123-3137.

Petsch, S.T., 2003. The global oxygen cycle. In: Holland, H.D., Turekian, K.K. (Eds.), *Treatise on Geochemistry*. Elsevier, Amsterdam, The Netherlands, pp. 515-555.

Petsch, S.T., Berner, R.A., Eglinton, T.I., 2000. A field study of the chemical weathering of ancient sedimentary organic matter. *Organic Geochemistry*, 31: 475-487.

Petsch, S.T., Eglinton, T.I., Edwards, K.J., 2001. ^{14}C -dead living biomass: Evidence for microbial assimilation of ancient organic carbon during shale weathering. *Science*, 292: 1127-1131.

Phillips, R.L., Grantz, A., Mullen, M.W., White, J.M., 1991. Preliminary lithostratigraphy of piston cores from the Beaufort Sea continental slope off northeastern Alaska. In: U.S. Geological Survey Open-File Report 91-34: 2 sheets.

Prahl, F.G., Ertel, J.R., Goñi, M.A., Sparrow, M.A., Eversmeyer, B., 1994. Terrestrial organic carbon contributions to sediments on the Washington margin. *Geochimica et Cosmochimica Acta*, 58: 3035-3048.

Rachold, V., Eicken, H., Gordeev, V.V., Grigoriev, M.N., Hubberten, H.-W., Lisitzin, A.P., Shevchenko, V.P., Schirrmeister, L., 2004. Modern terrigenous organic carbon input to the Arctic Ocean. In Stein and Macdonald (Eds.), *The Organic Carbon Cycle in the Arctic Ocean*. Springer, Berlin, Germany, pp. 33-55.

Raymond, P.A., Bauer, J.E., 2001. Use of ^{14}C and ^{13}C natural abundances for evaluating riverine, estuarine, and coastal DOC and POC sources and cycling: a review and synthesis. *Organic Geochemistry*, 32: 469-485.

Rethemeyer, J., Grootes, P.M., Bruhn, F., Andersen, N., Nadeau, M.J., Kramer, C., Gleixner, G., 2004a. Age heterogeneity of soil organic matter. *Nuclear Instruments and Methods in Physics Research B*, 223-224: 521-527.

Rethemeyer, J., Kramer, C., Gleixner, G., Wiesenberger, G.L.B., Schwark, L., Andersen, N., Nadeau, M.-J., Grootes, P.M., 2004b. Complexity of soil organic matter: AMS ^{14}C analysis of soil lipid fractions and individual compounds. *Radiocarbon*, 46: 465-473.

Ruttenberg, K.C., Goñi, M.A., 1997. Phosphorus distribution, C:N:P ratios, and $\delta^{13}\text{COC}$ in arctic, temperate, and tropical coastal sediments: tools for characterizing bulk sedimentary organic matter. *Marine Geology*, 139: 123-145.

Schiff, S.L., Aravena, R., Trumbore, S.E., Hinton, M.J., Elgood, R., Dillon, P.J., 1997. Export of DOC from forested catchments on the Precambrian Shield of central Ontario: Clues from ^{13}C and ^{14}C . *Biogeochemistry*, 36: 43-65.

Schubert, C.J., Calvert, S.E., 2001. Nitrogen and carbon isotopic composition of marine and terrestrial organic matter in Arctic Ocean sediments: implications for nutrient utilization and organic matter composition. *Deep Sea Research I*, 48: 789-810.

Schubert, C.J., Stein, R., 1997. Lipid distribution in surface sediments from the eastern central Arctic Ocean. *Marine Geology*, 138: 11-25.

Stein, R., Fahl, K., 2004. The Laptev Sea: Distribution, sources, variability, and burial of organic carbon. In Stein and Macdonald (Eds.), *The Organic Carbon Cycle in the Arctic Ocean*. Springer, Berlin, Germany, pp. 177-193.

Schouten, S., Breteler, W.C.M.K., Blokker, P., Schogt, N., Rupstra, I.C., Grice, K., Baas, M., Sinninghe Damsté, J.S., 1998. Biosynthetic effects on the stable carbon isotopic composition of algal lipids: Implications for deciphering the carbon isotopic biomarker record. *Geochimica et Cosmochimica Acta*, 62: 1397-1406.

Stendel, M., Christensen, J.H., 2002. Impact of global warming on permafrost conditions in a coupled GCM. *Geophysical Research Letters*, 29.

Sun, M.-Y., Zou, L., Dai, J., Ding, H., Culp, R.A., Scranton, M.I., 2004. Molecular carbon isotopic fractionation of algal lipids during decomposition in natural oxic and anoxic seawaters. *Organic Geochemistry*, 35: 895-908.

Trumbore, S.E., Bubier, J.L., Harden, J.W., Crill, P.M., 1999. Carbon cycling in boreal wetlands: A comparison of three approaches. *Journal of Geophysical Research*, 104: 27,673-27,682.

Uchida, M., Shibata, Y., Kawamura, K., Kumamoto, Y., Yoneda, M., Ohkushi, K., Harada, N., Hirota, M., Mukai, H., Tanaka, A., Kusakabe, M., Morita, M., 2001. Compound-specific radiocarbon ages of fatty acids in marine sediments from the western north Pacific. *Radiocarbon*, 43: 949-956.

Uchida, M., Shibata, Y., Kawamura, K., Yoneda, M., Mukai, H., Tanaka, A., Uehiro, T., Morita, M., 2000. Isolation of individual fatty acids in sediments using preparative capillary gas chromatography (PCGC) for radiocarbon analysis at NIES-TERRA. *Nuclear Instruments and Methods in Physics Research B*, 172: 583-588.

van Dongen, B.E., Schouten, S., Sinninghe Damste, J.S., 2002. Carbon isotope variability in monosaccharides and lipids of aquatic algae and terrestrial plants. *Marine Ecology Progress Series*, 232: 83-92.

Wakeham, S.G., Hedges, J.I., Lee, C., Peterson, M.L., Hernes, P.J., 1997. Compositions and transport of lipid biomarkers through the water column and surficial sediments of the equatorial Pacific Ocean. *Deep-Sea Research II*, 44: 2131-2162.

Wiesenberg, G.L.B., Schwarzbauer, J., Schmidt, M.W.I., Schwark, L., 2004. Source and turnover of organic matter in agricultural soils derived from *n*-alkane/*n*-carboxylic acid compositions and C-isotope signatures. *Organic Geochemistry*, 35: 1371-1393.

Yunker, M.B., Belicka, L.L., Harvey, H.R., Macdonald, R.W. Tracing the inputs and fate of marine and terrigenous organic matter in Arctic Ocean sediments: A multivariate analysis of lipid biomarkers. *Deep-Sea Research II*, in press.

Yunker, M.B., Macdonald, R.W., Cretney, W.J., Fowler, B.R., McLaughlin, F.A., 1993. Alkane, terpene and polycyclic aromatic hydrocarbon geochemistry of the Mackenzie River and Mackenzie shelf: Riverine contributions to Beaufort Sea coastal sediment. *Geochimica et Cosmochimica Acta*, 57: 3041-3061.

Yunker, M.B., Backus, S.M., Pannatier, E.G., Jeffries, D.S., Macdonald, R.W., 2002. Sources and significance of alkane and PAH hydrocarbons in Canadian arctic rivers. *Estuarine and Coastal Shelf Science*, 55: 1-31.

Yunker, M.B., Macdonald, R.W., Velthkamp, D.J., Cretney, W.J., 1995. Terrestrial and marine biomarkers in a seasonally ice-covered Arctic estuary – integration of multivariate and biomarker approaches. *Marine Chemistry*, 49: 1-50.

Yunker, M.B., Snowdon, L.R., Macdonald, R.W., Smith, J.N., Fowler, M.G., Skibo, D.N., McLaughlin, F.A., Danyushevskaya, A.I., Petrova, V.I., Ivanov, G.I., 1996. Polycyclic aromatic hydrocarbon composition and potential sources for sediment samples from the Beaufort and Barents Seas. *Environmental Science and Technology*, 30: 1310-1320.

Zegouagh, Y., Derenne, S., Largeau, C., Bardoux, G., Mariotti, A., 1998. Organic matter sources and early diagenetic alterations in Arctic surface sediments (Lena River delta and Laptev Sea, Eastern Siberia), II. Molecular and isotopic studies of hydrocarbons. *Organic Geochemistry*, 28: 571-583.

CHAPTER 3

APPLICATION OF THE COUPLED MOLECULAR ISOTOPE APPROACH TO A SMALL MOUNTAINOUS SYSTEM: THE EEL RIVER MARGIN

ABSTRACT

Recent radiocarbon-based studies have suggested that $\geq 50\%$ of the organic carbon (OC) currently being buried in continental margin sediments by small mountainous rivers might be the product of ancient sedimentary rock weathering. These investigations rely on the assumption that vascular plant detritus spends little time sequestered in terrestrial reservoirs such as soils and wetlands before delivery to adjacent shelves, and thus only minimally contributes to the extraneously old ^{14}C ages of total organic carbon often observed in margin sediments. Here I test this paradigm by measuring the $\Delta^{14}\text{C}$ compositions of individual fatty acids extracted from sediments from the Eel River Margin (coastal California). The signatures for the long chain homologues derived from the epicuticular coatings of leaves indicate that vascular plant OC has been 'pre-aged' on land for several thousand years before sedimentary incorporation. A coupled molecular isotope mass balance used to reassess the carbon budget on the shelf indicates that fossil material is less abundant than previous estimates, with pre-aged terrestrial detritus instead comprising the majority of OC. If these findings are characteristic of other shelf sediments adjacent to small mountainous rivers, then current

estimates of petrogenic OC burial in marine sediments world-wide may need to be adjusted downward.

3.0 INTRODUCTION

The transfer of terrigenous organic carbon (OC) from continents to the sea and its ultimate fate therein plays an important role in regulating the global carbon and oxygen cycles and hence past and future climate (Berner, 1989; Petsch, 2003; Burdige, 2005). Rivers are believed to carry the majority (~ 75 %) of this flux in either dissolved (DOC) or particulate (POC) form at a total rate of $400 \text{ to } 430 \times 10^{12} \text{ g yr}^{-1}$ (Hedges et al., 1997; Schlünz and Schneider, 2000), of which perhaps > 90 % undergoes abiotic and biotic remineralization using a succession of oxidants in both the water column and the upper meter or so of underlying sediments (Hedges et al., 1997). The majority of the remaining portion is presumably buried, with some structural modification, in the deeper sediments that build river deltas and on the adjacent continental margins (Hedges and Keil, 1995; Burdige, 2005). The ability of this OC to survive early diagenesis and the effect of its ultimate burial on the oxidation state of the atmosphere may likewise be influenced by its molecular composition and mineral association (Keil et al., 1997). For example, the rigidifying tissues of vascular plants (e.g. lignin and cutin) are more highly reduced and more likely to be closely associated with mineral matrices than other biopolymers such as proteins and carbohydrates, possibly enhancing their resistance to oxidation and increasing their residence times in soils (Hedges and Keil, 1995; Leavitt et al., 1996; Rethemeyer et al., 2004a, 2005).

Recent, primarily ^{14}C -based studies have also suggested that petrogenic OC (also known as fossil OC or kerogen) weathered from organic-rich sedimentary rocks (shales) might comprise a significant portion of the organic matter currently buried in certain

shelf sediments (Blair et al., 2003, 2004; Dickens et al., 2004; Komada et al., 2004, 2005; Goñi et al., 2005; Hwang et al., 2005). This material is radiocarbon ‘dead’ ($\Delta^{14}\text{C} = -1000$ ‰), presumably largely refractory, and likely associated with clay-sized minerals, having experienced late diagenetic and catagenetic modification in the lithosphere for $> 10^6$ years. It also represents the largest reservoir of organic matter on Earth at 15×10^{21} g (Hedges, 1992) (see Figure 4.1 in Chapter 4 of this thesis), from which perhaps 10^{14} g may be released each year (Di-Giovanni et al., 2002) through a combination of physical erosion and selective oxidation (Petsch et al., 2000, 2001a). Indeed, the persistence of non-contemporary radiocarbon ages in fluvial DOC, POC, bulk lipid fractions, and shallow sedimentary OC in an array of margin systems imply that some fossil material is able to evade further remineralization in these settings (Raymond and Bauer, 2001a,b; Komada et al., 2004, 2005; Goñi et al., 2005; Hwang et al., 2005; Yunker et al., in press). Although bacterial assimilation of petrogenic carbon has been demonstrated (Petsch et al., 2001b, 2003), the majority might therefore be efficiently recycled through the modern environment by rapid reburial in deep sediments.

However, anomalous bulk-level ^{14}C depletion may also result from the incorporation of vascular plant detritus that has been pre-aged in soils and wetlands for many millennia (Perruchoud et al., 1999; Masiello and Druffel, 2001; Rathemeyer et al., 2004a,b), confounding the exclusive attribution of this phenomenon to the presence of petrogenic OC. Such ambiguity can be mitigated by alternatively using the isotopic signatures of their corresponding biomarkers as endmembers in isotope mass balance calculations. Alkanoic (fatty) acids are particularly convenient in this regard as

homologues $\geq nC_{24}$ found in sediments are typically attributable to vascular plants, whereas those $\leq nC_{22}$ are usually derived mostly from marine algae and/or bacteria. Here I apply this approach to the Eel River Margin system using the $\delta^{13}C$ and $\Delta^{14}C$ compositions of individual fatty acids in an effort to more accurately apportion the sources of OC in coastal sediments adjacent to a small, mountainous river system.

Located between Cape Mendocino and Trinidad Head, CA (Figure 3.1), the ~ 20 km wide Eel shelf itself can be characterized as a subaqueous floodplain that sequesters roughly 20 % of the $\sim 14 \times 10^{10}$ g terrigenous OC supplied each year by the adjacent Eel River (Sommerfield and Nittrouer, 1999; Walsh and Nittrouer, 1999). The river and its tributaries drain a relatively small but rugged headwater terrain of some 8640 km² which is elevated ~ 2000 m above sea level at its maximum and largely underlain by readily erodible soils and shale *mélange* of the Mesozoic Franciscan Complex (Sommerfield and Nittrouer, 1999; Blair et al., 2003, 2004). Consequently, the annual sediment load of the Eel River (upwards of 23×10^{12} g) normalized to drainage basin size is the highest within the contiguous U.S. (Brown and Ritter, 1971), of which > 80 % is delivered to the adjacent margin during winter storms (Sommerfield and Nittrouer, 1999; Sommerfield et al., 1999). On an interannual timescale, major rainfall events resulting from large, climatically-driven storms have triggered the episodic deposition of clay-rich flood layers interbedded with the surrounding silts over much of the Eel shelf (Wheatcroft et al 1997; Sommerfield and Nittrouer, 1999; Sommerfield et al., 1999, 2002; Leithold and Blair, 2001; Leithold and Hope, 2001). Elemental and isotopic investigation of these flood deposits have lead previous investigators to conclude that they represent the primary

vehicle by which petrogenic input survives oxidation to overwhelm other sources of OC in Eel River Margin sediments (Leithold and Blair, 2001; Blair et al., 2003, 2004; Leithold et al., 2005). Here I test this interpretation using the coupled molecular isotope mass balance approach developed in Chapter 2.

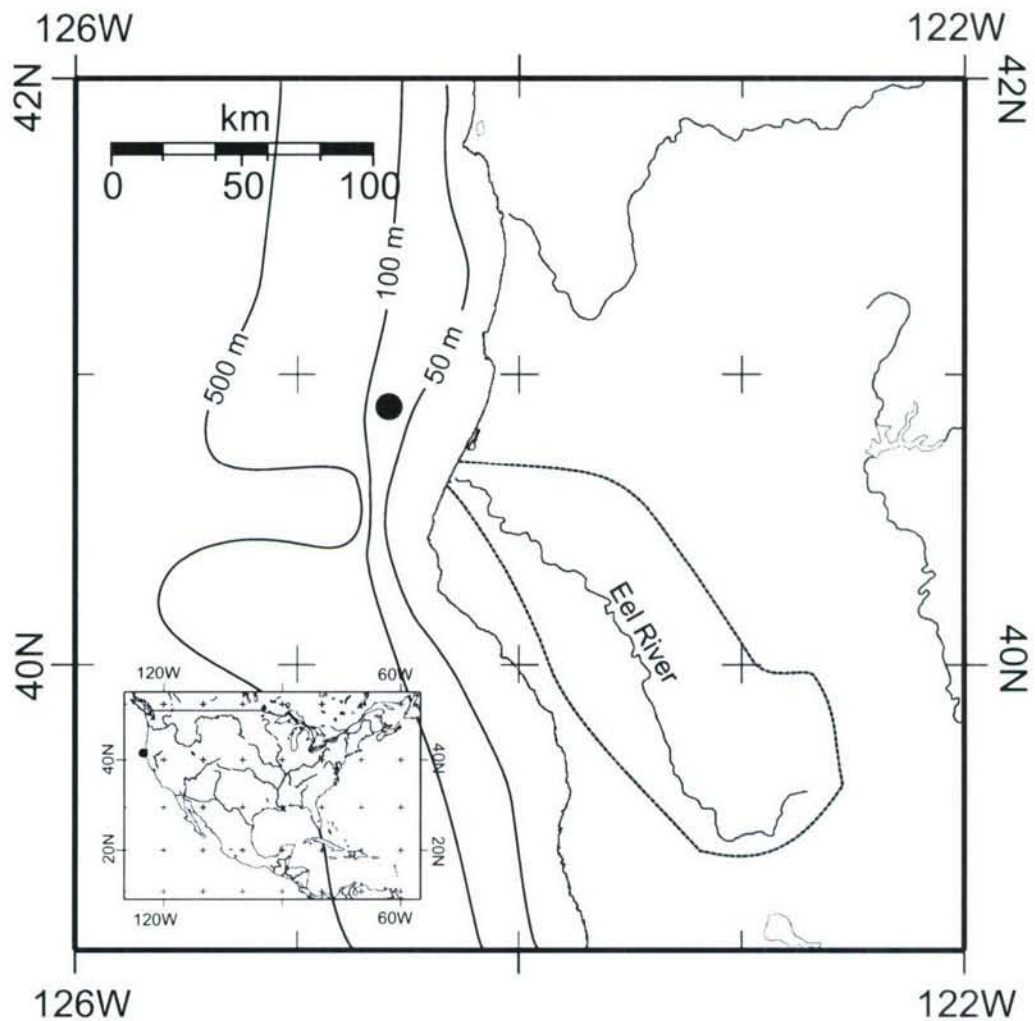


FIGURE 3.1 – Map of the Eel River Margin and the approximate boundaries of the adjacent Eel River drainage basin. The location from which GGC 5 and MC 36 were retrieved is also indicated.

3.1 METHODS

A 1.15 m long gravity core (GGC 5) and a 0.30 m long multicore (MC 36) (among others) were raised from 70 m water depth on the Eel River Margin during a cruise aboard the R/V *New Horizon* in June 2001. GGC 5 was transported back to Woods Hole Oceanographic Institution (WHOI) and stored at $\sim 4^{\circ}\text{C}$, whereas MC 36 was sectioned on deck into 1 cm intervals immediately after recovery and stored frozen. GGC 5 was subsequently split lengthwise and photographed. Light, clay-rich flood layers were visible in the upper portion of the split core, and likely represent deposition during previously recorded Eel River flood stages (Figure 3.2). The core surface was then scanned for the relative X-ray emission intensities of twenty six transition metals using a Cox Analytical Systems™ X-ray fluorescence (XRF) instrument (200 μm increments for 800 ms per step) in order to aid the identification of the flood deposits, though it should be noted that this technique only yields qualitative information. The entire core was then sectioned in 1 cm intervals for the ensuing geochemical analyses.

A detailed description of the remaining methods employed in this study can be found in Chapter 4 of this thesis. Briefly, every sediment horizon from GGC-5 and MC-36 was freeze dried, homogenized via grinding, and analyzed for their bulk elemental (C and N) compositions. Select horizons from both cores were measured for ^{210}Pb and ^{137}Cs activity by gamma spectrometry, and for the $\delta^{13}\text{C}$ and $\Delta^{14}\text{C}$ composition of TOC at the National Ocean Sciences Accelerator Mass Spectrometry (NOSAMS) facility at WHOI. Sediments from a subset of those GGC 5 intervals were then spiked with an internal recovery standard and extracted using an Accelerated Solvent Extractor (ASE) to obtain

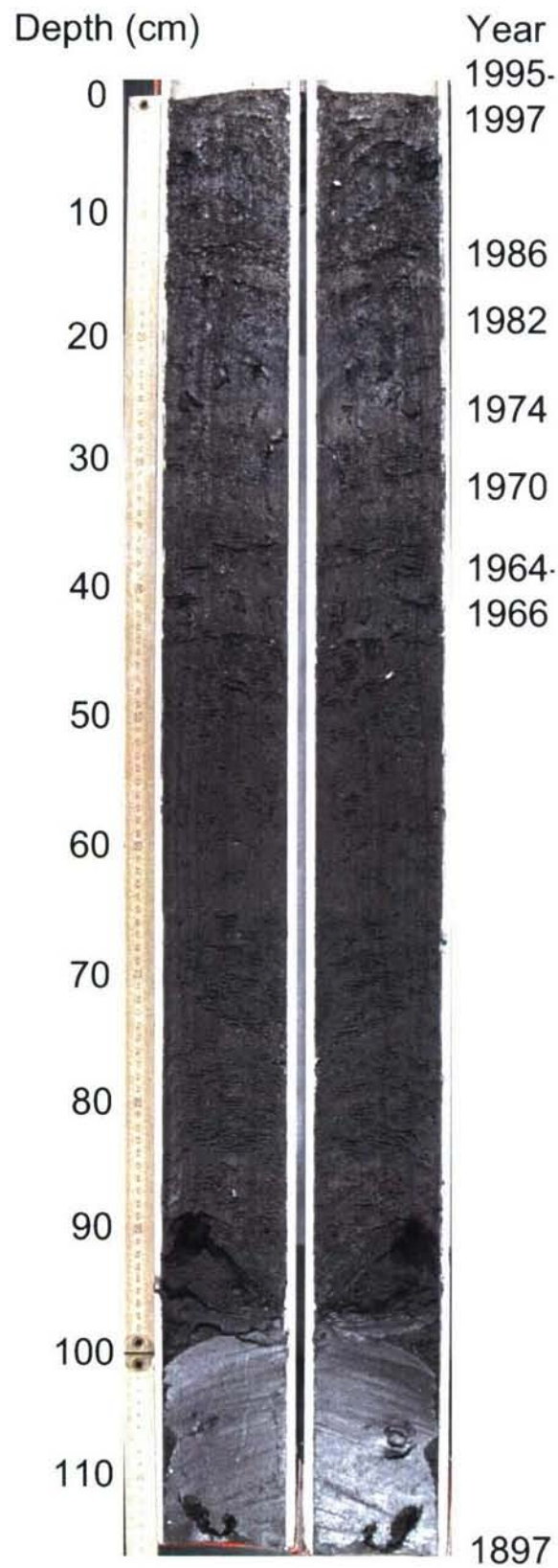


FIGURE 3.2 – Photograph of the split GGC 5 core with an approximate depth scale (cm) given at the left margin. Flood layers assigned to the years given in the right margin are visible as lighter (clay rich) bands. The approximate year of deposition for sediments at the base of the core is also given.

their total lipid extracts (TLEs). Each TLE was eluted through a fully activated silica gel column to isolate an unbound fatty acid fraction, which was subsequently esterified by acidic methanol of known isotopic composition and eluted through a second column containing 5 % deactivated silica gel to further purify a series of fatty acid methyl esters (FAMES). The abundance and $\delta^{13}\text{C}$ composition of each fatty acid homologue was determined by gas chromatography / flame ionization detection (GC/FID) and gas chromatography / isotope ratio mass spectrometry (GC/IRMS), respectively. Individual FAMES were then isolated by preparative capillary gas chromatography (PCGC), checked for purity and recovery by GC/FID, transferred to quartz tubes, combusted to CO_2 , stripped of impurities, reduced to graphite, and measured at either NOSAMS or at the Keck Carbon Cycle Accelerator Mass Spectrometry (KCCAMS) facility at the University of California, Irvine, along with several procedural standards. All of the $\delta^{13}\text{C}$ and $\Delta^{14}\text{C}$ compositions of fatty acids reported below have been corrected for the addition of a methyl group during esterification.

3.2 RESULTS & DISCUSSION

3.2.1 Chronology development

Episodic flood deposition and many subsequent resuspension cycles lead to abrupt changes in sedimentation rate across the Eel River Margin (Leithold and Hope, 1999; Sommerfield et al., 1999; Walsh and Nittrouer, 1999) and thus interfere with attempts to establish a coherent, down core age model. Flood deposits also contain low ^{210}Pb activities relative to surrounding sediments due to incomplete scavenging of ^{210}Pb from the overlying water column during their rapid emplacement (Sommerfield and

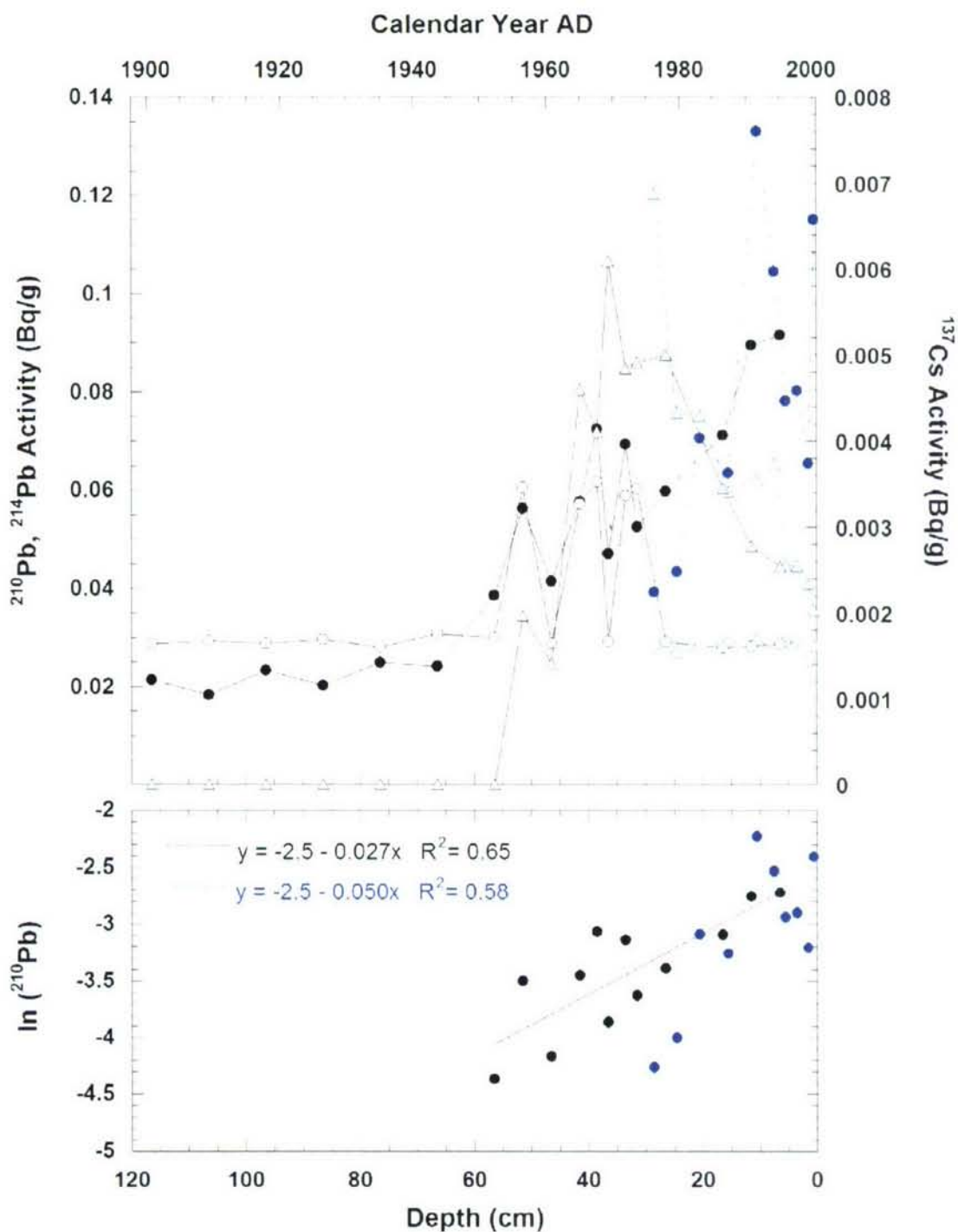


FIGURE 3.3 – Chronology development for Eel River Margin cores. Upper panel: Profiles of unsupported ^{210}Pb (filled circles), ^{214}Pb (open circles), and ^{137}Cs (open triangles) for GGC 5 (black symbols) and MC 36 (blue symbols). Analytical uncertainties for ^{210}Pb , ^{214}Pb , and ^{137}Cs measurements were generally ± 0.004 , 0.0008 , and 0.0003 Bq/g, respectively. Lower panel: Unsupported $\ln(^{210}\text{Pb})$ activity vs depth for both cores, with best fit regressions shown.

Nittrouer, 1999; Sommerfield et al., 1999), and yet may simultaneously exhibit higher ^{137}Cs activities weathered from the inventory in adjacent soils. Unsurprisingly then, both isotopes display complex down core profiles in GGC 5 and MC 36 (Figure 3.3; Appendix 3.1). The ^{210}Pb profile is further complicated by a departure from secular equilibrium with ^{214}Pb in the lower half of GGC 5. Using only the unsupported data above this interval, average sedimentation rates are calculated to be 1.1 and 0.6 cm yr^{-1} for GGC 5 and MC 36, respectively, in broad agreement with other estimates for the mid-shelf (Sommerfield and Nittrouer, 1999; Leithold et al., 2005). Since gravity coring usually displaces several centimeters of surficial sediments, the sedimentation rate for GGC 5 was linked to an absolute time scale through comparison of its ^{210}Pb and ^{137}Cs activities to those of MC 36, assuming surficial sediment in the latter core was indeed intact. This approach indicates that slightly less than 6 cm was lost from the upper portion of GGC 5, implying that the 0-1 cm horizon therein was deposited in 1995. Calendar years for underlying sediments were then assigned by applying the mean accumulation rate calculated for GGC 5. Although previous work suggests this rate increased by a factor of three or so after 1954 due to changes in Pacific climate, shelf geomorphology, flood frequency, and/or adjacent land use (Sommerfield et al., 2002; Leithold et al., 2005), the aforementioned decline in the $^{210}\text{Pb}/^{214}\text{Pb}$ activity ratios to values of < 1 in the lower half of the core make it impossible to evaluate this effect here.

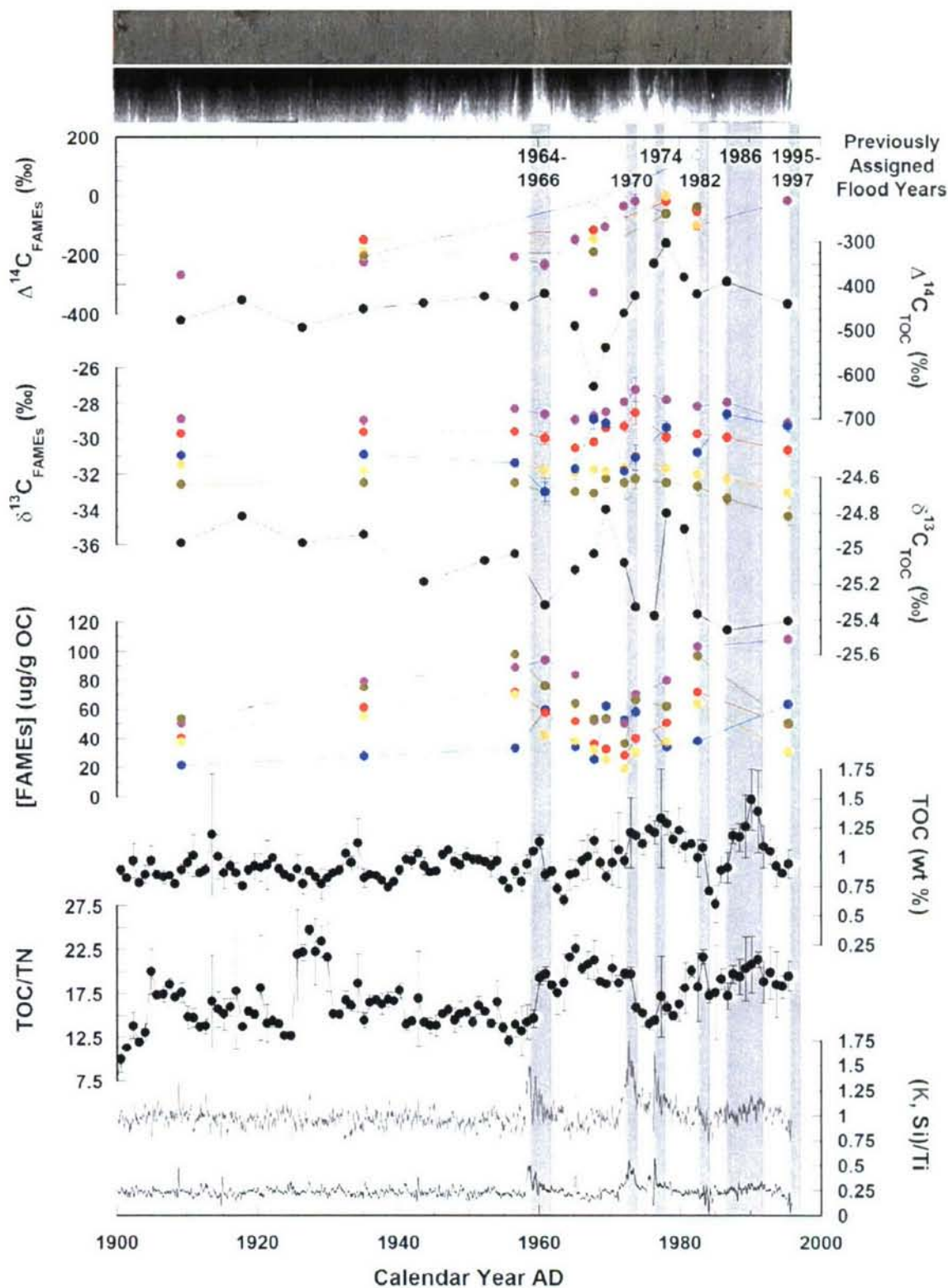


FIGURE 3.4 – Down core profiles for various bulk and molecular parameters in GGC 5. Colors for FAME data are as follows: nC_{16} (blue), nC_{24} (violet), nC_{26} (red), nC_{28} (orange), nC_{30+32} (olive). The $\Delta^{14}C$ values for nC_{16} are shown as open symbols as the analytical error bars exceed the given scale. Grey bars denote flood layers with previously assigned emplacement dates given at the top. Visible and X-radiographs of GGC 5 are shown above the plot; light regions in both correspond to clay-rich (flood) deposits.

3.2.2 Elemental and isotopic profiles

Bulk and molecular-level profiles of elemental and isotopic abundance are displayed in Figure 3.4 (also see Appendices 3.1 and 3.2). Comparisons amongst these proxies are robust since they are each plotted on the same chronology. As expected, high TOC/TN ratios and generally depleted values for $\delta^{13}\text{C}$ and $\Delta^{14}\text{C}$ relative to those expected for marine biomass both suggest that the OC in Eel River Margin sediments is primarily derived from pre-aged C_3 vegetation and/or shale erosion (Blair et al., 2003). Generally low abundances of short chain ($\leq n\text{C}_{22}$) fatty acids relative to their longer chain counterparts also suggest little input from autochthonous algal and/or bacterial production (Figure 3.5). Enrichments in their corresponding $\delta^{13}\text{C}$ signatures over those for the long chain homologues are likewise less than observed in most marine sediments, implying that the short chains are derived from a mixed vascular plant / marine algal source (Figure 3.6). The similar or somewhat more enriched $\Delta^{14}\text{C}$ compositions of $n\text{C}_{16}$ relative to $n\text{C}_{24}$, $n\text{C}_{26}$, $n\text{C}_{28}$, and $n\text{C}_{30+32}$ also support this notion, although analytical error associated with the former is large due to the ultra small mass of these particular samples ($< 4 \mu\text{g C}$; see Chapter 4 for a more detailed discussion). A notable exception is $n\text{C}_{18}$, whose $\delta^{13}\text{C}$ values [$\delta^{13}\text{C}_{18}$] are as much as $\sim 10 \text{ ‰}$ heavier, implying that this homologue might contain a larger contribution from the autotrophic fixation of mixed layer dissolved inorganic carbon (DIC). Irrespective of the above, the significant ^{14}C depletions in the more abundant long chain fatty acids and their apparent co-variation with those of TOC suggest a large portion of the terrigenous material is composed of pre-aged vascular plant detritus, and not only petrogenic carbon weathered from outcrops of the Franciscan

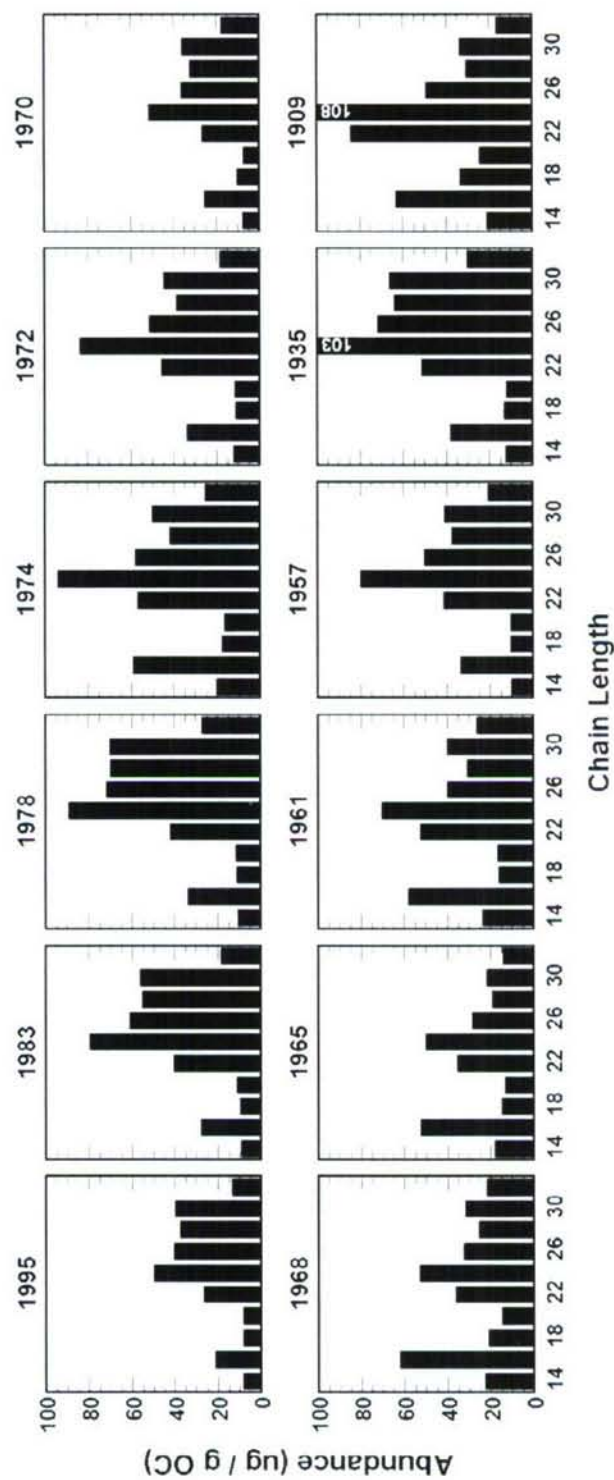


FIGURE 3.5 – Abundance of individual, even carbon numbered fatty acids normalized to sedimentary OC content for horizons investigated at the molecular level. Values for off-scale homologues are superimposed on their respective histogram bars.

Complex in the Eel River watershed as advanced by other investigations (Blair et al., 2003, 2004; Leithold et al., 2005),

Flood deposits can be readily identified by elevations in TOC/TN, K/Ti, and Si/Ti ratios in sediments and by light colored bands in visible and X-ray photographs (Leithold and Hope, 1999; Sommerfield and Nittrouer, 1999; Yarincik et al., 2000; Zabel et al., 2001) and are thus delineated by these criteria in Figure 3.4. Due to the uncertainty in the

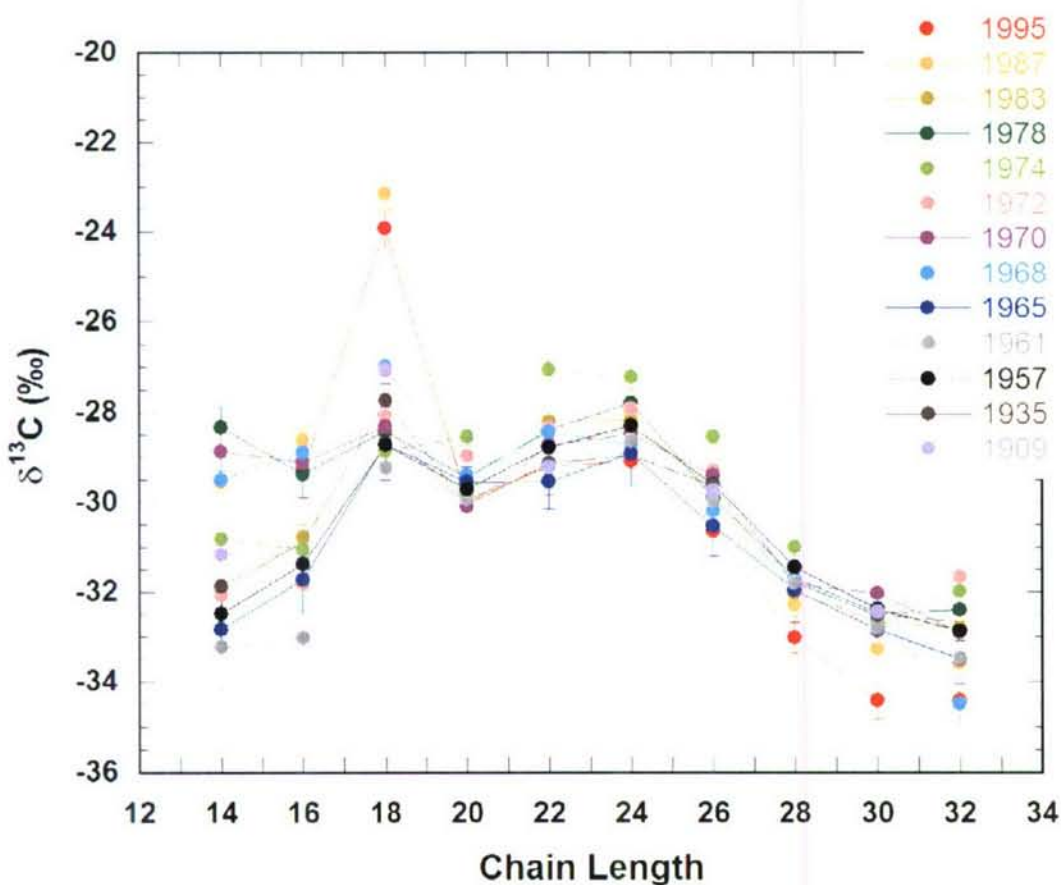


FIGURE 3.6 – Stable carbon isotopic compositions for individual, even carbon-numbered fatty acids as a function of chain length.

age model, it is not surprising that the dates for these events given by the chronology for GGC 5 do not exactly match those assigned in previous studies (Leithold and Blair, 2001; Sommerfield et al., 2002; Leithold et al., 2005), although they generally agree within a few years nonetheless. In accord with these investigations, however, major flood events only frequent the latter half of the century. Similar to observations by Leithold and Hope (1999), the accompanying TOC $\delta^{13}\text{C}$ depletions further suggest that the majority of the OC in these deposits is derived from vascular plants as opposed to sedimentary rocks, considering that the isotopic compositions for these endmembers are estimated as -26.5 and -24.3 ‰, respectively, in the Eel catchment (Blair et al., 2003). Additionally, noticeable depletions in the $\Delta^{14}\text{C}$ composition of TOC expected from the fossil signature of petrogenic carbon (i.e. -1000 ‰) are absent in these layers. In fact, the most depleted bulk $\Delta^{14}\text{C}$ values occur between flood layers and are coeval with some of the largest variations in ^{210}Pb and ^{214}Pb (Figure 3.3), possibly reflecting repeated cycles of physical scouring and/or redeposition from fast moving currents on the shelf (Leithold and Hope, 1999; Sommerfield et al., 1999; Walsh and Nittrouer, 1999).

3.2.3 Mass balance calculations

The proportion of pre-aged vascular plant ('terrestrial') OC in Eel River Margin sediments relative to those from petrogenic and marine sources can be more quantitatively estimated by incorporating their corresponding biomarker $\delta^{13}\text{C}$ and $\Delta^{14}\text{C}$ signatures as endmembers in the following dual isotope mass balance (see Chapter 2 for a more complete discussion),

$$f_T(\Delta^{14}C_T) + f_M(\Delta^{14}C_M) + f_P(\Delta^{14}C_P) = \Delta^{14}C_S \quad (1)$$

$$f_T(\delta^{13}C_T) + f_M(\delta^{13}C_M) + f_P(\delta^{13}C_P) = \delta^{13}C_S \quad (2)$$

$$f_T + f_M + f_P = 1 \quad (3)$$

where f is the fractional abundance and the subscripts T, M, P, and S are terrestrial, marine, and petrogenic carbon, and bulk sediment. Based on the source assignments discussed above, the stable carbon isotopic compositions of nC_{18} and nC_{32} are employed for $\delta^{13}C_M$ and $\delta^{13}C_T$, respectively, after being normalized for a 7 – 9 ‰ depletion from bulk biomass ($\delta^{13}C_{\text{biomass}} - \delta^{13}C_{\text{lipid}}$) (Collister et al., 1994; Schouten et al., 1998; van Dongen et al., 2002; Wiesenberg et al., 2004). Following correction for natural decay in the sedimentary column, the $\Delta^{14}C$ values of nC_{24} are equated to $\Delta^{14}C_T$ since they are similar to those for the longer homologues available but in greater number. Because of the large uncertainties and scant down-core coverage for the $\Delta^{14}C$ compositions of nC_{16} , and because its isotopic signatures suggest partial sourcing from vascular plants, $\Delta^{14}C_M$ values are instead derived from an annual re-sampling of the mixed layer $DI^{14}C$ record compiled by Pearson (1999) for the nearby southern California Bight. Finally, in the absence of molecular-level isotopic information for the petrogenic endmember, values of -24.3 ‰ (interpolated by Blair et al. [2003]) and -1000 ‰ (assumed) are used for $\delta^{13}C_P$ and $\Delta^{14}C_P$.

Results are shown in Figure 3.7. In agreement with the qualitative assessment given above, pre-aged vascular plant material dominates the OC budget at all depths in Eel Margin sediments, with petrogenic debris comprising the remainder. The slightly negative values calculated for f_M are likely a consequence of a mixed marine / vascular

plant source for $\delta^{13}\text{C}_{18}$ (and hence $\delta^{13}\text{C}_M$) and uncertainty in the value of $\delta^{13}\text{C}_P$, but nonetheless underscore the minimal marine contribution to TOC. Moreover, these fractional abundances do not appreciably change in flood deposits, suggesting that while floods increase the flux of pre-aged vascular plant and petrogenic OC to the margin, their relative proportions remain similar. The largest variations are driven by the period of

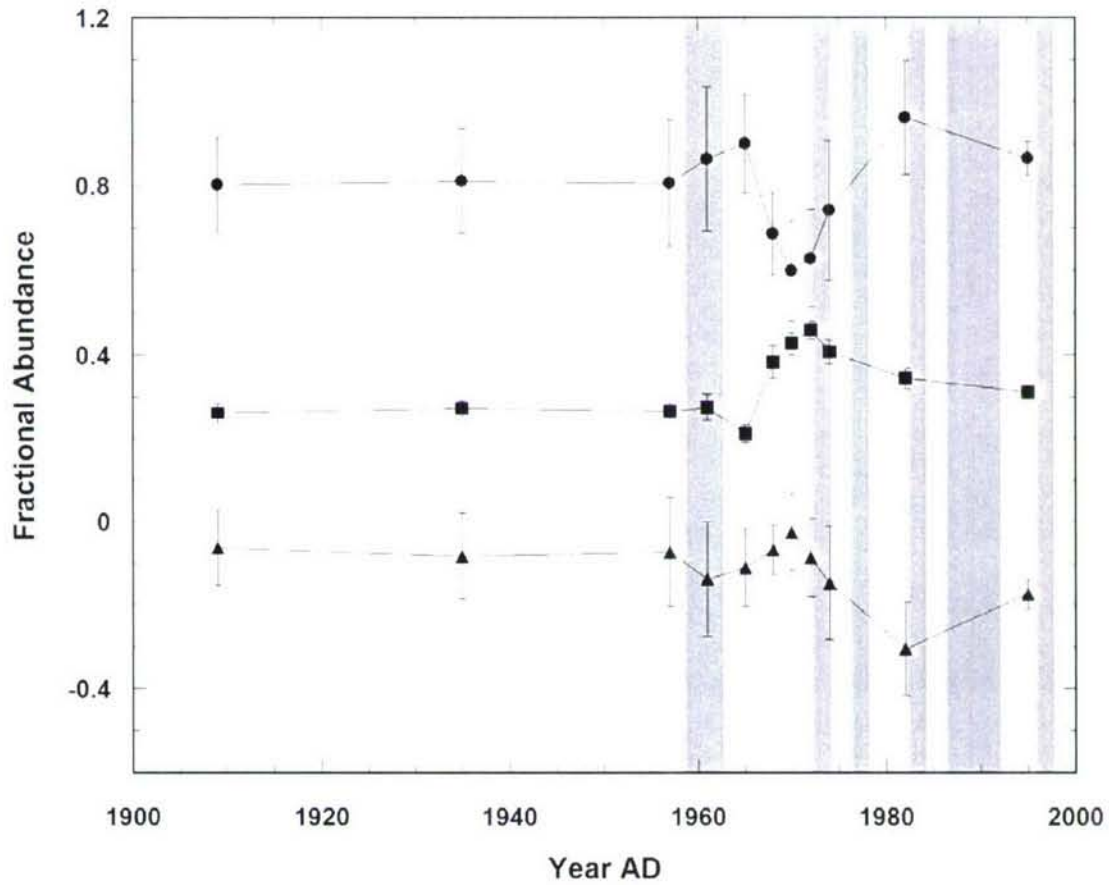


FIGURE 3.7 – Down core mass balance results for f_T (circles), f_P (squares), and f_M (triangles). Grey bars denote flood layers as established in Figure 3.4. Error bars represent 1σ of the solutions at each horizon for f_T , f_P , and f_M across a $\delta^{13}\text{C}_{\text{biomass}} - \delta^{13}\text{C}_{\text{lipid}}$ offset range of 7 – 9 ‰.

bulk $\Delta^{14}\text{C}$ depletions just before 1970, when f_P increases at the expense of f_T , concomitant with a decrease in the abundance of long chain fatty acids and an enrichment in the $\delta^{13}\text{C}$ of TOC during this interval (Figure 3.4). As the ^{210}Pb and ^{137}Cs evidence also implies (Figure 3.3), this is likely due to the local redeposition of fine-grained sediments scoured from shallower regions during storm events (Leithold and Hope, 1999; Sommerfield and Nittrouer, 1999; Sommerfield et al., 1999; Walsh at Nittrouer, 1999). Indeed, petrogenic OC has been shown to be concentrated in the clay sized fraction (Leithold and Blair, 2001; Blair et al., 2003, 2004; Leithold et al., 2005), consistent with the depleted $\Delta^{14}\text{C}$ and enriched $\delta^{13}\text{C}$ signatures exhibited by the $< 63\ \mu\text{m}$ pool relative to bulk sediment (Dickens et al., unpublished results). No other systematic down core trends are observed for f_T , or f_P , indicating that both forms of OC are resistant to diagenetic processes transpiring within the first meter or so of the sedimentary column.

3.3 CONCLUSIONS

Small mountainous rivers draining the world's active margins have been recently hypothesized to deliver $> 40 \times 10^{12}$ g of fossil organic carbon to the oceans annually based on the assumption that depleted $\Delta^{14}\text{C}$ values for TOC in their suspended loads and adjacent shelf sediments are primarily attributable to the presence of a petrogenic endmember (Blair et al., 2003, 2004; Komada et al., 2004; 2005). Here I show instead that, even in highly erodible watersheds, significant pre-aging of vascular plant OC in soils, wetlands, and intermediate flood plains might account for the majority of these $\Delta^{14}\text{C}$ signals. Further application of coupled molecular isotope mass balances in many different margin settings should refine our understanding of the age and composition of,

and hence the factors preserving, the OC that is ultimately buried in marine sediments world-wide.

ACKNOWLEDGEMENTS

This study is co-authored by Timothy Eglinton, Konrad Huguen, Daniel Montluçon, Liviu Giosan (all at Woods Hole Oceanographic Institution), Ellen Druffel, Guaciara dos Santos, and John Southon (all at the University of California at Irvine). I thank Ann McNichol and the entire prep lab staff at NOSAMS for accommodating my requests for rapid analyses and most especially for the frequent use of their PCGC. Margaret Sulanowska's help with the core photography and Sheila Griffin's laboratory assistance at UCI were most appreciated. Carl Johnson is thanked for his expertise in compound-specific $\delta^{13}\text{C}$ and elemental analyses, and the crew and scientific party members of the R/V *New Horizon* are acknowledged for their help in retrieving the sediment cores. N.J.D also gratefully acknowledges support from the Schlanger Ocean Drilling Graduate Fellowship and the EPA Star Graduate Fellowship. Additional funding was provided by NSF grants OCE-9907129 (T.I.E), OCE 0137005 (T.I.E and K.A.H.), and the Stanley Watson Chair for Excellence in Oceanography at WHOI (T.I.E.).

REFERENCES

Berner, R.A., 1989. Biogeochemical cycles of carbon and sulfur and their effect on atmospheric oxygen over Phanerozoic time. *Palaeogeography Palaeoclimatology Palaeoecology*, 73: 97-122.

Blair, N.E., Leithold, E.L., Aller, R.C., 2004. From bedrock to burial: the evolution of particulate organic carbon across coupled watershed-continental margin systems. *Marine Chemistry*, 92: 141-156.

Blair, N.E., Leithold, E.L., Ford, S.T., Peeler, K.A., Holmes, J.C., Perkey, D.W., 2003. The persistence of memory: The fate of ancient sedimentary organic carbon in a modern sedimentary system. *Geochimica et Cosmochimica Acta*, 67: 63-73.

Brown, W.M., Ritter, J.R., 1971. Sediment transport and turbidity in the Eel River Basin, California. U.S. Geological Survey Water Supply Paper no. 1986, 70 pp.

Burdige, D.J., 2005. Burial of terrestrial organic matter in marine sediments: A re-assessment. *Global Biogeochemical Cycles*, 19: doi: 10.1029/2004GB002368.

Collister, J.W., Rieley, G., Stern, B., Eglinton, G., Fry, B., 1994. Compound-specific $\delta^{13}\text{C}$ analyses of leaf lipids from plants with differing carbon dioxide metabolisms. *Organic Geochemistry*, 21: 619-627.

Dickens, A.F., Gélinais, Y., Masiello, C.A., Wakeham, S., Hedges, J.I., 2004. Reburial of fossil organic carbon in marine sediments. *Nature*, 427: 336-339.

Di-Giovanni, C., Disnar, J.R., Macaire, J.J., 2002. Estimation of the annual yield of organic carbon released from carbonates and shales by chemical weathering. *Global and Planetary Change*, 32: 195-210.

Goñi, M.A., Yunker, M.B., Macdonald, R.W., Eglinton, T.I., 2005. The supply and preservation of ancient and modern components of organic carbon in the Canadian Beaufort Shelf of the Arctic Ocean. *Marine Chemistry*, 93: 53-73.

Haberstroh, P.R., Brandes, J.A., Gélinais, Y., Dickens, A.F., Wirick, S., Cody, G., 2006. Chemical composition of the graphitic black carbon fraction in riverine and marine sediments at sub-micron scales using carbon X-ray spectromicroscopy. *Geochimica et Cosmochimica Acta*, 70: 1483-1494.

Hedges, J.I., 1992. Global biogeochemical cycles: Progress and problems. *Marine Chemistry*, 39: 67-93.

Hedges, J.I., Keil, R.G., 1995. Sedimentary organic matter preservation: An assessment and speculative synthesis. *Marine Chemistry*, 49: 81-115.

Hedges, J.I., Keil, R.G., Benner, R., 1997. What happens to terrestrial organic matter in the ocean? *Organic Geochemistry*, 27: 195-212.

Hwang, J., Druffel, E.R.M., Komada, T., 2005. Transport of organic carbon from the California coast to the slope region: A study of $\Delta^{14}\text{C}$ and $\delta^{13}\text{C}$ signatures of organic compound classes. *Global Biogeochemical Cycles*, 19: doi: 2004GB002422.

Keil, R.G., Mayer, L.M., Quay, P.D., Richey, J.E., Hedges, J.I., 1997. Loss of organic matter from riverine particles in deltas. *Geochimica et Cosmochimica Acta*, 61: 1507-1511.

Komada, T., Druffel, E.R.M., Hwang, J., 2005. Sedimentary rocks as sources of ancient organic carbon to the ocean: An investigation through $\Delta^{14}\text{C}$ and $\delta^{13}\text{C}$ signatures

of organic compound classes. *Global Biogeochemical Cycles*, 19: doi: 10.1029/2004GB002347.

Komada, T., Druffel, E.R.M., Trumbore, S.E., 2004. Oceanic export of relict carbon by small mountainous rivers. *Geophysical Research Letters*, 31: doi: 10.1029/2004GL019512.

Leavitt, S.W., Follett, R.F., Paul, E.A., 1996. Estimation of slow- and fast-cycling soil organic carbon pools from 6N HCl hydrolysis. *Radiocarbon*, 38: 231-239.

Leithold, E.L., Blair, N.E., 2001. Watershed control on the carbon loading of marine sedimentary particles. *Geochimica et Cosmochimica Acta*, 65: 2231-2240.

Leithold, E.L., Hope, R.S., 1999. Deposition and modification of a flood layer on the northern California shelf: Lessons from and about the fate of terrestrial particulate organic carbon. *Marine Geology*, 154: 183-195.

Leithold, E.L., Perkey, D.W., Blair, N.E., Creamer, T.N., 2005. Sedimentation and carbon burial on the northern California continental shelf: The signatures of land-use change. *Continental Shelf Research*, 25: 349-371.

Masiello, C.A., Druffel, E.R.M., 2001. Carbon isotope geochemistry of the Santa Clara River. *Global Biogeochemical Cycles*, 15: 407-416.

Pearson, A., 1999. Biogeochemical applications of compound-specific radiocarbon analysis. Ph.D. Thesis, MIT/WHOI Joint Program, Woods Hole, MA.

Perruchoud, D., Joos, F., Fischlin, A., Hajdas, I., Bonani, G., 1999. Evaluating timescales of carbon turnover in temperate forest soils with radiocarbon data. *Global Biogeochemical Cycles*, 13: 555-573.

Petsch, S.T., 2003. The global oxygen cycle. In: *Treatise on Geochemistry, Vol 8*, H.D. Holland and K.K. Turekian (eds): 515-555.

Petsch, S.T., Berner, R.A., Eglinton, T.I., 2000. A field study of the chemical weathering of ancient sedimentary organic matter. *Organic Geochemistry*, 31: 475-487.

Petsch, S.T., Edwards, K.J., Eglinton, T.I., 2003. Abundance, distribution, and $\delta^{13}\text{C}$ analysis of microbial phospholipid-derived fatty acids in a black shale weathering profile. *Organic Geochemistry*, 34: 731-743.

Petsch, S.T., Eglinton, T.I., Edwards, K.J., 2001b. ^{14}C -dead lipid biomass: Evidence for microbial assimilation of ancient organic carbon during shale weathering. *Science*, 292: 1127-1131.

Petsch, S.T., Smernik, R.J., Eglinton, T.I., Oades, J.M., 2001a. A solid state ^{13}C -NMR study of kerogen degradation during black shale weathering. *Geochimica et Cosmochimica Acta*, 65: 1867-1882.

Raymond, P.A., Bauer, J.E., 2001a. Riverine export of aged terrestrial organic matter to the North Atlantic Ocean. *Nature*, 409: 497-500.

Raymond, P.A., Bauer, J.E., 2001b. Use of ^{14}C and ^{13}C natural abundances for evaluating riverine, estuarine, and coastal DOC and POC sources and cycling: A review and synthesis. *Organic geochemistry*, 32: 469-485.

Rethemeyer, J., Grootes, P.M., Bruhn, F., Andersen, N., Nadeau, M.J., Kramer, C., Gleixner, G., 2004a. Age heterogeneity of soil organic matter. *Nuclear Instruments and Methods in Physics Research B*, 223-224: 521-527.

Rethemeyer, J., Kramer, C., Gleixner, G., John, B., Yamashita, T., Flessa, H., Andersen, N., Nadeau, M.-J., Grootes, P.M., 2005. Transformation of organic matter in agricultural soils: Radiocarbon concentration versus soil depth. *Geoderma*, 128: 94-105.

Rethemeyer, J., Kramer, C., Gleixner, G., Wiesenberger, G.L.B., Schwark, L., Andersen, N., Nadeau, M.-J., Grootes, P.M., 2004b. Complexity of soil organic matter: AMS ^{14}C analysis of soil lipid fractions and individual compounds. *Radiocarbon*, 46: 465-473.

Schlünz, B., Schneider, R.R., 2000. Transport of terrestrial organic carbon to the oceans by rivers: Re-estimating flux and burial rates. *International Journal of Earth Sciences*, 88: 599-606.

Schouten, S., Breteler, W.C.M.K., Blokker, P., Schogt, N., Rupstra, I.C., Grice, K., Baas, M., Sinninghe Damsté, J.S., 1998. Biosynthetic effects on the stable carbon isotopic composition of algal lipids: Implications for deciphering the carbon isotopic biomarker record. *Geochimica et Cosmochimica Acta*, 62: 1397-1406.

Sommerfield, C.K., Drake, D.E., Wheatcroft, R.A., 2002. Shelf record of climatic changes in flood magnitude and frequency, north-coastal California. *Geology*, 30: 395-398.

Sommerfield, C.K., Nittrouer, C.A., 1999. Modern accumulation rates and a sediment budget for the Eel shelf: A flood-dominated depositional environment. *Marine Geology*, 154: 227-241.

Sommerfield, C.K., Nittrouer, C.A., Alexander, C.R., 1999. ^7Be as a tracer of flood sedimentation on the northern California continental margin. *Continental Shelf Research*, 19: 335-361.

van Dongen, B.E., Schouten, S., Sinninghe Damsté, J.S., 2002. Carbon isotope variability in monosaccharides and lipids of aquatic algae and terrestrial plants. *Marine Ecology Progress Series*, 232: 83-92.

Walsh, J.P., Nittrouer, C.A., 1999. Observations of sediment flux to the Eel continental slope, northern California. *Marine Geology*, 154: 55-68.

Wiesenberger, G.L.B., Schwarzbauer, J., Schmidt, M.W.I., Schwark, L., 2004. Source and turnover of organic matter in agricultural soils derived from *n*-alkane/*n*-carboxylic acid compositions and C-isotope signatures. *Organic Geochemistry*, 35: 1371-1393.

Yarincik, K.M., Murray, R.W., Peterson, L.C., 2000. Climatically sensitive eolian and hemipelagic deposition in the Cariaco Basin, Venezuela, over the past 578,000 years: Results from Al/Ti and K/Al. *Paleoceanography*, 15: 210-228.

Yunker, M.B., Belicka, L.L., Harvey, H.R., Macdonald, R.W. Tracing the inputs and fate of marine and terrigenous organic matter in Arctic Ocean sediments: A multi-variate analysis of lipid biomarkers. *Deep-Sea Research II*, in press.

Zabel, M., Schneider, R.R., Wagner, T., Adegbe, A.T., de Vries, U., Kolonic, S., 2001. Late Quaternary climate changes in central Africa as inferred from terrigenous input to the Niger Fan. *Quaternary Research*, 56: 207-217.

CHAPTER 4

TEMPORAL CONSTRAINTS ON THE DELIVERY OF TERRESTRIAL BIOMARKERS TO MARINE SEDIMENTS

ABSTRACT

Little is known about the amount of time that lapses between vascular plant biomarker synthesis in the terrestrial biosphere and their ultimate incorporation into the marine sedimentary record. This information is critical for the application of these biomarkers in investigations of the global carbon cycle and climate, past and present. Here I use compound specific radiocarbon analysis to develop down core $\Delta^{14}\text{C}$ profiles of individual higher plant wax-derived fatty acids extracted from Cariaco Basin and Saanich Inlet sediments as a direct measure of the transport times these compounds experience. Their “terrestrial residence times” are evaluated by comparing these records to the $\Delta^{14}\text{C}$ evolution of atmospheric CO_2 . Using a simple modeling framework, I conclude that there are at least two pools of these compounds that exhibit markedly different residence times. Results indicate that 70 – 90 % of vascular plant leaf waxes in Cariaco and Saanich sediments were sequestered on land for an average of 2570 and 5170 years, respectively, with the remainder retarded for a much shorter time of only one or two decades. The fraction of each fatty acid homologue passing through these ‘millennial’ and ‘decadal’ reservoirs systematically decreased at shorter chain length, possibly reflecting the influence of different molecular-level properties such as degradation rate

and/or physiochemical sorption. The implications of these findings for climate and carbon cycle reconstructions are also explored.

4.0 INTRODUCTION

Some of the most promising archives of paleoclimatic information are high-deposition rate marine and lacustrine sediments, where organic geochemical analyses can provide high temporal resolution (sub-centennial) records of environmental change. The magnitude, type, provenance, and rate of organic carbon (OC) transport from continents to the aquatic environment and subsequent burial in sediments is an important indicator of past and present climate on a regional and global scale. Land-sea OC flux occurs mainly via rivers (Keil et al., 1997; Raymond and Bauer, 2001) in the form of dissolved organic carbon (DOC) and particulate organic carbon (POC) but may also be transported by aeolian mechanisms to many regions of the oceans (Gagosian and Peltzer, 1986; Ohkouchi et al., 1997; Huang et al., 2000; Conte and Weber, 2002a,b; Schefuß et al., 2003) (Figure 4.1). The sources of this OC include vascular plants, soils, desiccated lake beds, ancient OC-rich sedimentary rock (shale), and anthropogenic emissions (Hedges et al., 1997).

Organic compounds derived from terrigenous sources and subsequently preserved in marine sediments include homologous series of alkyl lipids such as alkanolic (fatty) acids, alkanes, and alcohols, various derivatives of steroid and hopanoid skeletons, and macromolecules such as lignin, cutin, and cellulose from rigidifying tissues (Eglinton and Hamilton, 1967; Kolattukudy, 1969; Hedges and Oades, 1997; Meyers, 1997, and references therein; Kunst and Samuels, 2003). The abundance and distribution of these molecular proxies are increasingly being employed in studies of past and present OC flux (e.g. Meyers, 1997; Huang et al., 1999; Holtvoeth et al., 2003; Zhao et al., 2003).

Coupling these measurements with their isotopic signatures provides an extra dimension of source and environmental information (e.g. Westerhausen et al., 1993; Goñi et al., 1996; Lockheart et al., 1997;) following the union of capillary gas chromatographs (GC) with isotope ratio monitoring mass spectrometers (*irmMS*) (Hayes et al., 1990) and the advent of compound-specific radiocarbon analysis by preparative capillary gas chromatography (PCGC) (Eglinton et al., 1996, 1997). One of the most powerful

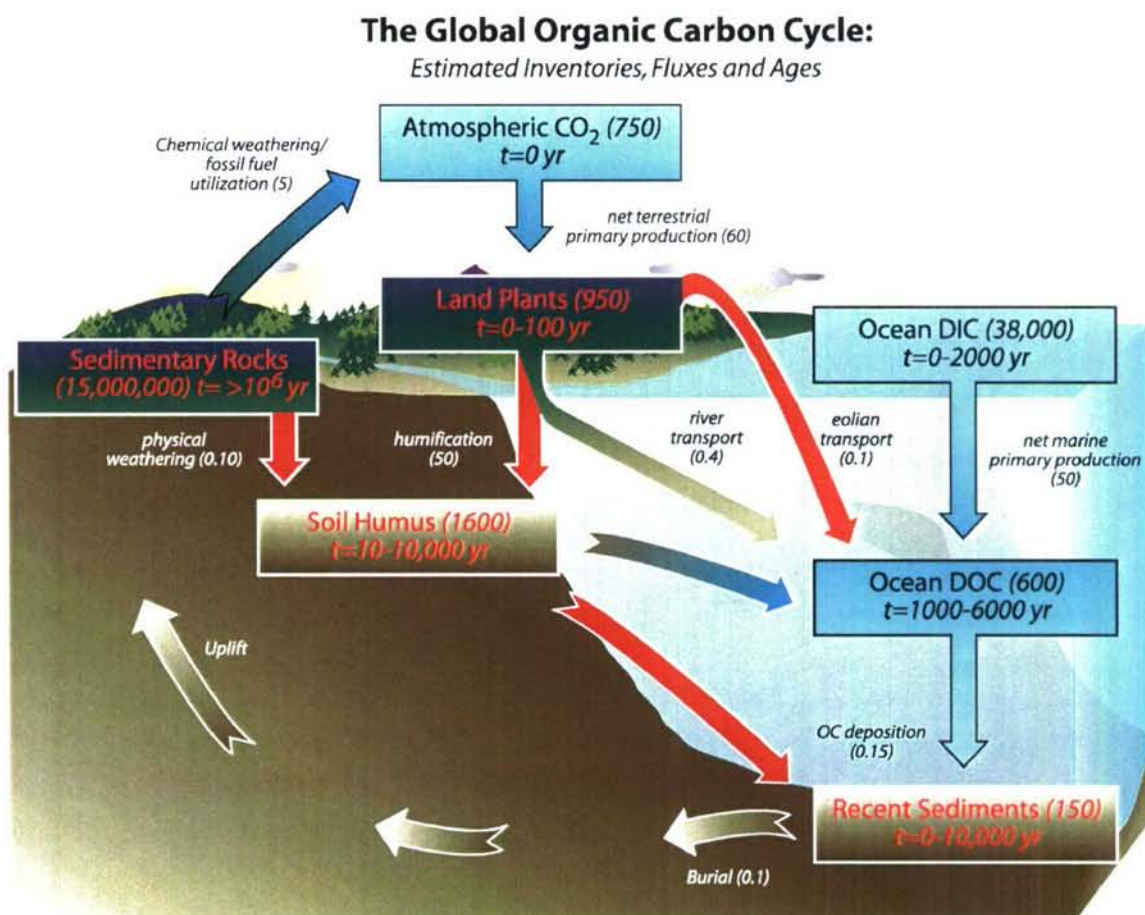


FIGURE 4.1 – Estimated inventories ($\times 10^{15}$ g C), fluxes ($\times 10^{15}$ g C yr⁻¹), and ¹⁴C ages associated with the global carbon cycle. Reservoirs and transfers highlighted in red delineate the focus of this study. Modified after Hedges (1992) and Pearson (1999).

applications of compound-specific stable carbon isotope analysis has been the assignment of biomarker source, since ^{13}C is discriminated against differently under different biosynthetic and environmental conditions (Hayes 1993, 2001). For example, the $\sim 14\text{‰}$ difference in stable carbon isotopic ($\delta^{13}\text{C}$) compositions of lipids from C_3 or C_4 plants (Collister et al., 1994; Hobbie and Werner, 2004; Bi et al., 2005) has been successfully used to trace continental aridity and OC inputs in marine (Bird et al., 1995; Goñi et al., 1998; Naraoka and Ishiwatari, 2000; Hughen et al., 2004; Rommerskirchen et al., 2006), estuarine (Shi et al., 2001), and lacustrine (Rieley et al., 1991; Huang et al., 1999; Fisher et al., 2003; Fuhrmann et al., 2003) sediments.

Radiocarbon analysis of individual fatty acids, alkanes, alcohols, ketols, diols, hopanols, sterols, alkenones, and polycyclic aromatic hydrocarbons extracted from marine sediments (Eglinton et al., 1997; Pearson, 1999; Pearson and Eglinton, 2000; Uchida et al., 2000, 2001, 2005; Pearson et al., 2001, 2005; Ohkouchi et al., 2002, 2003; Smittenberg, 2003; Mollenhauer et al., 2003, 2005; Lima, 2004; Ohkouchi and Eglinton, 2006; Smittenberg et al., 2006; Dickens et al., unpublished results; Schefuß et al., unpublished results; Chapters 2 and 3 of this thesis), soils (Rethemeyer et al., 2004a, 2005), and aerosols (Currie et al., 1997; Matsumoto et al., 2001) has also been used for biomarker provenance determination. Importantly, some of these studies have revealed the presence of significantly ‘pre-aged’ terrigenous components relative to other constituents, likely due to sequestration in soil and wetland reservoirs for up to millennia (Trumbore and Harden, 1997; Lichtfouse et al., 1998; Lichtfouse, 1999; Perruchoud et

al., 1999; Richter et al., 1999; Rethemeyer, 2004b, 2005; Swanston et al., 2005) before transport to the oceans and burial in marine sediments.

Yet the underlying mechanisms controlling the ages of individual vascular plant biomarkers in a given setting remain unclear. The period elapsing between the biosynthesis of a certain molecule and its ultimate burial in sediments, or its 'terrestrial residence time', may be expected to vary as a function of such physicochemical properties as structure, size, polarity, polymeric nature, reactivity, and mineral association, as well as environmental properties such as aridity, temperature, topography, soil type, wind stress, and the size and shape of a particular catchment basin (Trumbore, 1993, 1997; Trumbore and Harden, 1997; Rapalee et al., 1998; Wang et al., 1999; Parshotam et al., 2000; Quideau et al., 2001). Moreover, anthropogenic activities such as urbanization, deforestation, and cultivation of previously wooded landscapes in the last few centuries have not only shifted the type of OC delivered to the aquatic environment (Harrison et al., 1993; Bird et al., 1995; Fisher et al., 2003; Smittenberg et al., 2004; Wiesenberg et al., 2004) but have also altered its rate of discharge as water flow patterns and/or structural integrity of soils are modified (Richter et al., 1999; Wang et al., 1999; Smittenberg, 2003; Dalzell et al., 2007).

Large changes in global climate during the late Quaternary are also likely to have modified the terrestrial residence time of vascular plant biomarkers via alterations in both the chemical weathering of continents (Crowley, 1995; Oxburgh, 1998) and major precipitation and wind patterns, particularly in the tropics (Ruddiman, 1997; deMenocal et al., 2000; Leuschner and Sirocko, 2000). In northern South America, for example, the

decrease in precipitation during stadial events recorded by $\delta^{13}\text{C}$ compositions of leaf waxes (Hughen et al., 2004; Chapter 5 of this thesis) might result in a longer continental sequestration of these same compounds from a decrease in rainwater leaching of soils. If the effect is large enough or not properly taken into account, correlation with other climatic reconstructions from different sites or even different proxies from the same site will be impeded.

It is therefore imperative that the temporal relationship between terrestrial biomarker synthesis and sedimentary incorporation be accurately constrained. Here I construct $\Delta^{14}\text{C}$ profiles of several alkanolic (fatty) acid homologues, and combinations thereof, from sediment cores spanning the twentieth century. Long chain ($\geq n\text{C}_{24}$) fatty acids found in sediments are generally thought to derive from the epicuticular coating of vascular plant leaves (Eglinton and Hamilton, 1967; Kolattukudy, 1969; Kunst and Samuels, 2003; Lemieux, 1996), and inherit the $\Delta^{14}\text{C}$ signature of the CO_2 from which they are synthesized. Any departure in the $\Delta^{14}\text{C}$ signatures of these leaf waxes from that of the atmosphere can be attributed to retention in (perhaps a broad array of) terrestrial environments such as soils, wetlands, and/or other freshwater sediments (Figure 4.1). The large and well-documented change in the radiocarbon signature of CO_2 over the last half-century (Stuiver et al., 1998; Levin and Heshaimer, 2000; Hua and Barbetti, 2004; Levin and Kromer, 2004; McGee et al., 2004) brought about by the above-ground detonation of nearly 500 nuclear weapons between 1945 and 1963 can then be exploited to resolve the relative contribution and ages of such temporal reservoirs.

This approach is predicated on the assumption that the ^{14}C content of CO_2 used in the biosynthesis of terrestrial biomarkers and their subsequent retention on land exclusively control their radiocarbon signatures once incorporated into marine sediments. In other words, *in situ* decay and bioturbation must be either negligible or independently known. Anoxic basins therefore provide exceptional settings in which to conduct such a study, as the absence of bioturbation in their underlying sediments allows the establishment of robust ^{210}Pb and ^{137}Cs (and sometimes varved-based) chronologies by which lipid $\Delta^{14}\text{C}$ compositions can be decay-corrected to their values at the time of deposition. Such environments also typically exhibit high OC concentrations and deposition rates that allow lipids to be preserved in sufficient abundance for molecular level ^{14}C analysis at up to annual resolution.

Here I examine fatty acids extracted from the anoxic continental margin sediments of the Cariaco Basin (Caribbean Sea) and the Saanich Inlet (British Columbia) (Figure 4.2). Located off of the northern coast of Venezuela, the Cariaco Basin is a tectonic pull-apart depression consisting of two ~ 1400 m deep sub-basins separated by a ~ 900 m deep ridge. Its subsurface waters are effectively isolated from the abyssal Caribbean by a shallow (~ 150 m) sill, allowing only waters from the oxygen minimum zone to infill the deep basin. Strong wintertime trade winds accompanying a southward displacement of the Intertropical Convergence Zone (ITCZ) promote upwelling of nutrient rich waters that fuel high rates of primary production (Astor et al., 2003; Goñi et al., 2003), while the northward return of ITCZ during boreal summer deposits most of the

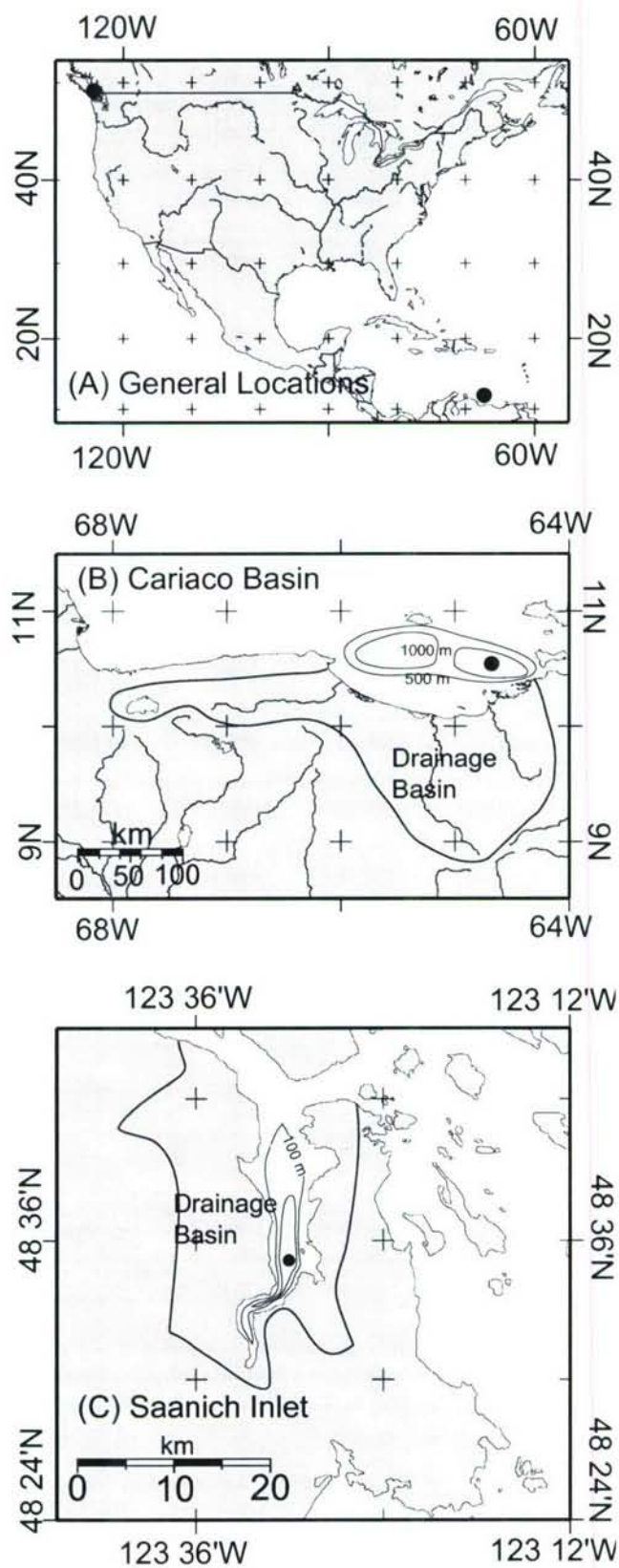


FIGURE 4.2 – Map showing the (a) general locations of the study sites, as well as the coring locations and drainage basins associated with the (b) Cariaco Basin, and (c) Saanich Inlet.

annual 677 mm of rainfall and increases terrigenous runoff from several rivers (including the Unare, Tuy, and Orinoco) that drain some 36,500 km² of tropical rainforest and grassy highland in northern South America. The large detrital carbon flux efficiently strips the remaining O₂ from deep waters below ~ 300 m (Ho et al., 2004) and leads to annually varved sedimentation that is virtually devoid of bioturbation (Hughen et al., 1996). Because of these redox characteristics and the Cariaco's sensitivity to the position of the ITCZ, a variety of biogeochemical (Wakeham, 1990; Thunell et al., 2000; Goñi et al., 2003; Muller-Karger et al., 2004; Werne and Hollander, 2004; Woodworth et al., 2004) and paleoceanographic studies (Peterson et al., 2000; Peterson and Haug, 2006; Hughen et al., 2004; Chapter 5 of this thesis) have been conducted there. Although lithogenic grains comprise several tens of percent by weight of the total sediment mass (Yarincik et al., 2000), the contribution of terrestrial organic matter to TOC is generally considered to be quite small (Thunell et al., 2000; and data presented below).

The Saanich Inlet is a 26 km long x 8 km wide, ~ 235 m deep coastal fjord in British Columbia, Canada, that likely receives the majority of its terrigenous sediment in the wintertime from the suspended load of the Cowichan River located approximately 10 km to the northwest (Blais-Stevens et al., 1997; Tunnicliffe, 2000), with lesser contributions from the small Goldstream River at the head of the fjord and the much larger Fraser River draining into the Strait of Georgia (Gucluer and Gross, 1964; Hamilton and Hedges, 1988; Tunnicliffe, 2000). The relatively steep topography within these drainage basins is overlain by thick forests of conifers, cedar, and oak characteristic of this cool, moist maritime climate (Pellatt et al., 2001) with a mean annual precipitation

of 846 mm. Deep water ventilation within the Saanich is limited by a ~ 65 m deep sill at the entrance to the fjord, which combined with high surface productivity maintains deepwater dysoxia and seasonal anoxia (Anderson and Devol, 1973; Timothy and Soon, 2001), preserving annual varves below 70 – 150 m depth (Gucluer and Gross, 1964). The sedimentology of this site has been well studied previously (Gucluer and Gross, 1964; Brown et al., 1972; Sancetta and Calvert, 1988; Cowie et al., 1992; Blais-Stevens et al., 1997; Tunnicliffe, 2000; Calvert et al., 2001; Johnson and Grimm, 2001; Nederbragt and Thurow, 2001; Whiticar and Elvert, 2001; Smittenberg, 2003; Smittenberg et al., 2004, 2006). In particular, analysis of lignin oxidation products led Hamilton and Hedges (1988) and Cowie et al. (1992) to conclude that vascular plant debris contributed between 10 and 25 % of the TOC in Saanich sediments, while Timothy et al. (2003) put the proportion of terrestrial OC closer to 40 % using bulk elemental and isotopic estimates.

4.1 METHODS

4.1.1 Sample recovery

As previously discussed, preservation of individual varves is highly desirable for this study. However, the waters of the Cariaco Basin are too warm and too deep for the recovery of intact freeze cores that are presently the most effective way of recovering intact varves (attempted for this study and failed). Hence, sediments from the northwestern flank of the eastern sub-basin (305 m water depth) were retrieved by a six-barreled multicorer during a cruise aboard the R/V *Hermano Gines* in May 2004 (Figure 4.2). Cores were immediately extruded and sectioned on deck at 0.5 cm intervals into pre-combusted glass jars and stored frozen until analysis. Three of these cores (MC 2, 5,

and 6) were subsequently chosen for this study. Additionally, water from several depths in the center of the eastern sub-basin were sampled in Niskin bottles, transferred to pre-combusted 500 mL Pyrex reagent bottles, and sterilized via the addition of 100 μ L of a saturated aqueous HgCl_2 solution for subsequent isotopic analysis of dissolved inorganic carbon (DIC).

Sediments from the depocenter (224 m water depth) of the Saanich Inlet were amenable to recovery via freeze corer during a cruise aboard the R/V *Clifford Barnes* in August 2003 (Figure 4.2). Briefly, a hollow aluminum freeze corer was filled with a dry ice / isopropanol slurry onboard the ship, capped, lowered into the sediments via hydrowire, and held there for ~ 30 minutes, during which time approximately 1 – 2 cm of surrounding sediment was frozen onto its non-insulated face. Upon return to the ship, this slab was gently scraped along the axis of the laminae to remove any unfrozen material, separated from the corer face, wrapped in Al foil and Saran WrapTM, and stored frozen. Water samples from several depths at the coring site were also recovered and preserved for DIC analysis by the procedures outlined above.

Each freeze core was subsequently photographed and stratigraphically correlated with each other through the comparison of episodic, earthquake-emplaced turbidites (Blais-Stevens et al., 1997) and particularly well defined laminae. The depth from the top and bottom of one very large turbidite to the base of each varve above and below it, respectively, was carefully noted to aid the development of an ancillary ^{210}Pb and ^{137}C -based age model (see below). Three cores (FC 3, 4, and 7) were then sectioned into individual varves (consisting of one light and one dark lamina from the marine bloom in

the spring and terrigenous runoff in the summer/fall, respectively) while still frozen using a band saw equipped with a diamond coated blade. Each varve was transferred to pre-combusted glass jars and stored frozen until analysis, with turbidites archived as a whole unit. The part of each core remaining to be sectioned was kept frozen during this process by periodic immersion in liquid nitrogen.

4.1.2 Chronology development

The resulting sedimentary horizons from both sites were freeze dried and homogenized via grinding in a mortar and pestle. Precisely 2.00 ± 0.01 grams (g) of each Cariaco horizon from MC 5 was transferred to individual tubes for ^{210}Pb and ^{137}Cs gamma counting. A mean sedimentation rate of 0.1 cm yr^{-1} (yielding a nominal sampling resolution of ~ 5 years) was obtained by a logarithmic fit to unsupported ^{210}Pb activity against depth and anchored to 1963 AD at the peak in ^{137}Cs activity (Figure 4.3; Appendix 4.1). On this timescale, the uppermost and lowermost horizons of MC 5 correspond to 1994 – 1998 and 1689 – 1693 AD, respectively. Analogous measurements in MC 2 and 6 revealed the ^{137}Cs spike to be one horizon lower in both of these cores; therefore, sediments from each MC 5 horizon were combined with those from one level below in MC 2 and 6 before lipid extraction.

For the Saanich Inlet, 1.00 ± 0.01 g aliquots from only select intervals in FC 3 were radiometrically dated as the chronology above and below the 1963 ^{137}Cs peak was principally established by annual varve counting. The average sedimentation rate derived from this approach is 0.85 cm yr^{-1} , in good agreement with that obtained from the unsupported ^{210}Pb profile (1.0 cm yr^{-1}) (Figure 4.4; Appendix 4.1). Based on the varve

counting chronology, the uppermost and lowermost varves of the core were thus deposited in 1987 and 1810 AD, respectively. The difference between the measured age of the core top (1987) and the date of sampling (2003) indicates that the surface-most sediments were not recovered due to the melting of most of the unconsolidated material during deployment. Since each varve in FC 3 was correlated to a unique equivalent in FC 4 and 7, individual varves representing the same year in each of these cores were combined to achieve sufficient lipid mass for extraction.

4.1.3 Bulk elemental and isotopic analysis

Aliquots of every horizon from Cariaco MC 6 and periodic varves from Saanich FC 3 were freeze dried, homogenized via grinding in a mortar and pestle, and measured in triplicate for total carbon (TC) and total nitrogen (TN) by high temperature combustion on a Carlo Erba 1108 Elemental Analyzer. Total organic carbon (TOC) was measured in triplicate by the same method after carbonate removal by exposure to HCl vapor for 8-10 hours followed by addition of a drop of 2N HCl_(aq) directly onto the sample. If any effervescence was noticed, an additional drop was added after drying overnight. TOC generated from additional sedimentary aliquots was measured for bulk ¹³C and ¹⁴C content (without replicates) at the National Ocean Sciences Accelerator Mass Spectrometry (NOSAMS) facility at Woods Hole Oceanographic Institution (WHOI).

4.1.4 Fatty acid isolation

Virtually all of the remaining sediment from Cariaco MC 2, 5, and 6 and Saanich FC 3, 4, and 7 was combined into chronologically equivalent horizons as described above, spiked with a recovery standard comprising 18 µg each of 5α-androstane, 1-

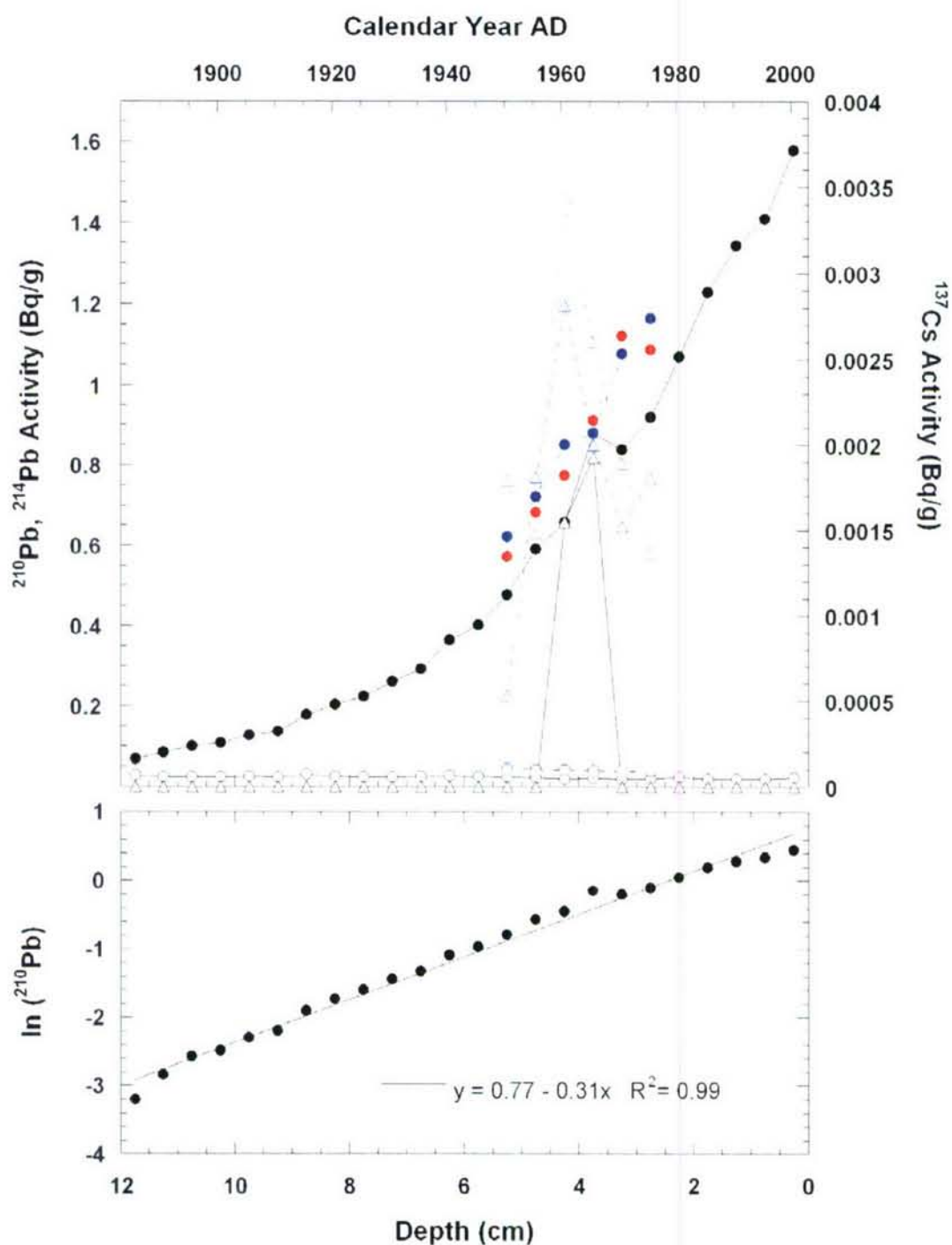


FIGURE 4.3 – Chronology development for Cariaco Basin sediments. Upper panel: ^{210}Pb (solid circles), ^{214}Pb (open circles), and ^{137}Cs (open triangles) activity for MC 5. Those for MC 2 and MC 6 are shown in blue and red, respectively. Bottom panel: Plot of unsupported $\ln(^{210}\text{Pb})$ activity vs. depth, with the least squares regression shown.

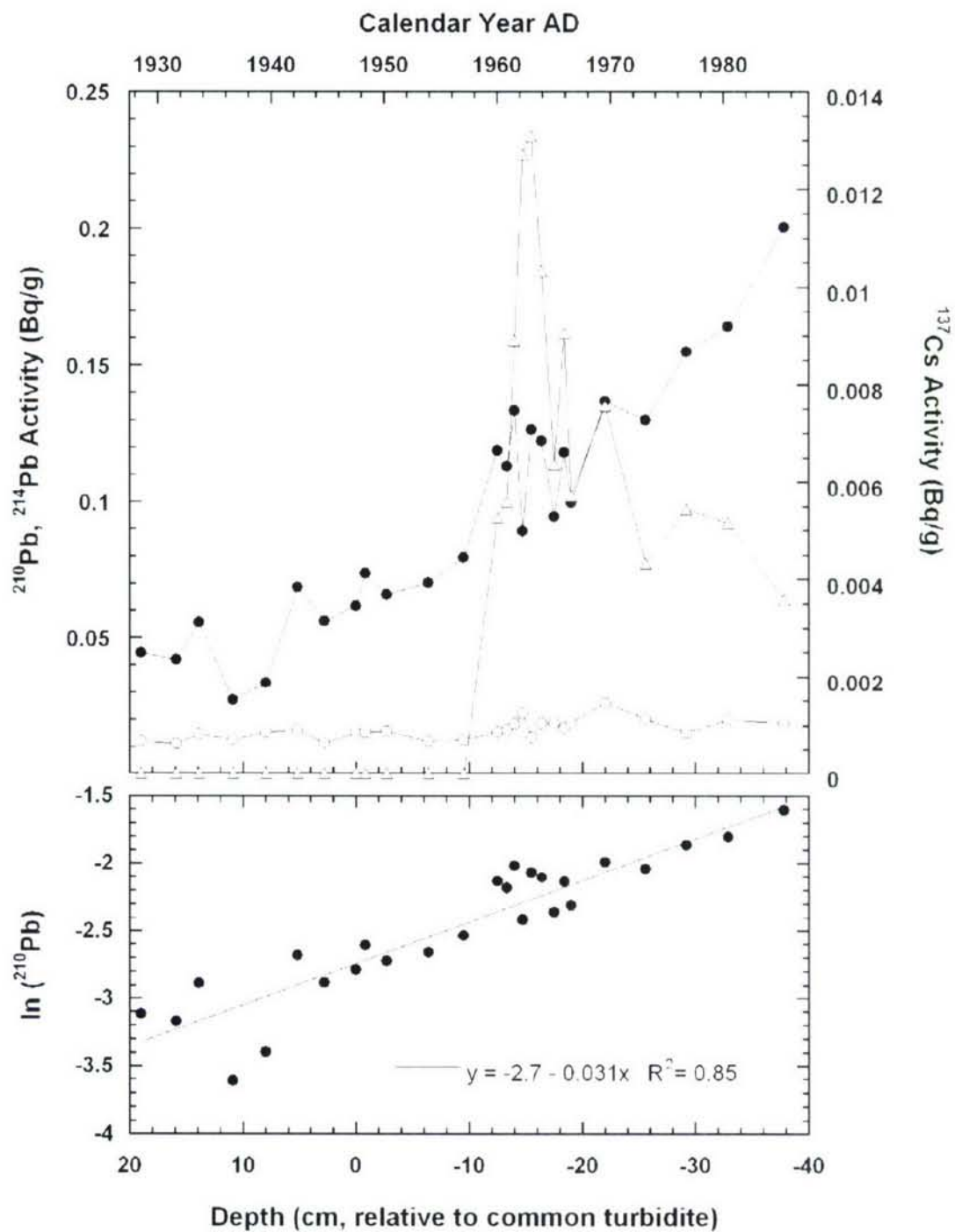


FIGURE 4.4 – Uranium-series chronology for Saanich Inlet FC 3 sediments. Upper panel: ^{210}Pb (solid circles), ^{214}Pb (open circles), and ^{137}Cs (open triangles) activity for FC 3. Bottom panel: Plot of unsupported $\ln(^{210}\text{Pb})$ activity vs. depth, with the least squares regression shown.

nonodecanol, heneicosanoic acid, and hexatriacontane, and extracted at 100°C using 1000 psi of a 90/10 (v/v) dichloromethane/methanol (DCM/MeOH) solvent mixture in an Accelerated Solvent Extractor (ASE). The resulting total lipid extracts were dried over sodium sulfate, solvent exchanged into 5 mL of hexane, and eluted through large bore (5 cm diameter) glass columns packed with ~ 85 g of fully activated silica gel into 300 mL of the following fractions: f1 = 100 % hexane (containing mostly non-aromatic hydrocarbons), f2 = 50/50 (vol %) hexane / toluene (polycyclic aromatic hydrocarbons), f3 = 80/20 hexane / diethyl ether (esterified acids), f4 = 75/25 hexane / ethyl acetate (cyclic and acyclic alcohols), f5 = 99.85/0.15 diethyl ether / acetic acid (unbound acids), and f6 = 100 % MeOH (highly polar compounds). Each fraction was reduced in volume via rotary evaporation, after which f1 – f4 and f6 were archived for future analysis. f5 was solvent exchanged into 100 % DCM and eluted through glass columns (1.25 cm diameter) containing 2.0 g of aminopropyl stationary phase with f1 = 15mL of 90/10 DCM / acetone, f2 = 20mL of 98/2 DCM/ formic acid, and f3 = 15mL of 100 % MeOH.

Following solvent reduction under nitrogen, the fatty acids in each f2 fraction were esterified overnight at 70°C with a solution of 5 % (by vol) hydrochloric acid in anhydrous MeOH of known isotopic composition. The resulting fatty acid methyl esters (FAMES) were subsequently back-extracted into 0.5 mL hexane, re-dried over sodium sulfate, and further purified by elution through Pasteur pipet columns containing 5 % deactivated silica gel into the following fractions: f1 = 4 mL hexane, f2 = 4 mL of 95/5 hexane / ethyl acetate, and f3 = 4 mL of MeOH. Each f2 (now containing the isolated FAMES) was then solvent exchanged into a known volume of hexane and injected along

with authentic standards on a gas chromatograph equipped with a flame ionization detector (GC/FID) to measure the abundance of individual FAME homologues. Molecular abundances reported here are corrected for any loss during wet chemical isolation using the heneicosanoic acid internal standard.

4.1.5 Compound-specific $\delta^{13}\text{C}$ analysis

Compound-specific $\delta^{13}\text{C}$ measurements on all even homologues between $n\text{C}_{16}$ and $n\text{C}_{32}$, along with a co-injected $n\text{C}_{36}$ alkane standard of known isotopic composition, were made on a HP6890 GC equipped with a CP-Sil 5 CB lowbleed/MS column (60 m x 0.25 mm i.d. x 0.25 μm film, operated under constant 1.0 mL/min helium carrier flow) coupled to a Finnigan Delta^{plus} Isotope Ratio Mass Spectrometer (IRMS) via a modified combustion interface. Results are reported as the mean of triplicate analyses (with 1 σ analytical uncertainties) in $\delta^{13}\text{C}$ (‰) notation on the VPDB scale, and have been corrected for the addition of the carboxyl methyl group during esterification via an isotope mass balance.

4.1.6 Compound-specific $\Delta^{14}\text{C}$ analysis

The procedures below describe the preparation of individual compounds for radiocarbon measurements that are reported in both this chapter and in chapter 3. Individual $n\text{C}_{16}$, $n\text{C}_{24}$, $n\text{C}_{26}$, $n\text{C}_{28}$ homologues as well as the combined $n\text{C}_{14+18}$ and $n\text{C}_{30+32}$ homologues were isolated for radiocarbon analysis by PCGC (an HP 5890 Series II or Agilent 6890 GC equipped with Gerstel CIS 3 or 4 injection systems, respectively, coupled to a Gerstel preparative fraction collector; see Eglinton et al., 1996 for a detailed description). PCGC traps were eluted with hexane and brought up to a known volume for

purity and recovery analysis by GC/FID. Individual compounds were generally > 99 % pure and recoveries averaged 61 %, which is standard for PCGC isolation. Selected isolates were then transferred into pre-combusted quartz tubes, the hexane evaporated, and pre-combusted cupric oxide added. These tubes were then attached to a vacuum line, evacuated, flame sealed, and combusted at 850°C for 5 hours.

Because this study required the Cariaco and Saanich sediment cores to be sectioned at ultra high resolution, isolated fatty acids often yielded less than the 20 µg carbon typically viewed as a minimum for reliable small scale ^{14}C analysis. However, recent advances in sample preparation and analysis techniques at the Keck Carbon Cycle Accelerator Mass Spectrometry (KCCAMS) facility at the University of California, Irvine allow precise ‘ultra small scale’ ^{14}C measurement on samples containing as little as a few micrograms of carbon (see Santos et al. [submitted] for a detailed description). Thus, 52 of the smallest samples (ranging in mass from 2 to 63 µg C, including those reported in this chapter as well as chapter 3; see Appendices 3.2 and 4.2) were processed and analyzed at the KCCAMS facility. Samples were stripped of impurities, graphitized over Fe powder within specially designed reactors containing $\text{Mg}(\text{ClO}_4)_2$ desiccant, pressed into custom targets, and analyzed on a modified, compact National Electrostatics Corporation AMS system.

Reported $\Delta^{14}\text{C}$ values for ≥ 60 µg C samples have been tentatively shown to be rather insensitive to isotopic fractionation and blank contamination during chromatographic isolation (Zencak et al., 2007). Since the fractional abundance of ‘modern’ (defined as 0 ‰) and ‘dead’ (-1000 ‰) blank contamination introduced during

this and other stages of sample preparation increases in proportion to decreases in total sample mass, however, measured $\Delta^{14}\text{C}$ values and their errors require corresponding adjustment for these influences at the ultra small sample level. Therefore, a solution of standards whose isotopic compositions encompassed the full $\Delta^{14}\text{C}$ scale ($n\text{C}_{19}$ alcohol, $\Delta^{14}\text{C} = -999\text{‰}$; $n\text{C}_{21}$ fatty acid, $\Delta^{14}\text{C} = -389\text{‰}$; *iso*- C_{21} fatty acid, $\Delta^{14}\text{C} = -32.9\text{‰}$) was prepared, apportioned into six aliquots whose masses spanned the range of those of the unknowns, isolated into individual compounds via the methods described above (i.e., from ASE extraction through graphitization), and co-analyzed along with the unknowns on the same AMS wheels. Twelve aliquots of the neat oxalic acid I (OX-I) and eight aliquots of the neat $n\text{C}_{19}$ alcohol standards (whose masses also spanned the range of those of the unknowns) were additionally loaded into quartz tubes, combusted, graphitized, and analyzed in the same wheels in order to assess the blank associated with these procedures alone. Detailed mathematical treatment of these blank corrections can be found in Santos et al. (submitted) and Pearson (1999). The total resultant mass and mass errors of modern and dead carbon measured for this standard suite were 0.8 ± 0.4 (all derived from combustion) and $1.0 \pm 0.5\text{ }\mu\text{g}$ (75 % derived from the sample preparation steps preceding combustion), respectively, and are applied to the corresponding $\Delta^{14}\text{C}$ values and errors reported hereafter.

An additional 38 molecular level samples (all $> 31\text{ }\mu\text{g C}$) were stripped of impurities, converted to graphite using a Co catalyst, and analyzed using standard procedures for small sample analysis at NOSAMS. Like KCCAMS, graphitization progress and yield was determined manometrically by monitoring the residual H_2 in the

reactor. All of the $\Delta^{14}\text{C}$ compositions of fatty acids reported below were also corrected for the addition of the derivative ester carbon via a simple two endmember isotope mass balance.

4.2 RESULTS & DISCUSSION

4.2.1 Bulk elemental and isotopic distributions

TOC abundance and TOC/TN ratio averages along with their corresponding 1σ replicate errors are plotted alongside the isotopic compositions of bulk sedimentary TOC and select FAMES in Figures 4.5 (Cariaco Basin) and 4.6 (Saanich Inlet). The full core data sets for TOC and TOC/TN, as well as those for TC and TC/TN, are given in Appendix 4.1. TOC is generally twice as high in Cariaco sediments ($\sim 6\%$) versus those from Saanich ($\sim 3\%$), whereas both exhibit rather low TOC/TN ratios of between 8 and 11 reflecting overwhelming contributions from marine production (at these high organic matter levels, contributions of inorganic nitrogen to the total nitrogen inventory can be assumed as negligible). The corresponding $\delta^{13}\text{C}$ and $\Delta^{14}\text{C}$ signatures of Saanich TOC are systematically depleted by ~ 2 and $\sim 100\text{‰}$, respectively, over those from the Cariaco, suggesting a greater influence of OC derived from pre-aged C_3 vascular plant debris in the former. Indeed, cross plotting $\delta^{13}\text{C}$ with TOC/TN supports the idea that the Saanich Inlet sediments likely contain a greater proportion of terrigenous organic carbon emanating from older soil detritus (Figure 4.7). The down-core bulk $\Delta^{14}\text{C}$ profiles at both sites generally trend toward markedly more positive values towards the present presumably reflecting biosynthetic incorporation of ^{14}C -enriched atmospheric CO_2 associated with the bomb effect (Stuiver and Quay, 1981).

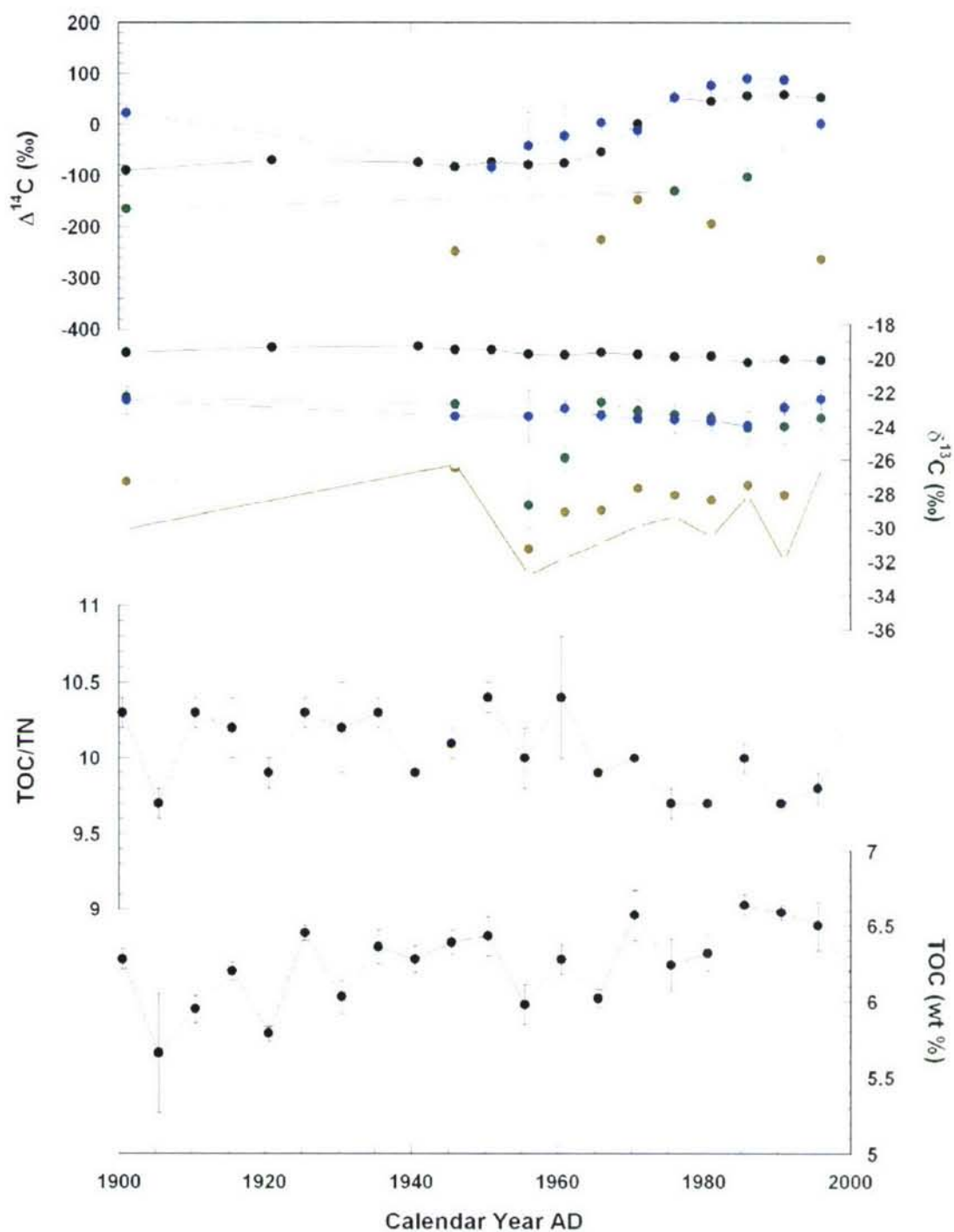


FIGURE 4.5 – Down-cores profiles for various Cariaco sediment parameters. From top to bottom: $\Delta^{14}\text{C}$ of TOC (black), $n\text{C}_{16}$ (blue), $n\text{C}_{26+28+30+32}$ (green), $n\text{C}_{30+32}$ (olive); their corresponding $\delta^{13}\text{C}$ compositions (that of $n\text{C}_{32}$ alone is given in open olive symbols); TOC/TN; and TOC (wt %).

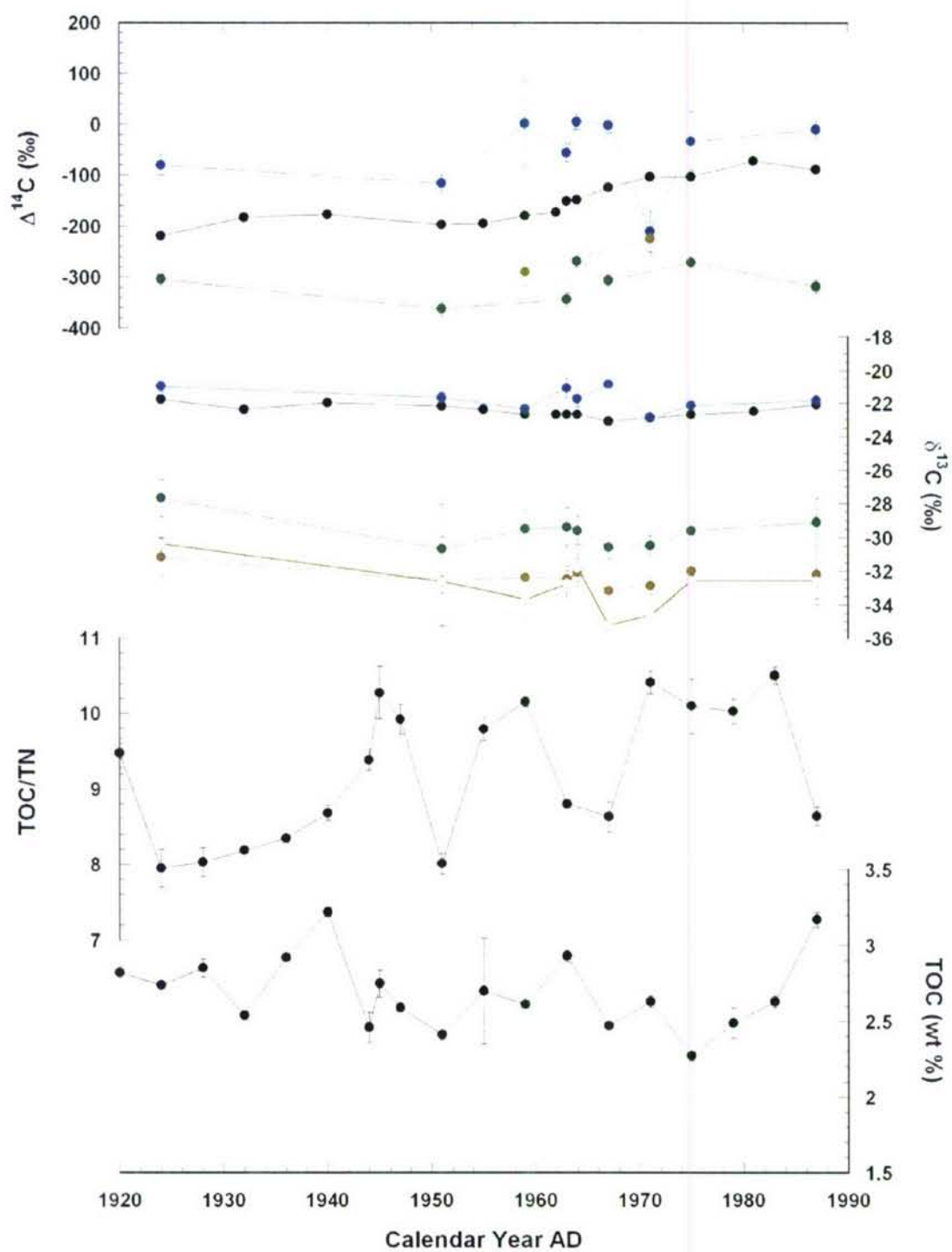


FIGURE 4.6 – Down-cores profiles for various Saanich sediment parameters. Symbols are as in Figure 4.5.

There are no systematic down core trends in either TOC or TOC/TN for the Cariaco record (slopes of 0.005 and 0.003% yr⁻¹ and r² values of 0.29 and 0.12, respectively; regressions not shown), suggesting that the flux and provenance of organic matter delivered to its sediments are in approximate steady state relative to the 100 year timeframe considered here. However, the Saanich TOC/TN profile varies in a more methodical fashion, with periods of consistently low ratios in the 1920s and 1930s giving way to generally higher ratios that are episodically punctuated by returns to lower values during the latter half of the twentieth century. These observations might reflect non-steady state behavior for OC inputs to Saanich sediments resulting from enhanced soil erosion in the latter half of the century following large scale deforestation from the late 1800s through 1960 (Tunncliffe, 2000). Additionally, the location and small size of the Saanich watershed may render it sensitive to multi-annual oscillations in large scale weather patterns (such as El Niño), which for example might alter the intensity of both marine production and terrigenous runoff (McQuoid and Hobson, 1997; Dean and Kemp, 2004; Krull et al., 2006).

4.2.2. Molecular distributions and isotopic signatures

At the molecular level, unbound fatty acids from both sites exhibit bimodal abundance distributions that are typical of marine sediments (Figures 4.8 and 4.9). Although extracts from leaf surfaces exhibit analogous patterns (Chikaraishi and Naraoka, 2006), it is typically assumed that faster degradation rates for the shorter chain homologues (Canuel, 1992; Haddad et al., 1992; Canuel and Martins, 1996; Camacho-Ibar et al., 2003) allow efficient replacement by those constantly emanating from algal

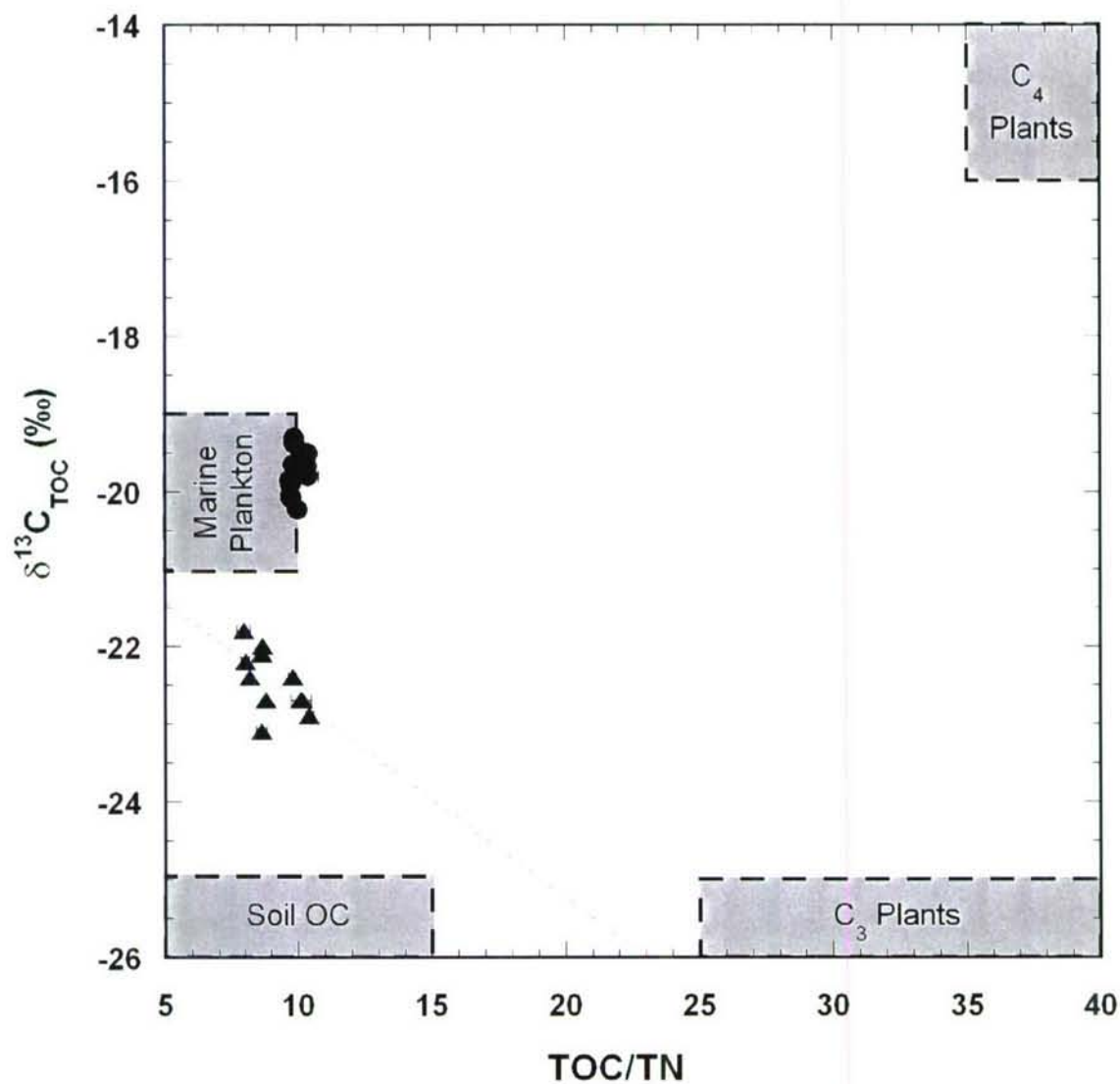


FIGURE 4.7 – Bulk OC $\delta^{13}\text{C}$ and TOC/TN cross plot for Cariaco (circles) and Saanich (triangles) sediments. Regions denoting general endmember compositions are given, along with the linear regression of the Saanich data. Endmember regions modified after Hedges and Oades (1997) and Meyers (1997).

and/or bacterial cell lysis in the marine environment (Gong and Hollander, 1997, and references therein). Their corresponding $\delta^{13}\text{C}$ and $\Delta^{14}\text{C}$ compositions can be used to confirm this tentative source assignment since (a) the $\delta^{13}\text{C}$ differences between different lipid homologues synthesized by the same terrestrial or aquatic plant is generally (though not always) no more than a few per mil (Collister et al., 1994; Lockheart et al., 1997; Schouten et al., 1998; Chikaraishi et al., 2004a,b; Nguyen Tu et al., 2004; Bi et al., 2005; Chikaraishi et al., 2006) and (b) all biomolecules inherit the $\Delta^{14}\text{C}$ of the carbon substrate from which they were synthesized (Pearson, 1999). Thus, both the roughly 5 ‰ (Cariaco) to 10 ‰ (Saanich) enrichment in the $\delta^{13}\text{C}$ compositions of the short chain homologues (Figure 4.10) and the similarity of their corresponding $\Delta^{14}\text{C}$ signatures to that of mixed layer DIC at both sites (Figure 4.11) implies a large contribution from photoautotrophic production.

This assignment can be further refined by considering the notable differences in the pattern of ^{13}C depletion with increasing chain length between the Cariaco and Saanich extracts. Specifically, fatty acid $\delta^{13}\text{C}$ signatures remain around -22 to -24 ‰ from $n\text{C}_{14}$ through $n\text{C}_{26}$ and then deplete rapidly towards $n\text{C}_{32}$ in the Cariaco, whereas mid chains ($n\text{C}_{20} - n\text{C}_{26}$) consistently display intermediate depletions in the Saanich (Figure 4.10; Appendix 4.2). The reasons for such dissimilarity amongst these two settings may include species-specific isotope effects associated with fatty acid chain elongation by the acetyl-CoA complex (e.g. Hayes, 2001), input from different species of terrestrial and aquatic plants (Collister et al., 1994; Chikaraishi et al., 2004b), seasonality (Lockheart et al., 1997), diagenetic fractionation (Nguyen Tu et al., 2004; Chikaraishi et al., 2006),

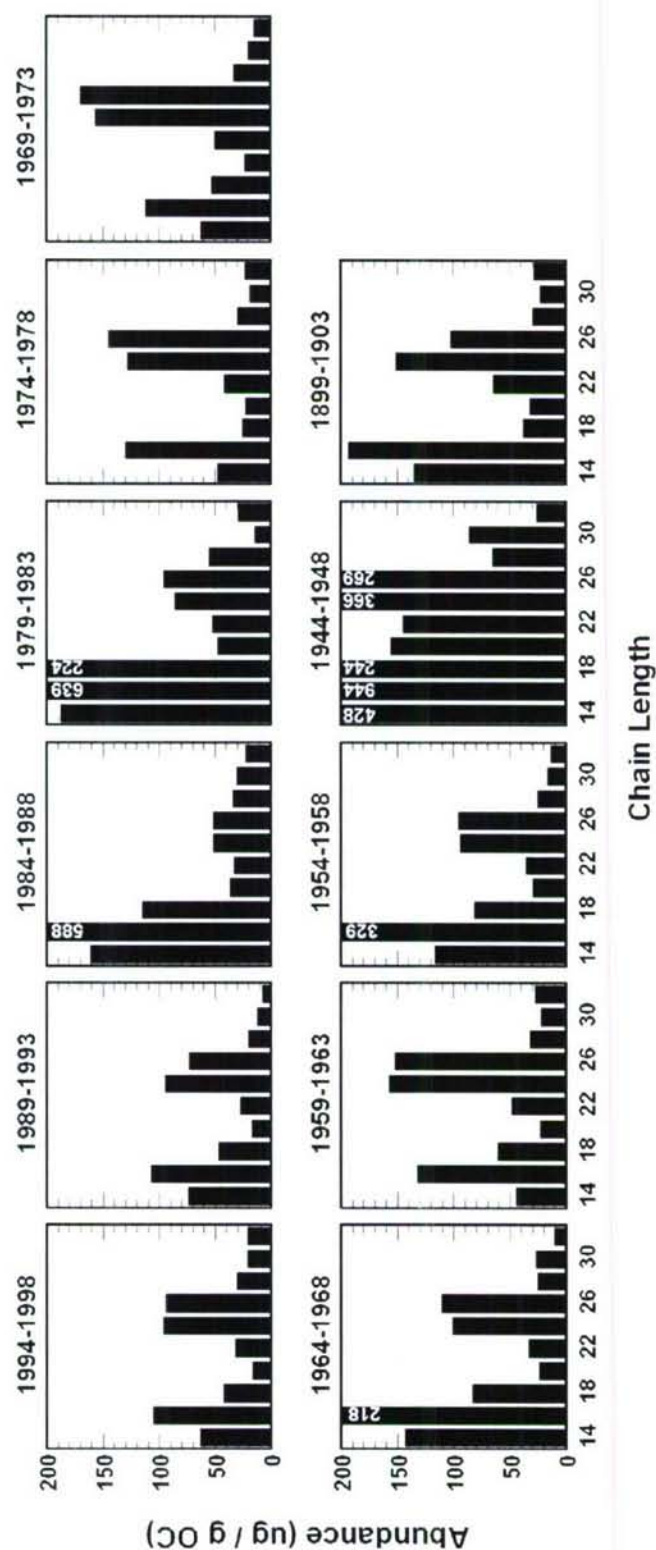


FIGURE 4.8 – Abundance of individual, even carbon numbered fatty acids from the Cariaco Basin normalized to sedimentary OC content. Values for off-scale homologues are superimposed on their respective histogram bars.

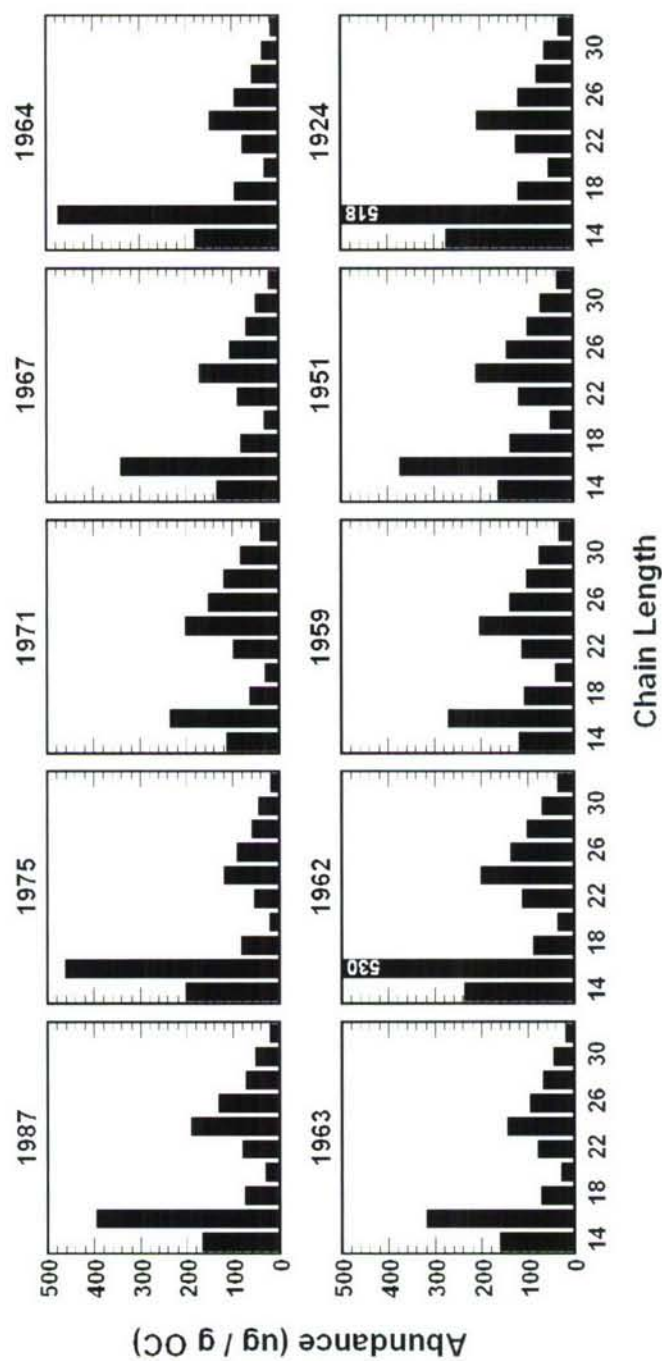


FIGURE 4.9 – Abundance of individual, even carbon numbered fatty acids from the Saanich Inlet normalized to sedimentary OC content. Values for off-scale homologues are superimposed on their respective histogram bars.

and/or the presence of algal (Schouten et al., 1998; Ratnayake et al., 2005) or bacterial (Gong and Hollander, 1997, and references therein; Abraham et al., 1998; Cifuentes and Salata, 2001) components. With respect to this last point, certain algae and bacteria have been shown to synthesize fatty acids up to nC_{28} (Schouten et al., 1998) and even as high as nC_{32} (Schweizer, 1988; Abraham et al., 1998), respectively, though this is rarely observed (and thus considered) in most applied studies. In any case, the molecular $\delta^{13}C$ evidence from the Cariaco Basin and Saanich Inlet suggests that a substantial fraction of those homologues $\leq nC_{26}$ might be derived from a marine source. The considerable spread in $\delta^{13}C$ of individual fatty acids values at both sites reveal additional information about their sources if plotted as a function of time (Figures 4.5 and 4.6). For example, the temporal covariance of nC_{32} and $nC_{26+28+30+32}$ and their collective decoupling from the $\delta^{13}C$ profiles of nC_{16} provides further evidence that the shorter chain compounds are predominantly marine in origin. Conversely, longer chain homologues are likely overwhelmed by vascular plant input. For example, the transition to more depleted $\delta^{13}C$ values for the nC_{32} acid around 1950 in the Cariaco Basin implies wetter conditions favored the expansion of C_3 vegetation in northern South America over the latter half of the 20th century. However, the relatively low temporal resolution of this profile precludes any statistically meaningful comparison between the first and second half of the century, as well as between the $\delta^{13}C$ composition of nC_{32} and TOC content.

The radiocarbon signatures of all fatty acid and TOC samples are compared to the annually averaged $\Delta^{14}C$ composition of CO_2 for the northern hemisphere in Figure 4.12 (see also Appendix 4.2). The $\Delta^{14}C$ values of nC_{16} appear to faithfully record both the

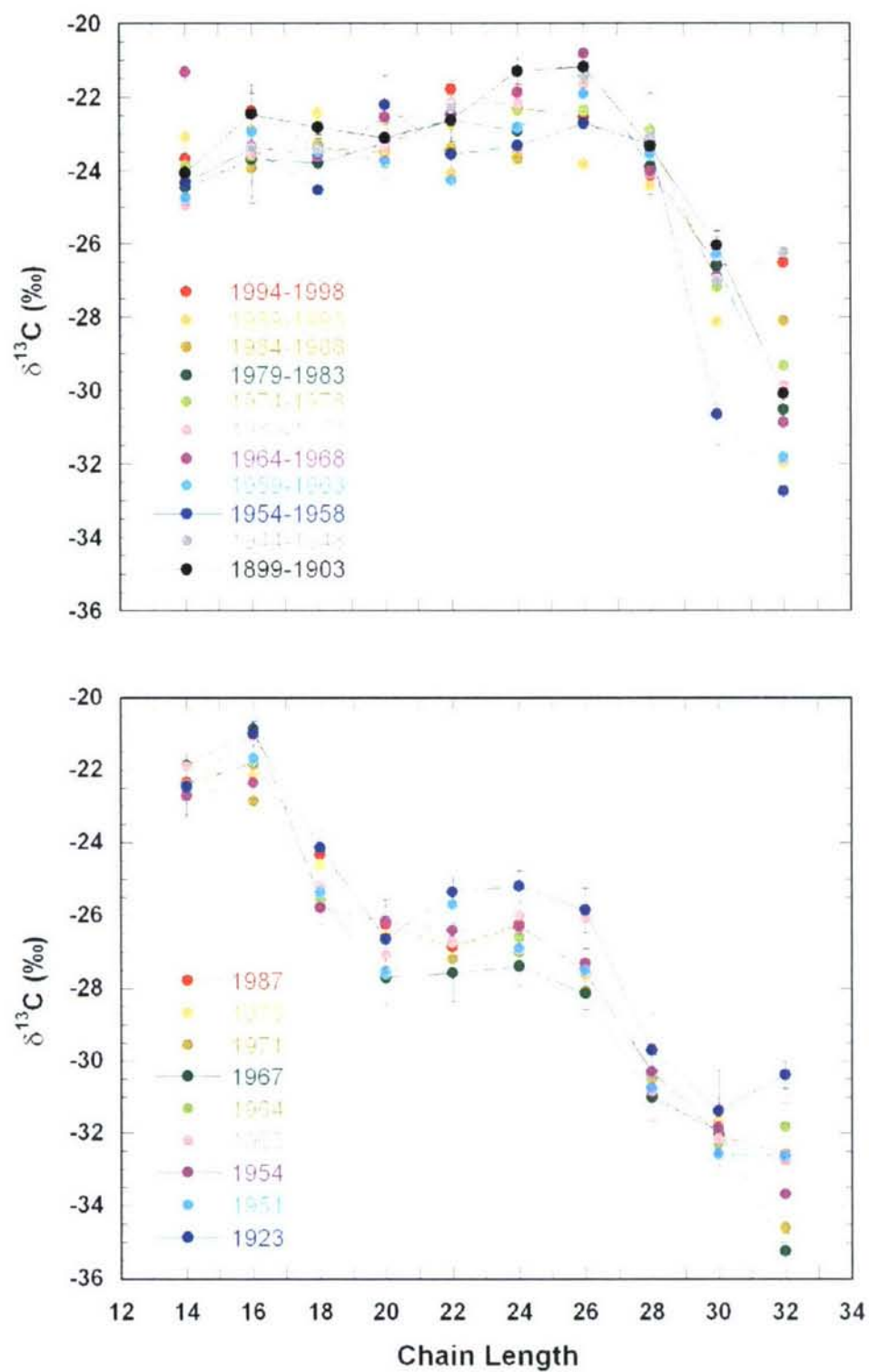


FIGURE 4.10 – Stable carbon isotopic compositions for individual fatty acids from (upper panel) Cariaco Basin, and (lower panel) Saanich Inlet.

pre-bomb (Guilderson et al., 2005) and post-bomb (Figure 4.11) $\Delta^{14}\text{C}$ composition of mixed layer DIC in the Cariaco Basin, and suggest that isotopic evolution of DIC in the surface waters of the Saanich Inlet was also similar in nature (though not exact value due to local hydrographic variability) to that of the global ocean due to the uptake of bomb-labeled $^{14}\text{CO}_2$ (Druffel, 1981, 1983, 1987, 1989, 1996; Weidman and Jones, 1993).

The individual $\Delta^{14}\text{C}$ values of the long chain homologues at any point in time likely represent a mixture of molecules that were pre-aged within a broad continuum of terrestrial reservoirs (Figure 4.1). Indeed, further insight into such processes can be attained when these molecular profiles are considered in relation to both the bomb spike and one another. Firstly, all long chain fatty acids in both records are depleted in ^{14}C relative to atmospheric CO_2 , and the magnitude of depletion systematically increases with increasing chain length. This general trend has been observed in virtually every molecular level radiocarbon study of sedimentary fatty acids thus far reported (Pearson, 1999; Uchida et al., 2000, 2001, 2005; Pearson et al., 2001; Ohkouchi et al., 2003; Dickens et al., unpublished results; Eglinton et al., unpublished results; Schefuß et al., unpublished results; Chapter 2 of this thesis), yet the underlying cause(s) of this phenomenon remain uncertain. As discussed above, it might be an artifact of mixing between the $\Delta^{14}\text{C}$ signatures of long chain homologues derived from autochthonous and allochthonous production. Alternatively, slower degradation rates for longer chain homologues (Canuel, 1992; Haddad et al., 1992; Canuel and Martins, 1996; Camacho-Ibar et al., 2003) might allow a more refractory component to survive continental sequestration for several millennia before delivery to the ocean. It should be noted that

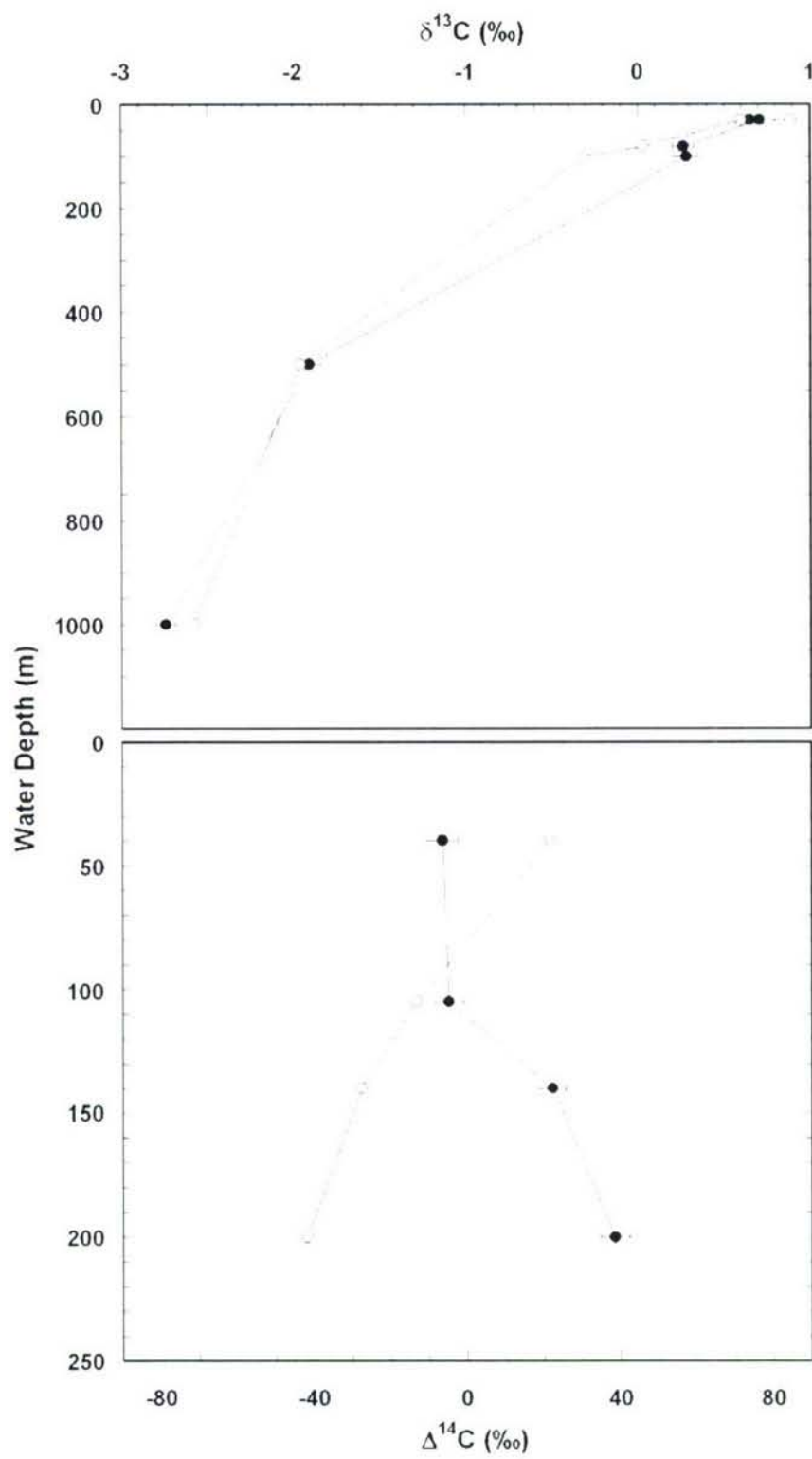


FIGURE 4.11 – The $\Delta^{14}\text{C}$ (filled) and $\delta^{13}\text{C}$ (open) profiles of water column DIC from (upper panel) Cariaco and (lower panel) Saanich.

this hypothesis appears to be more consistent with the observation of the same $\Delta^{14}\text{C}$ trend in an aerosol sample (Matsumoto et al., 2001). Thirdly, greater hydrophobicity of the longer chains may promote their association with soil organic matter and thus render them more resistant to rainwater leaching. It is nonetheless clear that, in the absence of any real bioturbation, exclusive production of these lipids from marine photoautotrophs cannot account for $\Delta^{14}\text{C}$ values much below that of mixed layer DIC, again invoking a significantly pre-aged vascular plant contribution to long chain fatty acid inventories in sediments.

Despite the overall depletion in ^{14}C relative to atmospheric CO_2 , the incorporation of bomb radiocarbon is clearly reflected in the ^{14}C enrichments displayed by long chain homologues extracted from post-1950 sediments over those from pre-1950 horizons. In the Cariaco Basin, maximum values are not seen until the early 1970s, a period when the ^{14}C content of the atmosphere was already in decline. Moreover, little enrichment over pre-bomb $\Delta^{14}\text{C}$ levels is generally observed during the peak in $^{14}\text{CO}_2$ activity. This delayed response implies that (a) some portion of these fatty acids were recently synthesized and subsequently deposited in Cariaco sediments within a decade or so, and (b) contributions from a more rapidly (e.g. seasonally, annually) delivered component are insignificant. These preliminary observations are consistent with the current configuration of the presumed terrestrial OC input pathways to the basin. Specifically, the small size of the two rivers (Unare and Tuy) that discharge directly onto the shelf adjacent to the Cariaco Basin likely foster a more direct seaward carbon flux than do larger, more developed, but more distal river systems (such as the Orinoco), whereas

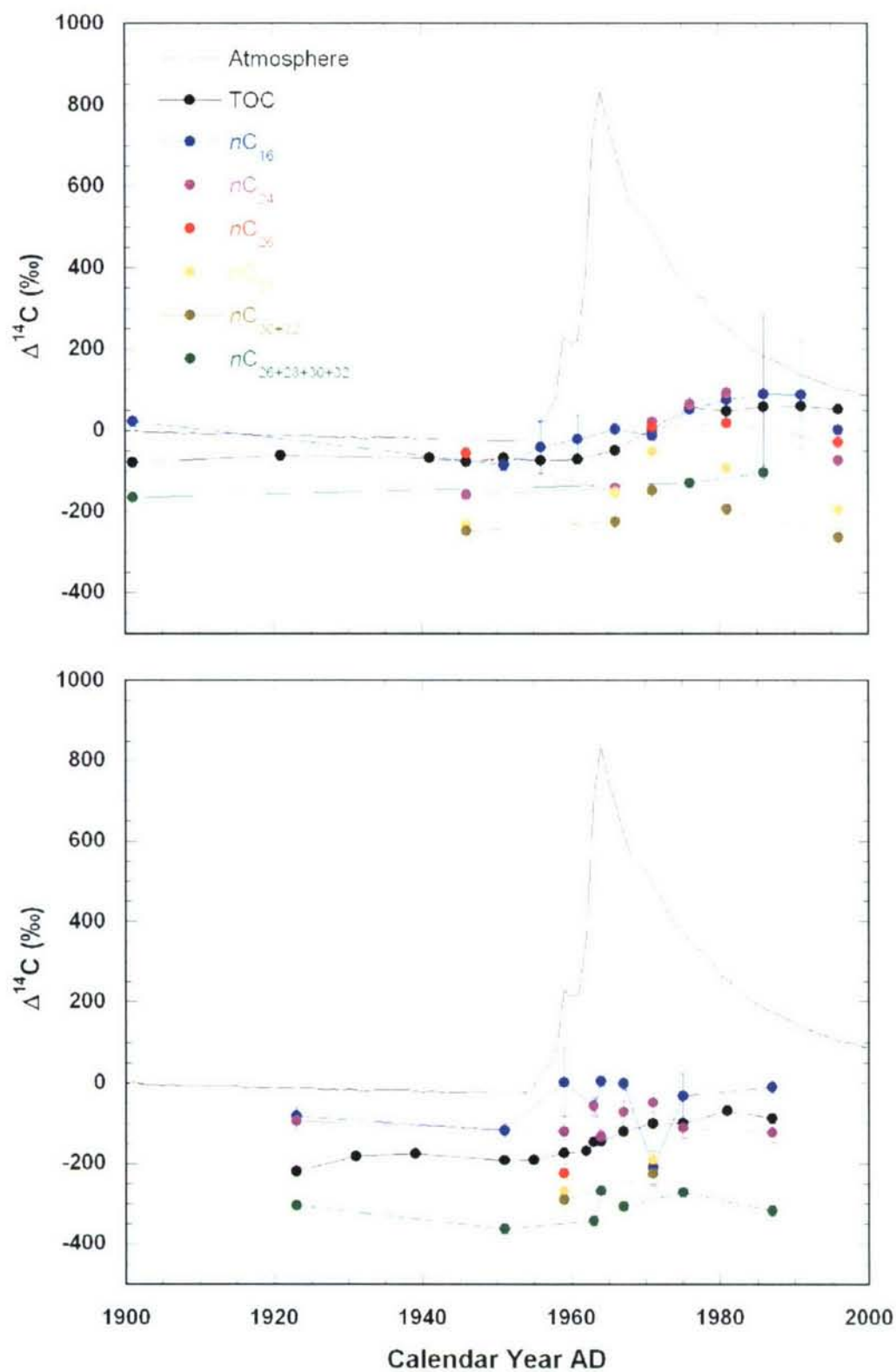


FIGURE 4.12 – Compound-specific $\Delta^{14}\text{C}$ profiles for fatty acids from (upper panel) Cariaco and (lower panel) Saanich plotted alongside those for TOC and atmospheric CO_2 . Values for fatty acids and TOC have been corrected for decay in sediments using the well-constrained chronologies developed for these sites.

significant aeolian transport of terrestrial matter on timescales as short as a year or less is improbable since the prevailing northeast trade winds establish a persistent onshore flow in this region.

In contrast, the maximum ^{14}C enrichment in the long chain fatty acids from the Saanich Inlet (measured as the combined $n\text{C}_{26+28+30+32}$) is coeval with the peak in bomb $^{14}\text{CO}_2$. Unlike the Cariaco Basin, the prevailing winds and inland setting of the Saanich likely allow either rapid aeolian delivery of some fraction of the leaf wax flux or direct runoff from the heavily vegetated hillsides surrounding the inlet. After this maximum, the $n\text{C}_{26+28+30+32}$ record displays a second peak roughly five years after that found in the separate $n\text{C}_{26}$, $n\text{C}_{28}$, and $n\text{C}_{30+32}$ homologues extracted from Cariaco sediments. This reveals the presence of another leaf wax component with a slightly longer terrestrial residence time over that experienced by its Cariaco counterpart. The amplitude of enrichment over pre-bomb values is smaller in the Saanich record, however, implying the presence of a larger component from old sources, an equivalently abundant component from even older sources, or some intermediate situation.

4.2.3. Quantitative model development and application

Resolution of the age and fractional contribution of every component of individual lipid biomarkers is beyond the scope of this study, as they likely integrate a broad continuum of temporal reservoirs ranging from those with very short (such as the atmosphere) to potentially very long (soils and wetlands) residence times. Nonetheless, the relationship between the evolution in the $\Delta^{14}\text{C}$ profiles of each fatty acid homologue and that of atmospheric CO_2 over the course of the bomb spike can be exploited in a

modeling framework to more quantitatively apportion their sedimentary inventories into several components. Based on the descriptions developed above, these are defined here as contributions from vascular plant material delivered to sediments in the same year of their synthesis, those from terrestrial reservoirs exhibiting ‘decadal’ and ‘millennial’ residence times (a dual apportionment broadly based on the soil studies of Harrison, Leavitt et al., Tegen and Dörr [all 1996], and Perruchoud et al. [1999]), and the contribution from marine production. The $\Delta^{14}\text{C}$ signatures of the annually delivered terrestrial and marine components are assumed to be equivalent to those of atmospheric CO_2 and mixed layer DIC in a given year, respectively, whereas those emanating from the decadal and millennial reservoirs should reflect the $\Delta^{14}\text{C}$ of atmospheric CO_2 integrated and decayed over the corresponding residence time τ .

This concept can be mathematically expressed for any biomarker $\Delta^{14}\text{C}$ value at time i by,

$$\Delta^{14}\text{C}_i = F_{\text{ATM}}(\Delta^{14}\text{C}_{\text{ATM}})_i + F_{\text{TER}}(\Delta^{14}\text{C}_{\text{TER}})_i + F_{\text{MAR}}(\Delta^{14}\text{C}_{\text{MAR}})_i \quad (1)$$

$$\Delta^{14}\text{C}_{\text{TER}} = f_{\text{D}}(\Delta^{14}\text{C}_{\tau} + \Delta^{14}\text{C}_{\text{decay}})_{\text{D}} + f_{\text{M}}(\Delta^{14}\text{C}_{\tau} + \Delta^{14}\text{C}_{\text{decay}})_{\text{M}} \quad (2)$$

$$F_{\text{TER}} + F_{\text{MAR}} + F_{\text{ATM}} = 1 \quad (3)$$

$$f_{\text{D}} + f_{\text{M}} = 1 \quad (4)$$

$$\Delta^{14}\text{C}_{\text{decay}} = 1000(e^{-\tau/\lambda} - 1) \quad (5)$$

where F_{ATM} , F_{TER} , and F_{MAR} , are the fractions of an individual homologue from the annual, decadal + millennial, and marine sources, f_{D} and f_{M} are the fractions of F_{TER} passing through decadal and millennial reservoirs, and $\Delta^{14}\text{C}_{\tau}$ is the residence time-dependant $\Delta^{14}\text{C}$ value of lipids released from the those reservoirs before accounting for

natural decay ($\Delta^{14}\text{C}_{\text{decay}}$) therein. Because equation (2) represents a deterministic system in the sense that $\Delta^{14}\text{C}_{\text{TER}}$ at time i is a function of those $\Delta^{14}\text{C}_{\text{TER}}$ values preceding it for τ years, solutions to these equations can only be iteratively calculated by modifying the atmospheric curve with appropriate values of terrestrial residence time in the box model until agreement with the biomarker $\Delta^{14}\text{C}$ profiles is achieved. This process can benefit from the introduction of a few simplifications. Since the concentration of radiocarbon in the atmosphere can be approximated as invariant over the past few thousand years, its integration into the millennial $\Delta^{14}\text{C}_{\tau,M}$ term will not appreciably depart from 0 ‰, such that the main contribution from the millennial reservoir to $\Delta^{14}\text{C}_{\text{TER}}$ will be the corresponding $\Delta^{14}\text{C}_{\text{decay},M}$. Conversely, radiocarbon decay within the decadal reservoir $\Delta^{14}\text{C}_{\text{decay},D}$ can be assumed to be minimal, while the bomb spike will cause a large change in the evolution of $\Delta^{14}\text{C}_{\tau,D}$. Best fit curves can thus be determined by minimizing the average residuals between calculated and measured $\Delta^{14}\text{C}_i$ values (that have been corrected for decay in sediments) as a function of the remaining variables.

This approach requires the imposition of additional boundary conditions, however. Based on discussions in earlier sections of this chapter, it is therefore further assumed that (a) the year of sedimentary deposition is known exactly, (b) bioturbation is non-existent, (c) values for $\Delta^{14}\text{C}_{\text{ATM}}$ and $\Delta^{14}\text{C}_{\text{MAR}}$ are equivalent to those of atmospheric CO_2 and $n\text{C}_{16}$, respectively, at any time point i , (d) $n\text{C}_{30+32}$ and $n\text{C}_{28}$ are exclusively derived from vascular plants (i.e. $F_{\text{MAR}} = 0$ for these homologues), and (e) the values of $\Delta^{14}\text{C}_{\text{decay},M}$ and $\Delta^{14}\text{C}_{\tau,D}$ are set by the solution for the longest chains at each site and do

not change for other homologues from those respective sites (i.e. only their fractional contributions are allowed to vary). In essence, this last condition represents a simple parameterization of the possible chain length-dependant differences in the rate of degradation and/or physiochemical weathering in real world systems mentioned earlier. Solutions are therefore first acquired for the nC_{30-32} and $nC_{26+28-30+32}$ profiles for Cariaco and Saanich, respectively, with those for shorter chain homologues at each site subsequently based on modifications in F_{ATM} , F_{TER} , F_{MAR} , f_D and f_M while $\Delta^{14}C_{decay,M}$ and $\Delta^{14}C_{\tau,D}$ remain constant.

Mean residuals were allowed to vary in both the positive and negative direction (i.e. not calculated as absolute values), such that best-fit curves neither overestimated nor underestimated most of the $\Delta^{14}C_i$ values in a given homologue's profile. Only one data point at each site was rejected *a priori* as an outlier by weighting their respective residuals to zero. These were nC_{26} in the 1944-1948 horizon for Cariaco Basin (as this sample is suspiciously enriched relative to marine-dominated TOC) and nC_{16} in 1971 for Saanich Inlet (as its $\Delta^{14}C$ value is well below that of ambient DIC in this interval interpolated from flanking data points). If unaffected by biases associated with procedural blanks that are particular to these two samples (such as PCGC co-elution with an unknown compound), their $\Delta^{14}C$ values might represent rapid departures from steady state conditions relative to the timescale considered here. However, the model described above was designed to constrain the average terrestrial residence times of vascular plant biomarkers; thus such transient behavior is not included in its solution. Lastly, it is important to point out that because these solutions were calculated iteratively for

variations in five to sometimes seven unknowns, it is possible that local – instead of global – residual minima were found even though a broad range of values for each parameter were considered. Future expansion of this study to other biomarkers and isotopes (i.e. δD) may impose more boundary conditions in which to better constrain this system.

The resulting model curves and associated best-fit parameter values for each considered homologue at both sites are shown in Figure 4.13 and Table 4.1. Mean residuals are usually $< 1\%$. For the Cariaco Basin system, terrestrial residence times are calculated to be 10 and 2570 years for the decadal and millennial reservoirs, respectively. Their fractional contributions to F_{TER} systematically increase from 0.11 to 0.31 for f_D and correspondingly decrease from 0.89 to 0.69 for f_M from the nC_{30+32} to nC_{24} homologues, suggesting that compound-specific rates of degradation and/or physiochemical weathering might indeed be important factor(s) in the delivery rates of vascular plant-derived fatty acids to marine sediments. Significant contributions from marine sources of some 44 and 60 % are also required in the solutions for the nC_{26} and nC_{24} , respectively, whereas an annually delivered (aeolian) component is absent for all homologues. Since it was not possible to apply a curve to the three lone data points for the $nC_{26+28+30+32}$ group in a statistically meaningful fashion, its particular solution represents the abundance-weighted average of those for nC_{30+32} , nC_{28} , and nC_{26} homologues as crude evaluation of the fidelity of these latter solutions. Figure 4.13 shows that the resulting curve intersects two of the three points, broadly insinuating that this approach describes some of the important mechanisms of fatty acid delivery to these sediments.

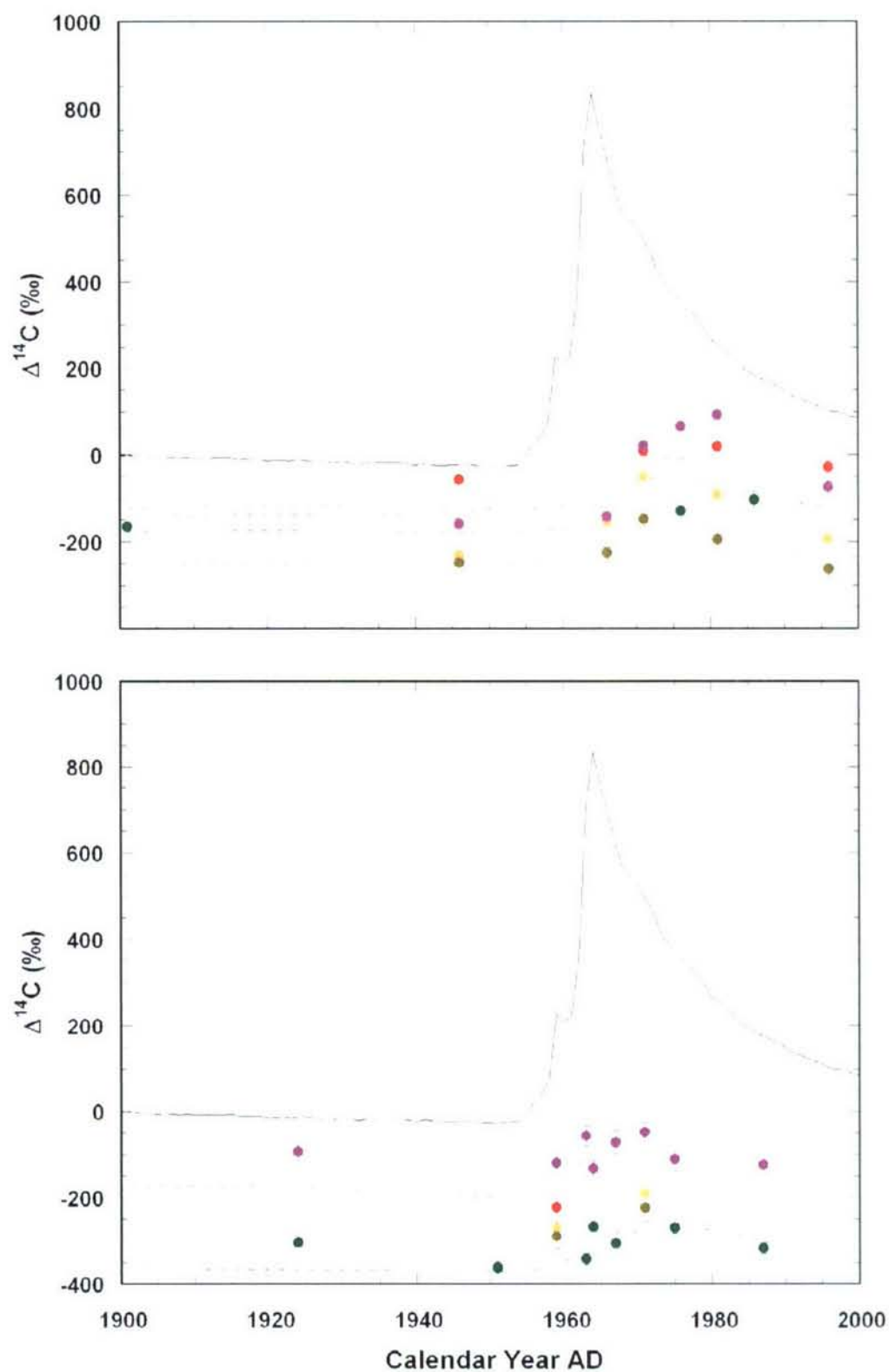


FIGURE 4.13 –Best fit model curves to the $\Delta^{14}\text{C}$ profiles for (upper panel) Cariaco and (lower panel) Saanich. Colors are as in Figure 4.12.

As anticipated, the decadal reservoir in the Saanich Inlet system sequesters material for only a slightly longer period than observed for the Cariaco Basin, while the millennial reservoir appears significantly older. The associated residence times are 20 and 5170 years for the decadal and millennial pools, respectively, with the vast majority of F_{TER} emanating from the latter for both $nC_{26+28+30+32}$ and nC_{24} . Like Cariaco, marine sources contribute 62 % of the nC_{24} flux (note again though that both systems were solved independently), but in contrast, there is a non-trivial (7 %) annually delivered

Homologue	F_{TER}	f_D	τ_D	f_M	τ_M	F_{MAR}	F_{ATM}
Cariaco Basin							
<i>Best-fit solutions</i>							
nC_{30+32}	1.00	0.11	10	0.89	2570	0.00	0.00
nC_{28}	1.00	0.28	...	0.77	...	0.00	0.00
nC_{26}	0.56	0.30	...	0.70	...	0.44	0.00
nC_{24}	0.40	0.31	...	0.69	...	0.60	0.00
<i>Sensitivity test</i>							
nC_{30+32}	1.00	0.16	10	0.84	2750	0.00	0.00
nC_{28}	1.00	0.28	...	0.72	...	0.00	0.00
Saanich Inlet							
$nC_{26+28+30+32}$	0.90	0.18	20	0.84	5170	0.03	0.07
nC_{24}	0.31	0.18	...	0.82	...	0.62	0.07

TABLE 4.1 – Best fit solutions to model parameters described in text. Colors are as in Figure 4.12. Dashed entries for τ_D and τ_M (expressed in ^{14}C years BP) indicate that their values were set by the solutions to the longest homologues first and then held constant for those of the shorter chains. Those italicized are imposed by the boundary conditions.

component required to simulate the initial rise in the $\Delta^{14}\text{C}$ signature of $n\text{C}_{26+28+30+32}$ at the onset of the atmospheric bomb spike.

All of these cost function-based solutions represent a compromise amongst equally weighted $\Delta^{14}\text{C}_i$ values for each homologue. Nonetheless, the most information-laden features of the molecular profiles with respect to residence time estimation are (a) the pre-bomb values relative to the atmosphere (for $\Delta^{14}\text{C}_{\text{decay},M}$), (b) the timing of the rise in response to the advent of the bomb spike (for $\Delta^{14}\text{C}_{\tau,D}$ and F_{ATM}), and (c) the timing and magnitude of the peak in $\Delta^{14}\text{C}_i$ achieved as the bomb spike evolves (also for $\Delta^{14}\text{C}_{\tau,D}$ and F_{ATM}). With respect to these last two points however, no value of $\Delta^{14}\text{C}_{\tau,D}$ can account for the rapid rise between $\Delta^{14}\text{C}_{1964-1968}$ and $\Delta^{14}\text{C}_{1969-1973}$ in the long chain homologues from the Cariaco Basin, whereas the addition of an annually delivered component (i.e. some nonzero F_{ATM}) would in fact reverse the direction of change in $\Delta^{14}\text{C}_i$ between those two horizons. Taken at face value, such behavior would rather imply that some of the leaf waxes synthesized every year are sequestered in individual reservoirs specific to that particular year, and that these reservoirs remain closed to any subsequent inputs or exchange until their entire inventory is instantaneously emptied into marine sediments approximately a decade later. This scenario is highly unlikely to operate in the real world, though, and the model employed here correspondingly fails to capture it. Nevertheless, the sensitivity of the model solution to the misfit as this critical interval can be ascertained by decreasing the weight of either one of these points in the calculation of residuals for a particular homologue. In order to test the extreme case, the weight of the data point in the 1964-1968 horizon as well as those in both horizons beyond the

$\Delta^{14}\text{C}_{1969-1973}$ maximum were set to zero, and the model was re-run for $n\text{C}_{30+32}$ and $n\text{C}_{28}$ (i.e. the homologues nominally ascribed exclusively to vascular plants). These sensitivity tests reveal only a modest increase in age and decrease in fractional contribution from the millennial reservoir, whereas the age of the decadal pool remains unchanged (Table 4.1). Thus, the quantitative description of the system given by the original model output appears to be robust.

Similarity in the terrestrial residence times for the decadal reservoirs within the Cariaco Basin and Saanich Inlet watersheds implies they are set by parameters that are similar at both sites, whereas the disparity in the age of their corresponding millennial reservoirs suggests these are controlled by parameters that are different. The environmental conditions that may influence these pools are the size and topographic relief of local rivers and their associated drainage basins, the age and development of the underlying soils, and annual and seasonal patterns in temperature and precipitation. The combined drainage area of the Unare and Tuy rivers in northern South America is 36,500 km², while the rivers directly proximal to the Saanich Inlet (Cowichan and Goldstream) only drain an estimated 380 km². However, there is still some uncertainty surrounding the importance of the Frazer River watershed, which encompasses some 248,000 km², to sedimentary OC in Saanich sediments. If its contribution is indeed minor, then the shorter decadal and millennial residence times observed for fatty acids from the Cariaco Basin are unlikely caused by the difference in overall drainage basin size, as larger basin/river systems might be expected to retard vascular plant OC on the continents for longer periods.

Many previous investigations have uncovered evidence for annual to multi-millennial residence times for lipids and bulk OC in soils (e.g. Harrison et al., 1993; Harrison, 1996; Huang et al., 1996; Leavitt et al., 1996; Tegen and Dörr, 1996; Perruchoud et al., 1999; Rethemeyer et al., 2004a,b; Swanston et al., 2005), though little information currently exists on the soil characteristics in these two particular areas. Nevertheless, Smittenberg et al. (2006) recently demonstrated that soil redevelopment following glacial retreat in British Columbia has led to a steady increase in the age of higher plant alkanes being delivered to Saanich Inlet sediments. Although the timescale of that study (the past ~ 12,000 years) was far too long to resolve a decadal component, the reported age of alkanes extracted from surficial sediments are equivalent to the residence time for the millennial pool calculated here. Such close correspondence suggests that the age of this reservoir may depend on the developmental extent soils in a particular drainage basin, and predicts that OC in soils surrounding the Saanich Inlet is more slowly cycled than those in northern South America.

The amount of precipitation falling on these two drainage basins may also play an important role, especially with respect to the decadal pool. While more seasonal over northern South America than in coastal British Columbia, annual mean rainfall is similar over both regions at 677 and 846 mm, respectively. Moreover, the mean residence time of groundwater in areas with similar river size and topographic relief has been estimated to be in the range of several months to one year (McGuire et al., 2002; Kabeya et al., 2007). It is thus possible that the ages of the fatty acids in the decadal reservoir reflect their physiochemical partitioning between more recalcitrant and highly retained

biopolymers (such as lignin and cutin) present in bulk soil OC and the more rapid flow of groundwater through that soil (Tegen and Dörr, 1996; Maraqa et al., 1999). Alternatively, they may represent an integrated signal from sequestration in surficial soils, wetlands, and riverbed sediments, each retarding the seaward transport of leaf waxes for years to decades. Such hypotheses may be tested in future molecular level ^{14}C investigations of soil OC, groundwater DOC, and freshwater DOC, POC, and sediment samples collected from each of these continental environments.

Lastly, it is important to point out that some portion of these residence times may not be exclusively attributable to terrestrial reservoirs. Rather, vascular plant OC might age significantly during repeated deposition/resuspension cycles in deltaic and inner shelf sediments before ultimate burial in the lower energy regions of the continental margins. Although not expected to be a major effect in the relatively small Saanich Inlet (turbidite deposits being the notable exception), this effect might play a role in setting the overall ^{14}C ages of fatty acids in the Cariaco Basin, and is even more likely to be a factor on the Eel River Margin (see Chapter 3).

4.3 CONCLUSIONS

Compound specific radiocarbon analysis of long chain fatty acids extracted from the Cariaco Basin and Saanich Inlet indicates that a portion of vascular plant OC is significantly pre-aged on the continents before delivery to marine sediments. Comparison of the down core profiles of several homologues to the $\Delta^{14}\text{C}$ composition of atmospheric CO_2 in a simple modeling framework suggests that 70 – 90 % of their annual input was sequestered on land for several millennia, while the remainder experienced a

much shorter delay of a decade or two. Along with petrogenic debris, this pre-aged terrestrial material likely represents one of the main sources of old OC currently being buried in many deltaic and margin sediments around the globe.

These findings also have important implications for the temporal relationship between, and interpretation of, paleoclimate records based on vascular plant biomarkers and other proxies of marine and terrestrial dynamics. Indeed, down core variations in the distributions and $\delta^{13}\text{C}$ and δD compositions of leaf waxes are being increasingly employed to reconstruct continental aridity fluctuations (Bird et al., 1995; Meyers, 1997; Huang et al., 1999; Freeman and Colarusso, 2001; Zhao et al., 2003; Hughen et al., 2004; Schefuß et al., 2005; Rommerskirchen et al., 2006; Makou et al., submitted; Chapter 5 of this thesis). Although decadal residence times alone would have a minimal impact on the interpretation of these records, pre-aging in substantially older pools has the potential to materially phase-shift signals relative to marine and other terrestrial proxies, especially across rapid transitions in temperature and precipitation accompanying deglacial and Dansgaard-Oeschger events. Modulation of the primary signal amplitude can also be expected due to the integration of several thousand years' worth of vegetation change (Chapter 6 of this thesis). Further research is therefore clearly needed to fully capture the extent and consequence of multi-millennial terrestrial residence times for vascular plant OC.

ACKNOWLEDGEMENTS

This study is co-authored by Timothy Eglinton, Konrad Huguen, Daniel Montluçon (all at Woods Hole Oceanographic Institution), Ellen Druffel, Guaciara dos Santos, and John Southon (all at the University of California at Irvine). I thank Ann McNichol and the entire prep lab staff at NOSAMS for accommodating my requests for rapid analyses and most especially for the frequent use of their PCGC over the years. Sheila Griffin's laboratory assistance at UCI and Ana Lima's guidance during the early stages of freeze core sectioning was most appreciated. Carl Johnson is thanked for his expertise in compound-specific $\delta^{13}\text{C}$ and elemental analyses, and the crews of the R/V *Clifford Barnes* and R/V *Hermano Gines* are acknowledged for their help in retrieving sediment cores from the Saanich Inlet and Cariaco Basin, respectively. Financial support for N.J.D. was provided by the Schlanger Ocean Drilling Graduate Fellowship and the EPA Star Graduate Fellowship. Additional support was provided by NSF grants OCE-0137005 (T.I.E and K.A.H.) and OCE-052626800 (T.I.E.).

REFERENCES

- Abraham, W.-R., Hesse, C., Pelz, O., 1998. Ratios of carbon isotopes in microbial lipids as an indicator of substrate usage. *Applied and Environmental Microbiology*, 64: 4202-4209.
- Anderson, J.J., Devol, A.H., 1973. Deep water renewal in Saanich Inlet, an intermittently anoxic basin. *Estuarine and Coastal Marine Science*, 1: 1-10.
- Astor, Y., Muller-Karger, F., Scranton, M.I., 2003. Seasonal and interannual variation in the hydrography of the Cariaco Basin: Implications for basin ventilation. *Continental Shelf Research*, 23: 125-144.
- Bi, X., Sheng, G., Liu, X., Li, C., Fu, J., 2005. Molecular and carbon and hydrogen isotopic composition of *n*-alkanes in plant leaf waxes. *Organic Geochemistry*, 36: 1405-1417.
- Bird, M.I., Summons, R.E., Gagan, M.K., Roksandic, Z., Dowling, L., Head, J., Fifield, L.K., Cresswell, R.G., Johnson, D.P., 1995. Terrestrial vegetation change inferred from *n*-alkane $\delta^{13}\text{C}$ analysis in the marine environment. *Geochimica et Cosmochimica Acta*, 59: 2853-2857.
- Blais-Stevens, A., Clague, J.J., Bobrowsky, P.T., Patterson, R.T., 1997. Late Holocene sedimentation in Saanich Inlet, British Columbia, and its paleoseismic implications. *Canadian Journal of Earth Sciences*, 34: 1345-1357.
- Brown, F.S., Baedeker, M.J., Nissenbaum, A., Kaplan, I.R., 1972. Early diagenesis in a reducing fjord, Saanich Inlet, British Columbia – III. Changes in organic constituents of sediment. *Geochimica et Cosmochimica Acta*, 36: 1185-1203.
- Calvert, S.E., Pedersen, T.F., Karlin, R.E., 2001. Geochemical and isotopic evidence for post-glacial paleoceanographic changes in Saanich Inlet, British Columbia. *Marine Geology*, 174: 287-305.
- Camacho-Ibar, V.F., Aveytua-Alcazar, L., Carriquiry, J.D., 2003. Fatty acid reactivities in sediment cores from the northern Gulf of California. *Organic Geochemistry*, 34: 425-439.
- Canuel, E.A., 1992. Seasonal variations in the sources and accumulation of organic matter in a coastal sediment. Ph.D. Thesis, University of North Carolina at Chapel Hill, Chapel Hill, NC.
- Canuel, E.A., Martens, C.S., 1996. Reactivity of recently deposited organic matter : Degradation of lipid compounds near the sediment-water interface. *Geochimica et Cosmochimica Acta*, 60: 1793-1806.
- Chikaraishi, Y., Naraoka, H., 2006. Carbon and hydrogen isotope variation of plant biomarkers in a plant-soil system. *Chemical Geology*, 231: 190-202.
- Chikaraishi, Y., Naraoka, H., Poulson, S.R., 2004a. Hydrogen and carbon isotopic fractionations of lipid biosynthesis among terrestrial (C3, C4, and CAM) and aquatic plants. *Phytochemistry*, 65: 1369-1381.
- Chikaraishi, Y., Suzuki, Y., Naraoka, H., 2004b. Hydrogen isotopic fractionations during desaturation and elongation associated with polyunsaturated fatty acid biosynthesis in marine macroalgae. *Phytochemistry*, 65: 2293-2300.

Cifuentes, L.A., Salata, G.G., 2001. Significance of carbon isotope discrimination between bulk carbon and extracted phospholipid fatty acids in selected terrestrial and marine environments. *Organic Geochemistry*, 32: 613-621.

Collister, J.W., Rieley, G., Stern, B., Eglinton, G., Fry, B., 1994. Compound-specific $\delta^{13}\text{C}$ analyses of leaf lipids from plants with differing carbon dioxide metabolisms. *Organic Geochemistry*, 21: 619-627.

Conte, M.H., Weber, J.C., 2002a. Long-range atmospheric transport of terrestrial biomarkers to the western North Atlantic. *Global Biogeochemical Cycles*, 16: doi: 10.1029/2002GB001922.

Conte, M.H., Weber, J.C., 2002b. Plant biomarkers in aerosols record isotopic discrimination of terrestrial photosynthesis. *Nature*, 417: 639-641.

Cowie, G.L., Hedges, J.I., Calvert, S.E., 1992. Sources and reactivities of amino acids, neutral sugars, and lignin in an intermittently anoxic marine environment. *Geochimica et Cosmochimica Acta*, 56: 1963-1978.

Crowley, T.J., 1995. Ice age terrestrial carbon changes revisited. *Global Biogeochemical Cycles*, 9: 377-389.

Currie, L.A., Eglinton, T.I., Benner Jr., B.A., Pearson, A., 1997. Radiocarbon "dating" of individual chemical compounds in atmospheric aerosol: First results comparing direct isotopic and multivariate statistical apportionment of specific polycyclic aromatic hydrocarbons. *Nuclear Instruments and Methods in Physics Research B*, 123: 475-486.

Dalzell, B.J., Filley, T.R., Harbor, J.M., 2007. The role of hydrology in annual organic carbon loads and terrestrial organic matter export from a Midwestern agricultural watershed. *Geochimica et Cosmochimica Acta*, 71: 1448-1462.

de Lima, A.L.C., 2004. Molecular and isotopic records of combustions inputs to the environment over the last 250 years. Ph.D. Thesis, MIT/WHOI Joint Program, Woods Hole, MA.

Dean, J.M., Kemp, A.E.S., 2004. A 2100 year BP record of the Pacific Decadal Oscillation, El Niño Southern Oscillation and Quasi-Biennial Oscillation in marine production and fluvial input from Saanich Inlet, British Columbia. *Palaeogeography, Palaeoclimatology, Palaeoecology*, 213: 207-229.

deMenocal, P., Ortiz, J., Guilderson, T., Sarnthein, M., 2000. Coherent high- and low-latitude climate variability during the Holocene warm period. *Science*, 288: 2198-2202.

Druffel, E.R.M., 1981. Radiocarbon in annual coral rings from the eastern tropical Pacific Ocean. *Geophysical Research Letters*, 8: 59-62.

Druffel, E.R.M., 1983. Long-term variability of temperature and carbon-14 in the Gulf Stream: Oceanographic implications. *Radiocarbon*, 25: 449-458.

Druffel, E.R.M., 1987. Bomb radiocarbon in the Pacific: Annual and seasonal timescale variations. *Journal of Marine Research*, 45: 667-698.

Druffel, E.R.M., 1989. Decade time scale variability of ventilation in the North Atlantic: High-precision measurements of bomb radiocarbon in banded corals. *Journal of Geophysical Research, Oceans*, 94: 3271-3285.

Druffel, E.R.M., 1996. Post-bomb radiocarbon records of surface corals from the tropical Atlantic Ocean. *Radiocarbon*, 38: 563-572.

Eglinton, T.I., Aluwihare L.I., Bauer J.E. and Druffel E.R.M., 1996. Gas Chromatographic isolation of individual compounds from complex matrices for radiocarbon dating. *Analytical Chemistry*, 68: 904-912.

Eglinton, T.I., Benitez-Nelson, B.C., Pearson, A., McNichol, A.P., Bauer, J.E., Druffel, E.R.M., 1997. Variability in radiocarbon ages of individual organic compounds from marine sediments. *Science*, 277: 796-799.

Eglinton, G., Hamilton, R.J., 1967. Leaf epicuticular waxes. *Science*, 156:1322-1335.

Fisher, E., Oldfield, F., Wake, R., Boyle, J., Appleby, P., Wolff, G.A., 2003. Molecular marker records of land use change. *Organic Chemistry*, 34: 105-119.

Freeman, K.H., Colarusso, L.A., 2001. Molecular and isotopic records of C₄ grassland expansion in the late Miocene. *Geochimica et Cosmochimica Acta*, 65: 1439-1454.

Fuhrmann, A., Mingram, J., Lucke, A., Lu, H., Horsfield, B., Liu, J., Negendank, J.F.W., Schleser, G.H., Wilkes, H., 2003. Variations in organic matter composition in sediments from Lake Huguang Maar (Huguangyan), south China during the last 68 ka: Implications for environmental and climatic change. *Organic Geochemistry*, 34: 1497-1515.

Gagosian, R.B., Peltzer, E.T., 1986. The importance of atmospheric input of terrestrial organic material to deep sea sediments. *Organic Geochemistry*, 10: 661-669.

Gong, C., Hollander, D.J., 1997. Differential contribution of bacteria to sedimentary organic matter in oxic and anoxic environments, Santa Monica Basin, California. *Organic Geochemistry*, 26: 545-563.

Goñi, M.A., Eglinton, T.I., 1996. Stable carbon isotopic analyses of lignin-derived CuO oxidation products by isotope ratio monitoring-gas chromatography-mass spectrometry (IRM-GC-MS). *Organic Geochemistry*, 24: 601-615.

Goñi, M.A., Ruttenberg, K.C., Eglinton, T.I., 1998. A reassessment of the sources and importance of land-derived organic matter in surface sediments from the Gulf of Mexico. *Geochimica et Cosmochimica Acta*, 62: 3055-3075.

Gucluer, S.M., Gross, M.G., 1964. Recent marine sediments in Saanich Inlet, a stagnant marine basin. *Limnology and Oceanography*, 9: 359-376.

Guilderson, T.P., Cole, J.E., Southon, J.R., 2005. Pre-bomb $\Delta^{14}\text{C}$ variability and the Suess effect in Cariaco Basin surface waters as recorded in hermatypic corals. *Radiocarbon*, 47: 57-65.

Haddad, R.I., Martens, C.S., Farrington, J.W., 1992. Quantifying early diagenesis of fatty acids in a rapidly accumulating coastal marine sediment. *Organic Geochemistry*, 19: 205-211.

Hamilton, S.E., Hedges, J.I., 1988. The comparative geochemistries of lignins and carbohydrates in an anoxic fjord. *Geochimica et Cosmochimica Acta*, 52: 129-142.

Harrison, K.G., 1996. Using bulk soil radiocarbon measurements to estimate soil organic matter turnover times: Implications for atmospheric CO₂ levels. *Radiocarbon*, 38: 181-190.

Harrison, K.G., Broecker, W.S., Bonani, G., 1993. The effect of changing land use on soil radiocarbon. *Science*, 262: 725-726.

Hayes, J.M., 1993. Factors controlling the ^{13}C content of sedimentary organic compounds: Principles and evidence. *Marine Geology*, 113: 111-125.

Hayes, J.M., 2001. Fractionation of the isotopes of carbon and hydrogen in biosynthetic processes. In *Stable Isotope Geochemistry, Reviews in Mineralogy and Geochemistry*, J.W. Valley and D.R. Cole (eds.): 225-278.

Hayes, J.M., Freeman, K.H., Popp, B.N., Hoham, C.H., 1990. Compound-specific isotopic analysis: A novel tool for reconstruction of ancient biogeochemical processes. *Organic Geochemistry*, 16: 1115-1128.

Hedges, J.I., 1992. Global biogeochemical cycles: Progress and problems. *Marine Chemistry*, 39: 67-93.

Hedges, J.I., Keil, R.G., Benner, R., 1997. What happens to terrestrial organic matter in the ocean? *Organic Geochemistry*, 27: 195-212.

Hedges, J.I., Oades, J.M., 1997. Comparative organic geochemistries of soils and marine sediments. *Organic Geochemistry*, 27: 319-361.

Ho, T.-Y., Taylor, G.T., Astor, Y., Varela, R., Müller-Karger, F., Scranton, M.I., 2004. Vertical and temporal variability of redox zonation in the water column of the Cariaco Basin: Implications for organic carbon oxidation pathways. *Marine Chemistry*, 86: 89-104.

Hobbie, E.A., Werner, R.A., 2004. Intramolecular, compound-specific, and bulk carbon isotope patterns in C_3 and C_4 plants: A review and synthesis. *New Phytologist*, 161: 371-385.

Holtvoeth, J., Wagner, T., Schubert, C.J., 2003. Organic matter in river-influenced continental margin sediments: The land-ocean and climate linkage at the Late Quaternary Congo fan (ODP site 1075). *Geochemistry Geophysics Geosystems*, 4: doi: 10.1029/2003GC000590.

Hua, Q., Barbetti, M., 2004. Review of tropospheric bomb ^{14}C data for carbon cycle modeling and age calibration purposes. *Radiocarbon*, 46: 1273-1298.

Huang, Y., Bol, R., Harkness, D.D., Ineson, P., Eglinton, G., 1996. Post-glacial variations in distributions, ^{13}C and ^{14}C contents of aliphatic hydrocarbons and bulk organic matter in three types of British acid upland soils. *Organic Geochemistry*, 24: 273-287.

Huang, Y., Dupont, L., Sarnthein, M., Hayes, J.M., Eglinton, G., 2000. Mapping of C_4 plant input from North West Africa into North East Atlantic sediments. *Geochimica et Cosmochimica Acta*, 64: 3505-3513.

Huang, Y., Street-Perrott, F.A., Perrott, R.A., Metzger, P., Eglinton, G., 1999. Glacial-interglacial environmental changes inferred from molecular and compound-specific $\delta^{13}\text{C}$ analyses of sediments from Sacred Lake, Mt. Kenya. *Geochimica et Cosmochimica Acta*, 63: 1383-1404.

Hughen, K.A., Eglinton, T.I., Xu, L., Makou, M., 2004. Abrupt tropical vegetation response to rapid climate change. *Science*, 304: 1955-1959.

Hughen, K.A., Overpeck, J.T., Peterson, L.C., Anderson, R.F., 1996. The nature of varved sedimentation in the Cariaco Basin, Venezuela, and its paleoclimate significance.

In *Palaeoclimatology and Palaeoceanography from Laminated Sediments*, A.E.S. Kemp (ed.): 171-183.

Johnson, K.M., Grimm, K.A., 2001. Opal and organic carbon in laminated diatomaceous sediments: Saanich Inlet, Santa Barbara Basin and the Miocene Monterey Formation. *Marine Geology*, 174: 159-175.

Kabeya, N., Katsuyama, M., Kawasaki, M., Ohte, N., Sugimoto, A., 2007. Estimation of mean residence times of subsurface waters using seasonal variation in deuterium excess in a small headwater catchment in Japan. *Hydrological Processes*, 21: 308-322.

Keil, R.G., Mayer, L.M., Quay, P.D., Richey, J.E., Hedges, J.I., 1997. Loss of organic matter from riverine particles in deltas. *Geochimica et Cosmochimica Acta*, 61: 1507-1511.

Keil, R.G., Tsamakis, E., Fuh, C.B., Giddings, J.C., Hedges, J.I., 1994. Mineralogical and textural controls on the organic composition of coastal marine sediments: Hydrodynamic separation using SPLITT-fractionation. *Geochimica et Cosmochimica Acta*, 56: 879-893.

Kolattukudy, P.E., 1969. Plant waxes. *Lipids*, 5: 259-275.

Krull, E., Sachse, D., Mügler, I., Thiele, A., Gleixner, G., 2006. Compound-specific $\delta^{13}\text{C}$ and $\delta^2\text{H}$ analyses of plant and soil organic matter: A preliminary assessment of the effects of vegetation change on ecosystem hydrology. *Soil Biology & Biochemistry*, 38: 3211-3221.

Kunst, L., Samuels, A.L., 2003. Biosynthesis and secretion of plant cuticular wax. *Progress in Lipid Research*, 42: 51-80.

Leavitt, S.W., Follett, R.F., Paul, E.A., 1996. Estimation of slow- and fast-cycling soil organic carbon pools from 6N HCl hydrolysis. *Radiocarbon*, 38: 231-239.

Leuschner, D.C., Sirocko, F., 2000. The low-latitude monsoon climate during Dansgaard-Oeschger cycles and Heinrich events. *Quaternary Science Reviews*, 19: 243-254.

Levin, I., Hesshaimer, V., 2000. Radiocarbon – A unique tracer of global carbon cycle dynamics. *Radiocarbon*, 42 : 69-80.

Levin, I., Kromer, B., 2004. The tropospheric $^{14}\text{CO}_2$ level in mid-latitudes of the northern hemisphere (1959-2003). *Radiocarbon*, 46: 1261-1272.

Lichtfouse, É., 1999. Temporal pools of individual organic substances in soil. *Analisis*, 27: 442-444.

Lichtfouse, É., Wehrung, P., Albrecht, P., 1998. Plant wax n-alkanes trapped in soil humin by noncovalent bonds. *Naturwissenschaften*, 85: 449-452.

Lockheart, M.J., Van Bergen, P.F., Evershed, R.P., 1997. Variations in the stable carbon isotope compositions of individual lipids from the leaves of modern angiosperms: implications for the study of higher plant-derived sedimentary organic matter. *Organic Geochemistry*, 26: 137-153.

Makou, M.C., Hughen, K.A., Xu, L., Sylva, S.P., Eglinton, T.I. Isotopic records of tropical vegetation and climate change from terrestrial vascular plant biomarkers preserved in Cariaco Basin sediments. Submitted.

Maraqa, M.A., Wallace, R.B., Voice, T.C., 1999. Effects of residence time and degree of water saturation on sorption nonequilibrium parameters. *Journal of Contaminant Hydrology*, 36: 53-72.

Matsumoto, K., Kawamura, K., Uchida, M., Shibata, Y., Yoneda, M., 2001. Compound-specific radiocarbon and $\delta^{13}\text{C}$ measurements of fatty acids in a continental aerosol sample. *Geophysical Research Letters*, 28: 4587-4590.

McGee, E.J., Gallagher, D., Mitchell, P.I., Baillie, M., Brown, D., Keogh, S.M., 2004. Recent chronologies for tree rings and terrestrial archives using ^{14}C bomb fallout history. *Geochimica et Cosmochimica Acta*, 68: 2509-2516.

McGuire, K.J., DeWalle, D.R., Gburek, W.J., 2002. Evaluation of mean residence time in subsurface waters using oxygen-18 fluctuations during drought conditions in the mid-Appalachians. *Journal of Hydrology*, 261: 132-149.

McQuoid, M.R., Hobson, L.A., 1997. A 91-year record of seasonal and interannual variability of diatoms from laminated sediments in Saanich Inlet, British Columbia. *Journal of Plankton Research*, 19: 173-194.

Meyers, P.A., 1997. Organic geochemical proxies of paleoceanographic, paleolimnologic, and paleoclimate processes. *Organic Geochemistry*, 27: 213-250.

Mollenhauer, G., Eglinton, T.I., Ohkouchi, N., Schneider, R.R., Müller, P.J., Grootes, P.M., Rullkötter, J., 2003. Asynchronous alkenone and foraminifera records from the Benguela upwelling system. *Geochimica et Cosmochimica Acta*, 67: 2157-2171.

Mollenhauer, G., Kienast, M., Lamy, F., Meggers, H., Schneider, R.R., Hayes, J.M., Eglinton, T.I., 2005. An evaluation of ^{14}C age relationships between co-occurring foraminifera, alkenones, and total organic carbon in continental margin sediments. *Paleoceanography*, 20: doi: 10.1029/2004PA001103.

Muller-Karger, F., Varela, R., Thunell, R., Astor, Y., Zhang, H., Luerksen, R., Chuanmin, H., 2004. Processes of coastal upwelling and carbon flux in the Cariaco Basin. *Deep-Sea Research II*, 51: 927-943/

Naraoka, H., Ishiwatari, R., 2000. Molecular and isotopic abundances of long-chain *n*-fatty acids in open marine sediments of the western North Pacific. *Chemical Geology*, 165: 23-36.

Nederbragt, A.J., Thurow, J.W., 2001. A 6000 yr varve record of Holocene climate in Saanich Inlet, British Columbia, from digital sediment colour analysis of ODP Leg 169S cores. *Marine Geology*, 174: 95-110.

Nguyen Tu, T.T., Derenne, S., Largeau, C., Bardoux, G., Mariotti, A., 2004. Diagenesis effects on specific carbon isotope composition of plant *n*-alkanes. *Organic Geochemistry*, 35: 317-329.

Ohkouchi, N., Eglinton, T.I., 2006. Radiocarbon constraint on relict organic carbon contributions to Ross Sea sediments. *Geochemistry Geophysics Geosystems*, 7: doi: 10.1029/2005GC001097.

Ohkouchi, N., Eglinton, T.I., Hayes, J.M., 2003. Radiocarbon dating of individual fatty acids as a tool for refining Antarctic margin sediment chronologies. *Radiocarbon*, 45: 17-24.

- Ohkouchi, N., Eglinton, T.I., Keigwin, L.D., Hayes, J.M., 2002. Spatial and temporal offsets between proxy records in a sediment drift. *Science*, 298: 1224-1227.
- Ohkouchi, N., Kawamura, K., Nakamura, T., Taira, A., 1997. Latitudinal distributions of terrestrial biomarkers in the sediments from the Central Pacific. *Geochimica et Cosmochimica Acta*, 61: 1911-1918.
- Oxburgh, R., 1998. Variations in the osmium isotope composition of seawater over the past 200,000 years. *Earth and Planetary Science Letters*, 159: 183-191.
- Parshotam, A., Saggar, S., Searle, P.L., Daly, B.K., Sparling, G.P., Parfitt, R.L., 2000. Carbon residence times obtained from labeled ryegrass decomposition in soils under contrasting environmental conditions. *Soil Biology & Biochemistry*, 32: 75-83.
- Pearson, A., 1999. Biogeochemical applications of compound-specific radiocarbon analysis. Ph.D. Thesis, MIT/WHOI Joint Program, Woods Hole, MA.
- Pearson, A., Eglinton, T.I., 2000. The origin of *n*-alkanes in Santa Monica Basin surface sediment: A model based on compound-specific $\Delta^{14}\text{C}$ and $\delta^{13}\text{C}$ data. *Organic Geochemistry*, 31: 1103-1116.
- Pearson, A., McNichol, A.P., Benitez-Nelson, B.C., Hayes, J.M., Eglinton, T.I., 2001. Origins of lipid biomarkers in Santa Monica Basin surface sediments: A case study using compound-specific $\Delta^{14}\text{C}$ analysis. *Geochimica et Cosmochimica Acta*, 65: 3123-3137.
- Pearson, A., Seewald, J.S., Eglinton, T.I., 2005. Bacterial incorporation of relict carbon in the hydrothermal environment of Guaymas Basin. *Geochimica et Cosmochimica Acta*, 69: 5477-5486.
- Pellatt, M.G., Hebda, R.J., Mathewes, R.W., 2001. High-resolution Holocene vegetation history and climate from hole 1034B, ODP leg 169S, Saanich Inlet, Canada. *Marine Geology*, 174: 211-226.
- Perruchoud, D., Joos, F., Fischlin, A., Hajdas, I., Bonani, G., 1999. Evaluating timescales of carbon turnover in temperate forest soils with radiocarbon data. *Global Biogeochemical Cycles*, 13: 555-573.
- Peterson, L.C., Haug, G.H., 2006. Variability in the mean latitude of the Atlantic Intertropical Convergence Zone as recorded by riverine input of sediments to the Cariaco Basin (Venezuela). *Palaeogeography, Palaeoclimatology, Palaeoecology*, 234: 97-113.
- Peterson, L.C., Haug, G.H., Hughen, K.A., Röhl, U., 2000. Rapid changes in the hydrologic cycle of the tropical Atlantic during the last glacial. *Science*, 290: 1947-1951.
- Quideau, S.A., Chadwick, O.A., Trumbore, S.E., Johnson-Maynard, J.L., Graham, R.C., Anderson, M.A., 2001. Vegetation control on soil organic matter dynamics. *Organic Geochemistry*, 32: 247-252.
- Rapalee, G., Trumbore, S.E., Davidson, E.A., Harden, J.W., Veldhuis, H., 1998. Soil carbon stocks and their rates of accumulation and loss in a boreal forest landscape. *Global Biogeochemical Cycles*, 12: 687-701.
- Ratnayake, N.P., Suzuki, N., Matsubara, M., 2005. Sources of long chain fatty acids in deep sea sediments from the Bering Sea and the North Pacific Ocean. *Organic Geochemistry*, 36: 531-541.

Raymond, P.A., Bauer, J.E., 2001. Use of ^{14}C and ^{13}C natural abundances for evaluating riverine, estuarine, and coastal DOC and POC sources and cycling: A review and synthesis. *Organic Geochemistry*, 32: 469-485.

Rieley, G., Collister, R.J., Jones, D.M., Eglinton, G., 1991. The biogeochemistry of Ellesmere Lake, U.K. – I: source correlation of leaf wax inputs to the sedimentary lipid record. *Organic Geochemistry*, 17: 901-912.

Rethemeyer, J., Grootes, P.M., Bruhn, F., Andersen, N., Nadeau, M.J., Kramer, C., Gleixner, G., 2004b. Age heterogeneity of soil organic matter. *Nuclear Instruments and Methods in Physics Research B*, 223-224: 521-527.

Rethemeyer, J., Kramer, C., Gleixner, G., John, B., Yamashita, T., Flessa, H., Andersen, N., Nadeau, M.-J., Grootes, P.M., 2005. Transformation of organic matter in agricultural soils: Radiocarbon concentration versus soil depth. *Geoderma*, 128: 94-105.

Rethemeyer, J., Kramer, C., Gleixner, G., Wiesenberger, G.L.B., Schwark, L., Andersen, N., Nadeau, M.-J., Grootes, P.M., 2004a. Complexity of soil organic matter: AMS ^{14}C analysis of soil lipid fractions and individual compounds. *Radiocarbon*, 46: 465-473.

Richter, D.D., Markewitz, D., Trumbore, S.E., Wells, C.G., 1999. Rapid accumulation and turnover of soil carbon in a re-establishing forest. *Nature*, 400: 56-58.

Rommerskirchen, F., Eglinton, G., Dupont, L., Rullkötter, J., 2006. Glacial/interglacial changes in southern Africa: Compound-specific $\delta^{13}\text{C}$ land plant biomarker and pollen records from southeast Atlantic continental margin sediments. *Geochemistry Geophysics Geosystems*, 7: doi: 10.1029/2005GC001223.

Ruddiman, W.F., 1997. Tropical Atlantic terrigenous fluxes since 25,000 yr BP. *Marine Geology*, 136: 189-207.

Sancetta, C., Calvert, S.E., 1988. The annual cycle of sedimentation in Saanich Inlet, British Columbia : Implications for the interpretation of diatom fossil assemblages. *Deep-Sea Research*, 35: 71-90.

Santos, G.M., Southon, J.R., Griffin, S., Beaupre, S.R., Druffel, E.R.M. Ultra small-mass AMS ^{14}C sample preparation and analyses at KCCAMS/UCI facility. Submitted.

Schefuß, E., Ratmeyer, V., Stuut, J.-B.W., Jansen, J.H.F., Sinninghe-Damsté, J.S., 2003. Carbon isotope analyses of *n*-alkanes in dust from the lower atmosphere over the central eastern Atlantic. *Geochimica et Cosmochimica Acta*, 67: 1757-1767.

Schefuß, E., Shouten, S., Schneider, R.R., 2005. Climatic controls on central African hydrology during the past 20,000 years. *Nature*, 437: 1003-1006.

Schouten, S., Klein Breteler, W.C.M., Blokker, P., Schogt, N., Rupstra, W.I.C., Grice, K., Baas, M., Sinninghe Damsté, J.S., 1998. Biosynthetic effects on the stable carbon isotopic compositions of algal lipids: Implications for deciphering the carbon isotopic biomarker record. *Geochimica et Cosmochimica Acta*, 62: 1397-1406.

Schweizer, E., 1988. Biosynthesis of fatty acids and related compounds. In *Microbial Lipids*, C. Ratledge and S.G. Wilkinson (eds): 3-50.

Shi, W., Sun, M.-Y., Molina, M., Hodson, R.E., 2001. Variability in the distribution of lipid biomarkers and their molecular compositions in Altamaha estuarine sediments: Implications for the relative contribution of organic matter from various sources. *Organic Geochemistry*, 32: 453-467.

Smittenberg, R.H., 2003. Holocene environmental changes disclosed from anoxic fjord sediments by biomarkers and their radiocarbon content. Ph.D. Thesis, University of Utrecht.

Smittenberg, R.H., Eglinton, T.I., Schouten, S., Sinninghe Damsté, J.S., 2006. Ongoing buildup of refractory organic carbon in boreal soils during the Holocene. *Science*, 314: 1283-1286.

Smittenberg, R.H., Hopmans, E.C., Schouten, S., Hayes, J.M., Eglinton, T.I., Sinninghe Damsté, J.S., 2004. Compound-specific radiocarbon dating of the varved Holocene sedimentary record of Saanich Inlet, Canada. *Paleoceanography*, 19: doi: 10.1029/2003PA000927.

Stuiver, M., Quay, P.D., 1981. Atmospheric ^{14}C changes resulting from fossil fuel CO_2 release and cosmic ray flux variability. *Earth and Planetary Science Letters*, 53: 349-362.

Stuiver, M., Reimer, P.J., Braziunas, T.F., 1998. High-precision radiocarbon age calibration for terrestrial and marine samples. *Radiocarbon*, 40: 1127-1151.

Swanston, C.W., Torn, M.S., Hanson, P.J., Southon, J.R., Garten, C.T., Hanlon, E.M., Ganio, L., 2005. Initial characterization of processes of soil carbon stabilization using forest stand-level radiocarbon enrichment. *Geoderma*, 128: 52-62.

Tegen, I., Dörr, H., 1996. ^{14}C measurements of soil organic matter, soil CO_2 and dissolved organic carbon (1987-1992). *Radiocarbon*, 38: 247-251.

Thunell, R.C., Varela, R., Llano, M., Collister, J., Muller-Karger, F., Bohrer, R., 2000. Organic carbon fluxes, degradation, and accumulation in an anoxic basin: Sediment trap results from the Cariaco Basin. *Limnology and Oceanography*, 45: 300-308.

Timothy, D.A., Soon, M.Y.S., 2001. Primary production and deep-water oxygen content of two British Columbian fjords. *Marine Chemistry*, 73: 37-51.

Timothy, D.A., Soon, M.Y.S., Calvert, S.E., 2003. Settling fluxes in Saanich and Jervis Inlets, British Columbia, Canada: Sources and seasonal patterns. *Progress in Oceanography*, 59: 31-73.

Trumbore, S.E., 1993. Comparison of carbon dynamics in tropical and temperate soils using radiocarbon measurements. *Global Biogeochemical Cycles*, 7: 275-290.

Trumbore, S.E., 1997. Potential responses of soil organic carbon to global environmental change. *Proceedings of the National Academy of Sciences of the United States of America*, 94: 8284-8291.

Trumbore, S.E., Harden, J.W., 1997. Accumulation and turnover of carbon in organic and mineral soils of the BOREAS northern study area. *Journal of Geophysical Research – Atmospheres*, 102: 28817-28830.

Tunncliffe, V., 2000. A fine-scale record of 130 years of organic carbon deposition in an anoxic fjord, Saanich Inlet, British Columbia. *Limnology and Oceanography*, 45: 1380-1387.

Uchida, M., Shibata, Y., Kawamura, K., Kumamoto, Y., Yoneda, M., Ohkushi, K., Harada, N., Hirota, M., Mukai, H., Tanaka, A., Kusakabe, M., Morita, M., 2001. Compound-specific radiocarbon ages of fatty acids in marine sediments from the western North Pacific. *Radiocarbon*, 43: 949-956.

Uchida, M., Shibata, Y., Kawamura, K., Yoneda, M., Mukai, H., Tanaka, A., Uehiro, T., Morita, M., 2000. Isolation of individual fatty acids in sediments using preparative capillary gas chromatography (PCGC) for radiocarbon analysis at NIES-TERRA. *Nuclear Instruments and Methods in Physics Research B*, 172: 583-588.

Uchida, M., Shibata, Y., Ohkushi, K., Yoneda, M., Kawamura, K., Morita, M., 2005. Age discrepancy between molecular biomarkers and calcareous foraminifera isolated from the same sediment horizons of Northwest Pacific sediments. *Chemical Geology*, 218: 73-89.

Wakeham, S.G., 1990. Algal and bacterial hydrocarbons in particulate organic matter and interfacial sediment of the Cariaco Trench. *Geochimica et Cosmochimica Acta*, 54: 1325-1336.

Wang, Y., Amundson, R., Trumbore, S., 1999. The impact of land use change on C turnover in soils. *Global Biogeochemical Cycles*, 13: 47-57.

Weidman, C.R., Jones, G.A., 1993. A shell-derived time history of bomb ^{14}C on Georges Bank and its Labrador Sea implications. *Journal of Geophysical Research*, 98: 14577-14588.

Werne, J.P., Hollander, D.J., 2004. Balancing supply and demand: Controls on the carbon isotopic fractionation in the Cariaco Basin (Venezuela) Younger Dryas to present. *Marine Chemistry*, 92: 275-293.

Westerhausen, L., Poynter, J., Eglinton, G., Erlenkeuser, H., Sarnthein, M., 1993. Marine and terrigenous origin of organic matter in modern sediments of the equatorial East Atlantic: the $\delta^{13}\text{C}$ and molecular record. *Deep-Sea Research I*, 40: 1087-1121.

Whiticar, M.J., Elvert, M.E., 2001. Organic geochemistry of Saanich Inlet, BC, during the Holocene as revealed by Ocean Drilling Program leg 169S. *Marine Geology*, 174: 249-271.

Wiesenberg, G.L.B., Schwartzbauer, J., Schmidt, M.W.I., Schwark, L., 2004. Source and turnover of organic matter in agricultural soils derived from n-alkane/n-carboxylic acid compositions and C-isotope signatures. *Organic Geochemistry*, 35: 1371-1393.

Woodworth, M., Goñi, M., Tappa, E., Tedesco, K., Thunell, R., Astor, Y., Varela, R., Diaz-Ramos, J.R., Müller-Karger, F., 2004. Oceanographic controls on the carbon isotopic compositions of sinking particles from the Cariaco Basin. *Deep-Sea Research I*, 51:1955-1974.

Yarincik, K.M., Murray, R.W., Lyons, T.W., Peterson, L.C., Haug, G.H., 2000. Oxygenation history of bottom waters in the Cariaco Basin, Venezuela, over the past 578,000 years: Results from redox-sensitive metals (Mo, V, Mn, and Fe). *Paleoceanography*, 15: 593-604.

Zencak, Z., Reddy, C.M., Teuten, E.L., Xu, L., McNichol, A.P., Gustafsson, Ö., 2007. Evaluation of gas chromatographic isotope fractionation and process contamination by carbon in compound-specific radiocarbon analysis. *Analytical Chemistry*, 79: 2042-2049.

Zhao, M., Dupont, L., Eglinton, G., Teece, M., 2003. *n*-Alkane and pollen reconstruction of terrestrial climate and vegetation for N.W. Africa over the last 160 kyr. *Organic Geochemistry*, 34: 131-143.

CHAPTER 5

ATLANTIC INTERTROPICAL CONVERGENCE ZONE VARIABILITY OVER THE LAST GLACIAL CYCLE

ABSTRACT

Precipitation changes in the western tropical Atlantic over the past 180 kyr are reconstructed using the stable carbon ($\delta^{13}\text{C}$) and deuterium (δD) isotopic compositions of higher plant leaf wax compounds preserved in Cariaco Basin sediments. Results indicate that less (more) precipitation fell over northern South America coincident with high latitude stadials (interstadials) relative to today. Moreover, this trend is highly modulated by precessionally driven oscillations in insolation at the end of the rainy season, such that dry events concurrent with periods of increased solar heating were less arid than those occurring when that heating was diminished (and vice versa). Together, these findings suggest that the duration of the seasonal displacement of the Intertropical Convergence Zone (ITCZ) during the last glacial cycle was modified in response to changes in both the high latitude North Atlantic (presumably due to variations in the rate of meridional overturning circulation) and local insolation during the last glacial cycle. An important link between seasonality and abrupt climate change is thus established, and used in the context of other environmental phenomena in the region to explore the possible origins of the millennial scale signals which permeate glacial climate records around the globe.

5.0 INTRODUCTION

Abrupt changes in temperature and precipitation patterns are a recurrent feature of late Quaternary climate records from many regions across the world, and have the potential to significantly impact future climate on the timescale of a human life. For example, air temperature in the high latitude northern hemisphere warmed repeatedly by as much as 10°C over just a few decades at certain times (interstadials) during the last glacial, followed by a more gradual return to periods of cooler temperatures (stadials) (Johnsen et al., 1992; Grootes et al., 1993). Twenty four such oscillations spaced at intervals of approximately 1.5 kyr or multiples thereof (1 kyr = 1000 years) have been identified over the last glacial period in ice cores recovered from Greenland (Dansgaard et al., 1993) and deep sea sediment cores (e.g. McManus et al., 1994) and are collectively known as ‘Dansgaard-Oeschger’ (D-O) events after the scientists who first discovered them (Dansgaard and Oeschger, 1989). Moreover, the rapid warmings are occasionally preceded by discharges of massive armadas of icebergs (Broecker et al., 1992) likely calved from the Hudson Strait region of the Laurentide ice sheet (Hemming, 2004). In fact, large lithogenic deposits attributed to ice rafting are one of the primary signatures of such ‘Heinrich’ events in North Atlantic sediments (Heinrich, 1988; Bond et al., 1992, 1993, 1995; McManus et al., 1999).

Evidence for millennial scale climate change is not confined to temperature or sedimentological variations at high latitudes. Voelker et al. (2002) examined climate records from around the globe spanning the particularly unstable period between 60 and 25 kyr BP known as Marine Isotope Stage (MIS) 3. D-O type variability is found in both

marine and terrestrial settings, and is expressed as changes in surface air temperature (SAT), sea surface temperature (SST), wind intensity, marine productivity and ventilation, atmospheric gas and aerosol composition, upwelling, precipitation, and vegetation. Leuschner and Sirocko (2000) also compiled a list of sites that display oscillations in the millennial band, though they focused their study on attendant modifications of the low latitude hydrologic cycle, particularly the Indian monsoon. Kiefer and Kienast (2005) recently provided a detailed comparison of numerous records documenting Pacific SST changes during Heinrich event 1.

The origin of millennial scale climatic fluctuations embedded in the last glacial cycle remains a matter of debate. Inherent oscillations in Earth's ocean or atmospheric circulation, nonlinearities arising from the coupling of these systems, and their amplified response to very small changes in solar insolation have all been advanced as possible triggers. Cause/effect relationships based on temporal lead/lag arguments have been difficult to establish, however, because of the same tight coupling and rapid dynamics amongst these systems (Xie and Tanimoto, 1998; Robertson et al., 2000; Marshall et al., 2001; Timmermann et al., 2005; Wang, 2005). The chronological uncertainties associated with mixing in, and the radiometric dating of, many paleoclimate archives present a significant hurdle to resolving such brief timescales.

Nevertheless, a great deal of evidence now points to variation in the rate of meridional overturning circulation (MOC) as a mechanism by which the underlying trigger – likely a change in the freshwater budget of Atlantic surface waters – may be translated into abrupt temperature change at high latitudes (e.g. Stocker, 1999, 2000;

Clark et al., 2001, 2002; Rahmstorf, 2002; Broecker, 2003). In its simplest form, this theory suggests that the component of poleward heat flux associated with MOC surface currents, primarily the Gulf Stream (Trenberth and Caron, 2001), was reduced during stadials as anomalous freshwater input weakened the density driven production of North Atlantic Deep Water (NADW) in the Labrador and Greenland Seas. Overturning circulation would be limited to Glacial North Atlantic Intermediate Water (GNAIW) formation in the northern edge of the North Atlantic gyre during these times, although these waters would only sink to ~ 1500 meters (m) depth, providing considerably less heat to the high latitude atmosphere. During Heinrich events, iceberg meltwater might have caused a dramatic decline in GNAIW as well. Warm tropical waters would alternatively be advected to high latitudes in the southern hemisphere, where enhanced overturning near Antarctica would fill the subsurface Atlantic basin with Antarctic Bottom Water (AABW) and Antarctic Intermediate Water (AAIW), leading to modest warming on the adjacent continent. As temperatures in the North Atlantic region gradually decline and salinity recovers (perhaps due to brine rejection associated with sea ice formation [van Kreveld et al., 2000] or decreased freshwater flux from smaller ice sheets following Heinrich events [Paillard and Labeyrie, 1994]), surface water densities would steadily increase. Upon crossing some threshold value, NADW formation would resume and initiate sudden interstadial warming, completing the cycle.

Support for abrupt MOC reorganizations in the past comes from $\delta^{13}\text{C}$ and $\delta^{18}\text{O}$ ratios in foraminifera (Boyle and Keigwin, 1987; Keigwin and Jones, 1994; Keigwin and Lehman, 1994; Keigwin et al., 1994; Keigwin and Boyle, 1999; Cortijo et al., 2000, and

references therein; van Kreveld et al., 2000; Elliot et al., 2002; Rühlemann et al., 2004; Lund and Curry, 2006; Lund et al., 2006; Peck et al., 2007), trace element and nutrient chemistry (Adkins et al., 1997; Marchitto and Broecker, 2006), atmospheric $\Delta^{14}\text{C}$ excursions (Hughen et al., 1998, 2000, 2004, 2006), sedimentological properties (Adkins et al., 1997; Bond et al., 1999; van Kreveld et al., 2000), and SST and SSS reconstructions (Rühlemann et al., 1999; Sachs and Lehman, 1999; Cortijo et al., 2000; van Kreveld et al., 2000; Lehman et al., 2002; Schmidt et al., 2004, 2006). Importantly, sedimentary $^{231}\text{Pa}/^{230}\text{Th}$ ratios have recently provided kinematic evidence for rapid changes in the rate of NADW production during the last deglaciation (McManus et al., 2004). This theory also has the advantage of offering qualified explanations for the saw-toothed shape of D-O cycles, their periodic association with Heinrich events, and the apparent asymmetry of millennial scale temperature fluctuations in Greenland versus Antarctica during the complete NADW shutdowns proposed for Heinrich events (Blunier and Brook, 2001).

In order for this scheme to be considered robust, the flux, duration, and especially location of freshwater anomalies required to significantly modify MOC require further constraint (Schmittner et al., 2000; Schmittner and Clement, 2002; Claussen et al., 2003; Lohmann, 2003; Romanova et al., 2004; Dahl et al., 2005). A high latitude source has been traditionally favored due to (a) the potential of ice sheets to produce large quantities of meltwater in a short amount of time (Fairbanks, 1989; Hyde and Crowley, 2002), (b) the injection of this meltwater directly into the region of NADW formation (Manabe and Stouffer, 2000), and (c) the ability of internal ice sheet instability to generate the

periodicities associated with D-O events (van Kreveld et al., 2000). This last point does not imply that internal dynamics are the only such ‘pacemaker’ of meltwater events from high latitude ice sheets. Indeed, the superposition of solar white noise (Hyde and Crowley, 2002) or more defined solar cycles (of some 210 and 87 years; Braun et al., 2005) have been simulated to trigger meltwater events at the requisite intervals.

The tropics have also garnered increased attention over the past decade as a potential trigger of abrupt climate change due to their importance as the heat engine powering the global hydrologic cycle. Atmospheric convection associated with low level wind convergence sustains a zonal band of strong maritime precipitation straddling the globe near the equator that is aptly termed the Intertropical Convergence Zone (ITCZ) (Chiang et al., 2002; Chiang and Vimont, 2004). In the Atlantic, the ITCZ migrates from $\sim 10^{\circ}\text{N}$ to $\sim 5^{\circ}\text{S}$ over the annual cycle in step with positive SST anomalies (Chiang et al., 2002; Biasutti et al., 2003), imparting distinct wet/dry seasonality to the coastal regions of Africa and South America (Figure 5.1). Interannual variations in the latitudinal position of the ITCZ can be thought of as an extension of this seasonal response to longer term changes in climate (Chiang, 2004). For instance, the position of the ITCZ has been shown to respond to SST anomalies associated with the strength of the MOC (Waliser and Gautier, 1993; Chiang et al., 2003; Chiang, 2004; Zhang and Delworth, 2005) as well as extratropical SAT (Broccoli et al., 2006), high latitude ice cover (Chiang et al., 2003; Chiang and Bitz, 2005), and centennial scale solar cycles (Poore et al., 2004). In fact, a SST cooling of just $\sim 1^{\circ}\text{C}$ in the northern tropics resulting from a MOC shutdown

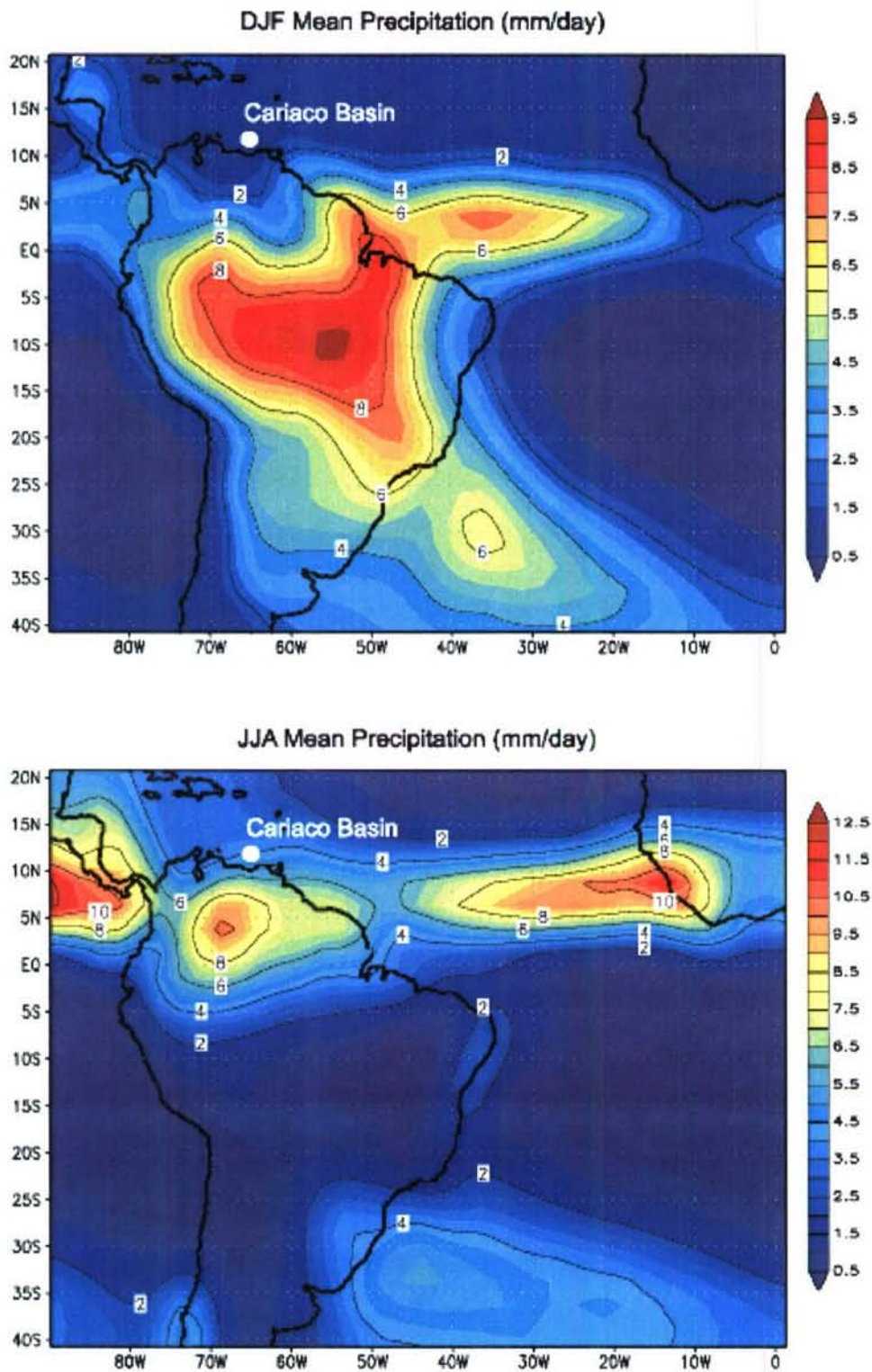


FIGURE 5.1 – Average (top) December, January, February (DJF) and (bottom) June, July, August (JJA) precipitation for South America and the adjoining Atlantic basin. Data provided by the Global Precipitation Climatology Project (GPCP) as archived at <http://www.cdc.noaa.gov/>. The band of high maritime precipitation corresponds to the ITCZ and that over central South America during DJF is the South American Summer Monsoon (SASM). The location of the Cariaco Basin is also shown.

(Rahmstorf, 2002) may have had the ability to shift the ITCZ southward by hundreds of kilometers (Chiang et al., 2002).

The tropics may in turn possess the ability to modify high latitude climate (Robertson et al., 2000; Hoerling et al., 2001; Okumura et al., 2001; Rodgers et al., 2003). In particular, the rate of NADW production associated with modern MOC (approximately 20-25 Sverdrups [Sv], $1 \text{ Sv} = 10^6 \text{ m}^3 \text{ s}^{-1}$) is thought to be influenced by the net atmospheric export of moisture from the Atlantic to Pacific oceans over the narrow Panamanian isthmus (Weyl, 1968; Weaver et al., 1999; Emile-Geay et al., 2003) as this helps to increase the salinity of the surface waters of the Atlantic, thereby preconditioning them to be dense enough to sink upon cooling at high latitudes (Zaucker et al., 1994; Benway and Mix, 2004). This inter-basin flux is attenuated over the annual cycle in response to the seasonal variations in solar insolation. SST cooling north of 5°N and warming south of the equator during the northern hemisphere winter displaces the ITCZ southward and strengthens the northeast trade winds, whereas a reduced SST gradient during summer leads to a more northward ITCZ position and relaxed trades (Chiang et al., 2002) (Figure 5.1). Thus, more freshwater is carried across the Panamanian atmospheric bridge on strong northeast trade winds during boreal wintertime than during summertime, causing noticeable tropical sea surface salinity (SSS) anomalies in the two basins (Levitus World Ocean Atlas, 1998; Benway and Mix, 2004).

Atlantic trade wind patterns and ITCZ position are also highly influenced by the atmospheric and oceanic dynamics of the tropical Pacific, particularly the El Niño – Southern Oscillation (ENSO) system (Chiang et al., 2000, 2002; Giannini et al., 2000,

2001). In the buildup preceding, and during mature El Niño phases, zonal trade winds in the Pacific weaken, allowing a deeper thermocline and warmer SSTs to develop in the eastern equatorial Pacific (EEP). This in turn enhances atmospheric convection over the central and eastern equatorial Pacific and causes anomalous subsidence over northern South America, leading to a southward deflection of the ITCZ. These changes are associated with a strengthening of the Atlantic trade winds, promoting more freshwater export to the EEP and higher surface salinities in the western tropical Atlantic (Schmittner et al., 2000). La Niña phases have the opposite effect: decreases in both SSTs and atmospheric convection in the central and eastern equatorial Pacific lead to less subsidence over the tropical North Atlantic basin and thus a more northward positioned ITCZ and slackened trade winds over the Panamanian isthmus.

A more sustained northward ITCZ position in response to more frequent La Niña events has therefore been proposed to reduce inter-basin freshwater export and create a considerable positive tropical Atlantic freshwater anomaly over time (Schmittner et al., 2000; Schmittner and Clement, 2002). Propagation of this anomaly to NADW formation regions via western boundary currents would thus gradually diminish MOC and progressively cool SATs and SSTs in the North Atlantic (Schmittner et al., 2000; Schmittner and Clement, 2002). Subsequent shift to more frequent El Niño events might then allow salt to pool in the surface waters of the southwestern subtropical gyre during stadial periods. Reduced Gulf Stream flow (Lynch-Stieglitz et al., 1999) would tend to exacerbate the buildup at low and mid latitudes until the anemic advection brought enough salt to the high latitude North Atlantic to destabilize the water column and revive

NADW production. Reinvigorated surface currents would then quickly transport the remaining salt excess poleward, intensifying MOC and generating abrupt warmth over Greenland. In line with this hypothesis, Schmidt et al. (2004, 2006) observed generally elevated surface salinities in the western subtropical Atlantic during stadials and a decrease in the SSS in the Caribbean Sea coincident with Bølling/Allerød (B/A) warming. Weldeab et al. (2006) also invoked MOC stagnation to explain increased SST and SSS in the North Brazil Current (a surface feeder for the Gulf Stream) during Heinrich event 1 (H1) and the Younger Dryas.

This scheme notably lacks a convincing mechanism by which 1500 year periodicities may be generated, although this is not to imply that no ideas have been advanced. Following a prediction that millennial scale ENSO variability would be unlikely to reside in narrow spectral bands (Cane and Clement, 1999; Clement and Cane, 1999), Clement et al. (2001) put forward the notion that abrupt changes in ENSO mode may in fact occur at relevant frequencies when forced by orbital changes in solar insolation. Indeed, there is empirical evidence for a persistent El Niño pattern during stadials (Koutavas et al., 2002; Stott et al., 2002).

Thus, millennial scale climate fluctuations have been proposed to originate in either the high latitude North Atlantic or equatorial Pacific, and each has the potential to reorganize the hydrologic cycle of the tropical Atlantic through changes in both the ITCZ position and the meridional temperature gradient (Chiang et al., 2000, 2002; Giannini et al., 2000, 2001; Münnich and Neelin, 2005; Wang, 2005). In this context, Cariaco Basin

sediments offer an invaluable archive of proxies able to document such high frequency climate variability throughout the late Quaternary.

Located off of the northern coast of Venezuela, the Cariaco Basin is a tectonic pull-apart depression consisting of two ~ 1400 m deep sub-basins separated by a ~ 900 m deep ridge. Its subsurface waters are effectively isolated from the abyssal Caribbean by a shallow (~ 150 m) sill, allowing only waters from the oxygen minimum zone to infill the deep basin today. Strong wintertime trade winds accompanying a southward displacement of the ITCZ promote upwelling of nutrient rich waters that fuel high rates of primary production (Astor et al., 2003; Goñi et al., 2003), while the northward return of ITCZ during summer (Figure 5.1) causes increased terrigenous runoff from the adjacent continent. The correspondingly large detrital carbon flux efficiently strips the remaining O₂ from deep waters below ~ 300 m (Ho et al., 2004) and leads to the preservation of annually varved sediments today that are virtually devoid of bioturbation (Hughen et al., 1996). Intermittent oxygenation of bottom waters during the last glacial period has been tied to sea level lowstands that allowed nutrient poor, O₂ rich surface waters to flush the basin (Haug et al., 1998; Yarincik et al., 2000).

The Cariaco sedimentary record also contains abundant evidence for millennial scale climate change in the tropical Atlantic region. Peterson et al. (2000) and Peterson and Haug (2006) cite variations in sedimentary metal abundances and reflectance as evidence for a tight coupling between stadial/interstadial sequences in Greenland and southward/northward displacements of the ITCZ. Lea et al. (2003) point to Mg/Ca-derived SST changes as an indication of similar co-variations over the B/A-YD

transition. Hughen et al. (2004) and Makou et al. (submitted) use the stable carbon and deuterium isotopic compositions of vascular plant leaf waxes to suggest that rapid terrestrial vegetation changes in northern South America were associated with abrupt shifts in the mean ITCZ position during deglaciation. Much smaller and shorter events are even captured during the Holocene (Haug et al., 2001; Peterson and Haug, 2006). The striking similarity between all of these records and Greenland ice cores has implicated a direct link between rapid environmental changes at high and low latitudes, yet the exact nature of this relationship remains unclear.

Here I extend the leaf wax isotope records as a direct proxy of ITCZ dynamics over the last full glacial cycle in an effort to better constrain the origin of millennial scale climate variability. Higher plants synthesize a homologous series of *n*-alkanoic (fatty) acids (among other biochemicals) that serve to regulate evapotranspiration (Eglinton and Hamilton, 1967). They are ablated from leaf surfaces and transported by either rivers or winds to marine sediments where their preservation over geologic timescales is likely aided by the intermittent anoxia in the Cariaco Basin.

The stable carbon isotopic composition ($\delta^{13}\text{C}$) of leaf waxes is largely prescribed by the particular biosynthetic pathway – C_3 , C_4 , or CAM – through which they are assembled. In general, the *n*-alkyl lipids of C_3 plants are 14.2 ± 6.5 (2σ) and 10.0 ± 4.0 (2σ) ‰ more depleted in ^{13}C than those of C_4 and CAM vegetation, respectively (Collister et al., 1994; Hobbie and Werner, 2004; Bi et al., 2005). CAM plants are rare and mainly confined to desert regions and are therefore not expected to significantly contribute to $\delta^{13}\text{C}$ variations in northern South America. The proportion of C_3 versus C_4

plants in a given ecosystem is thought to be largely controlled by ambient humidity (Huang et al., 2001), although lower $p\text{CO}_2$ during glacial intervals would tend to favor C_4 expansion as well. However, the isotopic discrimination in lipids of the same species grown under varying $p\text{CO}_2$ levels may be only 0.5 ‰ or less (Nguyen Tu et al., 2004a). The blend of C_3 and C_4 vegetation populating the drainage basins of the rivers that discharge into the Cariaco Basin (notably the Unare and Tuy) should therefore largely reflect fluctuations in the position of the ITCZ (Figure 5.2).

The factors influencing their corresponding deuterium isotopic compositions (δD) are presently less well constrained. The isotope effect strictly associated with lipid

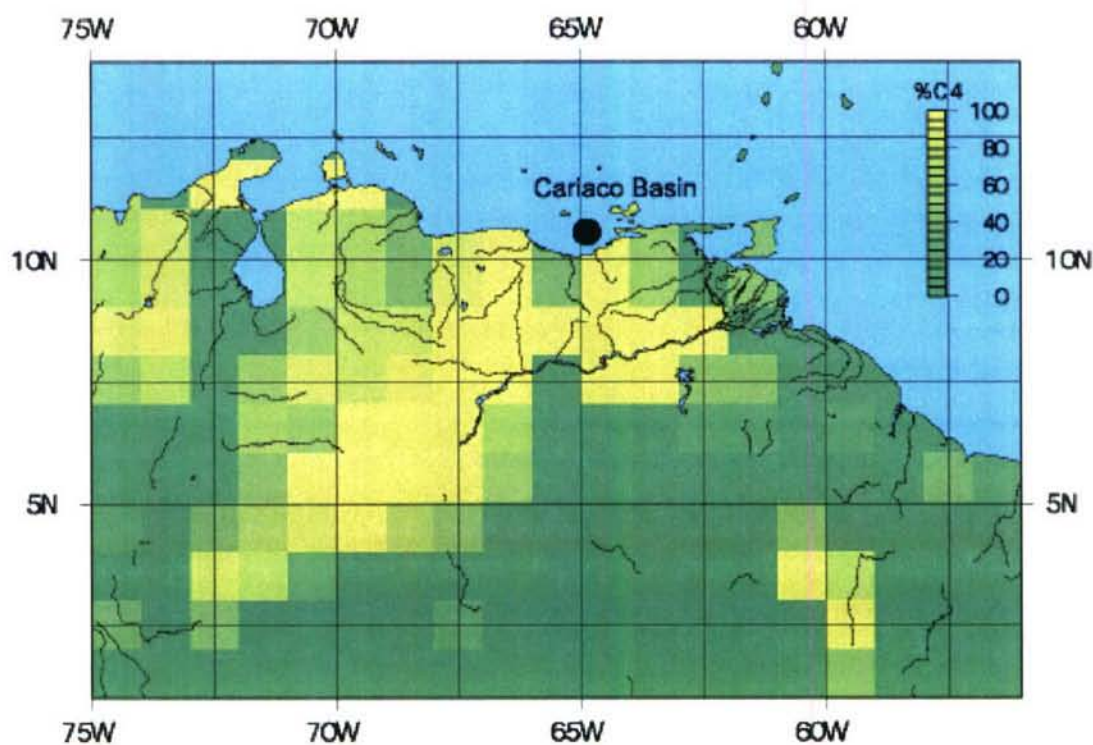


FIGURE 5.2 – Map of the relative proportion of C_3 vs C_4 vegetation in present day northern South America (data from Still et al., 2003). The location of the Cariaco Basin is also shown.

biosynthesis from the cellular water of leaves has been most readily reported for alkanes at -181 ‰ for C₃ plants (Smith and Freeman, 2006) and -157 ‰ for C₄ plants (Sessions et al., 1999, 2006; Smith and Freeman, 2006). That for their fatty acid precursors are likely to be approximately -156 ‰ and -132 ‰, respectively; i.e. some 25 ‰ more enriched (Chikaraishi and Naraoka, 2007). However, Sessions (2006) notes that a change in the substrate used for biosynthesis over the annual cycle can significantly alter the observed isotope effect. The apparent fractionation between the δD value of meteoric water and wax lipids is also usually at least 20 ‰ less than that from biosynthesis alone due to enrichment associated with evaporation from soils and evapotranspiration in the plants themselves (Sauer et al., 2001; Chikaraishi et al., 2004; Sachse et al., 2004, 2006a,b; Smith and Freeman, 2006). Leaf wax δD enrichments observed in accumulating sediments (i.e. integrated over many years) are therefore likely a consequence of both C₄ expansion and the dryer conditions that lead to it.

5.1 METHODS

5.1.1 Fatty acid extraction and isolation

Freeze-dried, ground sediment aliquots from Ocean Drilling Program (ODP) core 1002D were extracted at 100°C using 1000psi of a 90/10 (v/v) dichloromethane/methanol (DCM/MeOH) solvent mixture in an Accelerated Solvent Extractor (ASE). The resulting total lipid extracts were dried over sodium sulfate, solvent exchanged into 0.5mL of 100% DCM, and eluted through glass columns packed with 1.0g of aminopropyl-doped silica gel into the following fractions: f1 = 7mL of 90/10 (v/v) DCM/Acetone; f2 = 8mL of 2% formic acid in DCM (containing the free fatty acids). Following solvent reduction

under nitrogen, the fatty acids in each f2 fraction were esterified overnight at 70°C with a solution of 5% hydrochloric acid in anhydrous MeOH of known isotopic composition. The resulting fatty acid methyl esters (FAMES) were subsequently back-extracted into 0.5mL hexane, re-dried over sodium sulfate, and further purified by elution through a glass column containing 5% deactivated silica gel into the following fractions: f1 = 4mL hexane, f2 = 4mL of 5% ethyl acetate in hexane (containing isolated FAMES), and f3 = 4mL of MeOH. Each FAME fraction was then solvent exchanged into a known volume of hexane and injected along with authentic standards onto a gas chromatograph equipped with a flame ionization detector (GC/FID) to measure the abundance of individual FAME homologues (given in Appendix 5.1).

5.1.2 Compound-specific stable isotope analysis

Compound-specific $\delta^{13}\text{C}$ measurements on all even homologues between $n\text{C}_{16}$ and $n\text{C}_{32}$, along with a co-injected $n\text{C}_{36}$ alkane standard of known isotopic composition, were made on a HP6890 GC equipped with a CP-Sil 5 CB lowbleed/MS column (60 m x 0.25 mm i.d. x 0.25 μm film, operated under constant 1.0 mL/min helium carrier flow) coupled to a Finnigan Delta^{plus} Isotope Ratio Mass Spectrometer (IRMS) via a modified combustion interface. Results are reported as the mean of triplicate analyses (with 1 σ analytical error) in $\delta^{13}\text{C}$ (‰) notation on the VPDB scale, and have been corrected for the addition of the carboxyl methyl group during esterification via an isotopic mass balance.

Compound-specific δD measurements on the same homologues were performed on a ThermoFinnigan Trace GC equipped with a DB-5 column (30 m x 0.25 mm i.d. x 0.25 μm film) coupled to a ThermoFinnigan Delta+XP IRMS via a GC / TC (temperature

conversion) pyrolysis interface operated at 1440°C. Results are reported as the mean of duplicate or triplicate analyses (with 1σ analytical error) in δD notation (‰) relative to VSMOW by comparison to a periodically injected external standard containing a series of 15 *n*-alkanes of known δD composition, and were subsequently corrected for the addition of the carboxyl methyl group during esterification. The applied H_3^+ factor was determined daily.

5.1.3 Chronology development

Age model constraints from 10 – 75 kyr BP were provided by linking similar features of the Cariaco site 1002D sediment reflectance profile at 550nm (Hughen et al., 2006) with ^{230}Th -dated stalagmite $\delta^{18}\text{O}$ records from Hulu Cave, China (Wang et al., 2001) (Figure 5.3). Beyond 75 kyr BP, the down-core variation in the oxygen isotopic composition of planktonic foraminifer *Globigerinoides ruber* shells ($\delta^{18}\text{O}_{\text{ruber}}$) were tied to the LR04 global benthic foraminiferal $\delta^{18}\text{O}$ stack (Lisiecki and Raymo, 2005) (Figure 5.3; Appendix 5.2). Shell preservation in Cariaco sediments is generally excellent despite sedimentary organic carbon contents as high as 3 – 5 % (see Appendix 5.3 of this thesis) due to the high carbonate content of O_2 minimum zone waters spilling into the deep basin. The LR04 stack is in turn tuned to the NGRIP age model through 120 kyr BP and further anchored at 135 kyr BP by U-Th dating of fossil coral terraces from Termination II (Lisiecki and Raymo, 2005, and references therein).

The limitations inherent in this chronology should be carefully noted. For example, some of the D-O and Heinrich events recorded in the Cariaco Basin (see below) appear to be phase shifted from those in Greenland as a result of tying the Cariaco

chronology to that of Hulu Cave stalagmites, whose ^{230}Th -dated $\delta^{18}\text{O}$ curves differ from GISP2 and GRIP/NGRIP chronologies over certain intervals (Wang et al., 2001). Therefore, given the age model uncertainties, the direction of climate forcing between the two records cannot be ascertained through temporal lead/lag relationships at these timescales. Furthermore, the lack of remarkable features in the $\delta^{18}\text{O}_{\text{ruber}}$ and LR04 reconstructions beyond Termination II result in temporal uncertainties of a few millennia in the oldest part of the record.

Sedimentation rates calculated with this chronology average 33 cm kyr^{-1} , yielding a mean $\delta^{13}\text{C}$ sampling resolution of < 200 years in certain regions of interest (e.g. during MIS 2 and 3) and about 900 years overall (Figure 5.4). The corresponding D/H ratios were measured at considerably lower resolution due to the ca. 10-fold increase in required mass for δD versus $\delta^{13}\text{C}$ analyses combined with the limited abundance of fatty acids over some intervals (Appendix 5.1).

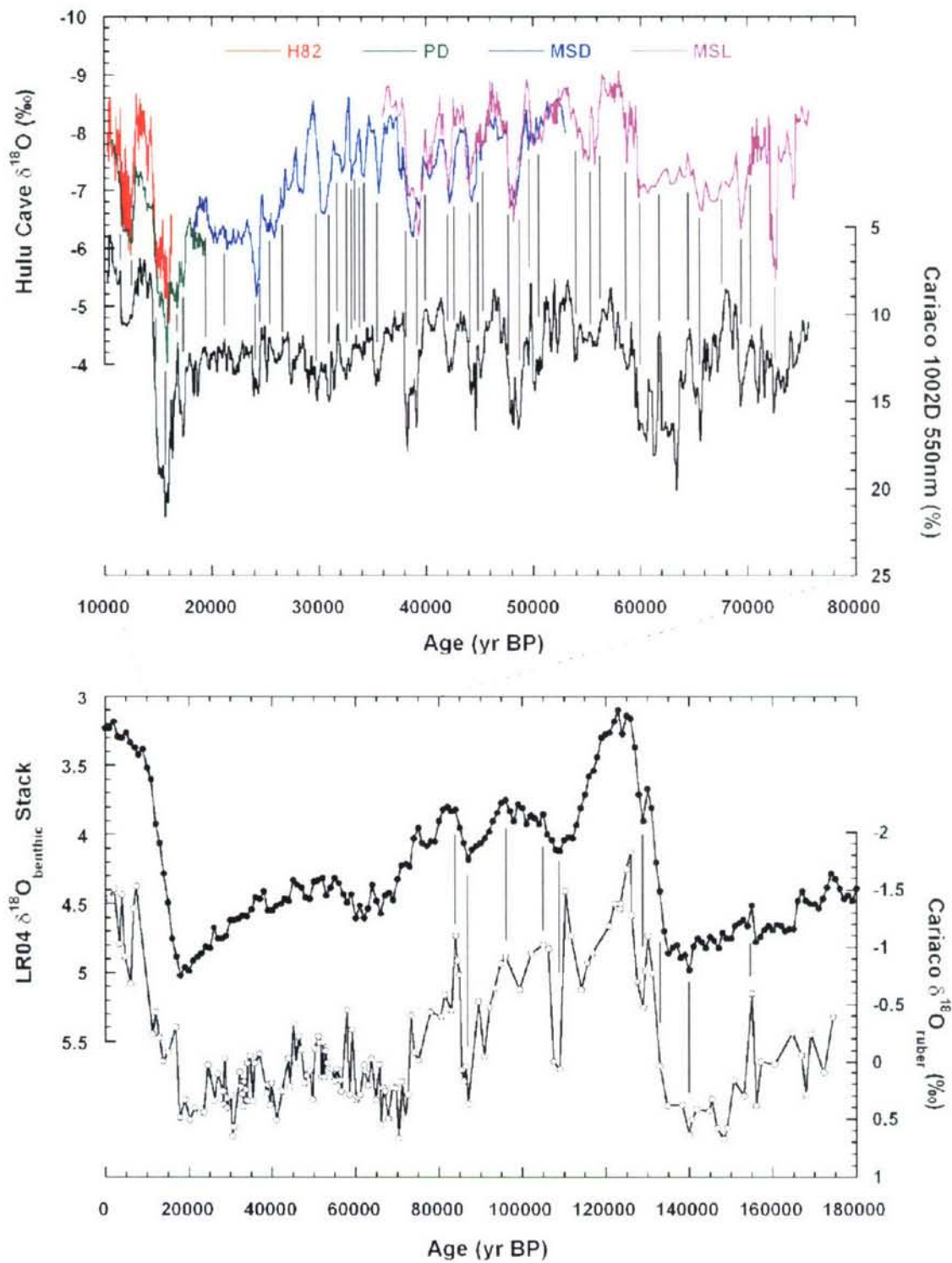


FIGURE 5.3 – Chronology development for (top) 10 – 75 kyr BP of Hulu Cave stalagmites, with colors corresponding to individual stalagmites (see Wang et al., 2001 for details); lower curve: Cariaco 1002D reflectance at 550nm] and (bottom) 75 – 180 kyr BP [upper curve: LR04 benthic stack; lower curve: Cariaco 1002D *G. ruber* $\delta^{18}\text{O}$ signatures]. Individual tiepoints among both sets of records are indicated by vertical bars.

5.2 RESULTS & DISCUSSION

5.2.1 Stable carbon isotope record

Increasing covariance between the $\delta^{13}\text{C}$ and δD compositions of the $n\text{C}_{24}$ through $n\text{C}_{30}$ (even numbered) fatty acid homologues and that of the relatively depleted $n\text{C}_{32}$ isolated from Cariaco Basin sediment indicates their increasing derivation from vascular plants and suggests that down-core variations in the isotopic composition of the latter accurately reflects changes the proportion of C_3 vs. C_4 vegetation on land (Figure 5.5). The stable carbon isotopic composition of $n\text{C}_{32}$ homologue ($\delta^{13}\text{C}_{32}$) is thus reported for the past ~ 180 kyr in Figure 5.6 and Appendix 5.2. The $\delta^{13}\text{C}_{32}$ values display large shifts

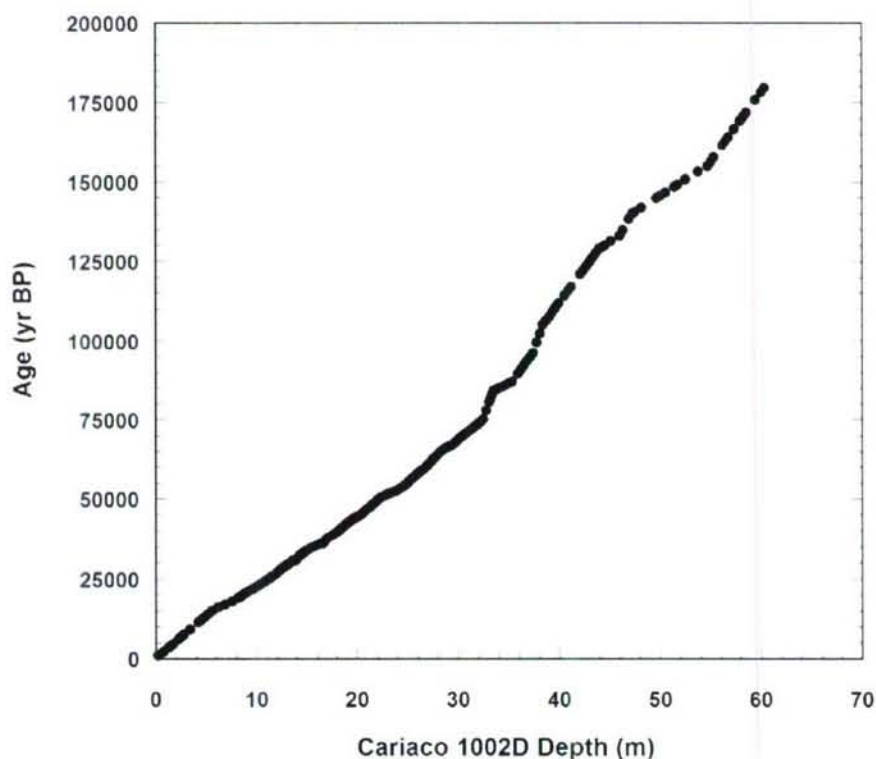


FIGURE 5.4 – Age vs. depth relationship for ODP core 1002D. Each data point corresponds to a $\delta^{13}\text{C}_{32}$ measurement reported in Figure 5.6.

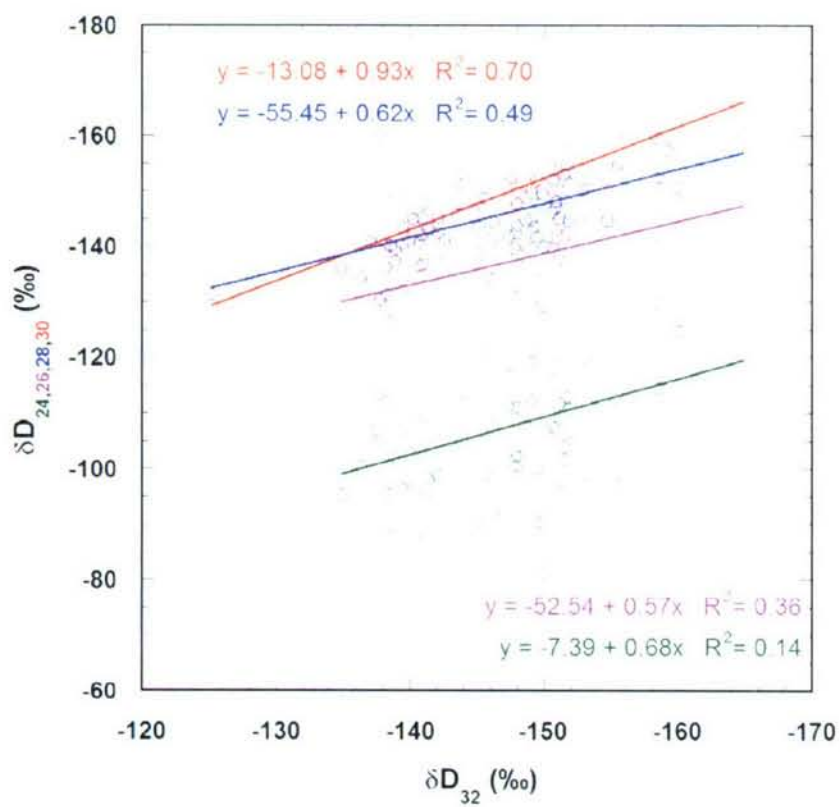
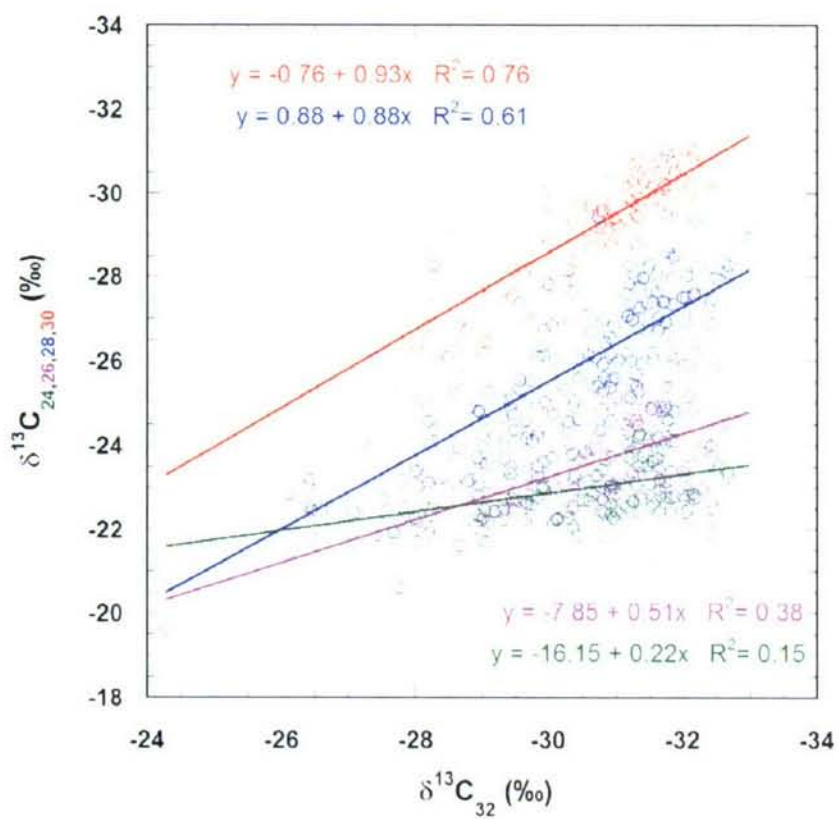


FIGURE 5.5 – Average (top) $\delta^{13}\text{C}$ and (bottom) δD signatures of long chain ($\geq n\text{C}_{24}$), even carbon-numbered fatty acids plotted against those of $n\text{C}_{32}$ from all samples discussed here. Best-fit regressions are shown.

in range from a maximum depletion of -32.9 ‰ at 140.6 kyr BP to their most enriched at -24.3 ‰ at 38.6 kyr BP. These values approach the endmember compositions for leaf waxes from C₃ and C₄ plants, respectively, and therefore indicate significant shifts in their relative abundances and correspondingly large fluctuations in precipitation over northern South America during the last glacial cycle.

In general, signatures between -30 and -33 ‰ suggest C₃ plants populated a large portion of the landscape from 20 to 180 kyr BP, indicating that a relatively humid environment prevailed over northern South America for much of this period. Rapid ¹³C enrichments periodically punctuate the record, however, reflecting the expansion of C₄ plants under extended drought conditions. These events are particularly large and frequent during MIS 3 and appear to correspond with D-O temperature cycles recorded in the oxygen isotopic composition of Greenland ice cores ($\delta^{18}\text{O}_{\text{ice}}$) (Figure 5.7). Specifically, warm intervals in the North Atlantic (characterized by enrichments in $\delta^{18}\text{O}_{\text{ice}}$) are associated with increased precipitation in northern South America (reflected by $\delta^{13}\text{C}_{32}$ depletions). The converse is true during stadial conditions. Unlike $\delta^{18}\text{O}_{\text{ice}}$ however, the amplitude of the $\delta^{13}\text{C}_{32}$ oscillations does not remain relatively uniform. For example, the ~ 4 ‰ enrichment in Greenland $\delta^{18}\text{O}_{\text{ice}}$ at the onset of major interstadial 8 is accompanied by a ~ 7 ‰ depletion in Cariaco $\delta^{13}\text{C}_{32}$, whereas a similar $\delta^{18}\text{O}_{\text{ice}}$ enrichment for major interstadial 12 is only accompanied by a ~ 2.5 ‰ $\delta^{13}\text{C}_{32}$ shift. Some D-O events are only weakly expressed in the $\delta^{13}\text{C}_{32}$ record and a few interstadials (such as 18) appear to be completely absent. Although some of this decoupling may be due to the difference in sampling interval between the earlier and latter half of the record,

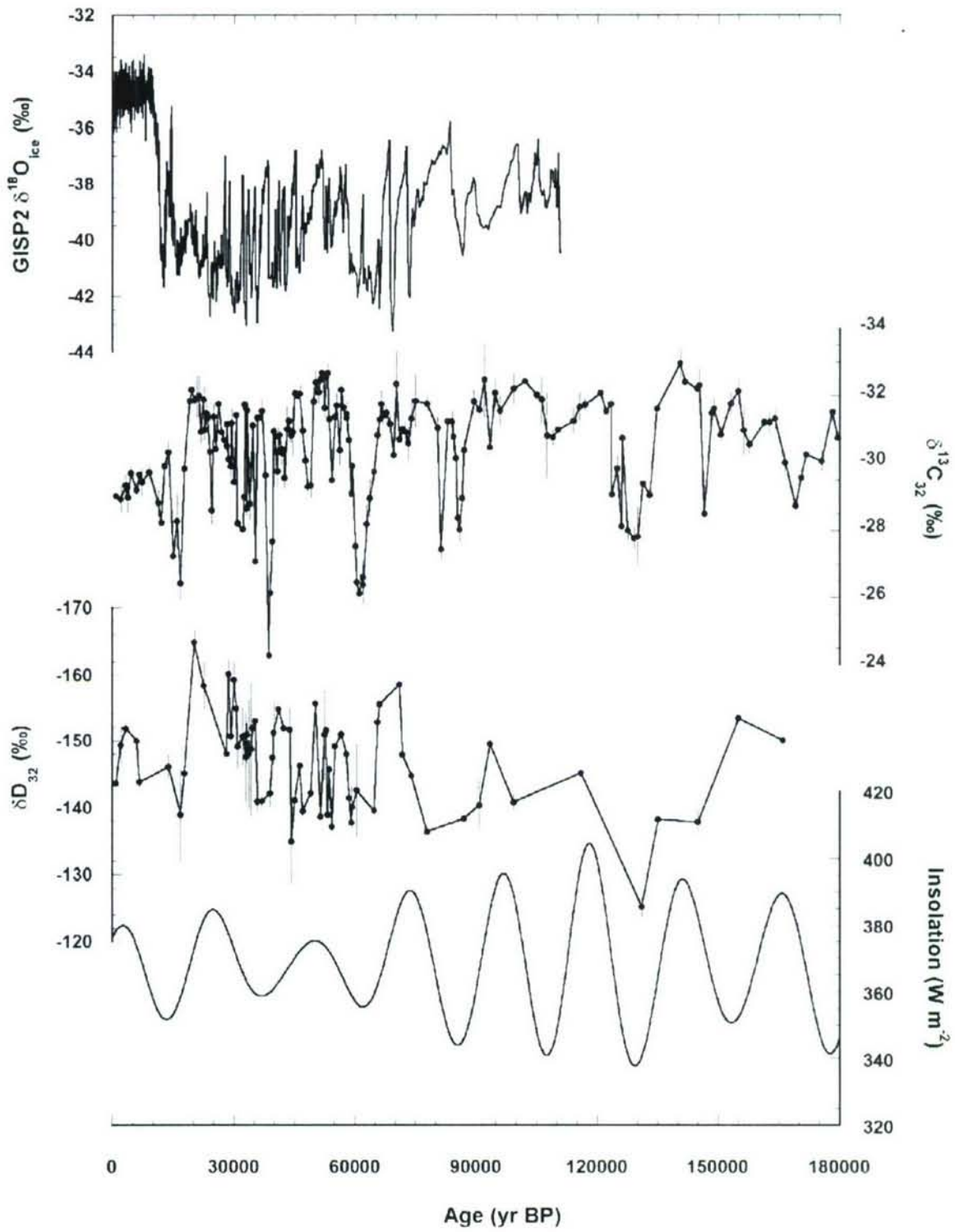


FIGURE 5.6 – (Top to bottom): GISP2 $\delta^{18}\text{O}_{\text{ice}}$, Cariaco $\delta^{13}\text{C}_{32}$, Cariaco δD_{32} , and November insolation at 10°N for the past 180 kyr. For the Cariaco records, each data point represents the mean of (generally) three replicates with the corresponding 1σ analytical uncertainty plotted as error bars.

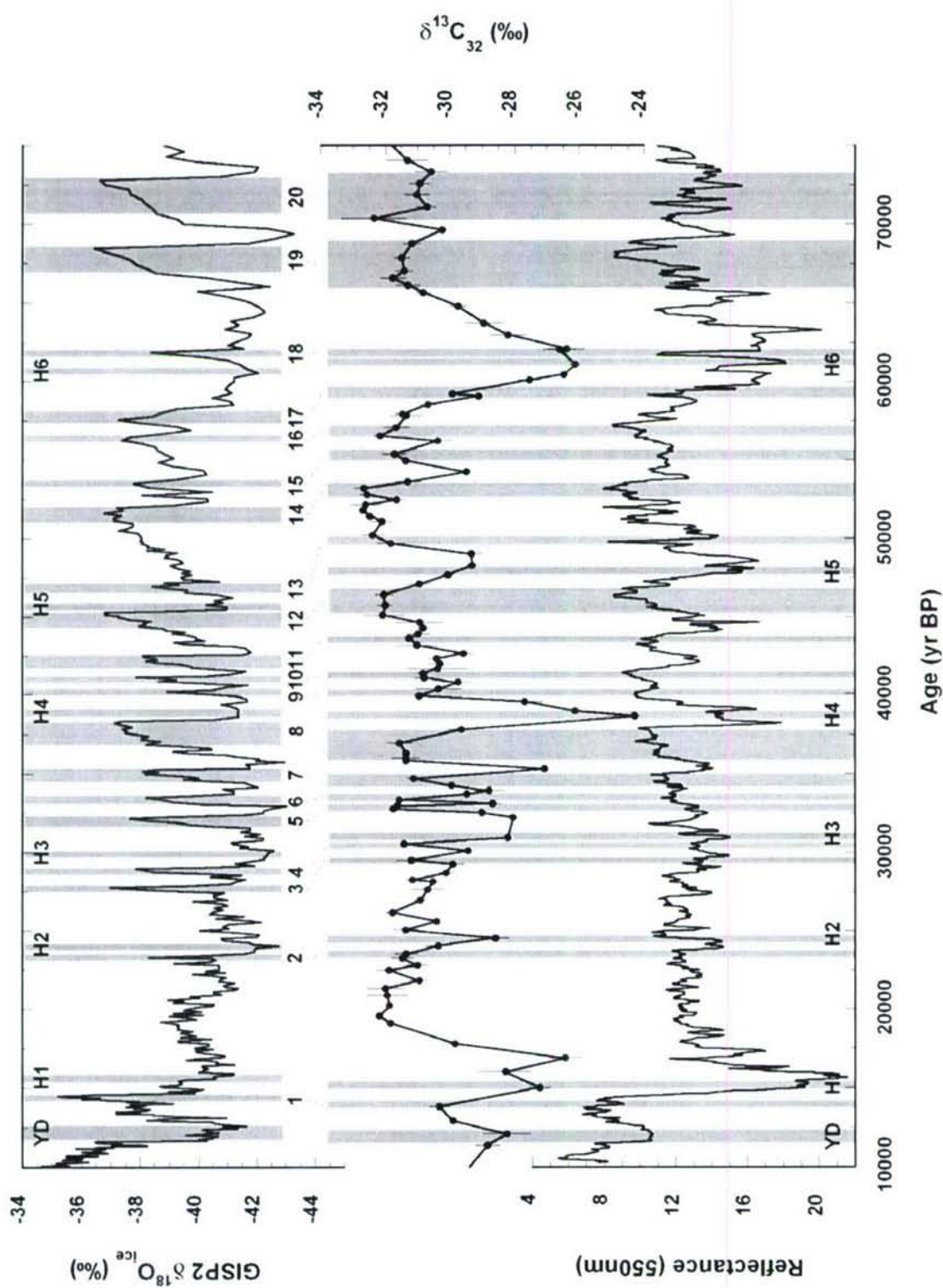


FIGURE 5.7 – (Top to bottom): GISP2 $\delta^{18}O_{ice}$, Cariaco $\delta^{13}C_{32}$, and Cariaco sediment reflectance at 550nm. The association of numbered interstadial and Heinrich events between the GISP2 and Cariaco records is shown by grey bars.

the resolution in MIS 3 & 4 with respect to the duration of the interstadial events defined by GISP2 $\delta^{18}\text{O}_{\text{ice}}$ is sufficient to accurately record an obvious decrease in oscillatory amplitude over ~ 11 kyr on either side of interstadials 8 and 17.

The hydrologic expression of Heinrich events in tropical South America appears to be similarly amplitude-modulated. The most enriched $\delta^{13}\text{C}_{32}$ value of the entire record (-24.3 ‰) is associated with H4, and serves as the inflection point from which the aforementioned ~ 7 ‰ transition to interstadial 8 proceeds. Heinrich events 6 and 1, ~ 23 kyr prior to and proceeding H4 respectively, likewise fall in $\delta^{13}\text{C}_{32}$ maxima, with smaller signal amplitudes associated with the intervening events of H0 (i.e. the Younger Dryas, YD), H2, H3, and H5.

Holocene $\delta^{13}\text{C}_{32}$ values are consistently enriched by > 2 ‰ over those from the last glacial maximum. This is unexpected as some empirical and model evidence suggest the ITCZ was displaced southward during the LGM relative to today (Chiang et al., 2003; Lea et al., 2003; Chiang and Bitz, 2005; Justino and Peltier, 2005; Broccoli et al., 2006). However, Peterson and Haug (2006) attribute a similar discrepancy in sedimentary titanium concentrations to a change in delivery caused by the ~ 120 m reduction in global sea level. One could therefore postulate that an exposed continental shelf populated by C_3 vegetation could account for the baseline $\delta^{13}\text{C}_{32}$ depletions during the glacial period. Holocene enrichments are not observed during the penultimate interglacial, however, with the values of approximately -32 ‰ that characterize MIS 2 also prevailing during MIS 5e. This difference is also unlikely to be diagenetically controlled since biological consumption has been shown to enrich the residual lipid pool in ^{13}C (Nguyen Tu et al.,

2004b; Chikaraishi and Naraoka, 2006). Thus, the data suggest the Holocene hydrological cycle in the tropical North Atlantic may be anomalous, as previously reported for Salar de Uyuni (Baker et al., 2001). On a more subtle scale, a ~ 0.7 ‰ $\delta^{13}\text{C}_{32}$ enrichment does accompany a decrease in sediment titanium and iron concentrations from the early to late Holocene (Haug et al., 2001), with both pointing to gradual drying during this time. Finally, it should be noted that the $\delta^{13}\text{C}$ values of long chain fatty acids extracted from modern sediments from the mouth of the Unare River (A. Dickens, personal communication), likely one of the major delivery pathways for leaf waxes to the Cariaco Basin, are similar to those from near-surface horizons of ODP Hole 1002D reported here.

5.2.2 Deuterium isotope record

In order to isolate the component attributable to local humidity fluctuations alone, it is necessary to account for the change in the leaf wax δD signal due to the isotopic evolution of mean ocean water over the glacial cycle. High latitude ice sheets preferentially incorporate H_2O over HDO as they grow, leaving the water remaining in the ocean enriched in HDO (Jouzel et al., 2000). Because the meteoric water used for biosynthesis in terrestrial plants is ultimately sourced from the ocean, their corresponding lipids will inherit this isotopic enrichment during intervals of extensive ice sheets. The fatty acid δD signatures reported here are therefore nominally corrected for global ice volume by multiplying the change in the $\delta^{18}\text{O}$ of mean ocean water from present, or $\Delta\delta^{18}\text{O}_w$ (constrained by the LR04 benthic foraminiferal $\delta^{18}\text{O}$ stack [Lisiecki and Raymo, 2005]), by the slope of the regression describing the modern meteoric $\delta^{18}\text{O}$ - δD

relationship for the globe (approximately 8, as compiled by the International Atomic Energy Agency [www.iaea.org]). It is important to bear in mind that the magnitude of this correction is nontrivial relative to the residual signal amplitudes and reaches a maximum of 14 ‰ during the LGM.

The variation in the deuterium isotopic composition of the nC_{32} fatty acids (δD_{32}) after normalization is shown in Figure 5.6 and Appendix 5.2. Enrichments (depletions) in δD_{32} generally accompany $\delta^{13}C_{32}$ shifts through stadial (interstadial) transitions, suggesting that the proportion of C_3 to C_4 plants was indeed sensitive to millennial scale changes in humidity. The amplitudes of these isotopic shifts are not correlated when considered over the entire length of the record, however ($r^2 \sim 0$). The reason for this observation is unclear and unrelated to the applied correction for the ice-volume effect ($r^2 \sim 0$ as well). It is possible that the expected lipid δD depletions associated with decreased evapotranspiration and greater C_3 biosynthesis during wet periods may be offset by a muted isotope effect associated with the uptake of more soil moisture by a larger vegetative inventory (Krull et al., 2006).

It also appears that millennial scale δD_{32} oscillations are superimposed on a longer term trend, amounting to a ~ 20 ‰ depletion in local isotopic minima from about 130 to 20 kyr BP (i.e. from the glacial inception to termination) (Figure 5.6). Abiotic exchange of carbon-bound hydrogen with interstitial water is unlikely in n -alkyl lipids $< 10^6$ years old at typical sedimentary temperatures (Sessions et al., 2004; Schimmelmann et al., 2006), and complete replacement of the carboxyl proton by virtually instantaneous exchange with interstitial water ($\delta D \sim 0$ ‰) would have an undetectable effect of only \sim

0.1 ‰. The isotopic consequences of biological metabolism are more poorly constrained, with both deuterium enrichments for *n*-alkanes (Pond et al., 2002; Sun et al., 2005) and depletions for *n*-alkanes, *n*-alcohols, and *n*-alkanoic acids (Chikaraishi and Naraoka, 2006) noted in the residual pool. In addition, the amount, source, and temperature of precipitation may play a large role in setting the δD composition of meteoric waters (Jouzel et al., 2000), but changes in these parameters for the tropics on glacial timescales are still too poorly known to make any quantitative arguments. It is worth noting that δD measurements of lipid biomarkers preserved from freshwater algae may be able to provide an empirical estimate of the isotopic evolution of meteoric waters over time (Sachse et al., 2006a), and should thus be explored in the future with an eye to the Cariaco record. At present though, in consideration of the ambiguity remaining in the paleoclimatic interpretation of lipid δD signatures relative to the more well-established systematics governing the corresponding stable carbon isotopic compositions, I focus hereafter on the climate implications of the $\delta^{13}C_{32}$ record.

5.2.3 Climate implications

Like Greenland, high frequency oscillations are a pervasive feature of the Cariaco $\delta^{13}C_{32}$ record during the last glacial cycle. As previously discussed, combined uncertainties in the Cariaco and Greenland ice core chronologies do not allow cause/effect relationships between the two archives to be established from temporal lead/lag arguments on these timescales. Causal relationships may be explored, however, by investigating the nature of the amplitude discrepancy between millennial scale activity expressed in high and low latitudes. Such activity displays highly variable amplitude in

the Cariaco record, where the impact of D-O and Heinrich events appears to be modified by a longer term oscillation. For example, more enriched $\delta^{13}\text{C}_{32}$ values tend to occur approximately every 23 kyr centered at 15, 38, 61, 84, 107, and 130 kyr BP, while more depleted values cluster in-between these intervals (Figure 5.6). Spectral analysis reveals significant power in the 1.7 and 7.7 kyr bands associated with D-O and Heinrich events, respectively; however, the greatest power lies at 22.8 kyr (at > 95 % confidence) and the corresponding harmonic at 11.4 kyr (Figure 5.8). These frequencies correspond to the precession of the Earth-Sun perihelion, an orbital parameter that seasonally re-distributes heat across the globe and therefore plays an important role in driving the hydrologic cycle. Indeed precessionally-driven changes in tropical insolation have been shown to be important in other reconstructions of late Quaternary climate (McIntyre and Molino, 1996; Clement et al., 2004; Cruz Jr. et al., 2005).

The Cariaco $\delta^{13}\text{C}_{32}$ record was band-pass filtered to isolate variability between the 14.3 to 33.3 kyr periods. Correlation of the resulting curve with average monthly insolation for the past 140 kyr (where the Cariaco chronology is best constrained) yields the highest coherence for November, a month which marks the end of the modern rainy season in Venezuela due to the southward migration of the ITCZ. Insolation maxima are associated with the most depleted $\delta^{13}\text{C}_{32}$ values, whereas enrichments tend to occur during insolation minima. Moreover, the magnitude of the insolation peaks is correlated with the amplitude of the superimposed millennial scale activity. For example, the decline in insolation maxima from $\sim 405 \text{ W m}^{-2}$ at 118 kyr BP to $\sim 375 \text{ W m}^{-2}$ at 50 kyr BP is accompanied by a rise in the expression of stadial enrichments.

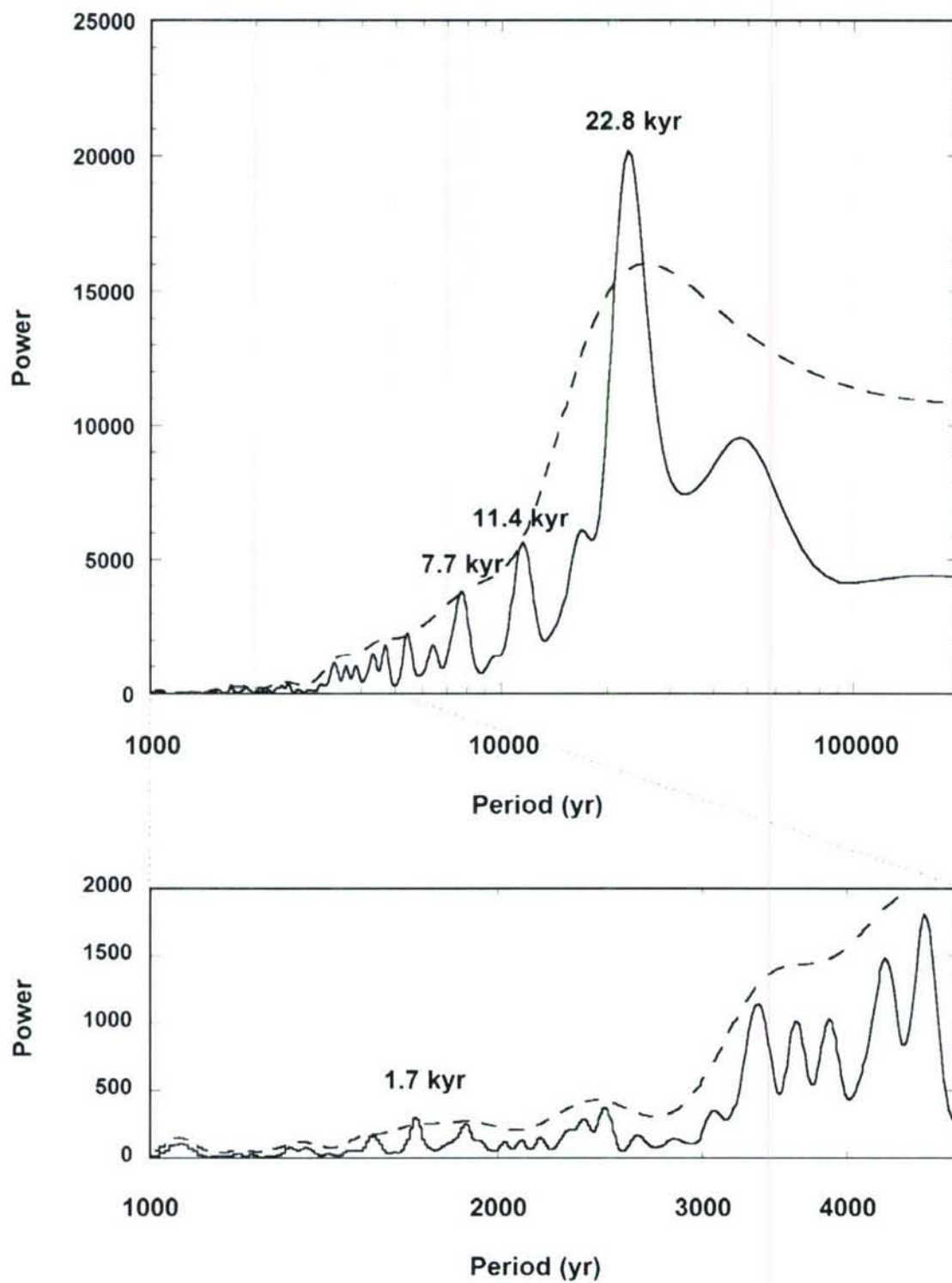


FIGURE 5.8 – Spectral analysis of the unfiltered Cariaco $\delta^{13}\text{C}_{32}$ record (solid line) with the 95 % confidence limit superimposed (dotted line) for periods 1 – 200 kyr (top) and a 1 – 5 kyr zoom (bottom).

These observations suggest that higher local insolation in November enhanced the thermally-driven atmospheric convection over the northern tropical Atlantic, effectively delaying the seasonal southward migration of the ITCZ. A prolonged rainy season over northern South America would favor C_3 plants over their C_4 counterparts, leading to the observed depletions in the carbon isotopic signatures of the corresponding leaf waxes delivered to the Cariaco Basin. Conversely, insolation minima would shorten the rainy season, leading to C_4 plant expansion. The dependence of the C_3/C_4 balance on the *duration* of rainy season precipitation is reasonable, as C_3 vegetation might not be expected to survive a prolonged dry season.

It appears, therefore, that the response of the ITCZ to low frequency solar forcing effectively modulated its sensitivity to millennial scale changes in SST gradients induced by D-O and Heinrich events in the North Atlantic. For instance, stadial coolings during the early glacial, possibly associated with MOC reductions (Lehman et al., 2002), would have tended to cool SSTs north of the equator, thus displacing the ITCZ southward for a longer period of time during the annual cycle. However, this effect appears to have been locally overwhelmed by greater wintertime heating from the sun during the relatively high insolation maxima at that time. Convective precipitation was thus sustained north of the equator for a longer proportion of the annual cycle, effectively muting the vegetation response to D-O stadial cooling. As the glacial cycle continued, the decline in the peak magnitudes of November insolation weakened the local hydrological circulation, thereby increasing the exposure of the ITCZ to the influence of large climate events in the North Atlantic. In this case, SST increases (decreases) possibly associated with MOC re-

invigorations (reductions) displaced the ITCZ southward for less (more) time in the annual cycle, efficiently imprinting D-O signals into the tropical hydrologic cycle.

Similar arguments can be made concerning the shoaling of insolation minima as the glacial cycle progressed. For example, the relatively deep insolation well at the end of the Eemian interglacial occurred during a time of brief, modest reductions MOC (Adkins et al., 1997; Lehman et al., 2002), and therefore resulted in only moderate $\delta^{13}\text{C}_{32}$ enrichments reflecting a shorter rainy season. The following minimum (centered at ~ 85 kyr BP) was coincident with higher amplitude D-O variability (especially the warming into interstadial 21) and a more prolonged MOC reduction beforehand in the North Atlantic, and is duely recorded as abrupt wettenings interspaced with more intense dry intervals in northern South America. Subsequent insolation minima, though progressively more shallow, are characterized by the largest $\delta^{13}\text{C}_{32}$ shifts, again highlighting the tight coupling of the seasonal ITCZ adjustments to MOC in the absence of high solar forcing overhead. Indeed, the most enriched $\delta^{13}\text{C}_{32}$ values of the entire record (i.e. driest periods) occur when local insolation minima are coincident with the some of the coldest stadial periods in the North Atlantic (Heinrich events 6, 4, and 1), reflecting the combined influence of low solar flux and high latitude cooling on the hydrology of northern South America. Consequently, the ITCZ was displaced southward for much of the year. Thus, the interplay between precessionally modulated November insolation and MOC forcing, periodically co-directional and opposed, is recorded as an 'obvious decrease in $[\delta^{13}\text{C}_{32}]$ oscillatory amplitude over ~ 11 kyr on either side of interstadials 8 and 17' so noted above.

Upon return to a more stable MOC regime during the Holocene, the seasonal duration of the ITCZ was again principally driven by local insolation that was some 25 W m^{-2} lower than during penultimate interglacial. Hence, the ITCZ was not held north of the equator for as long, resulting in modest $\delta^{13}\text{C}_{32}$ enrichments over those observed in the Eemian. This hypothesis may be bolstered if similar behavior is found during the transition between MIS 12 and 11, an period in which Earth's orbital configuration was analogous to that in the LGM / Holocene.

Interestingly, Denton et al. (2005) recently postulated that abrupt climate oscillations in the North Atlantic region during the last glacial primarily arose from MOC perturbations of sea ice associated with changes in wintertime seasonality. They also went on to predict that the ITCZ must respond most sensitively to high latitude forcing during boreal winter, even though the existing records from the Cariaco Basin at the time did not contain enough seasonal information to address this assertion. The extended $\delta^{13}\text{C}_{32}$ record presented here documents just such a response and therefore supports the notion that seasonality changes (as opposed to uniform adjustments in all months of the year) were the dominant mode of millennial scale climate fluctuations in the past.

The hydrologic implications of these findings can best understood by considering other regional paleoclimate records in the context of the seasonal dynamics of the modern system. The southward displacement of ITCZ over the tropical Atlantic during boreal winter is accompanied by the development of the South American Summer Monsoon (SASM) over southern tropical South America (Figure 5.1). This results in precipitation which is in broad antiphase to that in northern South America when viewed from the

geologic record. Oxygen isotope variations in stalagmites from southern Brazil indicate that increases (decreases) in monsoon intensity over the past 116 kyr are tied to increases (decreases) in insolation during February, with some modulation associated with Heinrich events (Cruz Jr. et al., 2005, 2006). In northeast Brazil, closer to the influence of the ITCZ in its southernmost position, wet events tend to occur during stadial (mostly Heinrich) events (Jennerjahn et al., 2004) that have been further demonstrated to be coincident with periods of high isolation from February – May (Wang et al., 2004). These observations provide additional evidence that seasonal shifts in meridional position of the ITCZ still occurred in the past (as opposed to wholesale displacements on an interannual basis), but that the duration of these shifts varied in response to changes in seasonal heat distribution patterns resulting from orbital and MOC forcing.

Does the amplitude modulation of D-O events in the tropics necessarily imply that such millennial scale variability originated at high latitudes? If MOC rearrangements were indeed responsible, then the nature of its reaction to both high and low latitude freshwater anomalies requires careful consideration. Today, the net freshwater export of the entire Atlantic basin is roughly 0.35 – 0.45 Sv, of which anywhere between 30 – 100 % flows as vapor across the Panamanian isthmus (Zaucker et al., 1994; Benway and Mix, 2004). The response of MOC to fractional perturbation of this balance in ocean circulation models is roughly linear, although the slope of the relationship differs among individual simulations. Under modern boundary conditions, a 0.1 Sv freshwater anomaly applied for only ~ 100 years in either the high or low latitude Atlantic has been found to change simulated MOC by 2 to 10 Sv (Zaucker et al., 1994; Schmittner et al., 2000;

Schmittner and Clement, 2002; Dahl et al., 2005), although at least one model simulates a greater response of MOC to high latitude freshwater flux (Manabe and Stouffer, 2000). This relationship becomes nonlinear only near a critical shutdown threshold (Zaucker et al., 1994), with perhaps 0.25 Sv for ~ 200 years leading to total collapse (Lohmann, 2003).

The response is amplified when glacial boundary conditions are imposed. An already reduced MOC (as might characterize ‘background’ GNAIW production) primes the system for an even more rapid collapse when the freshwater balance is similarly perturbed (e.g. during Heinrich events) (Schmittner and Clement, 2002; Claussen et al., 2003; Romanova et al., 2004). This effect may be monotonically counterbalanced by the increased salt content of the glacial ocean due to an overall increase in evaporation and ice sheet growth (Schmittner and Clement, 2002; Romanova et al., 2004), thereby imparting transient behavior to MOC shifts as opposed to irreversible mode changes.

Therefore, if ENSO-driven ITCZ displacements were responsible for linear MOC reorganizations through the modulation of Atlantic freshwater export in the tropics, North Atlantic temperature records would reasonably be expected to display similar amplitude modulation to that of the Cariaco $\delta^{13}\text{C}_{32}$ record. Since this is not observed, it can be concluded that (a) this mechanism is nonlinear, (b) this mechanism is linear, but that relatively uniform signals propagating from the North Atlantic are amplitude modulated by precession upon arrival in the tropics, or (c) a different mechanism operates. Although argument (a) is provisionally rejected based on the simulated MOC responses highlighted above, model representations of real world processes are only as good as the

parameterizations employed in their construction. Additional work with different model realizations initiated under ever more realistic boundary conditions is clearly needed to either support or repudiate this scenario.

With respect to argument (c), modifications in atmospheric circulation stand out as the only other viable conduit for the rapid propagation of tropical signals to the high latitudes. Although previous studies have suggested that high ice sheet albedo and cooler SSTs in the North Atlantic may enhance the subtropical high pressure cell, intensify the northeast trade winds, and displace the ITCZ southwards (Chiang et al., 2003; Chiang and Bitz, 2005; Justino and Peltier, 2005; Broccoli et al., 2006), much less is known about the capacity of low latitude systems to imprint themselves on high latitude climate (Cane and Clement, 1999; Clement and Cane, 1999; Kerr, 2001; Okumura et al., 2001; Yin and Battisti, 2001). In the modern world, El Niño events are correlated with warmer than average conditions in northern North America, whereas La Niña events have the opposite effect (Cane and Clement, 1999). The mechanisms hypothesized to be associated with these teleconnections, such as convectively-driven modifications in atmospheric planetary waves, are best described by nonlinearities arising from the interaction with underlying SST anomalies (Hoerling et al., 1997; Visbeck et al., 1998, 2001; Robertson et al., 2000; Giannini et al., 2000, 2001; Kushnir et al., 2002; Justino and Peltier, 2005), and may therefore provide a medium through which the purported ability of ENSO to lock to the seasonal cycle for several centuries (Clement et al., 2001) may translate into fairly uniform abrupt temperature oscillations in the high latitude North Atlantic. Yet it is still unclear if the atmospheric meridional mode itself can

effectively transmit periodicities longer than several decades either today or during the last glacial (Marshall et al., 2001; Justino and Peltier, 2005). If not, then the millennial scale shifts in the seasonality of the tropical hydrologic cycle (as documented by the Cariaco $\delta^{13}\text{C}_{32}$ record) must be interpreted in a manner consistent with argument (b), that is as a locally modulated response to a high latitude MOC trigger.

5.3 CONCLUSIONS

The development of a continuous leaf wax $\delta^{13}\text{C}$ record from the Cariaco Basin for the last ~ 180 kyr indicates a strong link between the seasonal migration of the Atlantic ITCZ and abrupt climate events recorded in Greenland ice. Corresponding δD compositions support the case for rapid fluctuations in precipitation but a quantitative interpretation is currently limited. Unlike Greenland $\delta^{18}\text{O}_{\text{ice}}$ records, the millennial scale $\delta^{13}\text{C}_{32}$ oscillations are amplitude-modulated by precessionally driven changes in local insolation, suggesting that the D-O events originated in the high latitude North Atlantic and were propagated to the tropics via reorganizations in either MOC or atmospheric circulation. Freshwater perturbations in the tropics associated with an increase in ITCZ seasonality seem unlikely to have modified MOC themselves as this would have been expected to produce a similarly amplitude-modulated temperature response over Greenland given the provisionally linear MOC response simulated for freshwater forcing. It also remains unclear if the atmospheric meridional mode, though likely a nonlinear conduit, can sustain a particular configuration for more than a few decades when forced from either location. Thus, the incoherent relationship between abrupt events in methane-synchronized ice cores from Greenland and Antarctica (Blunier and Brook,

2001) and increasing evidence that millennial scale changes (especially Heinrich events) were marked by abrupt MOC reorganizations (e.g. McManus et al., 2004) still provide a compelling, albeit circumstantial (Boyle, 2000) case that past variations in high and low latitude Atlantic climate were linked by MOC reorganizations triggered in the former.

In this context, the Cariaco $\delta^{13}\text{C}_{32}$ record provides a benchmark view of tropical Atlantic ITCZ variability over the last full glacial cycle against which these hypotheses may be more rigorously tested. Specifically, it is recommended that more attention be paid to the relative amplitude of the signals themselves when attempting to evaluate the relative influence of high vs. low latitude systems. Future research should also be directed towards a greater utilization of proxies that record changes in seasonality (such as some foraminiferal assemblages), constraining the isotopic composition of paleoprecipitation, refining the physics used to describe oceanic and atmospheric perturbations, and investigating the interglacial carbon isotope discrepancy noted above.

ACKNOWLEDGEMENTS

This study is co-authored by Konrad Huguen, Marley Bice, Timothy Eglinton (all at Woods Hole Oceanographic Institution), and Alex Sessions (at California Institute of Technology). I thank Carl Johnson for his expertise in compound-specific $\delta^{13}\text{C}$ analysis, Daniel Montluçon for laboratory assistance, Jerry McManus, Enno Schefuß, Matt Makou, and Candace Major for stimulating discussions, and Walter Hale and the Ocean Drilling Program for providing sediments from core 1002D. I also gratefully acknowledge financial support from the Schlanger Ocean Drilling Graduate Fellowship and the EPA Star Graduate Fellowship. Additional support was provided by NSF DEB-0447281 to K.A.H.

REFERENCES

- Adkins, J.F., Boyle, E.A., Keigwin, L., Cortijo, E., 1997. Variability of the North Atlantic thermohaline circulation during the last interglacial period. *Nature*, 390: 154-156.
- Astor, Y., Muller-Karger, F., Scranton, M.I., 2003. Seasonal and interannual variation in the hydrography of the Cariaco Basin: Implications for basin ventilation. *Continental Shelf Research*, 23: 125-144.
- Baker, P.A., Rigsby, C.A., Seltzer, G.O., Fritz, S.C., Lowenstein, T.K., Bacher, N.P., Veliz, C., 2001. Tropical climate changes at millennial orbital timescales on the Bolivian Altiplano. *Nature*, 409: 698-701.
- Benway, H.M., Mix, A.C., 2004. Oxygen isotopes, upper ocean salinity, and precipitation sources in the eastern tropical Pacific. *Earth and Planetary Science Letters*, 224: 493-507.
- Bi, X., Sheng, G., Liu, X., Li, C., Fu, J., 2005. Molecular and carbon and hydrogen isotopic composition of *n*-alkanes in plant leaf waxes. *Organic Geochemistry*, 36: 1405-1417.
- Biasutti, M., Battisti, D.S., Sarachik, E.S., 2003. The annual cycle over the tropical Atlantic, South America, and Africa. *Journal of Climate*, 16: 2491-2508.
- Blunier, T., Brook, E.J., 2001. Timing of millennial-scale climate change in Antarctica and Greenland during the last glacial period. *Science*, 291: 109-112.
- Bond, G., Broecker, W., Johnsen, S., McManus, J., Labeyrie, L., Jouzel, J., Bonani, G., 1993. Correlations between climate records from North Atlantic sediments and Greenland ice. *Nature*, 365: 143-147.
- Bond, G., Heinrich, H., Broecker, W., Labeyrie, L., McManus, J., Andrews, J., Huon, S., Jantschik, R., Clasen, S., Simet, C., Tedesco, K., Kias, M., Bonani, G., Ivy, S., 1992. Evidence for massive discharges of icebergs into the North Atlantic ocean during the last glacial period. *Nature*, 360: 245-249.
- Bond, G.C., Lotti, R., 1995. Iceberg discharges into the North Atlantic on millennial time scales during the last glaciation. *Science*, 267: 1005-1010.
- Bond, G.C., Showers, W., Elliot, M., Evans, M., Lotti, R., Hajdas, I., Bonani, G., Johnson, S., 1999. The North Atlantic's 1-2 kyr climate rhythm: Relation to Heinrich events, Dansgaard/Oeschger cycles and the little ice age. In *Mechanisms of Global Climate Change at Millennial Time Scales*, P.U. Clark, R.S. Webb, L.D. Keigwin (eds.): 35-58.
- Boyle, E.A., 2000. Is ocean thermohaline circulation linked to abrupt stadial/interstadial transitions? *Quaternary Science Reviews*, 19: 255-272.
- Boyle, E.A., Keigwin, L.D., 1987. North Atlantic thermohaline circulation during the last 20,000 years: Link to high latitude surface temperature. *Nature*, 330: 35-40.
- Braun, H., Christi, M., Rahmstorf, S., Ganopolski, A., Mangini, A., Kubatzki, C., Roth, K., Kromer, B., 2005. Possible solar origin of the 1,470-year glacial climate cycle demonstrated in a coupled model. *Nature*, 438: 208-211.
- Broccoli, A.J., Dahl, K.A., Stouffer, R.J., 2006. Response of the ITCZ to northern hemisphere cooling. *Geophysical Research Letters*, 33: doi: 10.1029/2005GL024546.

Broecker, W.S., 2003. Does the trigger for abrupt climate change reside in the ocean or in the atmosphere? *Science*, 300: 1519-1522.

Broecker, W.S., Bond, G.C., Klas, M., Clark, E., McManus, J.F., 1992. Origin of the northern Atlantic's Heinrich events. *Climate Dynamics*, 6: 265-273.

Cane, M., Clement, A.C., 1999. A role for the tropical Pacific coupled ocean-atmosphere system on Milankovitch timescales: Part II: Global impacts. In *Mechanisms of Global Climate Change at Millennial Time Scales*, P.U. Clark, R.S. Webb, L.D. Keigwin (eds.): 373-383.

Chiang, J.C.H., 2004. Present-day climate variability in the tropical Atlantic: a model for paleoclimate changes? In *The Hadley Circulation: Past, Present, and Future*, H.F. Diaz and R. Bradley (eds.): 465-488.

Chiang, J.C.H., Biasutti, M., Battisti, D.S., 2003. Sensitivity of the Atlantic Intertropical Convergence Zone to Last Glacial Maximum boundary conditions. *Paleoceanography*, 18: doi: 10.1029/2003PA000916.

Chiang, J.C.H., Bitz, C.M., 2005. Influence of high latitude ice cover on the marine Intertropical Convergence Zone. *Climate Dynamics*, 25: 477-496.

Chiang, J.C.H., Kushnir, Y., Giannini, A., 2002. Deconstructing Atlantic Intertropical Convergence Zone variability: Influence of the local cross-equatorial sea surface temperature gradient and remote forcing from the eastern equatorial Pacific. *Journal of Geophysical Research*, 107: doi: 10.1029/2000JD000307.

Chiang, J.C.H., Kushnir, Y., Zebiak, S.E., 2000. Interdecadal changes in eastern Pacific ITCZ variability and its influence on the Atlantic ITCZ. *Geophysical Research Letters*, 27: 3687-3690.

Chiang, J.C.H., Vimont, D.J., 2004. Analogous Pacific and Atlantic meridional modes of tropical atmosphere-ocean variability. *Journal of Climate*, 17: 4143-4158.

Chikaraishi, Y., Naraoka, H., 2006. Carbon and hydrogen isotope variation of plant biomarkers in a plant-soil system. *Chemical Geology*, 231: 190-202.

Chikaraishi, Y., Naraoka, H., 2007. $\delta^{13}\text{C}$ and δD relationships among three *n*-alkyl compound classes (*n*-alkanoic acids, *n*-alkane, and *n*-alkanol) of terrestrial higher plants. *Organic Geochemistry*, 38: 198-215.

Chikaraishi, Y., Naraoka, H., Poulson, S.R., 2004. Hydrogen and carbon isotopic fractionations of lipid biosynthesis among terrestrial (C3, C4, and CAM) and aquatic plants. *Phytochemistry*, 65: 1369-1381.

Clark, P.U., Marshall, S.J., Clarke, G.K.C., Hostetler, S.W., Licciardi, J.M., Teller, J.T., 2001. Freshwater forcing of abrupt climate change during the last glaciation. *Science*, 293: 283-287.

Clark, P.U., Pisias, N.G., Stocker, T.F., Weaver, A.J., 2002. The role of the thermohaline circulation in abrupt climate change. *Nature*, 415: 863-869.

Claussen, M., Ganopolski, A., Brovkin, V., Gerstengarbe, F.-W., Werner, P., 2003. Simulated global-scale response of the climate system to Dansgaard/Oeschger and Heinrich events. *Climate Dynamics*, 21: 361-370.

Clement, A.C., Cane, M., 1999. A role for the tropical Pacific coupled ocean-atmosphere system on Milankovitch timescales: Part I: A modeling study of tropical

Pacific variability. In *Mechanisms of Global Climate Change at Millennial Time Scales*, P.U. Clark, R.S. Webb, L.D. Keigwin (eds.): 363-371.

Clement, A.C., Cane, M.A., Seager, R., 2001. An orbitally driven tropical source for abrupt climate change. *Journal of Climate*, 14: 2369-2375.

Clement, A.C., Hall, A., Broccoli, A.J., 2004. The importance of precessional signals in tropical climate. *Climate Dynamics*, 22: 327-341.

Collister, J.W., Rieley, G., Stern, B., Eglinton, G., Fry, B., 1994. Compound-specific $\delta^{13}\text{C}$ analyses of leaf lipids from plants with differing carbon dioxide metabolisms. *Organic Geochemistry*, 21: 619-627.

Cortijo, E., Labeyrie, L., Elliot, M., Balbon, E., Tisnerat, N., 2000. Rapid climatic variability of the North Atlantic Ocean and global climate: a focus of the IMAGES program. *Quaternary Science Reviews*, 19: 227-241.

Cruz Jr., F.W., Burns, S.J., Karmann, I., Sharp, W.D., Vuille, M., 2006. Reconstruction of regional atmospheric circulation features during the late Pleistocene in subtropical Brazil from oxygen isotope composition of speleothems. *Earth and Planetary Science Letters*, 248: 495-507.

Cruz Jr., F.W., Burns, S.J., Karmann, I., Sharp, W.D., Vuille, M., Cardoso, A.O., Ferrari, J.A., Silva Dias, P.L., Viana Jr., O., 2005. Insolation-driven changes in atmospheric circulation over the past 116,000 years in subtropical Brazil. *Nature*, 434: 63-66.

Dahl, K.A., Broccoli, A.J., Stouffer, R.J., 2005. Assessing the role of North Atlantic freshwater forcing in millennial scale climate variability: a tropical Atlantic perspective. *Climate Dynamics*, 24: 325-346.

Dansgaard, W., Oeschger, H., 1989. In *The Environmental Record in Glaciers and Ice Sheets*, H. Oeschger and C.C. Langway (eds): 287-318.

Denton, G.H., Alley, R.B., Comer, G.C., Broecker, W.S., 2005. The role of seasonality in abrupt climate change. *Quaternary Science Reviews*, 24: 1159-1182.

Eglinton, G., Hamilton, R.J., 1967. Leaf epicuticular waxes. *Science*, 156:1322-1335.

Elliot, M., Labeyrie, L., Duplessy, J.-C., 2002. Changes in North Atlantic deep-water formation associated with the Dansgaard-Oeschger temperature oscillations (60-10ka). *Quaternary Science Reviews*, 21: 1153-1165.

Emile-Geay, J., Cane, M.A., Naik, N., Seager, R., Clement, A.C., van Green, A., 2003. Warren revisited: Atmospheric freshwater fluxes and "Why is no deep water formed in the North Pacific". *Journal of Geophysical Research*, 108: doi: 10.1029/2001JC001058.

Fairbanks, R.G., 1989. A 17,000-year glacio-eustatic sea level record: influence of glacial melting rates on the Younger Dryas event and deep-ocean circulation. *Nature*, 342: 637-642.

Giannini, A., Chiang, J.C.H., Cane, M.A., Kushnir, Y., Seager, R., 2001. The ENSO teleconnection to the tropical Atlantic Ocean: Contributions of the remote and local SSTs to rainfall variability in the tropical Americas. *Journal of Climate*, 14: 4530-4544.

Giannini, A., Kushnir, Y., Cane, M.A., 2000. Interannual variability of Caribbean rainfall, ENSO, and the Atlantic Ocean. *Journal of Climate*, 13: 297-311.

Goñi, M.A., Aceves, H.L., Thunell, R.C., Tappa, E., Black, D., Astor, Y., Varela, R., Muller-Karger, F., 2003. Biogenic fluxes in the Cariaco Basin: a combined study of sinking particulates and underlying sediments. *Deep-Sea Research I*, 50: 781-807.

Grootes, P.M., Stuiver, M., White, J.W.C., Johnsen, S., Jouzel, J., 1993. Comparison of oxygen isotope records from the GISP2 and GRIP Greenland ice cores. *Nature*, 366: 552-554.

Haug, G.H., Hughen, K.A., Sigman, D.M., Peterson, L.C., Röhl, U., 2001. Southward migration of the intertropical convergence zone through the Holocene. *Science*, 293: 1304-1308.

Haug, G.H., Pedersen, T.F., Sigman, D.M., Calvert, S.E., Nielsen, B., Peterson, L.C., 1998. Glacial/interglacial variations in production and nitrogen fixation in the Cariaco Basin during the last 580 kyr. *Paleoceanography*, 13: 427-432.

Heinrich, H., 1988. Origin and consequences of cyclic rafting in the northeast Atlantic ocean during the past 130,000 years. *Quaternary Research*, 29: 142-152.

Hemming, S.R., 2004. Heinrich events: Massive late Pleistocene detritus layer of the North Atlantic and their global climate imprint. *Review of Geophysics*, 42: 8755-1209/04/2003RG000128.

Ho, T.-Y., Taylor, G.T., Astor, Y., Varela, R., Müller-Karger, F., Scranton, M.I., 2004. Vertical and temporal variability of redox zonation in the water column of the Cariaco Basin: Implications for organic carbon oxidation pathways. *Marine Chemistry*, 86: 89-104.

Hobbie, E.A., Werner, R.A., 2004. Intramolecular, compound-specific, and bulk carbon isotope patterns in C₃ and C₄ plants: A review and synthesis. *New Phytologist*, 161: 371-385.

Hoerling, M.P., Hurrell, J.W., Xu, T., 2001. Tropical origins for recent north Atlantic climate change. *Science*, 292: 90-92.

Hoerling, M.P., Kumar, A., Zhong, M., 1997. El Niño, La Niña, and the nonlinearity of their teleconnections. *Journal of Climate*, 10: 1769-1786.

Huang, Y., Street-Perrott, F.A., Metcalfe, S.E., Brenner, M., Moreland, M., Freeman, K.H., 2001. Climate change as the dominant control on the glacial-interglacial variations in C₃ and C₄ plant abundance. *Science*, 293: 1647-1651.

Hughen, K.A., Eglinton, T.I., Xu, L., Makou, M., 2004. Abrupt tropical vegetation response to rapid climate change. *Science*, 304: 1955-1959.

Hughen, K.A., Lehman, S., Southon, J., Overpeck, J., Marchal, O., Herring, C., Turnbull, J., 2004. ¹⁴C activity and global carbon cycle changes over the past 50,000 years. *Science*, 303: 202-207.

Hughen, K.A., Overpeck, J.T., Lehman, S.J., Kashgarian, M., Southon, J., Peterson, L.C., Alley, R., Sigman, D.M., 1998. Deglacial changes in ocean circulation from an extended radiocarbon calibration. *Nature*, 391: 65-68.

Hughen, K.A., Overpeck, J.T., Peterson, L.C., Anderson, R.F., 1996. The nature of varved sedimentation in the Cariaco Basin, Venezuela, and its paleoclimate significance. In *Palaeoclimatology and Palaeoceanography from Laminated Sediments*, A.E.S. Kemp (ed.): 171-183.

Hughen, K., Southon, J., Lehman, S., Bertrand, C., Turnbell, J., 2006. Marine-derived ^{14}C calibration and activity record for the past 50,000 years updated from the Cariaco Basin. *Quaternary Science Reviews*, 25: 3216-3227.

Hughen, K.A., Southon, J.R., Lehman, S.J., Overpeck, J.T., 2000. Synchronous radiocarbon and climate shifts during the last deglaciation. *Science*, 290: 1951-1954.

Hyde, W.T., Crowley, T.J., 2002. Stochastic forcing of Pleistocene ice sheet: Implications for the origin of millennial-scale climate oscillations. *Paleoceanography*, 17: doi: 10.1029/2001PA000669.

Jennerjahn, T.C., Ittekkot, V., Arz, H.W., Behling, H., Pätzold, J., Wefer, G., 2004. Asynchronous terrestrial and marine signals of climate change during Heinrich events. *Science*, 306: 2236-2239.

Johnsen, S.J., Clausen, H.B., Dansgaard, W., Fuhrer, K., Gundestrup, N., Hammer, C.U., Iversen, P., Jouzel, J., Stauffer, B., Steffensen, J.P., 1992. Irregular glacial interstadials recorded in a new Greenland ice core. *Nature*, 359: 311-313.

Jouzel, J., Hoffmann, G., Koster, R.D., Masson, V., 2000. Water isotopes in precipitation: Data/model comparison for present-day and past climates. *Quaternary Science Reviews*, 19: 363-379.

Justino, F., Peltier, W.R., 2005. The glacial North Atlantic Oscillation. *Geophysical Research Letters*, 32: doi: 10.1029/2005GL023822.

Keigwin, L.D., Boyle, E.A., 1999. Surface and deep ocean variability in the northern Sargasso Sea during marine isotope stage 3. *Paleoceanography*, 14: 164-170.

Keigwin, L.D., Curry, W.B., Lehman, S.J., Johnsen, S., 1994. The role of the deep ocean in North Atlantic climate change between 70 and 130 kyr ago. *Nature*, 371: 323-326.

Keigwin, L.D., Jones, G.A., 1994. Western North Atlantic evidence for millennial-scale changes in ocean circulation and climate. *Journal of Geophysical Research*, 99: 12,397-12,410.

Keigwin, L.D., Lehman, S.J., 1994. Deep circulation change linked to Heinrich event 1 and Younger Dryas in a middepth North Atlantic core. *Paleoceanography*, 9: 185-194.

Kerr, R.A., 2001. The tropics return to the climate system. *Science*, 292: 660-661.

Kiefer, T., Kienast, M., 2005. Patterns of deglacial warming in the Pacific ocean: A review with emphasis on the time interval of Heinrich event 1. *Quaternary Science reviews*, 24: 1063-1081.

Koutavas, A., Lynch-Stieglitz, J., Marchitto Jr., T.M., Sachs, J.P., 2002. El Niño-like pattern in ice age tropical Pacific sea surface temperature. *Science*, 297: 226-230.

Krull, E., Sachse, D., Mügler, I., Thiele, A., Gleixner, G., 2006. Compound-specific $\delta^{13}\text{C}$ and $\delta^2\text{H}$ analyses of plant and soil organic matter: A preliminary assessment of the effects of vegetation change on ecosystem hydrology. *Soil Biology & Biochemistry*, 38: 3211-3221.

Kushnir, Y., Seager, R., Miller, J., Chiang, J.C.H., 2002. A simple model of tropical Atlantic decadal climate variability. *Geophysical Research Letters*, 21: doi: 10.1029/2002GL015847.

Lea, D.W., Pak, D.K., Peterson, L.C., Hughen, K.A., 2003. Synchronicity of tropical and high-latitude Atlantic temperatures over the last glacial termination. *Science*, 301: 1361-1364.

Lehman, S.J., Sachs, J.P., Crotwell, A.M., Keigwin, L.D., Boyle, E.A., 2002. Relation of subtropical Atlantic temperature, high-latitude ice rafting, deep water formation, and European climate 130,000-60,000 years ago. *Quaternary Science Reviews*, 21: 1917-1924.

Leuschner, D.C., Sirocko, F., 2000. The low-latitude monsoon climate during Dansgaard-Oeschger cycles and Heinrich events. *Quaternary Science Reviews*, 19: 243-254.

Levitus NODC_WOA98 data provided by the NOAA/OAR/ESRL PSD, Boulder, Colorado, USA, from their Web site at <http://www.cdc.noaa.gov/>

Lisiecki, L.E., Raymo, M.E., 2005. A Pliocene-Pleistocene stack of 57 globally distributed benthic $\delta^{18}\text{O}$ records. *Paleoceanography*, 20: doi: 10.1029/2004PA001071.

Lohmann, G., 2003. Atmospheric and oceanic freshwater transport during weak Atlantic overturning circulation. *Tellus*, 55A: 438-449.

Lund, D.C., Curry, W., 2006. Florida current surface temperature and salinity variability during the last millennium. *Paleoceanography*, 21: doi: 10.1029/2005PA001218.

Lund, D.C., Lynch-Stieglitz, J., Curry, W.B., 2006. Gulf Stream density structure and transport during the past millennium. *Nature*, 444: 601-604.

Lynch-Stieglitz, J., Curry, W.B., Slowey, N., 1999. Weaker Gulf Stream in the Florida straits during the Last Glacial Maximum. *Nature*, 402: 644-648.

Makou, M.C., Hughen, K.A., Xu, L., Sylva, S.P., Eglinton, T.I. Isotopic records of tropical vegetation and climate change from terrestrial vascular plant biomarkers preserved in Cariaco Basin sediments. Submitted.

Manabe, S., Stouffer, R.J., 2000. Study of abrupt climate change by a coupled ocean-atmosphere model. *Quaternary Science Reviews*, 19: 285-299.

Marchitto, T.M., Broecker, W.S., 2006. Deep water mass geometry in the glacial Atlantic Ocean: A review of constraints from the paleonutrient proxy Cd/Ca. *Geochemistry Geophysics Geosystems*, 7: doi: 10.1029/2006GC001323.

Marshall, J., Kushnir, Y., Battisti, D., Chang, P., Czaja, A., Dickson, R., Hurrell, J., McCartney, M., Saravanan, R., Visbeck, M., 2001. North Atlantic climate variability: Phenomena, impacts, and mechanisms. *International Journal of Climatology*, 21: 1863-1898.

McIntyre, A., Molino, B., 1996. Forcing of Atlantic equatorial and subpolar millennial cycles by precession. *Science*, 274: 1867-1870.

McManus, J.F., Bond, G.C., Broecker, W.S., Johnsen, S., Labeyrie, L., Higgins, S., 1994. High-resolution climate records from the north Atlantic during the last interglacial. *Nature*, 371: 326-329.

McManus, J.F., François, R., Gherardi, J.-M., Keigwin, L.D., Brown-Leger, S., 2004. Collapse and rapid resumption of Atlantic meridional circulation linked to deglacial climate changes. *Nature*, 428: 834-837.

McManus, J.F., Oppo, D.W., Cullen, J.L., 1999. A 0.5-million-year record of millennial-scale climate variability in the north Atlantic. *Science*, 283: 971-975.

Münnich, M., Neelin, J.D., 2005. Seasonal influence of ENSO on the Atlantic ITCZ and equatorial South America. *Geophysical Research Letters*, 32: doi: 10.1029/2005GL023900.

Nguyen Tu, T.T., Kurschner, W.M., Schouten, S., Van Bergen, P.F., 2004a. Leaf carbon isotope composition of fossil and extant oaks grown under differing atmosphere CO₂ levels. *Palaeogeography, Palaeoclimatology, Palaeoecology*, 212: 199-213.

Nguyen Tu, T.T., Derenne, S., Largeau, C., Bardoux, G., Mariotti, A., 2004b. Diagenesis effects on specific carbon isotope composition of plant *n*-alkanes. *Organic Geochemistry*, 35: 317-329.

Okumura, Y., Xie, S.-P., Numaguti, A., Tanimoto, Y., 2001. Tropical Atlantic air-sea interaction and its influence on the NAO. *Geophysical Research Letters*, 28: 1507-1510.

Paillard, D., Labeyrie, L., 1994. Role of the thermohaline circulation in the abrupt warming after Heinrich events. *Nature*, 372: 162-164.

Peck, V.L., Hall, I.R., Zahn, R., Scourse, J.D., 2007. Progressive reduction in NE Atlantic intermediate water ventilation prior to Heinrich events: Response to NW European ice sheet instabilities? *Geochemistry Geophysics Geosystems*, 8: doi: 10.1029/2006GC001321.

Peterson, L.C., Haug, G.H., 2006. Variability in the mean latitude of the Atlantic Intertropical Convergence Zone as recorded by riverine input of sediments to the Cariaco Basin. *Palaeogeography, Palaeoclimatology, Palaeoecology*, 234: 97-113.

Peterson, L.C., Haug, G.H., Hughen, K.A., Röhl, U., 2000. Rapid changes in the hydrologic cycle of the tropical Atlantic during the last glacial. *Science*, 290: 1947-1951.

Pond, K.L., Huang, Y., Wang, Y., Kulpa, C.F., 2002. Hydrogen isotopic composition of individual *n*-alkanes as an intrinsic tracer for bioremediation and source identification of petroleum contamination. *Environmental Science and Technology*, 36: 724-728.

Poore, R.Z., Quinn, T.M., Verardo, S., 2004. Century-scale movement of the Atlantic Intertropical Convergence Zone linked to solar variability. *Geophysical Research Letters*, 31: doi: 10.1029/2004GL019940.

Rahmstorf, S., 2002. Ocean circulation and climate during the past 120,000 years. *Nature*, 419: 207-214.

Robertson, A.W., Mechoso, C.R., Kim, Y.-J., 2000. The influence of Atlantic sea surface temperature anomalies on the North Atlantic Oscillation. *Journal of Climate*, 13: 122-138.

Rogers, K.B., Lohmann, G., Lorenz, S., Schneider, R., Henderson, G.M., 2003. A tropical mechanism for northern hemisphere deglaciation. *Geochemistry Geophysics Geosystems*, 4: doi: 10.1029/2003GC000508.

Romanova, V., Prange, M., Lohmann, 2004. Stability of the glacial thermohaline circulation and its dependence on the background hydrological cycle. *Climate Dynamics*, 22 : 527-538.

Rühlemann, C., Mulitza, S., Muller, P.J., Wefer, G., Zahn, R., 1999. Warming of the tropical Atlantic ocean and slowdown of thermohaline circulation during the last deglaciation. *Nature*, 402: 511-514.

- Rühlemann, C., Mulitza, S., Lohmann, G., Paul, A., Prange, M., Wefer, G., 2004. Intermediate depth warming in the tropical Atlantic related to weakened thermohaline circulation: Combining paleoclimate data and modeling results for the last deglaciation. *Paleoceanography*, 19: doi: 10.1029/2003PA000948.
- Sachs, J.P., Lehman, S.J., 1999. Subtropical North Atlantic temperatures 60,000 to 30,000 years ago. *Science*, 286: 756-759.
- Sachse, D., Radke, J., Gleixner, G., 2004. Hydrogen isotope ratios of recent lacustrine sedimentary n-alkanes record modern climate variability. *Geochimica et Cosmochimica Acta*, 68: 4877-4889.
- Sachse, D., Radke, J., Gleixner, G., 2006a. δD values of individual *n*-alkanes from terrestrial plants along a climatic gradient – Implications for the sedimentary biomarker record. *Organic Geochemistry*, 37: 469-483.
- Sachse, D., Radke, J., Gleixner, G., 2006b. Hydrogen isotope ratios of recent lacustrine sedimentary n-alkanes record modern climate variability. *Geochimica et Cosmochimica Acta*, 68: 4877-4889.
- Sauer, P.E., Eglinton, T.I., Hayes, J.M., Schimmelmann, A., Sessions, A.L., 2001. Compound-specific D/H ratios of lipid biomarkers from sediments as a proxy for environmental and climatic conditions. *Geochimica et Cosmochimica Acta*, 65: 213-222.
- Schimmelmann, A., Sessions, A.L., Mastalerz, M., 2006. Hydrogen isotopic (D/H) composition of organic matter during diagenesis and thermal maturation. *Annual Review of Earth and Planetary Science*, 34: 501-533.
- Schmidt, M.W., Spero, H.J., Lea, D.W., 2004. Links between salinity variation in the Caribbean and North Atlantic thermohaline circulation. *Nature*, 428: 160-163.
- Schmidt, M.W., Vautravers, M.J., Spero, H.J., 2006. Rapid subtropical North Atlantic salinity oscillations across Dansgaard-Oeschger cycles. *Nature*, 443: 561-564.
- Schmittner, A., Appenzeller, C., Stocker, T.F., 2000. Enhanced Atlantic freshwater export during El Niño. *Geophysical Research Letters*, 27: 1163-1166.
- Schmittner, A., Clement, A.C., 2002. Sensitivity of the thermohaline circulation to tropical and high latitude freshwater forcing during the last glacial-interglacial cycle. *Paleoceanography*, 17: doi: 10.1029/2000PA000591.
- Sessions, A.L., 2006. Seasonal changes in D/H fractionation accompanying lipid biosynthesis in *Spartina alterniflora*. *Geochimica et Cosmochimica Acta*, 70: 2153-2162.
- Sessions, A.L., Burgoyne, T.W., Schimmelmann, A., Hayes, J.M., 1999. Fractionation of hydrogen isotopes in lipid biosynthesis. *Organic Geochemistry*, 30: 1193-1200.
- Sessions, A.L., Sylva, S.P., Summons, R.E., Hayes, J.M., 2004. Isotopic exchange of carbon-bound hydrogen over geologic timescales. *Geochimica et Cosmochimica Acta*, 68: 1545-1559.
- Smith, F.A., Freeman, K.H., 2006. Influence of physiology and climate on δD of leaf wax n-alkanes from C_3 and C_4 grasses. *Geochimica et Cosmochimica Acta*, 70: 1172-1187.
- Stocker, T.F., 1999. Abrupt climate changes: from the past to the future – a review. *International Journal of Earth Sciences*, 88: 365-374.

Stocker, T.F., 2000. Past and future reorganizations in the climate system. *Quaternary Science Reviews*, 19: 301-319.

Stott, L., Poulsen, C., Lund, S., Thunell, R., 2002. Super ENSO and global climate oscillations at millennial time scales. *Science*, 297: 222-226.

Sun, Y., Chen, Z., Xu, S., Cai, P., 2005. Stable carbon and hydrogen isotopic fractionation of individual n-alkanes accompanying biodegradation : Evidence from a group of progressively biodegraded oils. *Organic Geochemistry*, 36: 225-238.

Timmermann, A., Krebs, U., Justino, F., Goosse, H., Ivanochko, T., 2005. Mechanism for millennial-scale global synchronization during the last glacial period. *Paleoceanography*, 20: doi: 10.1029/2004PA001090.

Trenberth, K.E., Caron, J.M., 2001. Estimates of meridional atmosphere and ocean heat transports. *Journal of Climate*, 14: 3433-3443.

van Kreveld, S., Sarinthein, M., Erlenkeuser, H., Grootes, P., Jung, S., Nadeau, M.J., Pflaumann, U., Voelker, A., 2000. Potential links between surging ice sheets, circulation changes, and the Dansgaard-Oeschger cycles in the Irminger Sea, 60-18 kyr. *Paleoceanography*, 15: 425-442.

Visbeck, M., Cullen, H., Krahnemann, G., Naik, N., 1998. *Geophysical Research Letters*, 25: 4521-4524.

Visbeck, M.H., Hurrell, J.W., Polvani, L., Cullen, H.M., 2001. The North Atlantic Oscillation: Past, present, and future. *Proceedings of the National Academy of Sciences*, 98: 12,876-12,877.

Voelker, A.H.L., and the SCOR-IMAGES workshop participants, 2002. Global distribution of centennial-scale records for Marine Isotope Stage (MIS) 3: A database. *Quaternary Science Reviews*, 21: 1185-1212.

Waliser, D.E., Gautier, C., 1993. A satellite-derived climatology of the ITCZ. *Journal of Climate*, 6: 2162-2174.

Wang, C., 2005. ENSO, Atlantic climate variability, and the walker and Hadley circulations. In *The Hadley Circulation: Present, Past, and Future*, H.F. Diaz and R.S. Bradley (eds): 173-202.

Wang, X., Auler, A.S., Edwards, R.L., Cheng, H., Cristalli, P.S., Smart, P.L., Richards, D.A., Shen, C.-C., 2004. Wet periods in northeastern Brazil over the past 210 kyr linked to distant climate anomalies. *Nature*, 432: 740-743.

Wang, Y.J., Cheng, H., Edwards, R.L., An, Z.S., Wu, J.Y., Shen, C.-C., Dorale, J.A., 2001. A high-resolution absolute-dated late Pleistocene monsoon record from Hulu Cave, China. *Science*, 294: 2345-2348.

Weaver, A.J., Bitz, C.M., Fanning, A.F., Holland, M.M., 1999. Thermohaline circulation: High-latitude phenomena and the difference between the Pacific and Atlantic. *Annual Review of Earth and Planetary Science*, 27: 231-285.

Weldeab, S., Schneider, R.R., Kölling, M., 2006. Deglacial sea surface temperature and salinity increase in the western tropical Atlantic in synchrony with high latitude climate instabilities. *Earth and Planetary Science Letters*, 241: 699-706.

Weyl, P.K., 1968. The role of the oceans in climatic change: a theory of the ice ages. *Meteorological Monographs*, 8: 37-62.

Xie, S.-P., Tanimoto, Y., 1998. A pan-Atlantic decadal climate oscillation. *Geophysical Research Letters*, 25: 2185-2188.

Yarincik, K.M., Murray, R.W., Lyons, T.W., Peterson, L.C., Haug, G.H., 2000. Oxygenation history of bottom waters in the Cariaco Basin, Venezuela, over the past 578,000 years: Results from redox-sensitive metals (Mo, V, Mn, and Fe). *Paleoceanography*, 15: 593-604.

Yin, J.H., Battisti, D.S., 2001. The importance of tropical sea surface temperature patterns in simulations of last glacial maximum climate. *Journal of Climate*, 14: 565-581.

Zaucker, F., Stocker, T.F., Broecker, W.S., 1994. Atmospheric freshwater fluxes and their effect on the global thermohaline circulation. *Journal of Geophysical Research*, 99: 12,443-12,457.

Zhang, R., Delworth, T.L., 2005. Simulated tropical response to a substantial weakening of the Atlantic thermohaline circulation. *Journal of Climate*, 18: 1853-1860.

CHAPTER 6

CONCLUSIONS AND THOUGHTS ON FUTURE RESEARCH DIRECTIONS

The distributions and carbon isotopic ($\delta^{13}\text{C}$, $\Delta^{14}\text{C}$) signatures of organic biomarkers preserved in marine sediments provide a wealth of information on the operation of present and past global carbon cycle, and have accordingly been employed to address a broad spectrum of geochemical questions. Importantly though, a decade of compound-specific radiocarbon analysis has revealed substantial temporal discrepancies between some of these compounds and surrounding sedimentary archive. In the case of vascular plant biomarkers, these offsets are likely attributable to sequestration in an array of reservoirs on land compounded by redistribution processes upon arrival in the sea. Until now, however, it remained unclear if the ^{14}C depletions of bulk organic carbon (OC) observed in many rivers and adjacent margin sediments were also symptomatic of such ‘terrestrial residence times’, or instead largely reflected a truly fossil endmember weathering from ancient sedimentary rocks.

The studies comprising this thesis developed an initial framework in which to both address these challenges and circumnavigate (in effect) the associated consequences for biomarker-based climate reconstructions. In Chapters 2 and 3, coupled molecular isotope mass balances demonstrated that the amount of petrogenic OC residing on the Beaufort and Eel River margins had been previously overestimated due to the presence of significantly ‘pre-aged’ terrestrial OC. However, even though its contribution may be

smaller, these results reinforce the emerging notion that organic matter housed in sedimentary rocks is not completely oxidized during weathering and subsequent seaward transport. Moreover, the relative invariance in the down-core abundance of petrogenic OC on the Eel River Margin (calculated by multiplying its fractional abundance with the mass of TOC in each horizon) further insinuates that little additional attenuation occurs in the redox-active zone of marine sediments. Together, these results suggest that some portion of petrogenic OC transits passively through the ‘active’ branch of the carbon cycle. If relevant on a global scale, such observations carry profound implications for the current cycling and geologic evolution of atmospheric O₂ on Earth. Thus, if additional constraints can be placed on lipid-biomass $\delta^{13}\text{C}$ offsets, the coupled molecular isotope approach developed here will warrant much wider application to both active and passive margin systems in the future.

Chapter 4 refocused attention on the temporal dynamics of vascular plant OC transfer to the oceans using two disparate settings where sediment redistribution processes are likely to be minimal: the Cariaco Basin and Saanich Inlet. Comparison of the down-core $\Delta^{14}\text{C}$ profiles for long chain fatty acids at both sites with the $\Delta^{14}\text{C}$ history of atmospheric CO₂ within a simple model framework reveals that the vast majority of these vascular plant biomarkers at both sites suffer from multi-millennial residence times on land. Most of the remaining inventory is deposited in sediments within one or two decades (with only a small component delivered annually to the Saanich Inlet), providing direct evidence that very little terrestrial organic matter is rapidly transferred to the marine environment. Again, if symptomatic of a broader scale phenomenon, these

findings not only suggest that the inherent age of terrestrial OC might exert substantial control on the ability of some components to survive remineralization in the ocean, but also that continental soils and wetlands represent a more significant long-term sink for atmospheric CO₂ than previously considered.

Reconstructions of carbon cycle and climate dynamics using terrestrial biomarker proxies are likewise prone to such temporal offsets, likely confounding the assessment of cause/effect relationships founded on lead/lag arguments. In fact, this technique may need to be abandoned altogether, especially when investigating abrupt climate events. Therefore, the striking modulation in the signal amplitude of a $\delta^{13}\text{C}$ -based tropical paleoaridity record presented in Chapter 5 is instead used to evaluate the role of low versus high latitude phenomena in abrupt paleoclimate oscillations during the last full glacial cycle. Using this approach, seasonal variations in the position of the Intertropical Convergence Zone are interpreted to be a response to both high latitude adjustments in meridional overturning circulation and precessionally-driven modifications in local insolation.

It bears noting, however, that significant pre-aging of a large component of the leaf wax inventory also has the potential to attenuate the amplitude of the $\delta^{13}\text{C}$ shifts. If, for demonstration purposes only, this record is considered to accurately reflect the primarily climate signal (even though, as discussed above, it likely does not), passage through the box model developed in Chapter 4 for the Cariaco Basin system effectively mutes the amplitude of change during many D-O cycles, especially those that are particularly short-lived (Figure 6.1). Thus, even the large $\delta^{13}\text{C}$ shifts documented here

might not adequately capture the full response of vegetation to the more abrupt climate events in the presence of substantial (i.e. multi-millennial) terrestrial residence times. It should nevertheless be noted that the sheer presence of rapid $\delta^{13}\text{C}$ shifts across abrupt climate transitions during both MIS 3 (Chapter 5) and last deglaciation (Hughen et al., 2004) implies that some fraction of these biomarkers are transferred to marine sediments far more rapidly, in agreement with the observation (in Chapter 4) of a considerably abundant portion of decadally-delivered fatty acids in the Cariaco Basin. These results suggest that a premium should be placed on maximizing the temporal resolution of such biomarker-based paleoclimate records in future studies.

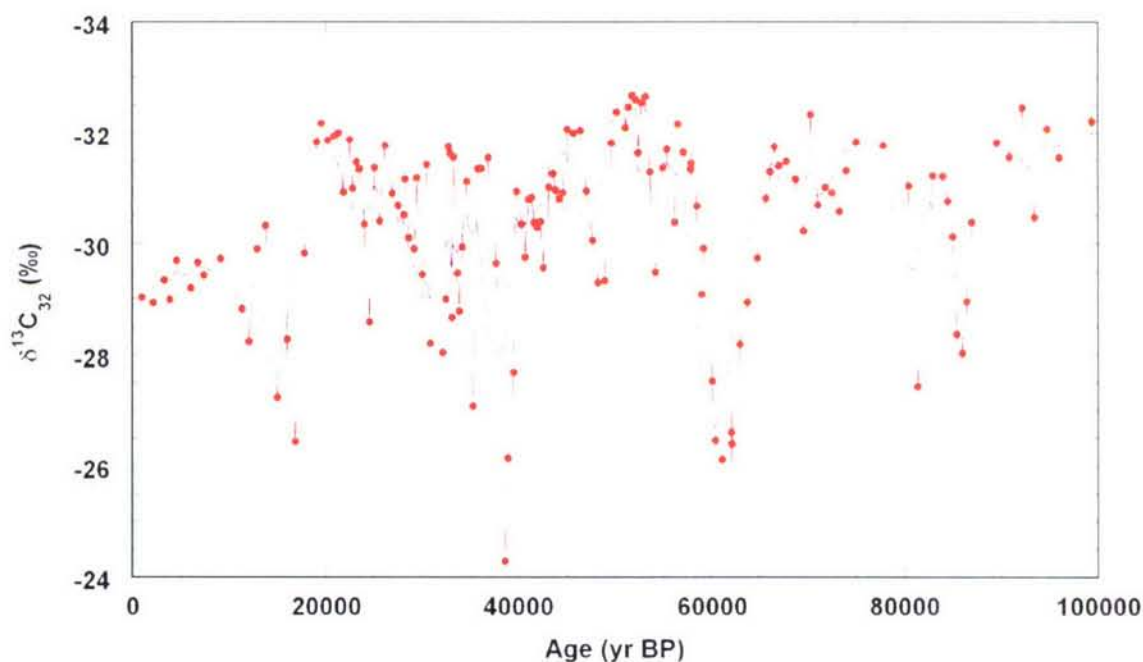


FIGURE 6.1 – The last 100 kyr of the Cariaco Hole 1002D $\delta^{13}\text{C}$ record presented in Chapter 5 (red) along with the curve that results from passing it through the multi-component residence time box model developed in Chapter 4 (blue).

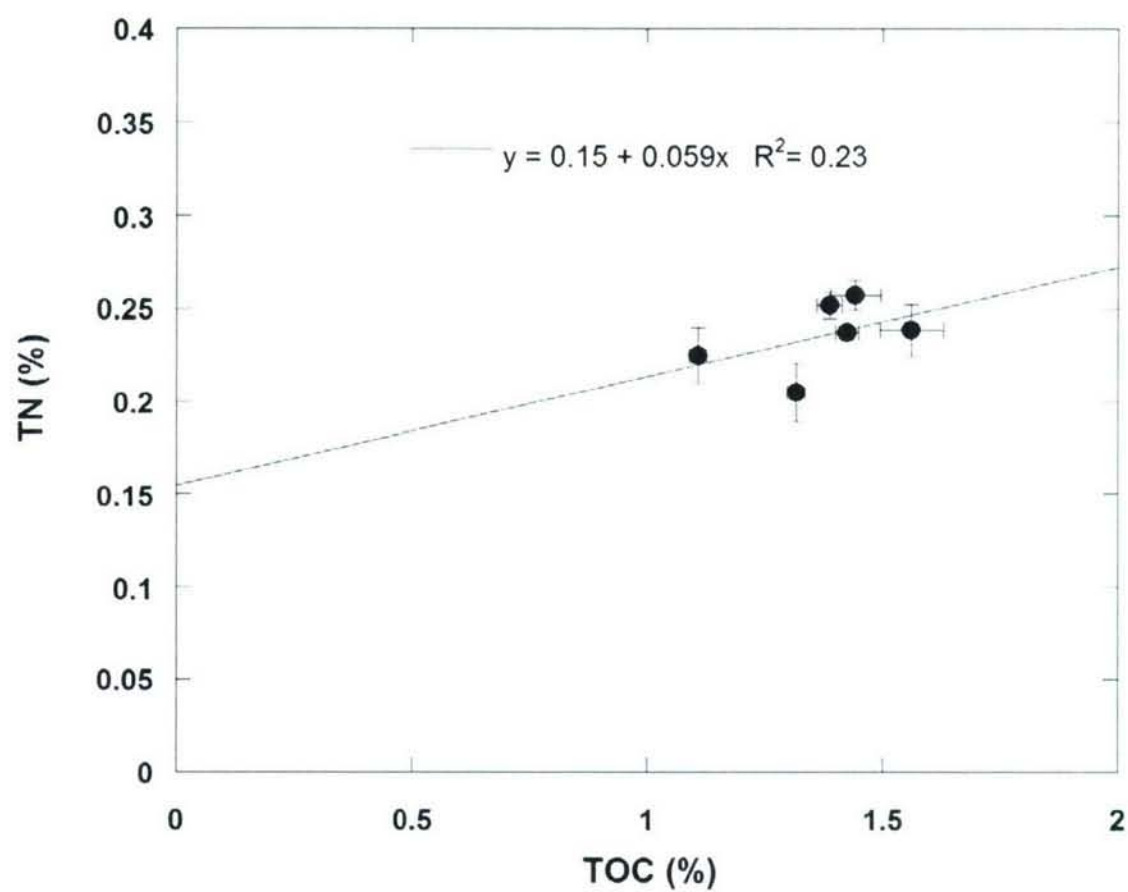
REFERENCES

Hughen, K.A., Eglinton, T.I., Xu, L., Makou, M., 2004. Abrupt tropical vegetation response to rapid climate change. *Science*, 304: 1955-1959.

APPENDICES

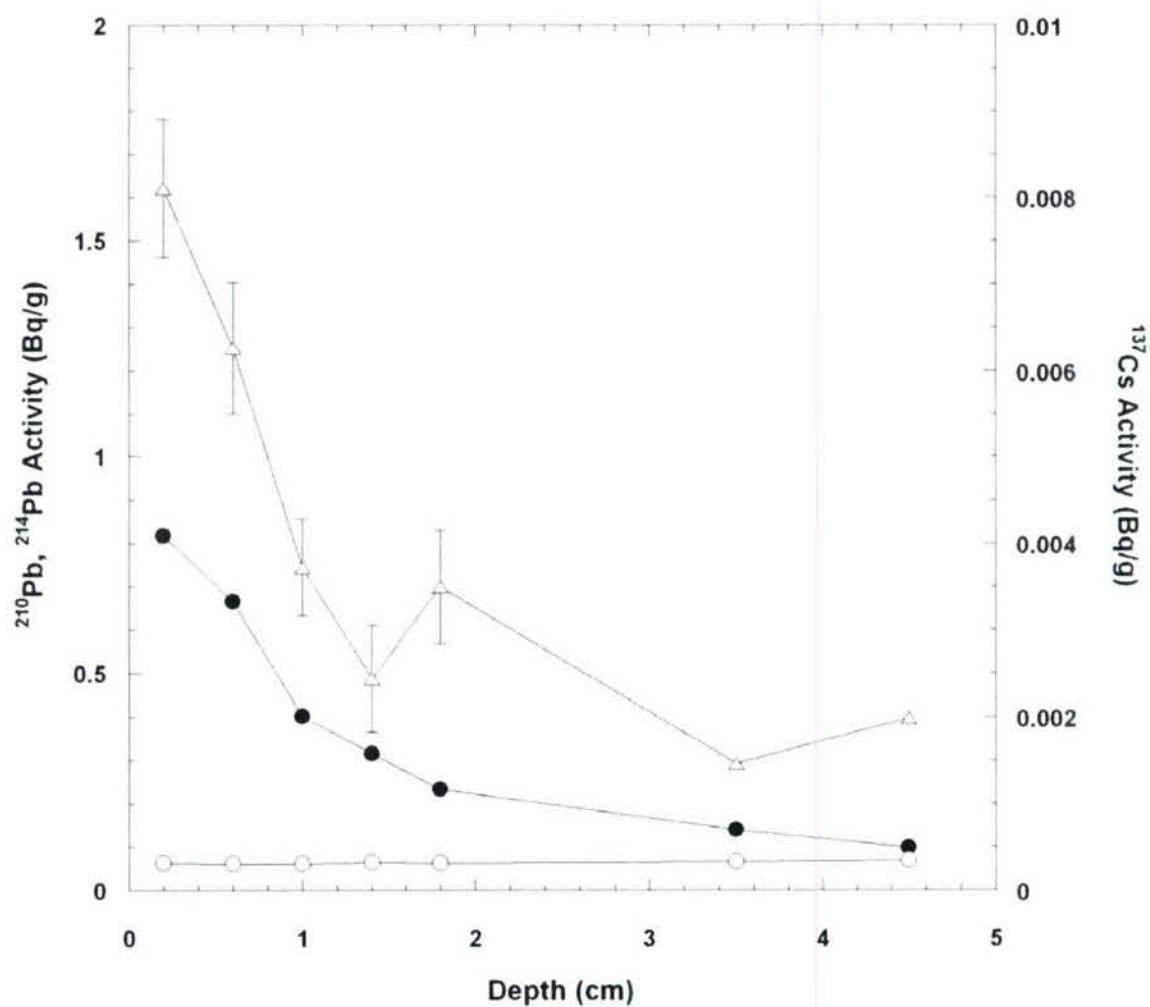
APPENDIX 2.1

Beaufort Shelf sedimentary total nitrogen (TN) vs. total organic carbon (TOC) concentrations for all stations. Best fit linear regression is shown.



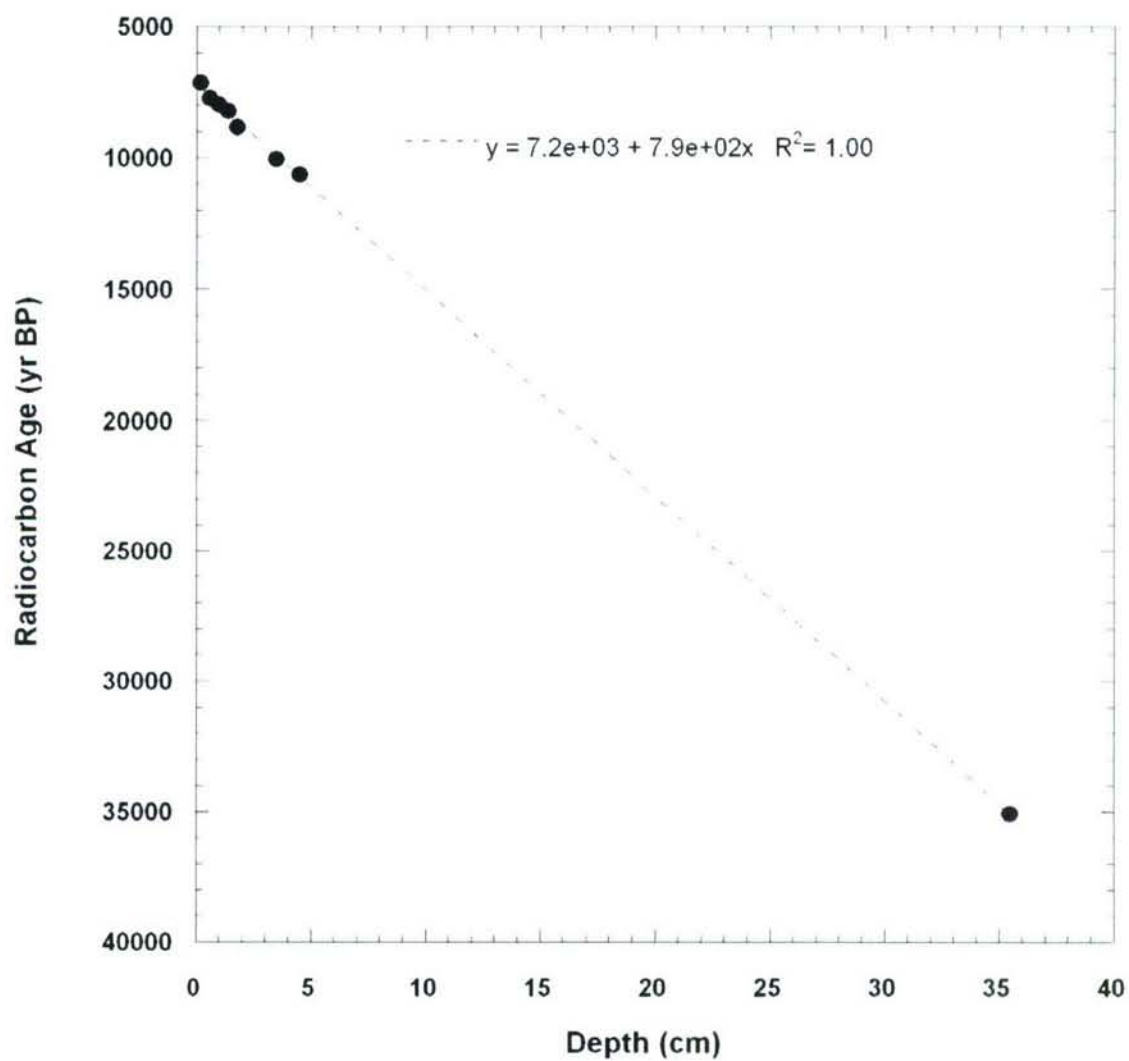
APPENDIX 2.2

Beaufort Shelf Station 144 down core profiles of ^{210}Pb (filled circles), ^{214}Pb (open circles), and ^{137}Cs (open triangles).



APPENDIX 2.3

Beaufort Shelf Station 144 TOC radiocarbon age vs. depth. Least squares regression fit is shown, yielding an average sedimentation rate of 1.2 cm kyr^{-1}



APPENDIX 3.1

Bulk elemental and isotopic properties of Eel River Margin sediment cores. $^{210}\text{Pb}_{\text{xs}}$ = excess (unsupported) ^{210}Pb activity, TC = total carbon, TOC = total organic carbon, TN = total nitrogen, TON = total organic nitrogen. Bulk $\delta^{13}\text{C}$ and $\Delta^{14}\text{C}$ values were measured for TOC. Table continued on three subsequent pages.

Depth (cm)	Adj Depth (cm)	Year (AD)	$^{210}\text{Pb}_{\text{xs}}$ (Bq/g)	^{214}Pb (Bq/g)	^{137}Cs (Bq/g)	TC (wt%)	TC/TN	TOC (wt%)	TOC/TON	$\delta^{13}\text{C}_{\text{TOC}}$	$\Delta^{14}\text{C}_{\text{TOC}}$
GGC 5											
0.5	7.0	1995.4	0.0655	0.0286	0.0025	0.88	15.63	0.94	19.51	-25.4	-441
1.5	8.0	1994.5				0.79	14.65	0.86	18.35		
2.5	9.0	1993.7				0.81	13.96	0.92	18.56		
3.5	10.0	1992.8				1.04	17.36	1.05	19.90		
4.5	11.0	1991.9				1.07	16.64	1.09	18.84		
5.5	12.0	1991.1	0.0635	0.0282	0.0028	1.01	16.45	1.39	21.37		
6.5	13.0	1990.2				1.21	17.25	1.49	20.82		
7.5	14.0	1989.4				1.00	15.95	1.26	20.36		
8.5	15.0	1988.5				1.10	18.02	1.17	19.43		
9.5	16.0	1987.6				1.04	17.07	1.18	19.71		
10.5	17.0	1986.8	0.0452	0.0279	0.0035	0.96	17.25	0.91	17.26	-25.5	-390
11.5	18.0	1985.9				0.76	16.70	0.89	19.20		
12.5	19.0	1985.1				0.53	13.59	0.60	17.65		
13.5	20.0	1984.2				0.69	15.14	0.71	17.30		
14.5	21.0	1983.3				0.99	17.05	1.08	21.68		
15.5	22.0	1982.5				0.97	16.59	0.99	18.23	-25.4	-418
16.5	23.0	1981.6				0.94	15.40	1.11	20.09		
17.5	24.0	1980.7				0.99	15.38	1.09	18.14	-24.9	-380
18.5	25.0	1979.9				0.95	14.91	1.23	16.35		
19.5	26.0	1979.0				1.10	16.81	1.15	14.96		
20.5	27.0	1978.2	0.0338	0.0290	0.0050	1.10	16.16	1.29	15.91	-24.8	-303
21.5	28.0	1977.3				1.11	17.04	1.33	17.18		
22.5	29.0	1976.4				1.07	16.61	1.21	14.48	-25.4	-349
23.5	30.0	1975.6				1.04	14.49	1.24	14.09		
24.5	31.0	1974.7				1.01	14.02	1.11	15.30		
25.5	32.0	1973.8	0.0266	0.0604	0.0049	1.19	15.61	1.18	15.94	-25.3	-422
26.5	33.0	1973.0				1.06	14.18	1.21	19.75		
27.5	34.0	1972.1	0.0434	0.0589	0.0048	0.91	14.96	0.97	19.80	-25.1	-461
28.5	35.0	1971.3				0.74	13.25	1.06	18.70		
29.5	36.0	1970.4				0.80	14.28	0.95	20.39		
30.5	37.0	1969.5	0.0210	0.0293	0.0061	0.77	14.06	0.83	18.60	-24.8	-539

APPENDIX 3.1 (CONTINUED)

Depth (cm)	Adj Depth (cm)	Year (AD)	²¹⁰ Pb _{ex} (Bq/g)	²¹⁴ Pb (Bq/g)	¹³⁷ Cs (Bq/g)	TC (wt%)	TC/TN	TOC (wt%)	TOC/TON	δ ¹³ C _{Toc}	Δ ¹⁴ C _{Toc}
GGC 5											
31.5	38.0	1968.7				0.85	14.65	0.95	18.88		
32.5	39.0	1967.8	0.0465	0.0618	0.0041	0.77	13.66	1.14	21.36	-25.0	-627
33.5	40.0	1966.9				0.87	14.79	1.00	20.82		
34.5	41.0	1966.1				0.77	14.59	0.97	20.36		
35.5	42.0	1965.2	0.0318	0.0572	0.0046	0.78	16.14	0.86	22.65	-25.1	-490
36.5	43.0	1964.4				0.80	16.04	0.85	21.66		
37.5	44.0	1963.5				0.65	14.96	0.63	18.77		
38.5	45.0	1962.6				0.68	14.61	0.73	17.59		
39.5	46.0	1961.8				0.82	14.93	0.88	18.48		
40.5	47.0	1960.9	0.0155	0.0288	0.0014	0.83	15.05	0.85	19.73	-25.3	-417
41.5	48.0	1960.1				1.01	14.56	1.13	19.32		
42.5	49.0	1959.2				0.89	12.55	1.05	14.68		
43.5	50.0	1958.3				0.95	12.74	0.94	14.26		
44.5	51.0	1957.5				0.84	13.88	0.79	13.24		
45.5	52.0	1956.6	0.0302	0.0605	0.0020	0.90	14.25	0.88	13.97	-25.0	-445
46.5	53.0	1955.7				0.81	13.81	0.73	12.13		
47.5	54.0	1954.9				0.84	13.63	0.80	13.65		
48.5	55.0	1954.0				1.07	17.67	0.97	16.60		
49.5	56.0	1953.2				1.02	16.97	0.92	14.13		
50.5	57.0	1952.3	0.0127	0.0300	0.0000	0.99	16.76	0.96	15.48	-25.1	-423
51.5	58.0	1951.4				0.97	16.68	0.98	16.15		
52.5	59.0	1950.6				0.98	17.30	0.98	14.22		
53.5	60.0	1949.7				0.88	14.89	1.00	15.38		
54.5	61.0	1948.8				0.84	17.23	0.93	15.20		
55.5	62.0	1948.0				1.00	19.19	0.96	14.50		
56.5	63.0	1947.1				1.10	19.39	1.06	15.65		
57.5	64.0	1946.3				1.07	21.06	1.02	15.19		
58.5	65.0	1945.4				0.89	18.40	0.88	13.85		
59.5	66.0	1944.5				0.95	18.97	0.87	13.84		

APPENDIX 3.1 (CONTINUED)

Depth (cm)	Adj Depth (cm)	Year (AD)	²¹⁰ Pb _{ex} (Bq/g)	²¹⁴ Pb (Bq/g)	¹³⁷ Cs (Bq/g)	TC (wt%)	TC/TN	TOC (wt%)	TOC/TON	δ ¹³ C _{Toc}	Δ ¹⁴ C _{Toc}
GGC 5											
60.5	67.0	1943.7	-0.0019	0.0307	0.0000	1.02	31.69	0.92	14.21	-25.2	-439
61.5	68.0	1942.8				1.08	25.10	1.03	16.93		
62.5	69.0	1941.9				0.95	27.96	0.97	14.37		
63.5	70.0	1941.1				0.98	29.14	0.98	13.97		
64.5	71.0	1940.2				0.88	29.11	0.89	17.86		
65.5	72.0	1939.4				0.78	23.96	0.79	16.68		
66.5	73.0	1938.5				0.79	19.57	0.74	16.84		
67.5	74.0	1937.6				0.80	19.16	0.80	16.31		
68.5	75.0	1936.8				0.77	18.88	0.84	16.74		
69.5	76.0	1935.9				0.81	18.44	0.85	16.52		
70.5	77.0	1935.1	-0.0010	0.0280	0.0000	0.84	19.94	0.82	14.44	-24.9	-451
71.5	78.0	1934.2				0.83	20.39	1.12	18.66		
72.5	79.0	1933.3				0.99	15.09	0.95	16.11		
73.5	80.0	1932.5				1.07	15.72	1.03	16.79		
74.5	81.0	1931.6				0.93	14.99	0.89	15.10		
75.5	82.0	1930.7				0.97	14.37	0.86	15.16		
76.5	83.0	1929.9				0.88	13.23	0.82	21.62		
77.5	84.0	1929.0				0.85	13.64	0.77	23.43		
78.5	85.0	1928.2				0.85	18.50	0.83	22.28		
79.5	86.0	1927.3				0.89	18.92	0.88	24.75		
80.5	87.0	1926.4	-0.0058	0.0295	0.0000	0.79	17.34	0.77	22.18	-25.0	-494
81.5	88.0	1925.6				0.83	18.15	0.90	21.97		
82.5	89.0	1924.7				0.88	18.93	0.82	12.71		
83.5	90.0	1923.8				0.95	18.74	0.85	12.67		
84.5	91.0	1923.0				0.93	16.96	0.90	14.06		
85.5	92.0	1922.1				0.93	17.58	0.99	14.38		
86.5	93.0	1921.3				1.05	20.53	0.93	14.12		
87.5	94.0	1920.4				0.82	16.53	0.91	18.13		
88.5	95.0	1919.5				1.07	20.53	0.92	15.08		
89.5	96.0	1918.7				0.95	18.73	0.89	15.50		

APPENDIX 3.1 (CONTINUED)

Depth (cm)	Adj Depth (cm)	Year (AD)	²¹⁰ Pb _{xs} (Bq/g)	²¹⁴ Pb (Bq/g)	¹³⁷ Cs (Bq/g)	TC (wt%)	TC/TN	TOC (wt%)	TOC/TN	δ ¹³ C _{Toc}	Δ ¹⁴ C _{Toc}
GGC 5											
90.5	97.0	1917.8	-0.0026	0.0289	0.0000	0.82	15.20	0.75	13.70	-24.8	-432
91.5	98.0	1916.9				0.93	17.03	0.86	17.80		
92.5	99.0	1916.1				0.82	14.89	0.92	15.98		
93.5	100.0	1915.2				0.87	15.20	0.86	15.14		
94.5	101.0	1914.4				0.93	15.85	1.00	15.69		
95.5	102.0	1913.5				0.92	16.90	1.19	16.64		
96.5	103.0	1912.6				0.91	13.17	0.89	13.79		
97.5	104.0	1911.8				0.87	12.60	0.86	13.73		
98.5	105.0	1910.9				0.93	13.52	1.01	14.74		
99.5	106.0	1910.1				0.97	13.47	0.95	14.83		
100.5	107.0	1909.2				0.89	13.19	0.89	17.63	-25.0	-477
101.5	108.0	1908.3	-0.0077	0.0293	0.0000	0.84	12.89	0.77	17.09		
102.5	109.0	1907.5				0.84	14.32	0.84	18.56		
103.5	110.0	1906.6				0.84	14.81	0.83	17.45		
104.5	111.0	1905.7				0.93	14.83	0.85	17.35		
105.5	112.0	1904.9				0.89	15.22	0.97	19.99		
106.5	113.0	1904.0				0.87	15.87	0.85	13.05		
107.5	114.0	1903.2				0.87	17.05	0.78	11.94		
108.5	115.0	1902.3				0.94	18.35	0.97	13.82		
109.5	116.0	1901.4				1.04	20.38	0.82	11.31		
110.5	117.0	1900.6				1.08	21.23	0.89	9.95		
111.5	118.0	1899.7		0.0287	0.0000	0.99	20.78	0.99	6.63		
112.5	119.0	1898.8				0.84	18.50	0.85	16.01		
113.5	120.0	1898.0	-0.0046			0.88	19.60	0.92	18.46		
114.5	121.0	1897.1				0.93	19.80	0.91	17.88		
MC 36											
0.5			0.0900	0.0282	0.0020					-25.4	-367
1.5			0.0404	0.0254	0.0024						
3.5			0.0552	0.0290	0.0026						
5.5			0.0531	0.0290	0.0026						-410
7.5			0.0794	0.0275	0.0037						
10.5			0.1079	0.0295	0.0036					-25.1	-363
15.5			0.0385	0.0289	0.0034						
20.5			0.0456	0.0281	0.0043					-25.1	-413
24.5			0.0183	0.0268	0.0043						
28.5			0.0141	0.0280	0.0069					-26.3	-274

Compound-specific $\delta^{13}\text{C}$ and $\Delta^{14}\text{C}$ values and 1σ analytical uncertainties of fatty acids extracted from Eel River Margin core GGC 5. Italicized $\Delta^{14}\text{C}$ values were measured at the KCCAMS facility, while all others were analyzed at NOSAMS. Final sample masses (μg carbon measured manometrically as CO_2) are given next to each reported $\Delta^{14}\text{C}$ number in parentheses.

209

APPENDIX 4.1

Bulk elemental and isotopic properties of Cariaco Basin and Saanich Inlet sediment cores. $^{210}\text{Pb}_{\text{xs}}$ = excess (unsupported) ^{210}Pb activity, TC = total carbon, TOC = total organic carbon, TN = total nitrogen, TON = total organic nitrogen. Bulk $\delta^{13}\text{C}$ and $\Delta^{14}\text{C}$ values were measured for TOC. Saanich Inlet horizons are given as varve numbers relative to a turbidite common to all freeze cores. Table continued on three subsequent pages.

Depth (cm)	Year (AD)	$^{210}\text{Pb}_{\text{xs}}$ (Bq/g)	^{214}Pb (Bq/g)	^{137}Cs (Bq/g)	TC (wt%)	TC/TN	TOC (wt%)	TON	$\delta^{13}\text{C}_{\text{TOC}}$	$\Delta^{14}\text{C}_{\text{TOC}}$
Cariaco MC 5										
0.25	2001	1.5551	0.0226	n/d	9.07	13.06	6.16	10.29		
0.75	1996	1.3916	0.0183	n/d	9.20	13.10	6.50	9.77	-20.1	53
1.25	1991	1.3244	0.0190	n/d	9.15	13.58	6.59	9.75	-20.1	59
1.75	1986	1.2096	0.0194	n/d	9.64	13.82	6.64	10.00	-20.2	57
2.25	1981	1.0455	0.0232	n/d	9.26	14.12	6.32	9.70	-19.9	46
2.75	1976	0.8988	0.0200	n/d	9.15	13.82	6.24	9.74	-19.9	54
3.25	1971	0.8179	0.0194	n/d	9.17	13.53	6.57	10.02	-19.8	1
3.75	1966	0.8585	0.0208	0.0019	8.59	13.49	6.02	9.85	-19.7	-53
4.25	1961	0.6365	0.0202	0.0016	9.04	13.70	6.28	10.38	-19.8	-76
4.75	1956	0.5675	0.0225	n/d	8.68	13.99	5.98	10.00	-19.8	-78
5.25	1951	0.4532	0.0236	n/d	8.97	13.68	6.43	10.40	-19.5	-74
5.75	1946	0.3771	0.0253	n/d	9.18	13.88	6.39	10.11	-19.5	-82
6.25	1941	0.3367	0.0267	n/d	8.81	13.92	6.28	9.87	-19.3	-74
6.75	1936	0.2656	0.0261	n/d	8.58	13.00	6.36	10.28		
7.25	1931	0.2358	0.0239	n/d	8.33	13.07	6.03	10.22		
7.75	1926	0.2010	0.0231	n/d	8.63	12.78	6.45	10.25		
8.25	1921	0.1767	0.0258	n/d	7.89	12.89	5.79	9.87	-19.4	-70
8.75	1916	0.1481	0.0306	n/d	8.40	12.86	6.20	10.25		
9.25	1911	0.1109	0.0248	n/d	8.33	13.10	5.95	10.30		
9.75	1906	0.1000	0.0261	n/d	7.79	13.38	5.66	9.67		
10.25	1901	0.0830	0.0236	n/d	8.54	13.14	6.28	10.34	-19.7	-90
10.75	1896	0.0762	0.0237	n/d	8.34	13.08	6.11	9.99		
11.25	1891	0.0583	0.0247	n/d	8.48	13.94	5.66	9.83		
11.75	1886	0.0404	0.0282	n/d	7.92	13.12	5.75	10.23		
12.25	1881				8.69	13.16	6.34	9.83		
12.75	1876				8.52	13.25	6.04	10.22		
13.25	1871				8.74	13.44	6.15	10.04		
13.75	1866				8.45	13.19	6.22	9.93		
14.25	1861				8.72	12.88	6.56	9.87		
14.75	1856				8.61	13.04	6.23	10.06		

APPENDIX 4.1 (CONTINUED)

Depth (cm)	Year (AD)	²¹⁰ Pb _{ex} (Bq/g)	²¹⁴ Pb (Bq/g)	¹³⁷ Cs (Bq/g)	TC (wt%)	TC/TN	TOC (wt%)	TOC/TN	δ ¹³ C _{Toc}	Δ ¹⁴ C _{Toc}
Carliaco MC 5										
15.25	1851				8.66	13.59	6.10	10.08		
16.25	1841				8.67	14.57	5.75	10.15		
16.75	1836				8.66	15.29	5.55	9.26		
17.25	1831				8.60	14.28	5.94	10.15		
17.75	1826				8.60	14.05	5.86	9.90		
18.25	1821				8.34	13.27	5.89	10.13		
18.75	1816				9.14	12.84	6.92	10.02		
19.25	1811				8.88	13.31	6.44	9.93		
19.75	1806				8.92	13.37	6.42	10.35		
20.25	1801				8.82	14.23	6.07	10.08		
20.75	1796				8.82	13.62	6.15	10.07		
21.25	1791				8.67	13.79	6.05	9.47		
21.75	1786				8.58	14.17				
22.25	1781				9.14	13.28	6.66	10.02		
22.75	1776				9.16	13.16	6.72	10.78		
23.25	1771				8.68	14.29	6.42	9.54		
23.75	1766				9.37	13.79	6.87	10.13		
24.25	1761				9.09	13.39	6.86	10.10		
24.75	1756				8.37	13.72	6.46	10.34		
25.25	1751				8.55	14.14	6.05	10.13		
25.75	1746				8.60	13.53	6.28	9.65		
26.25	1741				8.57	14.41	6.04	10.20		
26.75	1736				8.74	14.50	6.19	10.23		
27.25	1731				7.91	13.69	5.56	10.14		
27.75	1726				8.48	13.80	6.10	9.61		
28.25	1721				8.68	14.11	6.18	10.44		
28.75	1716				9.11	13.81	6.60	10.20		
29.25	1711				7.63	13.34	5.73	10.28		
29.75	1706				7.95	14.86	5.81	10.18		
30.25	1701				7.92	14.25	5.59	10.53		
30.75	1696				8.52	13.83	6.11	9.90		
31.25	1691				9.20	14.35	6.46	10.62		

APPENDIX 4.1 (CONTINUED)

Depth (cm)	Year (AD)	²¹⁰ Pb _{ex} (Bq/g)	²¹⁴ Pb (Bq/g)	¹³⁷ Cs (Bq/g)	TC (wt%)	TC/TN	TOC (wt%)	TOC/TON	δ ¹³ C _{TOC}	Δ ¹⁴ C _{TOC}
Cariaco MC 2										
2.75	1976	1.1257	0.0375	0.0018						
3.25	1971	1.0367	0.0394	0.0015						
3.75	1966	0.8380	0.0405	0.0020						
4.25	1961	0.8077	0.0436	0.0028						
4.75	1956	0.6789	0.0428	0.0018						
5.25	1951	0.5761	0.0453	0.0020						
Cariaco MC 6										
2.75	1976	1.0475	0.0394	0.0014						
3.25	1971	1.0818	0.0392	0.0019						
3.75	1966	0.8738	0.0356	0.0026						
4.25	1961	0.7315	0.0413	0.0034						
4.75	1956	0.6418	0.0398	0.0015						
5.25	1951	0.5298	0.0412	0.0018						
Saanich FC 3										
Varve 85 Below	1860				2.57	8.97	2.36	9.15		
Varve 77 Below	1868				2.73	8.98	2.37	9.19		
Varve 69 Below	1876				2.73	9.03	2.71	7.57		
Varve 61 Below	1884				3.05	9.79	2.92	7.94		
Varve 53 Below	1892				2.58	9.63	2.73	7.99		
Varve 45 Below	1900				2.74	9.14	2.62	8.70		
Varve 41 Below	1904				2.91	9.39	2.78	7.59		
Varve 37 Below	1908				2.68	9.45	2.51	8.99		
Turbidite	1908				2.13	10.97	2.13	8.37		
Varve 36 Below	1909				2.28	10.25	2.04	9.79		
Varve 33 Below	1912				2.57	9.55	2.41	8.89		
Varve 29 Below	1916				2.60	9.63	2.50	9.51		
Varve 25 Below	1920	0.0444	0.0120	n/d	2.89	10.78	2.82	9.48		

APPENDIX 4.1 (CONTINUED)

Depth (cm)	Year (AD)	²¹⁰ Pb _{xs} (Bq/g)	²¹⁴ Pb (Bq/g)	¹³⁷ Cs (Bq/g)	TC (wt%)	TC/TN	TOC (wt%)	TOC/TON	δ ¹³ C _{Toc}	Δ ¹⁴ C _{Toc}
Saanich FC 3										
Varve 21 Below	1924	0.0420	0.0111	n/d	2.82	10.23	2.74	7.95	-21.8	-225
Varve 17 Below	1928	0.0556	0.0146	n/d	3.05	9.90	2.85	8.03		
Varve 13 Below	1932	0.0270	0.0127	n/d	2.59	10.11	2.54	8.19	-22.4	-189
Varve 9 Below	1936	0.0335	0.0155	n/d	2.95	10.21	2.92	8.35		
Varve 5 Below	1940	0.0686	0.0162	n/d	3.30	10.84	3.22	8.68	-22.0	-181
Varve 1 Below	1944	0.0560	0.0113	n/d	2.53	10.44	2.46	9.39		
Reference Turbidite	1944	0.0615	0.0150	n/d	2.49	10.58	2.31	9.67		
Varve 1 Above	1945	0.0737	0.0154	n/d	2.83	10.80	2.75	10.28		
Varve 3 Above	1947	0.0658	0.0158	n/d	2.98	11.10	2.59	9.92		
Varve 7 Above	1951	0.0702	0.0122	n/d	2.59	11.25	2.41	8.01	-22.2	-197
Varve 11 Above	1955	0.0794	0.0125	n/d	3.04	11.59	2.70	9.79	-22.4	-195
Varve 15 Above	1959	0.1189	0.0155	0.0053	3.15	12.02	2.61	10.16	-22.7	-178
Varve 16 Above	1960	0.1130	0.0163	0.0056						
Varve 17 Above	1961	0.1332	0.0184	0.0089						
Varve 18 Above	1962	0.0892	0.0219	0.0127					-22.7	-172
Varve 19 Above	1963	0.1264	0.0134	0.0131	3.23	11.43	2.93	8.80	-22.7	-151
Varve 20 Above	1964	0.1222	0.0186	0.0103					-22.7	-148
Varve 21 Above	1965	0.0944	0.0189	0.0064						
Varve 22 Above	1966	0.1182	0.0170	0.0091						
Varve 23 Above	1967	0.0995	0.0188	0.0057						
Varve 27 Above	1971	0.1368	0.0260	0.0076					-23.1	-125
Varve 31 Above	1975	0.1298	0.0203	0.0043	3.14	13.38	2.27	10.42	-22.9	-104
Varve 35 Above	1979	0.1549	0.0153	0.0054	3.64	12.88	2.49	10.03	-22.7	-103
Varve 37 Above	1981									
Varve 39 Above	1983	0.1642	0.0199	0.0052	2.87	11.10	2.63	10.51	-22.5	-72
Varve 43 Above	1987	0.2005	0.0188	0.0036	3.14	10.51	3.17	8.64	-22.1	-88

Compound-specific $\delta^{13}\text{C}$ and $\Delta^{14}\text{C}$ values and 1σ analytical uncertainties of fatty acids extracted from the Cariaco Basin and Saanich Inlet. *Italicized $\Delta^{14}\text{C}$ values were measured at the KCCAMS facility, while all others were analyzed at NOSAMS. Final sample masses (μg carbon measured manometrically as CO_2) are given next to each reported $\Delta^{14}\text{C}$ number in parentheses. Table continued on subsequent page.*

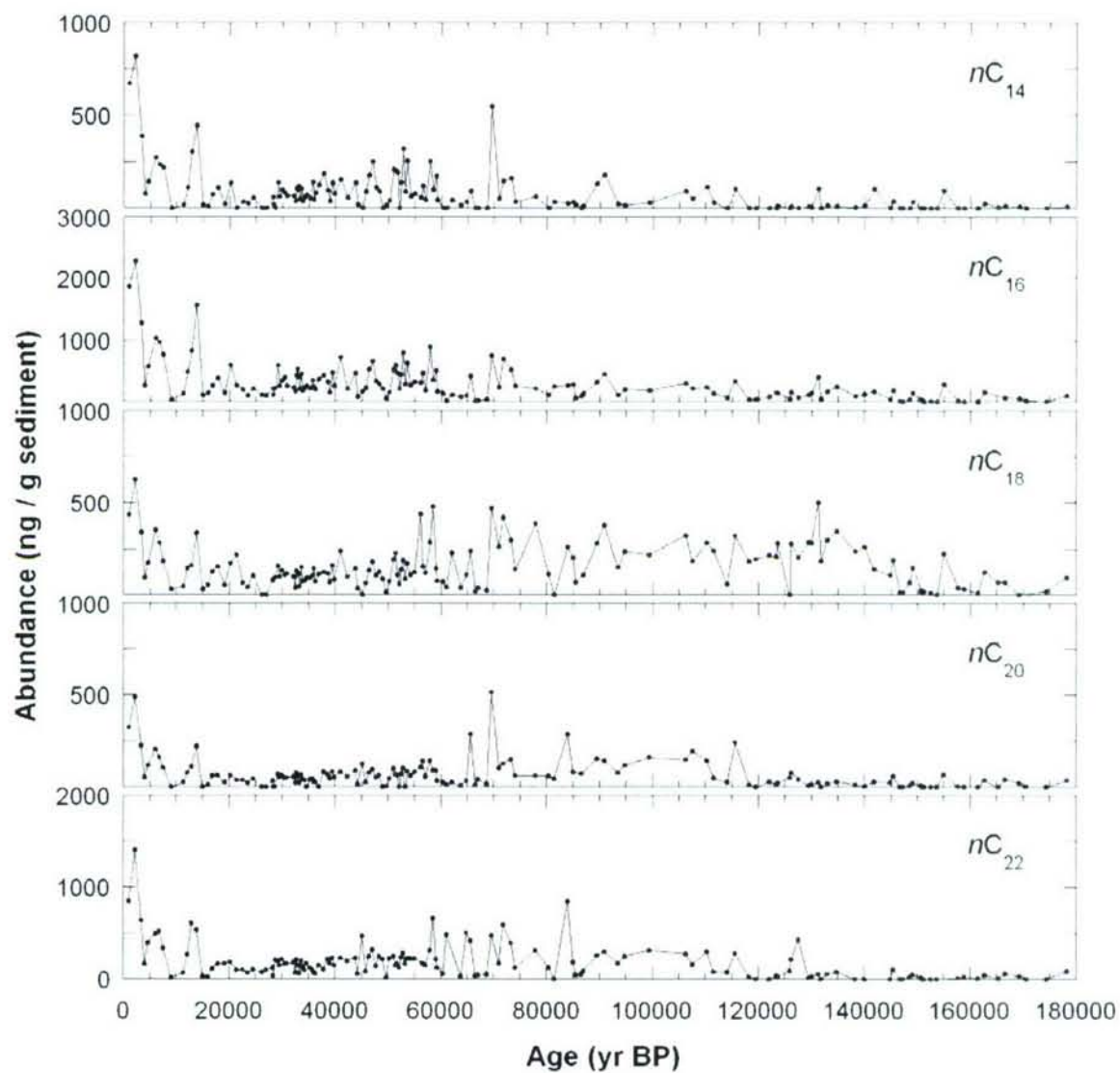
214

APPENDIX 4.2 (CONTINUED)

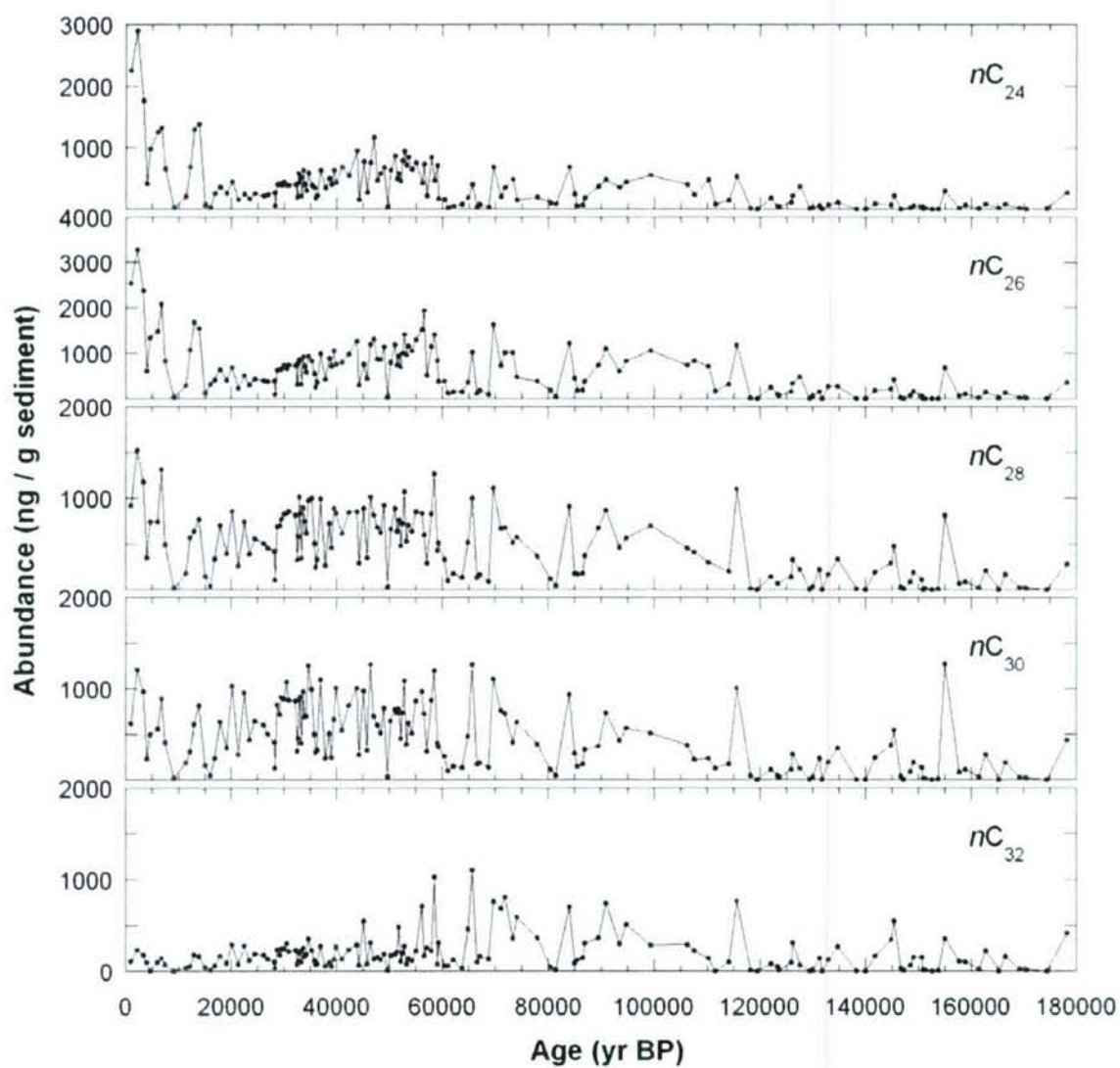
Year	nC_{14}	error	nC_{15}	error	nC_{18}	error	nC_{20}	error	nC_{22}	error	nC_{24}	error	nC_{25}	error	nC_{28}	error	nC_{30}	error	nC_{32}	error	nC_{30+32}	error	$nC_{20+28+30+32}$	error
$\delta^{13}C$																								
1924	-22.5	0.9	-21.0	0.4	-24.1	0.5	-26.6	1.1	-25.4	0.4	-25.2	0.4	-25.8	0.6	-29.7	1.0	-31.4	1.1	-30.4	0.4				
1951			-21.7	0.3	-25.4	0.7	-27.6	0.3	-25.7	0.7	-26.9	0.3	-27.5	0.3	-30.7	0.4	-32.6	1.5	-32.6	2.6				
1959	-22.7	0.5	-22.4	0.2	-25.8	0.5	-26.2	0.1	-26.4	0.2	-26.3	0.1	-27.3	0.4	-30.3	0.8	-31.8	0.7	-33.7	1.1				
1963	-21.9	0.5	-21.1	0.6	-25.2	0.7	-27.1	1.0	-26.7	0.9	-26.0	0.9	-26.1	0.6	-30.8	1.1	-32.2	0.8	-32.8	0.8				
1964	-22.4	0.5	-21.8	0.5	-25.6	0.4	-27.6	0.6	-26.7	0.2	-26.6	0.3	-27.4	0.6	-30.4	0.3	-32.3	0.7	-31.8	0.8				
1967	-21.9	0.4	-20.8	0.3	-25.5	0.2	-27.7	0.8	-27.6	0.8	-27.4	0.5	-28.1	0.4	-31.0	0.6	-31.9	0.7	-35.2	0.2				
1971	-22.7	0.4	-22.8	0.2	-25.4	0.3	-27.5	0.3	-27.2	0.4	-27.0	0.3	-28.1	0.6	-30.9	0.6	-31.8	0.5	-34.6	0.2				
1975	-22.6	0.2	-22.1	0.3	-24.6	0.3	-26.6	0.2	-26.7	0.5	-26.3	0.3	-27.6	0.1	-30.5	0.2	-31.7	0.3	-32.6	0.0				
1987	-22.3	0.0	-21.8	0.1	-24.3	0.2	-26.2	0.5	-26.8	0.2	-26.3	0.2	-27.5	0.6	-30.3	0.6	-32.1	0.8	-32.6	1.4				
$\Delta^{14}C$																								
1924			-81 (31.1)	21																			-304 (38.7)	11
1951			-117 (31.7)	16																			-362 (29.8)	13
1959			1 (7.8)	85																				
1963			-56 (33.5)	18																			-290 (15.9)	28
1964			5 (36.5)	15																			-342 (30.9)	13
1967			-2 (40.8)	15																			-268 (38.0)	11
1971			-210 (12.2)	40																			-307 (36.1)	11
1975			-33 (10.2)	58																				
1987			-10 (32.9)	17																			-224 (14.8)	32
																							-271 (34.3)	12
																							-318 (31.1)	13

APPENDIX 5.1

Abundance profiles for individual even numbered fatty acids from ODP Hole 1002D in the Cariaco Basin. Note change in scale between homologues.



APPENDIX 5.1 (CONTINUED)



APPENDIX 5.2

Stable carbon and oxygen isotopic compositions of *Globigerinoides ruber* shells, and the stable carbon and hydrogen isotopic composition of nC_{32} fatty acids from Cariaco Basin ODP Hole 1002D. Table continued on three subsequent pages.

Sample ID	Depth (m)	Age (Cal yr BP)	Ruber $\delta^{13}C$ (‰)	Ruber $\delta^{18}O$ (‰)	$\delta^{13}C_{32}$ (‰)	error (‰)	δD_{32} (‰)	error (‰)
1H-1 25-27.5	0.263	1015	1.10	-1.43	-29.0	0.2	-143.6	
1H-1 75-77.5	0.763	2185	1.32	-1.51	-28.9	0.4	-149.3	2.9
1H-1 125-127.5	1.263	3354	1.05	-1.03	-29.3	0.3	-151.8	0.8
1H-2 0-2.5	1.513	3940	0.86	-1.46	-29.0	0.5		
1H-2 25-27.5	1.763	4645	1.32	-0.93	-29.7	0.3		
1H-2 75-77.5	2.263	6055	1.24	-0.68	-29.2	0.1	-149.9	
1H-2 100-102.5	2.513	6760	0.96	-1.34	-29.7	0.1	-143.8	0.9
1H-2 125-127.5	2.763	7420	1.40	-1.54	-29.4	0.4		
1H-3 40-42.5	3.413	9136			-29.7	0.2		
1H-4 25-27.5	4.263	11380	0.81	-0.24	-28.8	0.4		
1H-CC 0-2.5	4.523	12102	0.58	-0.43	-28.2	0.7		
2H-1 10-12.5	4.813	12908	0.48	-0.21	-29.9	0.0		
2H-1 45-47.5	5.163	13836	0.58	-0.01	-30.3	0.3	-146.1	1.7
2H-1 90-92.5	5.613	15027	0.17	-0.09	-27.2	0.3		
2H-2 0-2.5	6.213	16024			-28.3	0.8		
2H-2 65-67.5	6.863	16875	0.34	-0.30	-26.4	0.5	-138.9	7.0
2H-2 135-137.5	7.563	17791	0.53	0.48	-29.8	0.2	-145.1	2.0
2H-3 50-52.5	8.213	19113	0.78	0.33	-31.8	0.1		
2H-3 75-77.5	8.463	19569			-32.2	0.1		
2H-3 105-107.5	8.763	20242	0.74	0.50	-31.9	0.1	-164.8	1.9
2H-3 140-142.5	9.113	20864			-31.9	0.6		
2H-4 20-22.5	9.413	21334	0.87	0.40	-32.0	0.6		
2H-4 45-47.5	9.663	21812			-30.9	0.3		
2H-4 80-82.5	10.013	22517	0.89	0.45	-31.9	0.4	-158.3	3.6
2H-4 95-97.5	10.163	22819			-31.0	0.4		
2H-4 115-117.5	10.363	23223			-31.5	0.4		
2H-4 130-132.5	10.513	23526	0.84	0.43	-31.3	0.3		
2H-5 5-7.5	10.763	24029			-30.3	0.4		
2H-5 30-32.5	11.013	24533	0.50	0.03	-28.6	0.4		
2H-5 53-54.5	11.243	25039			-31.4	0.4		
2H-5 80-82.5	11.513	25634			-30.4	0.1		
2H-5 105-107.5	11.763	26175	0.89	0.34	-31.8	0.2		
2H-5 130-132.5	12.013	26945	0.93	0.11	-30.9	0.2		
2H-6 5-7.5	12.263	27630			-30.7	0.5		
2H-6 30-32.5	12.513	28167	1.06	0.25	-30.5	0.2	-148.0	0.3
2H-6 35-37.5	12.563	28274	0.98	0.37	-31.2	0.2		
2H-6 55-57.5	12.763	28705	0.93	-0.04	-30.1	0.2	-160.1	2.1
2H-6 80-82.5	13.013	29258	1.22	0.40	-29.9	0.3	-150.7	0.7
2H-6 90-92.5	13.113	29491	0.92	0.31	-31.2	0.5		
2H-6 115-117.5	13.363	30076	0.69	0.29	-29.4	0.1	-159.3	2.7
2H-6 135-137.5	13.563	30543	0.80	0.65	-31.4	0.1	-154.8	0.7
2H-7 20-22.5	13.913	30906	0.87	0.57	-28.2	0.1	-149.1	3.4
3H-1 5-7.5	14.263	32222	1.11	0.09	-28.0	0.1	-150.6	4.3
3H-1 15-17.5	14.353	32513	0.92	0.22	-29.0	0.1		
3H-1 25-27.5	14.453	32752	1.10	0.28	-31.7	0.1		
3H-1 35-37.5	14.543	32935	0.81	0.18	-31.6	0.2	-147.6	6.6
3H-1 45-47.5	14.643	33117	0.69	0.39	-28.7	0.2	-150.9	1.7
3H-1 55-57.5	14.733	33333	1.27	0.17	-31.6	0.1	-149.6	3.0
3H-1 70-72.5	14.882	33690	0.93	0.25	-29.5	0.2	-148.0	8.2

APPENDIX 5.2 (CONTINUED)

Sample ID	Depth (m)	Age (Cal yr BP)	Ruber $\delta^{13}\text{C}$ (‰)	Ruber $\delta^{18}\text{O}$ (‰)	$\delta^{13}\text{C}_{32}$ (‰)	error (‰)	δD_{32} (‰)	error (‰)
3H-1 80-82.5	14.973	33909	0.92	0.33	-28.8	0.5		
3H-1 105-107.5	15.213	34219	0.82	0.01	-29.9	0.2	-148.7	10.1
3H-1 130-132.5	15.453	34681	1.61	-0.06	-31.1	0.2	-151.9	2.8
3H-2 30-32.5	15.923	35307	0.64	0.34	-27.1	0.1	-152.9	0.7
3H-2 80-82.5	16.403	35819	0.67	0.00	-31.3	0.0	-140.9	1.4
3H-2 95-97.5	16.543	36008			-31.4	0.4		
3H-2 105-107.5	16.643	36257			-31.3	0.0		
3H-2 130-132.5	16.873	36944	0.76	-0.08	-31.5	0.4	-140.9	1.0
3H-3 5-7.5	17.113	37789			-29.6	0.4		
3H-3 50-52.5	17.563	38631	0.85	0.28	-24.3	0.2		
3H-3 70-72.5	17.733	38948	1.02	0.20	-26.1	0.1	-142.1	2.1
3H-3 100-102.5	18.033	39529	1.08	0.38	-27.7	0.6	-147.4	2.6
3H-3 120-122.5	18.213	39878	1.12	0.19	-30.9	0.2	-151.2	4.8
3H-3 135-137.5	18.363	40347			-30.3	0.7		
3H-4 0-2.5	18.497	40766			-29.8	0.5		
3H-4 10-12.5	18.590	41060	1.08	0.51	-30.8	0.3	-154.7	0.3
3H-4 20-22.5	18.683	41356			-30.8	0.2		
3H-4 30-32.5	18.783	41672			-30.4	0.9		
3H-4 40-42.5	18.873	41957			-30.3	0.3		
3H-4 55-57.5	19.023	42338	1.27	0.25	-30.4	0.3	-151.9	0.8
3H-4 70-72.5	19.163	42636			-29.6	0.3		
3H-4 95-97.5	19.413	43171			-31.0	0.7		
3H-4 115-117.5	19.613	43600			-31.3	0.1		
3H-4 130-132.5	19.733	43857	0.98	-0.03	-31.0	0.3	-151.6	3.5
3H-5 5-7.5	19.973	44269	1.07	0.22	-30.8	0.2	-134.9	6.2
3H-5 30-32.5	20.213	44609			-30.9	0.7		
3H-5 55-57.5	20.443	45112	1.20	-0.34	-32.1	0.6	-141.0	0.2
3H-5 80-82.5	20.683	45758	1.00	0.01	-32.0	0.2		
3H-5 105-107.5	20.923	46415	1.10	-0.23	-32.0	0.3	-146.3	0.2
3H-5 130-132.5	21.163	47071	0.92	-0.11	-31.0	0.4	-139.4	0.9
3H-6 5-7.5	21.403	47693	0.93	0.18	-30.1	0.2		
3H-6 30-32.5	21.633	48283	0.87	0.12	-29.3	0.2		
3H-6 55-57.5	21.873	49012	0.80	0.08	-29.3	0.4	-142.2	0.7
3H-6 80-82.5	22.113	49697	0.93	0.33	-31.8	0.4		
3H-6 105-107.5	22.353	50215	1.20	-0.12	-32.4	0.4	-155.6	0.3
3H-7 5-7.5	22.823	51095	0.88	-0.23	-32.1	0.3		
3H-7 30-32.5	23.063	51429	0.82	-0.17	-32.5	0.2	-138.6	2.2
3H-7 55-57.5	23.313	51794	0.78	0.13	-32.7	0.1		
3H-CC 20-22.5	23.573	52173	0.90	-0.17	-32.6	0.5		
4H-1 10-12.5	23.793	52458	1.10	0.14	-31.6	0.3	-150.9	6.7
4H-1 35-37.5	24.043	52779	0.76	-0.10	-32.6	0.2	-151.5	5.0
4H-1 60-62.5	24.293	53219	1.12	0.00	-32.7	0.3	-138.9	0.3
4H-1 85-87.5	24.516	53614	0.87	0.05	-31.3	0.4	-145.7	4.2
4H-1 110-112.5	24.743	54262	0.94	0.06	-29.5	0.2	-137.1	2.2
4H-1 135-137.5	24.993	54974	0.55	0.17	-31.4	0.0	-149.1	0.3
4H-2 3-4.5	25.143	55387	0.65	0.06	-31.7	0.4		
4H-2 33-34.5	25.443	56215	0.67	0.16	-30.4	0.5		
4H-2 45-47.5	25.563	56547	0.36	0.26	-32.2	0.2	-150.9	0.8
4H-2 63-64.5	25.743	57071			-31.6	0.4		

APPENDIX 5.2 (CONTINUED)

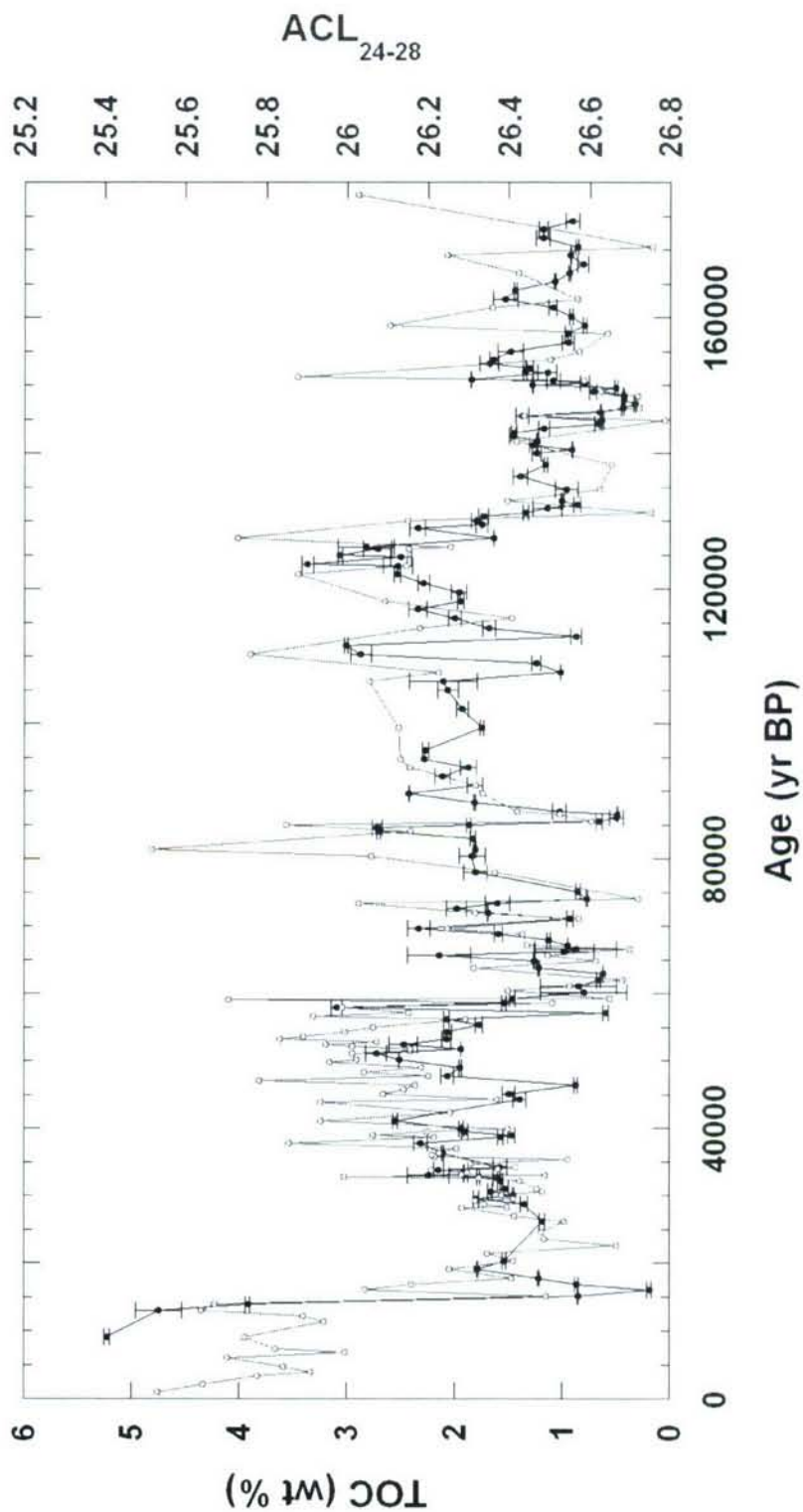
Sample ID	Depth (m)	Age (Cal yr BP)	Ruber $\delta^{13}\text{C}$ (‰)	Ruber $\delta^{18}\text{O}$ (‰)	$\delta^{13}\text{C}_{32}$ (‰)	error (‰)	δD_{32} (‰)	error (‰)
4H-2 93-94.5	26.013	57860	0.84	-0.46	-31.3	0.5		
4H-2 95-97.5	26.033	57919			-31.5	0.2	-147.9	0.6
4H-2 123-124.5	26.283	58519	0.75	0.28	-30.7	0.3	-141.4	1.8
4H-2 145-147.5	26.503	59046			-29.1	0.1	-137.7	1.9
4H-3 3-4.5	26.563	59223	1.12	-0.28	-29.9	0.1	-140.0	3.3
4H-3 33-34.5	26.863	60101	0.30	0.33	-27.5	0.4		
4H-3 45-47.5	26.983	60451	0.35	0.31	-26.5	0.1	-142.6	6.9
4H-3 63-64.5	27.163	61098	0.35	0.28	-26.1	0.2		
4H-3 93-94.5	27.433	62067	0.50	0.02	-26.6	0.5		
4H-3 95-97.5	27.453	62138	0.35	0.07	-26.4	0.6		
4H-3 123-124.5	27.703	62997	0.54	0.21	-28.2	0.6		
4H-3 145-147.5	27.923	63754	0.55	-0.03	-28.9	0.6		
4H-4 3-4.5	28.263	64804	0.89	0.33	-29.7	0.3	-139.5	0.7
4H-4 33-34.5	28.563	65661	1.02	0.02	-30.8	0.2	-152.7	0.1
4H-4 63-64.5	28.863	66121	0.95	0.55	-31.3	0.4	-155.4	6.8
4H-4 93-94.5	29.163	66582	0.86	0.23	-31.8	0.4		
4H-4 123-124.5	29.463	67043	0.79	0.25	-31.4	0.3		
4H-5 3-4.5	29.763	67842	0.90	0.49	-31.5	0.2		
4H-5 33-34.5	30.063	68780	0.97	0.22	-31.2	0.3		
4H-5 63-64.5	30.363	69626	0.75	0.23	-30.2	0.1		
4H-5 93-94.5	30.663	70342	1.03	0.66	-32.3	1.0		
4H-5 123-124.5	30.963	71058	0.72	0.18	-30.7	0.3	-158.5	1.0
4H-6 3-4.5	31.293	71846	0.59	0.49	-31.0	0.4	-147.8	5.2
4H-6 33-34.5	31.593	72566	0.99	0.28	-30.9	0.3		
4H-6 63-64.5	31.893	73304	1.84	-0.41	-30.6	0.5		
4H-6 93-94.5	32.193	74043	1.01	-0.08	-31.3	0.7	-144.8	0.4
4H-6 123-124.5	32.493	75042	1.15	-0.02	-31.8	0.8		
4H-7 3-4.5	32.823	77885	1.35	-0.44	-31.8	0.2	-136.4	
4H-7 33-34.5	33.123	80470	1.41	-0.40	-31.0	0.3		
5H-1 3-4.5	33.233	81417	1.31	-0.45	-27.4	0.3		
4H-7 62-63.5	33.413	82968	1.63	-0.59	-31.2	0.5		
5H-1 33-34.5	33.533	84000	1.35	-1.10	-31.2	0.3		
5H-1 63-64.5	33.833	84490	1.19	-0.89	-30.8	0.5		
5H-1 93-94.5	34.133	84982	1.39	-0.76	-30.1	0.3		
5H-1 123-124.5	34.433	85474	0.72	0.07	-28.4	0.4		
5H-2 3-4.5	34.763	86015	0.72	0.17	-28.0	0.4		
5H-2 33-34.5	35.063	86507	1.01	0.04	-29.0	0.2		
5H-2 63-64.5	35.363	87000	0.61	0.37	-30.4	0.3	-138.3	
5H-2 123-124.5	35.963	89571	1.24	-0.53	-31.8	0.4		
5H-3 3-4.5	36.263	90856	1.25	-0.05	-31.6	0.1	-140.3	3.7
5H-3 33-34.5	36.563	92142	1.33	-0.48	-32.5	1.1		
5H-3 63-64.5	36.863	93428	1.40	-0.65	-30.5	0.4	-149.5	6.6
5H-3 93-94.5	37.163	94713	1.05	-0.86	-32.1	0.4		
5H-3 123-124.5	37.463	96000	1.24	-0.92	-31.5	0.4		
5H-4 3-4.5	37.823	99375	1.35	-0.63	-32.2	0.5	-140.7	1.3
5H-4 33-34.5	38.123	102187	1.42	-0.95	-32.4	0.0		
5H-4 63-64.5	38.423	105000	1.52	-1.02	-32.0	0.1		
5H-4 93-94.5	38.723	106288	1.35	-0.99	-31.9	0.7		
5H-4 123-124.5	39.023	107578	1.32	0.00	-30.8	1.3		

APPENDIX 5.2 (CONTINUED)

Sample ID	Depth (m)	Age (Cal yr BP)	Ruber $\delta^{13}\text{C}$ (‰)	Ruber $\delta^{18}\text{O}$ (‰)	$\delta^{13}\text{C}_{32}$ (‰)	error (‰)	δD_{32} (‰)	error (‰)
5H-5 3-4.5	39.353	109000	1.01	0.07	-30.8	0.3		
5H-5 33-34.5	39.653	110298	1.23	-1.50	-31.0	0.8		
5H-5 63-64.5	39.953	111594	1.15	-1.10				
5H-5 123-124.5	40.553	114186	0.88	-0.63	-31.2	0.4		
5H-6 3-4.5	40.883	115611	1.19	-0.87	-31.7	0.4	-145.2	0.1
5H-6 33-34.5	41.183	116907	0.82	-0.96	-31.7	0.2		
5H-6 123-124.5	42.083	120795	1.18	-1.19	-32.1	0.1		
5H-7 3-4.5	42.383	122091	0.93	-1.38	-31.5	0.1		
5H-7 33-34.5	42.683	123387	1.11	-1.33	-31.8	0.2		
6H-1 3-4.5	42.733	123603	1.11	-1.68	-29.1	0.4		
6H-1 33-34.5	43.033	124899	0.81	-1.83	-29.8	0.4		
5H-CC 3-4.5	43.273	125935	1.54	-1.39	-28.1	0.1		
6H-1 63-64.5	43.333	126195	0.83	-1.28	-30.7	0.1		
6H-1 93-94.5	43.633	127490	0.47	-0.70	-28.0	0.3		
6H-1 128-129.5	43.983	129000	0.72	-0.48	-27.8	0.3		
6H-2 3-4.5	44.233	129487	0.63	-0.80				
6H-2 33-34.5	44.533	130073	0.48	-1.10	-27.8	0.9		
6H-2 93-94.5	45.133	131244	0.00	-0.78	-29.4	0.7	-125.2	
6H-3 33-34.5	46.033	133000	0.02	0.04	-29.0	0.2		
6H-3 63-64.5	46.333	134748	0.31	0.38	-31.6	0.2	-138.2	1.6
6H-3 123-124.5	46.933	138248	0.33	0.37				
6H-4 3-4.5	47.233	140000	0.37	0.63				
6H-4 33-34.5	47.533	140603	0.43	0.50	-33.0	0.4		
6H-4 93-94.5	48.133	141811	0.67	0.41	-32.4	0.2		
6H-5 93-94.5	49.633	144831	0.45	0.42	-32.2	0.1		
6H-5 123-124.5	49.933	145435	0.36	0.32	-32.3	0.5	-137.8	1.8
6H-6 33-34.5	50.533	146643	0.45	0.58	-28.5	0.2		
6H-6 123-124.5	51.433	148455	0.22	0.67	-31.5	0.1		
6H-7 3-4.5	51.733	149059	0.53	0.58	-31.6	0.3		
7H-1 33-34.5	52.533	150670	0.85	0.16	-30.8	0.2		
7H-2 63-64.5	53.783	153187	0.83	0.30	-31.8	0.3		
7H-3 3-4.5	54.683	155000	0.79	-0.60	-32.1	0.4	-153.3	0.3
7H-3 33-34.5	54.983	156290	0.62	0.38	-31.0	0.7		
7H-3 65-66.5	55.303	157666	0.74	0.00	-30.5	0.3		
7H-4 3-4.5	56.183	161450	0.80	0.01	-31.2	0.2		
7H-4 33-34.5	56.483	162740			-31.2	0.4		
7H-4 63-64.5	56.783	164030			-31.3	0.3		
7H-4 123-124.5	57.383	166610	0.62	-0.25	-30.0	0.3		
7H-5 33-34.5	57.983	169190	0.61	-0.06	-28.7	1.8		
7H-5 63-64.5	58.283	170480	0.28	0.29	-29.6	0.6		
7H-5 93-94.5	58.583	171770	0.78	-0.25	-30.3	0.1		
7H-6 33-34.5	59.483	175640	0.54	0.09	-30.1	0.3		
7H-6 93-94.5	60.083	178220	0.98	-0.39	-31.5	0.3	-150.0	0.5
7H-6 123-124.5	60.383	179510			-30.7	0.1		

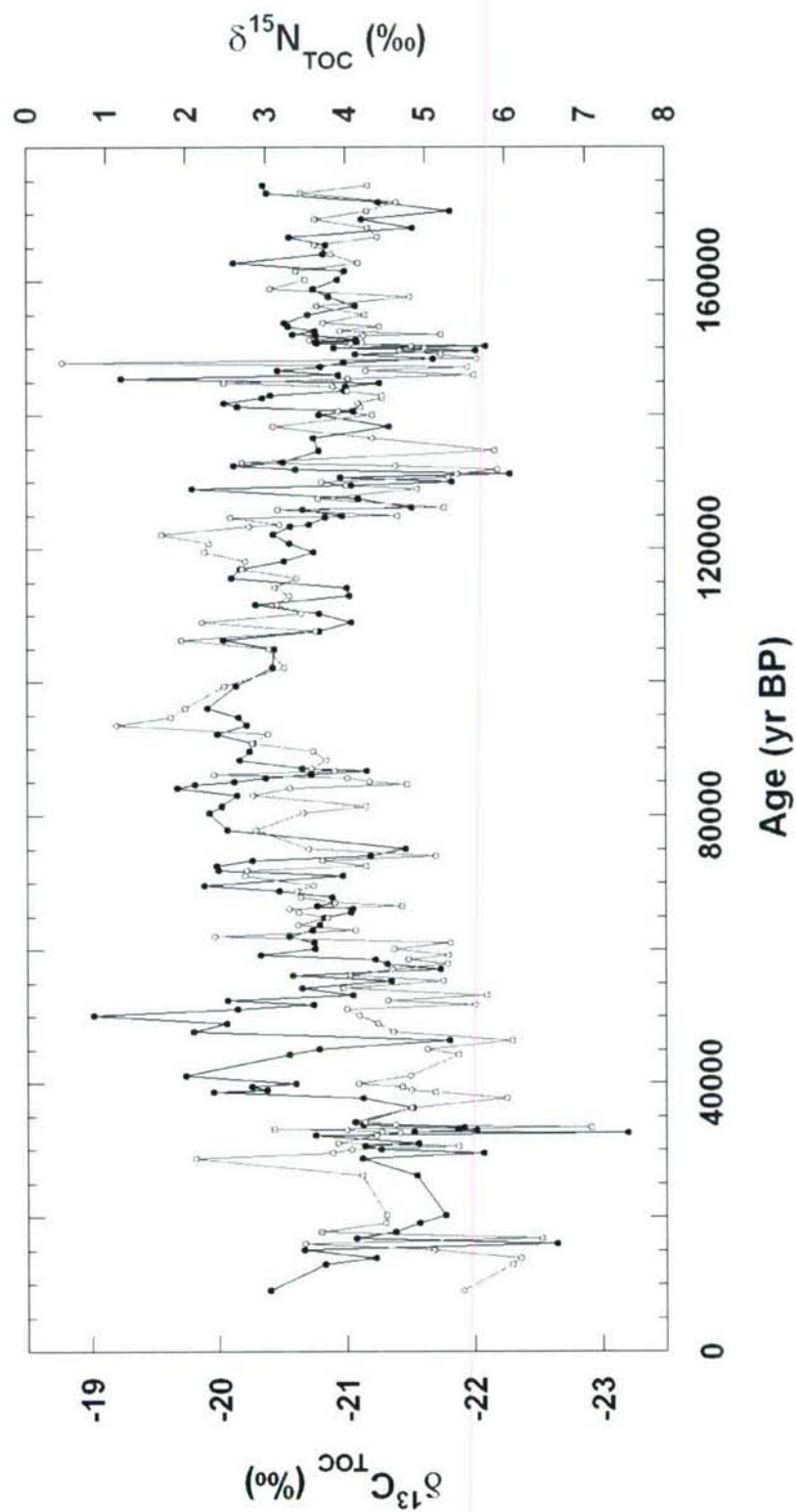
APPENDIX 5.3

Profiles of bulk TOC (black) and the average chain length of the $nC_{24} - nC_{28}$ fatty acids (ACL_{24-28} ; grey) from ODP Hole 1002D in the Cariaco Basin. Triplicate means and 1σ analytical error bars are shown for the TOC values.



APPENDIX 5.4

Profiles of $\delta^{13}\text{C}$ (black) and $\delta^{15}\text{N}$ (grey) in bulk TOC from ODP Hole 1002D in the Cariaco Basin. Triplicate means for both isotopes are given; analytical error bars are not shown for the sake of visual clarity.



REPORT DOCUMENTATION PAGE	1. REPORT NO. MIT/WHOI 2007-14	2.	3. Recipient's Accession No.
4. Title and Subtitle The Temporal Dynamics of Terrestrial Organic Matter Transfer to the Oceans: Initial Assessment and Application			5. Report Date June 2007
7. Author(s) Nicholas J. Drenzek			6.
9. Performing Organization Name and Address MIT/WHOI Joint Program in Oceanography/Applied Ocean Science & Engineering			8. Performing Organization Rept. No.
12. Sponsoring Organization Name and Address National Science Foundation Stanley Watson Foundation Schlanger Ocean Drilling Program Environmental Protection Agency			10. Project/Task/Work Unit No. MIT/WHOI 2007-14
			11. Contract(C) or Grant(G) No. (C) OCE-9907129 (C) OCE-052626800 (G) OCE-0137005 DEB-0447281
15. Supplementary Notes This thesis should be cited as: Nicholas J. Drenzek, 2007. The Temporal Dynamics of Terrestrial Organic Matter Transfer to the Oceans: Initial Assessment and Application. Ph.D. Thesis. MIT/WHOI, 2007-14.			13. Type of Report & Period Covered Ph.D. Thesis
			14.
16. Abstract (Limit: 200 words) This thesis employs compound-specific stable carbon and radiocarbon isotopic analysis of organic biomarkers to (a) resolve petrogenic from pre-aged vascular plant organic carbon (OC) in continental margin sediments, (b) investigate the underlying mechanisms controlling the anomalously old ages that are often observed for the terrestrial component of sedimentary OC, and (c) address the associated consequences for biomarker-based climate reconstructions. Coupled molecular isotope mass balances demonstrate that the amount of petrogenic OC in margin sediments has been previously overestimated due to the presence of significantly 'pre-aged' terrestrial OC, but is nonetheless still significant. Additionally, the vast majority of terrestrial OC at two study sites was determined to experience multi-millennial residence times on land prior to entering the sea. With this in mind, the striking modulation in the signal amplitude of a biomarker-based tropical paleoaridity record was instead used to evaluate the role of low versus high latitude forcing in abrupt paleoclimate oscillations during the last full glacial cycle. Seasonal variations in the position of the Intertropical Convergence Zone were interpreted to be a response to both high latitude adjustments in meridional overturning circulation and local insolation.			
17. Document Analysis a. Descriptors Radiocarbon Paleoclimate Biomarkers b. Identifiers/Open-Ended Terms c. COSATI Field/Group			
18. Availability Statement Approved for publication; distribution unlimited.		19. Security Class (This Report) UNCLASSIFIED	21. No. of Pages 223
		20. Security Class (This Page)	22. Price